Visually Mediated Control of Flight in *Drosophila*: Not Lost in Translation

Thesis by
Michael B. Reiser

In Partial Fulfillment of the Requirements
for the Degree of
Doctor of Philosophy

California Institute of Technology
Pasadena, California

2007
(Defended December 15, 2006)

This thesis is dedicated to the memory of my grandfathers: Dr. Bernard Abel, a true gentleman whom I never had the chance to meet, and my saba, Ephraim Reiser, a mountain of a man who is dearly missed.

Acknowledgements

I owe a considerable debt of gratitude to my advisor, Michael Dickinson. Not only did he take a chance on a rather desperate electrical engineer, but he has allowed me virtually unlimited intellectual freedom during my time in his laboratory. Most valuable of all, Michael—in his quiet manner—has provided me with the finest example of what doing science is all about.

I am grateful to the members of my committee, Joel Burdick, Christof Koch, Richard Murray, and Pietro Perona, for providing necessary guidance and finding time to fit me into their incredibly busy lives.

Spending years in peculiar underground settings, building robots and gluing flies to sticks would not have been nearly as much fun without the entire Dickinson Lab crew, past and present. I am especially indebted to the original Berkeley group for making my transition over to *real* science such a hoot. Whether given some duct tape and a few servo motors or a thorny whiteboard problem, Will Dickson was always available for impromptu, and often impractical, pursuits. I have been fortunate to have two great office-mates over the past few years—chats with Seth Budick and Alice Robie were always a pleasant distraction. Special thanks are owed to Mark Frye who has unwittingly served as a second mentor and taught me a few priceless phrases along the way.

I wish to thank Robert Bailey for his brilliant assistance in getting the panels to progress from concept to reality. I also thank Andrew Straw for assistance with cameras and teaching me a few things about fly motion vision, and Allan Wong for being a generally great guy and always letting me take over the 'miscroscopy room' or his computer when I needed to squeeze out that last drop of data. Major thanks are

owed to Ofer Mazor for the generous use of his very nice LaTeX templates.

I am grateful to Domitilla Del Vecchio, Mary Dunlop, Sean Humbert,and Richard Murray (again) for the short-lived collaboration (as part of CDS 270) that resulted in the vision-based upwind flight model that is described in Chapter 6.

I am indebted to an interesting group of people for friendships that have made my time in graduate school such a strange pleasure that I would eagerly do it again—Sarah Bergbreiter, Dan Gold, Vivek Jayaraman, Wyatt Korff, Attila Kovacs, Tim Lebestky, Connie Lu, Ofer Mazor, Ben Rubin, Jasper Simon, the CNS 2002 class, and many others who have contributed to my Caltech experience.

To my parents, Barbara and Sammy, I owe nothing short of everything, they gave me life, and have provided me with years of unending support. I am fortunate to have such a wonderful family, both by birth and by marriage; they provide the context that makes all else worthwhile.

And finally, I must thanks my incredible wife Judy. As I look back with fondness (and a bit of horror) on our graduate school years, first at Berkeley and then at Caltech, it is absolutely clear that I could not have done any of this without her. Judy understands me as no one else can...she's just about perfect.

Abstract

Flying insects exhibit stunning behavioral repertoires that are largely mediated by the visual control of flight. For this reason, presenting a controlled visual environment to tethered insects has been and continues to be a powerful tool for studying the sensory control of complex behaviors. The work presented in this dissertation concerns several robust behavioral responses exhibited by *Drosophila* that shed light on some of the challenges of visual navigation. To address questions of visual flight control in *Drosophila*, a modular display system has been designed and has proven to be a robust experimental instrument. The display system has enabled the wide variety of experimental paradigms presented in the thesis.

Much is known about the responses of tethered *Drosophila* to rotational stimuli. However, the processing of the more complex patterns of motion that occur during translatory flight is largely unknown. Recent experimental results have demonstrated that *Drosophila* turn away from visual patterns of expansion. However, the avoidance of expansion is so vigorous, that flies robustly orient towards the focus of contraction of a translating flow field. Much of the effort documented in this thesis has sought to explain this paradox.

The paradox has been largely resolved by several significant findings. When undergoing flight directed towards a prominent object, *Drosophila* will tolerate a level of expansion that would otherwise induce avoidance. The expansion-avoidance behavior is also critically dependent on the speed of image motion; in response to reduced speeds of expansion, *Drosophila* exhibit a centering response in which they steer towards the focus of expansion by balancing the image motion seen by both eyes. Taken together, these behaviors contribute to a model of *Drosophila*'s visual flight

control as emerging from multiple behavioral modules that operate concurrently.

Simple computational models of *Drosophila*'s visual system are used to demonstrate that the experimental results arrived at by doing psychophysics on tethered animals actually yield sensible navigation strategies. This final component of the thesis documents an effort to close the feedback loop around the experimenter, by using computational models of *Drosophila* behavior to constrain the design of future experiments.

Contents

List of Figures

List of Tables

Chapter 1

Introduction

Flying insects exhibit stunning behavioral repertoires that are largely mediated by the visual control of flight. For decades these impressive animals have served as model systems for neurobiological studies of the sensory control of complex behaviors (Buchner, 1984; Frye and Dickinson, 2001; Egelhaaf et al., 2002; Borst and Haag, 2002). There is still much that is unknown about the visual processing underlying the robust flight control of flies. Fortunately, current research can draw on recent advances in our understanding of the aerodynamics of insect flight control (Taylor, 2001; Fry et al., 2003) and the neural basis of visual processing in flies.[1]

1.1 Fly sensory systems

Although this document focuses on the visual control of flight, it is essential to emphasize that flies integrate feedback from many complementary sensory systems to control flight behavior (Figure 1.1). For example, eight separate mechanosensory and visual systems are responsible for the control of visual gaze in the blowfly, *Calliphora* (Hengstenberg, 1991).

Flies possess mechanosensory structures, called halteres, which function as gyroscopes. The halteres are small modified hind wings that beat antiphase to the wings (Nalbach, 1993) and are sensitive to Coriolis forces, inertial forces acting on

[1] Since the fruit fly, *Drosophila melanogaster*, is the model system used in this thesis, the discussion in this introduction will focus on the *Drosophila* flight control system wherever possible.

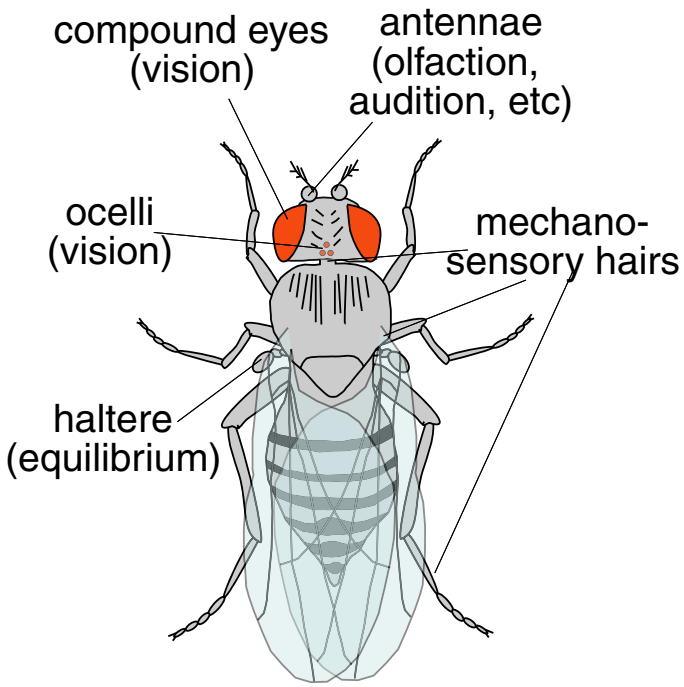

Figure 1.1. Summary of the various sensory systems present in *Drosophila* that contribute to the control of flight.

bodies moving in a rotating reference frame. The Coriolis forces measured by the halteres are proportional to the angular velocity of the fly's body. It is theoretically possible for the pair of halteres to measure roll, pitch, and yaw velocities, although experimental results indicate that their response may be explained as the linear sum of two orthogonal systems, one most sensitive to pitch, and the other most sensitive about a combined yaw-roll axis (Dickinson, 1999). The halteres are used to maintain the equilibrium reflexes of the fly, minimizing rotations of the body during flight. When fixed to a mechanically rotating environment, and receiving no visual feedback, flies modify their wing kinematics to counteract the applied rotation sensed by the halteres (Dickinson, 1999; Sherman and Dickinson, 2003). Flies possess several other mechanosensory organs used in flight, including campaniform sensilla on the wings sensitive to wing load and neck sense organs that detect the posture of the head (Hengstenberg, 1991).

In addition to eyes, flies, like many insects, have three photosensitive organs called

ocelli that are arranged in a triangle on the dorsal part of the head (Chapman, 1998). The ocelli are underfocused, and thus are unlikely to play a role in the detection of motion. Rather they are used to measure brightness and are thought to contribute to the dorsal light response, in which the fly aligns its head with sources of brightness (Schuppe and Hengstenberg, 1993). There is strong evidence suggesting ocelli may also be used in more complicated tasks, such as horizon detection in locusts (Wilson, 1978) and dragonflies (Stange, 1981), and orientation towards edges in walking houseflies (Wehrhahn, 1984). Wilson (1978) observes that the ocelli of locusts act as high-pass temporal and low-pass spatial filters, implying they are sensitive to sudden movements of the visual world as would be experienced during flight instabilities. Furthermore, by recording from ocellar nerves, Wilson (1978) demonstrates that the ocelli are most sensitive to UV light, the wavelength at which ground and sky contrast are maximal.

Perhaps most intricate of all, the fly antennae are home to multiple sensory systems. The antennae are known to be the primary nose (Vosshall, 2000) and ear (Gopfert and Robert, 2002) of *Drosophila*, and they have also been shown to be temperature and humidity sensors (Sayeed and Benzer, 1996). In a brief note, Götz and Biesinger (1983) report that when tethered *Drosophila* are confronted with a head and tail wind, significant changes are observed in motor responses to visual motion, and these changes are largely removed when the antennae are fixed.

The integration mechanism of these different modalities is likely to be complicated. For example, the control muscles of the blowfly's halteres receive input from the visual system; thus visual motion perceived by the fly might alter mechanosensory sensitivity during flight (Chan et al., 1998). The halteres in turn provide feedback to the wing steering muscles. This 'control loop' may explain a system by which a fly could alter gains or override the equilibrium reflex to initiate a voluntary behavior. This design in which one sensory modality controls the sensitivity of another via efferent pathways appears to be a common feature of the flight control architecture (Hengstenberg, 1991). Other findings suggest that multimodal information is integrated in neurons that play a role in flight control; Olberg (1981) reports dragonfly interneurons that encode directional information from at least four sensory modalities, and (Parsons

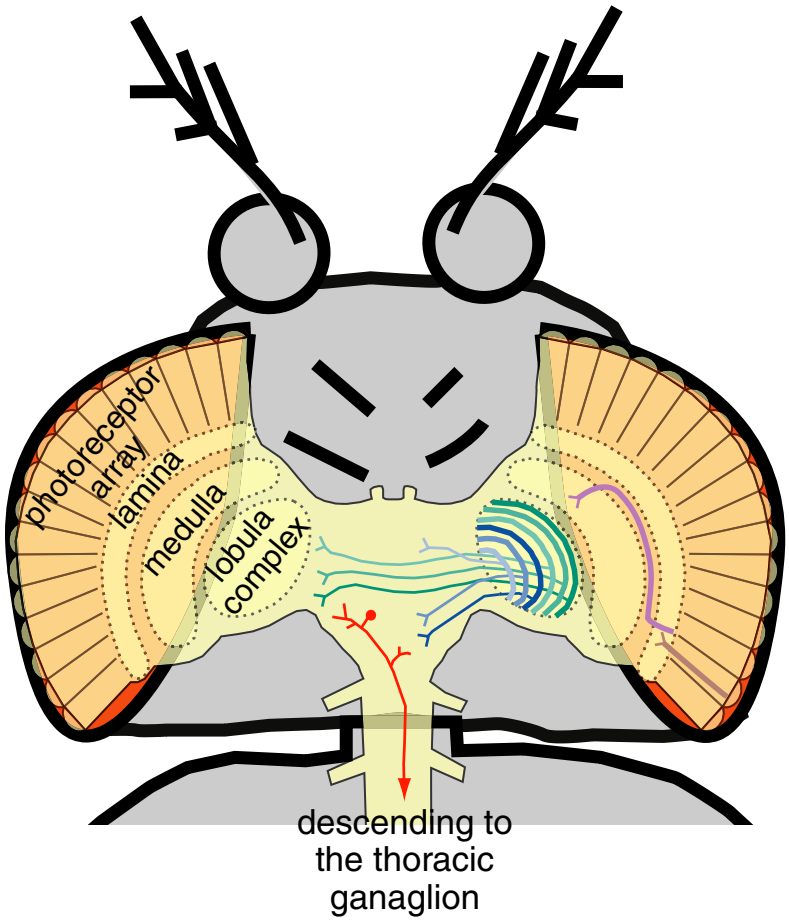

Figure 1.2. A horizontal cross section through the fly's head in schematic form, emphasizing the visual system. Vision begins with the ommatidia, the individual elements of the eye. Visual information is processed by three successive ganglia in a retinotopic arrangement. The motion-sensitive neurons of the lobula plate transmit information to descending interneurons that project to motor centers in the thorax. Figure modified from M. Frye.

et al., 2006) finds multimodal responses in neurons that were previously thought to respond exclusively to visual motion. At present, we are far from an understanding of the general principles underlying the multisensory control of flight.

1.2 Dipteran visual system

While flies use many sensory modalities, most of the behaviors we casually observe are dominated by visual control. Flying insects use visual feedback to stabilize flight, track objects, land, measure self-motion, estimate distances traveled, and perceive

depth (Egelhaaf and Kern, 2002; Srinivasan et al., 1999; Borst and Egelhaaf, 1989). The architecture of the fly visual system is schematized in Figure 1.2.

Any discussion of vision must begin at the periphery; each compound eye of *Drosophila* consists of approximately 700 units, called ommatidia, arranged in a hexagonal array. The optical axis of each ommatidium is directed at a different point in space, while the diffraction-limited optics (Snyder, 1979; Land, 1997) of the facet lens collect light from a round patch of about 5° of the visual world. The 1400 ommatidia can sample roughly 85% of visual space (Heisenberg and Wolf, 1984). As an adaptation for capturing photons in low light while maximizing visual acuity, the visual systems of Diptera have evolved a neural superposition architecture, a rather complex optical arrangement, whereby the photoreceptors pointing to one region of space (but located in neighboring ommatidia) are pooled at the neural level (Land and Fernald, 1992). Once pooled, the signals from each ommatidia are processed by four successive optical ganglia—the lamina, the medulla, the lobula, and the lobula plate, in a system composed of thousands of intricately organized neurons that maintain a retinotopic columnar structure such that neighboring optical 'cartridges' process information from neighboring eye facets (Strausfeld, 1989; Borst and Haag, 2002). In the lamina the retinotopic signals from the photoreceptors are spatially and temporally filtered (Laughlin, 1994) before being sent to the medulla, which is involved in motion processing (Buchner et al., 1979; Borst and Haag, 2002).

1.3 Computational modeling of fly visual system

Since the influential work of Gibson (1950), the notion that an optic flow field is a source of important information for animal navigation has inspired a detailed analysis of the motion vision of many organisms.[2] The motion detection system of flies has an extensive history of detailed investigation. The basic, correlation-type motion detector was originally proposed by Hassenstein and Reichardt (1956) to explain

[2]It is important to note the distinction between the velocity field, a purely geometric quantity of motion projected onto the retina, and the optic flow field, which is the pattern of intensity motion across the retina, transduced by a motion detecting system. The optic flow field can ideally be thought of as an estimate of the velocity field.

the optomotor response of the beetle *Clorophanus*. A local motion detector must theoretically consist of at least two inputs passing through asymmetrical channels and combined via a nonlinear element (Borst and Egelhaaf, 1989). Two of these half detectors are combined (with mirror symmetry) to form a directionally selective motion detector. In the Hassenstein-Reichardt (HR) model, a temporal delay provides the asymmetry, and a multiplication is the nonlinear interaction (Figure 6.2A). In the simulations of Chapter 6, further details on the practical issues involved with modeling the HR motion detector are provided.

An alternative class of optic flow computations has been developed within the computer vision community. These so-called gradient methods assume that intensity across the image is constant, yielding output that is (desirably) independent of contrast. Some studies on humans support a biological basis for gradient methods, but as discussed by Borst and Egelhaaf (1989), practical implementations of gradient-based vision begin to resemble correlation-type motion detectors. This suggests that mechanisms underlying motion detection in biological systems are, in some sense, equivalent to the Hassenstein-Reichardt motion detector.

A variety of behavioral and neurobiological studies have shown that the Hassenstein-Reichardt model coheres with many aspects of insect behavior and physiology (Srinivasan et al., 1999; Egelhaaf et al., 1989, and the discussion in §4.6.1). The HR model does not provide a true measurement of velocity, since the response also depends on luminance, contrast, and the distribution of features in the environment (Zanker et al., 1999). A recent trend has seen the proposal of many elaborated versions of the HR model. For example, Dror et al. (2001) demonstrate that with appropriate modification (spatial and temporal prefiltering, compressive nonlinearities, temporal integration, and spatial summation), the reliability of the HR model as a velocity estimator is significantly enhanced. Furthermore, this enhanced model proves more useful when presented with natural image statistics as opposed to artificial patterns as we have used. In other work, Lindemann et al. (2005) have incorporated elaborations into the HR model to explicitly account for the response properties of motion-sensitive neurons of the lobula plate.

1.4 Lobula plate tangential cells and the matched filter hypothesis

Most attention to the visual processing in flies has focused on the neuronal activity of a class of large motion-sensitive cells in the lobula plate, referred to as the lobula plate tangential cells (LPTCs). The experimental accessibility of these cells and their presumed importance in visual processing relevant to flight control has motivated this disproportionate effort. There are approximately 60 of these visual interneurons in the well-studied lobula plate of the blowfly *Calliphora* (Hausen, 1984), and a recent Golgi analysis has anatomically identified many analogous neurons in *Drosophila* (Rajashekhar and Shamprasad, 2004). Much of the current understanding of the LPTCs originates with the pioneering work of Hausen, who recorded (both intra- and extracellularly) from several of these identified cells while presenting a local motion stimulus, and showed that each cell type encodes a certain orientation of local motion that is consistent with that cell's dendritic arborization (Hausen, 1982a,b, 1984). Further, Hausen (1984) observed that the receptive fields and preferred directions of the LPTCs appeared to be tuned to specific patterns of optic flow that might be relevant to flight control. This observation was made more rigorous by the detailed investigations of Krapp and Hengstenberg (1996), who made use of an elaborate system for providing fast local motion stimuli (Krapp and Hengstenberg, 1997). By mapping the locally preferred direction and sensitivity, Krapp and Hengstenberg (1996) generated receptive-field maps for the motion sensitivity of several LPTCs that were strikingly similar to particular features of the optic flow field that the fly would experience by self-motion during flight.

This observation has given rise to the idea that the LPTCs function as 'matched filters' to patterns of optic flow that could directly drive flight (Egelhaaf et al., 2002). Although some recent studies have provided challenges to the specific mechanism of the matched filter hypothesis (Karmeier et al., 2003; Straw et al., 2006), other recent work has focused on the decoding of the response properties of certain LPTCs; Kern et al. (2005) suggest that both rotational and translational motion may be encoded in

different frequency bands in the HS cell, and Karmeier et al. (2005) have shown that the information encoded in the VS cells is sufficient to predict the axis of rotation. The matched filter hypothesis has also inspired several (dozen) artificial visual systems that use a simplified motion-detection and a matched filter model to estimate the self-motion of (virtual or actual) robots (Franz et al., 1999; Neumann and Bülthoff, 2002; Reiser and Dickinson, 2003).

1.5 A brief history of experimental flight control

Much of what is known about the aerodynamic and sensory control of flight is based on many important free flight studies (Land and Collett, 1974; Srinivasan et al., 1991; Schilstra and Van Hateren, 1999; Tammero and Dickinson, 2002b; Fry et al., 2003). An alternative approach has been to use visual stimuli in conjunction with behavioral studies of the visuomotor responses of restrained insects, which is an established laboratory technique with a rich history of cleverly designed stimulus generating systems. Early experiments used patterned cylinders that were mechanically rotated to provide a moving visual stimulus. Behavior observed using these types of experiments led to the development of the principle of reafference (Von Holst and Mittlestaedt, 1950), the formulation of the Hassenstein-Reichardt model for visual motion detection (Reichardt, 1961), and the discovery of the syndirectional optomotor response, measured in flies using a torque compensator (Götz, 1964). The invention of the torque compensator and the subsequent optical wingbeat analyzer (Götz, 1987), enabled a variety of closed-loop experiments, in which the measured turning response of tethered flies was used to set the velocity of the rotating panorama (Reichardt and Wenking, 1969). Revolving static patterns are an appropriate stimulus for studying the response of flies to coherent rotatory motion, but even with many creative modifications, large classes of motion stimuli cannot be presented with such a system. To develop a model for the response of *Drosophila* to progressive and regressive motion, Götz (1968) used two independently controlled projectors to present moving stimuli to each eye. Even better spatial control of the motion stimulus was necessary

for electrophysiological investigations of motion sensitive neurons in blowflies; Hausen (1982a) used pattern projectors mounted on a gimbal and Krapp and Hengstenberg (1997) developed an elaborate system consisting of multiple servomotors, each moving a small dot attached to a stage that can be positioned at various locations relative to the fly's retina. Continuing the practice of incorporating newer electronic technologies with enhanced performance, LED-based systems have recently come into standard usage (Strauss et al., 1997; Lehmann and Dickinson, 1997; Lindemann et al., 2003). Unlike systems used in the past, LED-based systems are capable of displaying panoramic visual motion with suitable spatial and temporal control. Chapter 2 documents a modular LED-based system that is a suitable display for a large class of laboratory experiments.

1.6 *Drosophila* flight control

In the classic open-loop experiments that elucidated many of *Drosophila*'s optomotor reactions, Götz (1968) demonstrates that motion on the lateral portions of the eye controls the yaw and thrust produced by tethered *Drosophila*, and shows that a strong correlation exists between thrust and the difference in the bilateral *sum* of wingbeat amplitudes, and between the torque and the bilateral *difference* of wingbeat amplitudes. Götz (1968) provided early evidence that visual motion influences the magnitude of the flight force, but not its inclination relative to the body. This finding, that the mean flight vector is at a fixed angle to the body (in *Drosophila* and *Musca*) was confirmed in more detailed experiments by Götz and Wandel (1984) and David (1978), and has lead to the notion that *Drosophila* employ a helicopter-like control scheme. Since the orientation of the force vector is fixed to the body axis, the modulation of wingbeat amplitude must be considered as the input to a system that controls thrust-pitch-lift via adjustments in the magnitude of the force produced by the wings and the pitch angle of the body. Recent studies (Fry et al., 2003), making use of high-speed video to capture free-flight kinematics and a dynamically scaled robotic model wing to measure the forces produced by these kinematics, have established two

surprising facts—the dynamics of body motion in flight are governed by inertia rather than friction, and that very subtle changes to the wingstroke trajectories result in large body movements. These subtle steering commands are present, but exaggerated under tethered flight conditions (Fry et al., 2005).

The free flight behavior of *Drosophila* is characterized by segments of extremely straight flight, interspersed with rapid turns, called saccades (Tammero and Dickinson, 2002b). This flight strategy has also been demonstrated in several other species of flies (Collett and Land, 1975; Wagner, 1986; Schilstra and Van Hateren, 1999). Much has been made of the likelihood that 'torque spikes'—short bursts of torque in one direction are the tethered flight analog of free-flight body saccades (Heisenberg and Wolf, 1979, 1984, 1988; Tammero and Dickinson, 2002a). The time course of the torque spikes produced by rigidly tethered flies is much longer than the rapid free flight body saccades, but this time course is significantly reduced when *Drosophila* are tethered to a thread so that they are fixed in space but free to turn (Mayer et al., 1988). Recent work with a magnetic tether (an improved method for fixing a fly in space but enabling body rotations) has confirmed that the visual stimuli that have been shown to evoke torque spikes in rigidly tethered flies also evoke saccade-like turns in *Drosophila* at the magnetic tether (Bender and Dickinson, 2006b). Further evidence suggests that the initial motor activity during a free flight saccade and the tethered flight torque spike are very similar, and the discrepancy in time course is due to the lack of mechanosensory haltere feedback prevented by the rigid tether (Bender and Dickinson, 2006a). Nonetheless, the domination of saccade and torque spike based steering on navigation should not be overstated; there is evidence that in addition to the saccadic flight strategy *Drosophila* can also steer via a smooth (e.g., proportional/derivative) control system. Examples of the action of a smooth control system are the weak centering seen in free flight (David, 1985; Tammero and Dickinson, 2002b), the tethered flight closed-loop expansion-avoidance (Tammero et al. (2004);Figure 1.4F), and the tethered flight closed-loop stripe fixation Götz (1987). It is likely that the prominence of torque spikes in the closed-loop tethered flight experiments of Heisenberg and Wolf (1988) is a response of *Drosophila* to sluggish

feedback due to the low-pass filtering of the mechanical torque meter and the low gain used in these experiments.

1.7 The optomotor equilibrium hypothesis of flight control

An early model of locomotory control in flies was the optomotor equilibrium reflex [3] A fly presented with a visually rotating environment will turn in the direction of the rotation (Von Holst and Mittlestaedt, 1950; Götz, 1968). This response is thought to minimize image rotation during flight and stabilize the course of the fly. The most thorough exposition on the use of this reflex in controlling locomotion is provided by Götz (1975). However, recent studies in flies, bees, and locusts have identified several other visually elicited behaviors that cannot be explained by optomotor equilibrium (Tammero et al., 2004; Srinivasan et al., 1999). The optomotor equilibrium strategy fails in several regards:

- The strategy does not account for the complexities of realistic optic flow (idealized in Figure 1.3) during translation.

- When flying close to a surface, the motion on the eye closest to the surface will be stronger, thus the predicted turn is towards/into the surface.

- The typical disturbances during flight are not likely to cause pure rotation of the body, therefore it is not likely that a system that seeks to maintain rotational equilibrium could yield straight flight.

- Egelhaaf (1987) shows that the optomotor response has slower dynamics than small field tracking system. Additionally, *Drosophila* will only fly in an optomotor equilibrium assay if the coupling between torque and rotational velocity of the display is much lower than for other behaviors (§4.1). These observations suggest that the syndirectional optomotor response is a slow, weak correction

[3] The term *optomotor* is often used to refer to any visually induced motor response, also sometimes referred to as *visuomotor*. The turning response described here should properly be called the *syndirectional* optomotor response, because the animal turns in the direction of the perceived motion.

for small deviations from straight flight that only emerge when the animal is not particularly close to objects, and motion on the retina is not too fast.

1.8 Visual control of flight velocity?

In the classic open-loop experiments that elucidated many of *Drosophila*'s optomotor reactions, Götz (1968) demonstrates that the orientation of motion on the lateral portions of the eye controls the torque and thrust produced by tethered *Drosophila*. Further, the directions yielding zero thrust and zero torque are roughly orthogonal, suggesting that the orientation of motion detectors drives different motor output—horizontal for the torque response and vertical for the thrust response. When progressive and regressive motion are presented along the direction in line with the body axis, the measured thrust responses are identical, therefore it seems as if the 'thrust' response reported by Götz (1968) is much more likely to be related to the control of lift.

Strong evidence suggests that flying insects adjust their airspeed to maintain a preferred level of visually transduced groundspeed. This theory was originally proposed by Kennedy (1940) to explain observed behavior in mosquitoes. Further support for this theory has been found by Kennedy and colleagues in locusts (Kennedy, 1951), in moths (Marsh et al., 1978), and in *Drosophila* (David, 1982a). Owing to the helicopter-like control of thrust in *Drosophila* (§1.6), the bilateral sum of wingbeat amplitude is clearly related to the control of flight speed in some nontrivial way that couples the control of thrust, lift, and pitch.

The velocity control of trained honeybees flying down a tunnel has been the subject of considerable investigation. Bees navigate down the center of the tunnel by balancing the image motion seen by the right and left eyes (Srinivasan et al., 1991, 1996). The strongest evidence for this balancing is obtained via a simple experiment—if the pattern on one wall of the tunnel is translated in the direction of flight motion, then (on average) the bees fly closer to the moving wall; if one wall is translated against the flight direction, then the bees fly away from the moving wall (Srinivasan et al., 1991). The bees are able to fly down the center of a corridor (with stationary walls)

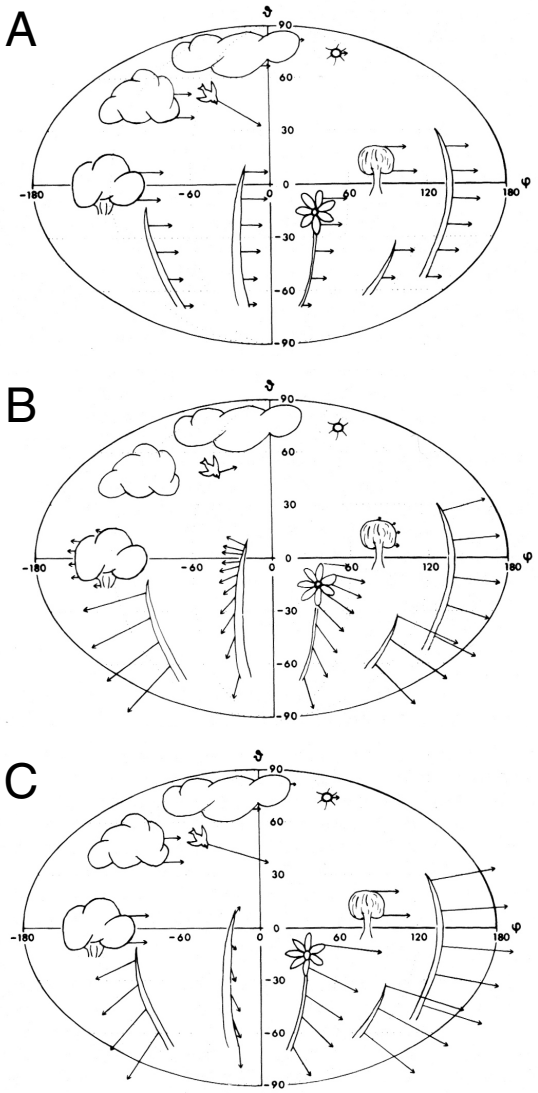

Figure 1.3. Summary of the environmental influence on optic flow perceived during flight. (A) The optic flow perceived as a result of pure rotation of the retina relative to the environment. All features (regardless of distance) move on the retina with the same angular velocity. (B) The optic flow field during forward translation is dominated by a frontal focus of expansion, and the angular velocities of environmental features projected onto the retina depend on the distance to the objects and their position relative to the flight direction. (C) The effects of simultaneous translation and rotation are combined in the optic flow field. This figure has been modified from Buchner (1984).

even when the spatial frequency of the pattern is different between the two walls. This finding suggests that the centering response of bees is sensitive to image velocity and is independent of the spatial-frequency dependence that is predicted by HR-like motion detectors. The velocity control of bees in the centering paradigm has also been studied. Bees show a 'clutter' response, whereby they will decrease flight speed as they approach a narrowing tunnel and increase their speed as the tunnel widens (Srinivasan et al., 1996). Further manipulation of the visual texture on the walls of the corridor has revealed that honeybees fly at a preferred groundspeed that is independent of many of the parameters of the wall patterns (Srinivasan et al., 1996; Baird et al., 2005). Even in the face of a strong headwind, bees will maintain their preferred groundspeed by increasing their airspeed to maintain a constant rate of optic flow (Barron and Srinivasan, 2006). The one manipulation in which the speed preference of bees is 'fooled' involves lining the tunnel with horizontal stripes oriented axially down the tunnel, bees fly much faster in this condition than even in a bare wall treatment (Baird et al., 2005). The high contrast horizontal stripes prevent contrast adaptation from exploiting the weak horizontal motion, and thus the bees increase their airspeed in an attempt to achieve the desired level of translatory (horizontal) optic flow.

The apparent discrepancy between the motion processing of bees and flies resulted in an interesting discussion contrasting the optomotor equilibrium response (flies) with the centering response (bees) (Egelhaaf and Borst, 1992; Srinivasan et al., 1993). In retrospect, it is unlikely that motion processing in bees and flies is fundamentally different; recent results demonstrate that flies do exhibit some form of a centering response (Tammero and Dickinson, 2002b; Frye et al., 2003; Budick and Dickinson, 2006) that is tuned to 'true' velocity (Fry et al. in prep.). The apparent difference between bees and flies is almost certainly due to the differences in the experimental procedures and not in alternative solutions to motion processing. The stimuli presented to tethered flies and used as a basis for formulating the optomotor equilibrium hypothesis, is drastically different from the more complex visual conditions in free-flight experiments, which provide many relative motion cues that are simply not

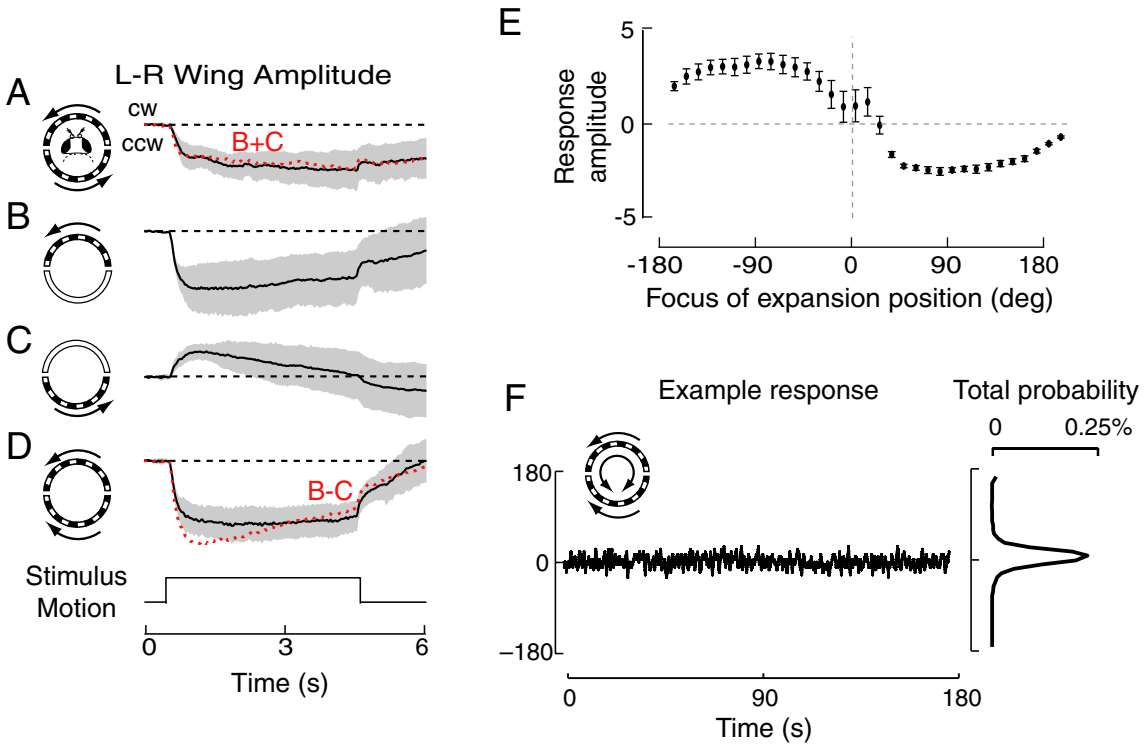

Figure 1.4. Summary of the expansion-avoidance behavior on tethered *Drosophila*. The sum of the turning responses to half-field motion (B and C), predict the response to the optomotor stimulus (A) and the expansion stimulus (D). The position-dependent response to open-loop expansion (F) reveals that the maximal turn is away from a laterally positioned focus of expansion. (E) When the fly is given closed-loop control over the rotational velocity of the position of the focus of expansion, long lasting, stable orientation towards the focus of contraction is observed. This figure has been rearranged from Tammero et al. (2004).

there when the fly is tethered and placed in the center of a cylinder. An additional confirmation of the similarity between bees and flies is the radically altered trajectories of freely flying flies when a cylindrical environment is lined with horizontal stripes (Frye et al., 2003)—the flies fly much faster and closer to the walls, much as bees were observed to fly faster in the corridor equivalent of this treatment.

1.9 The expansion-avoidance paradox

Presenting freely flying *Drosophila* with different visual environments shows that the initiation of saccades is largely controlled by visual detection of relative motion within the environment. Reconstructions of the optic flow seen by the fly during

flight has suggested a model of saccade initiation based on the detection of visual expansion (Tammero and Dickinson, 2002b), a hypothesis that is consistent with open-loop presentation of expanding stimuli to tethered flies (Tammero and Dickinson, 2002a). To better approximate the optic flow seen during translatory flight (Figure 1.3), Tammero et al. (2004) simulated a simplified translatory flow field. Figure 1.4 summarizes several of the results of Tammero et al. (2004) on tethered *Drosophila*. In these experiments large-field motion stimuli were presented in open-loop to tethered flies. Figure 1.4 A–D shows the averaged turning response of the flies measured from an optical sensor that records wing activity. Figure 1.4A corresponds to the classic (syndirectional) optomotor response (Götz, 1968), in which the fly responds to coherent full field rotatory motion by turning to minimize retinal slip. The plots in B and C show the mean response of the fly to front- and rear-field rotatory motion. The response in A is shown to be the sum of the responses in B and C (red line). However, the response in C clearly contradicts the predictions of the optomotor response, since the attempted turn is not in the direction that would minimize the rotatory stimuli. The response in D shows that the strongest response is obtained when the fly attempts to orient towards a contracting focus of the motion stimulus. This shows that the fly can detect the location of the visual focus of contraction (or is doing something functionally equivalent). The focus of contraction (expansion) is the point of no motion in a velocity field induced by pure translation that all motion vectors point towards (away from). As further confirmation of this finding, the pattern was presented to flies from many azimuthal positions around the cylindrical arena; the tuning curve resulting from this experiment is shown in E. Finally, in F are the results of a novel closed-loop paradigm, where the fly is given control over the rotational velocity of the position of the focus of expansion. The results of the closed-loop assay are predicted by the expansion-avoidance tuning curve in E—but are surprising nonetheless—the flies robustly orient towards the focus of contraction. These data suggest that a control algorithm based on feedback of the movement of the visual focus of contraction could be used to detect wind direction, since upwind flight induces a frontally centered focus of the visual motion field, a hypothesis that is tested with a closed-loop simulation in

Chapter 6.

The expansion-avoidance behavior that is clearly seen in the results of Tammero et al. (2004) (Figure 1.4) is a response that can be simply interpreted as an attempt to prevent an imminent collision. However, the paradox arises when one considers forward (translatory) flight. As soon as a fly begins to move forward in its environment (at any speed in 'still' air, or faster than the wind speed when flying upwind), the animal should encounter an optic flow field dominated by a frontally centered, sustained focus of expansion (as shown in Figure 1.3B). *If this visual motion perceived during forward flight is strongly aversive, how does the animal ever fly forward?*

1.10 Plan for thesis

The focus of the work presented in this thesis is on elucidating the control of visually guided flight by *Drosophila* in response to a broad class of visual stimuli that are related to visual motion seen by a flying animal as it translates around in its environment. The methods used in pursuit of this goal are presented in Chapter 2. The successful design and implementation of a novel display system that was used for all presented experiments is discussed in detail. Chapters 3–5 cover the results of a series of experiments undertaken to resolve the expansion-avoidance paradox. The proposed solutions to the paradox are listed below. Finally, Chapter 6 documents the computational modeling of the expansion-avoidance behavior.

1.11 Proposed solutions to the expansion-avoidance paradox

The resolution of the expansion-avoidance paradox (see §1.9) must involve an acknowledgment of the simple fact that tethered flight experiments present an imperfect approximation of the sensory experience of a *Drosophila* in free flight. Therefore, it is not surprising that a result obtained in tethered flight (even a robust one), might lead to an interpretation that is at odds with what is known about free flight (and common sense). It is clear that flies tolerate expansion while flying forward, and since they vigorously avoid expansion in the experiments of Tammero et al. (2004), the logical

conclusion is that those experiments are a poor approximation of 'reality.' However, we believe that tethered flight is an extremely valuable experimental technique for studying a rather complex behavior—flight—and that the value of the experiment increases as attempts are made to increase the fidelity of the simulation. The original simulation may have been imperfect for these reasons:

1. Perhaps flies only tolerate expansion during directed flight, or flight towards some prominent visual object. If valid, this hypothesis suggests that object-orientation behavior likely plays a far more central role in *Drosophila* flight control than previously thought.

2. The flies are being overstimulated—the strength of the expansion cue that a freely flying fly would encounter must be much weaker then the cues delivered in the flight arena experiments of Tammero et al. (2004). For example, the pattern velocities and the contrast of the pattern may be inappropriately high.

3. There is good evidence to suggest that *Drosophila* rely heavily on ground motion (David, 1978, 1979, 1982b). The complete absence of any ground motion in tethered flight experiment in a cylindrical flight arena may contribute to the surprising results.

4. Flies might also rely heavily on mechanosensory wind cues which are again absent in the original experiments. Perhaps the perception of a headwind is necessary to maintain 'forward' flight.

5. The stimuli used in the original experiment only crudely approximate the geometry of optic flow that would be experienced by a flying fly (Figure 1.3). Typical optic flow fields rarely contain perceptible poles, so perhaps this simplification is sufficient to cause the paradox. This hypothesis would suggest a much more nuanced use of visual motion than is typically thought to be relevant to *Drosophila*. The sampling of the visual world performed by *Drosophila* is extremely coarse, and thus it would be somewhat surprising if subtle corrections in the geometry of the visual stimuli yielded significant changes in behavioral responses.

Chapter 2

Experimental Methods

2.1 Modular display system for visual stimuli

A large portion of the effort documented in this thesis went towards the design and development of a modular system of displays that enable the experimental results presented in the following chapter.[1] Conventional display technologies, such as cathode ray tubes and liquid crystal displays, are not well-suited for use as stimuli for insect experiments because their refresh rates are typically much slower than the flicker fusion rates of insect visual systems (Miall, 1978). The new display system described in this chapter is based on LEDs, and was designed as a stimulus for the fly visual system. Because LEDs can be rapidly refreshed, the displays can be used to present apparent motion stimuli. The system we have developed reinforces the many advantages of modern electronic technologies in enabling powerful, low-cost laboratory instruments that are a welcomed addition to the neurobiologist's toolkit. The display system is not the result of an effort to design one specific stimulus-generating apparatus for flies. Rather, the system makes it possible to introduce an affordable and programmable visual stimulus into virtually any fly behavior experiment. The system has been designed to address the challenges of conducting experiments on insect vision—it accommodates electrophysiological recordings, can be configured into many geometries, supports high rates of pattern refresh, and can deliver bright visual stimuli over a

[1] Much of the text describing the modular display system has been taken from the manuscript "Modular displays for rapid development of behavioral stimuli" by M. B. Reiser and M. H. Dickinson, submitted to the *Journal of Neuroscience Methods* and currently in review.

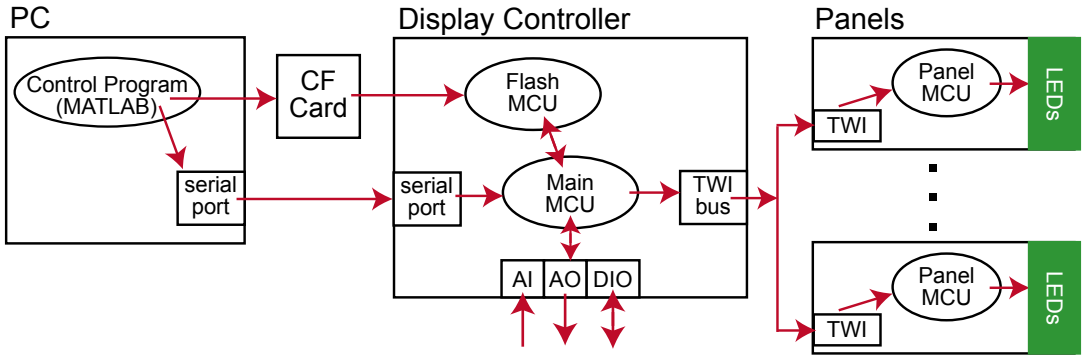

Figure 2.1. The panel-based display system has been designed to rapidly transmit pattern data from storage to the panels. Patterns are created using custom-written software, and stored on a CompactFlash (CF) card. The display controller contains two microcontroller units (MCUs). The flash MCU reads pattern data from the CF card and sends it to the main MCU. The main MCU receives directives from the PC control program over the serial port and maintains the timing of display updates. The main MCU communicates with external devices over Analog Input (AI), Analog Output (AO), and Digital Input/Output (DIO) ports. Once fetched from the flash MCU, the updated pattern frames are sent out to the individual panels over the Two Wire Interface (TWI). On each panel, an MCU receives the pattern data and refreshes the display of LEDs.

wide range of contrast levels.

2.1.1 System overview

The display system has been designed to allow for the rapid development of behaviorally relevant visual stimuli. The files needed to build, program, and control the system are available from the project web site.[2]. To achieve the additional flexibility of a reconfigurable display, the system has been designed around a programmable display module. The system consists of three major components:

- PC software—set of tools for generating and storing patterns and conducting experiments by communicating with the display controller.
- Panel display controller (PDC)—dual microcontroller circuit that retrieves pattern data from memory, sends the appropriate segment to each panel, and receives commands from the PC control program.

[2]Permanent address: http://www.dickinson.caltech.edu/PanelsPage

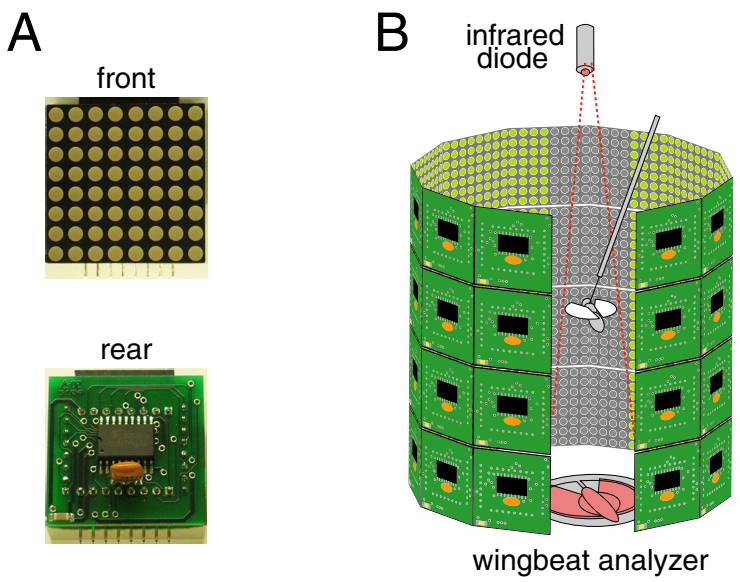

Figure 2.2. The panel modules are connected to form controllable displays of varying geometries. (A) Photographs of an individual panel showing the 64-LED display. The panels are joined by 8-pin connectors: a male header on the bottom and a female header on the top of each panel. The LEDs in the dot matrix display (3 mm diameter, each), are covered with a translucent lens and are embedded in opaque black plastic. (B) To assay the sensorimotor responses of flies in rotational closed loop, the panels are configured as a flight arena, constructed as a 4×11 cylinder of panels, height of 128 mm, diameter of 123 mm.

- Panels—individually addressed display modules with an 8×8 dot matrix array of LEDs, and supporting electronics to locally refresh the display (photographs in Figure 2.2A).

The general flow of information is shown in Figure 2.1. A display is constructed using a circuit board as an electrical and architectural substrate to which panels are connected. This circuit board is powered separately from the PDC, and contains a connection from the PDC, through which pattern data pass onto the panels. In the results presented, two types of displays are used: a cylindrical flight arena (Figure 2.2B) and a planar 'screen' (Figure 5.1), although many other display geometries are possible.

2.1.2 PC software components

The display system is supported by a set of software tools that run on a Windows-based PC. The software, all developed and run under MATLAB (Mathworks, Inc.), serves two distinct functions: (1) the creation, testing, and storage of patterns, and (2) the coordination of the PDC output while the system is in operation. The overall system has been designed to eliminate the need for low-latency computations to originate on the PC. The essential timing operations for transmitting pattern data to the display are implemented on the PDC, while the less timing-critical functions are implemented on the PC using a comprehensible, high-level language. The complex task of rendering pattern data is not performed while the display is being updated. Rather all patterns are compiled in advance, and stored on an inexpensive CompactFlash (CF) card, which is then transferred to the PDC.

PATTERN CREATION AND STORAGE

Each *pattern* consists of a sequence of *frames*, and each *frame* is a sequence of binary data specifying the activity of the LEDs for each panel. Each frame of a binary-valued pattern is created in MATLAB as a matrix consisting of zeros and ones, where zero values correspond to inactive pixels, and one values correspond to active pixels. The system also supports patterns that can display one of eight intensity levels at each pixel. Such patterns require three binary-valued matrices for each frame (see §2.1.4). Any pattern that can be created using this simple bitmap-like scheme can be displayed on the panels. Once a sequence of frames is created in MATLAB, a program determines the portion of each frame that maps to each panel and then arranges these data into 8 bytes (or 24 for 8-level patterns). Finally, these data are 'flattened' into a one-dimensional array, each byte corresponding to the activation sequence for one column of one panel in one frame (3 bytes are necessary per column in the 8-level case). Because a pattern is stored as a linear array, each frame is identified by a unique index. However, it is convenient to implement two degrees-of-freedom for the pattern data. The usage of these degrees-of-freedom need not correspond to physical directions of motion. For example, in the pattern used in the experiment

of §3.1, one index is used to map the azimuthal position of a single stripe as it is rotated around the cylindrical display, and the second is used as an index into a set of contrast levels between the stripe and the background. In another example, (§5.1), one index maps rotations of a striped pattern, and the other maps the translation motion component. It is not impossible to conceive of experiments that would require three or more degrees-of-freedom. For example, simulating flight through a virtual two-dimensional landscape requires azimuthal rotation (about the yaw axis) and two degrees of translational motion, along the longitudinal (front-to-back, or Y) axis and the transverse (side-to-side, or X) axis. Adding this functionality is a simple software extension of the currently implemented system.

Patterns generated on a PC are stored on readily available CF cards. Even low-capacity cards can accommodate dozens of patterns. A desirable feature of CF media is that it can be formatted with the FAT file system and can be used as removable storage on any computer running a modern operating system. Unfortunately, this approach does not produce the performance necessary for the display—frequent accessing of the File Attribute Table is much too time-consuming, especially in cases where pattern data cannot be read sequentially. Our solution is to do away with the file system altogether, and instead, copy a binary image containing the patterns directly to the CF media. At the head of the image is a sequence of slots containing information about each pattern: the number of frames, size of each frame, number of panels for this pattern, a bit specifying whether multi-level intensities are used, and the address on the CF card where the pattern begins. After this header, the data for each frame are stored sequentially. To further optimize the speed of pattern access, the data for each frame begin at the start of a block in the CF memory.

COMPUTER CONTROL

The PDC, and thus the display, is controlled from MATLAB through the PC's serial port. The implemented software uses a single function for all commands that pass through the serial port. This function is called by a graphical user interface, and can also be called from the MATLAB command line or in scripts. While the PDC

is running, the PC control commands can modify its operations. The supported commands allow a user to (among other options) change the current pattern, display a specific frame, set the controller mode and specify relevant run-time parameters (§2.1.3), start and stop the updating of the display, change the address of a panel, benchmark the maximal frame rate of a pattern, and update the PDC's internal function generator. These directives can be concatenated into scripts for conducting controlled, repeatable experiments.

2.1.3 Panel display controller

The PDC coordinates the updating of the panels by reading pattern data from a CF memory card and executing commands sent by the PC control program. The PDC contains two ATmega128 (Atmel Corp.) microcontroller units (MCUs) connected to 8 analog input lines, 2 analog output lines, and 4 digital input/output lines. One MCU is dedicated to reading the pattern data from the CF card and placing it into a synchronous FIFO memory (CY7C4251V-15AC, Cypress Semiconductor Corp.). The second, or main, MCU maintains the timing of pattern updates. The software running on the main MCU decodes the commands sent from the PC control program (detailed in §2.1.2), and requests new frames from the CF-reading MCU via a dedicated serial connection. Further, the main MCU reads the data from the FIFO buffer and transmits the appropriate part of the current frame to each panel. The PDC has been implemented such that most users can control the system directly from MATLAB with no need to modify the PDC's code. However, the PDC is fully programmable, and adaptable to future tasks.

The PDC software has been designed to maintain fast rates of pattern data transmission from the CF card to the panels—all other tasks are handled with lower priority. There are two basic ways to control the sequence of displayed frames: the controller can determine the update rate ('velocity control'), or the frame index can be specified directly, while the timing is handled elsewhere ('position control'). The current frame is determined by an interrupt service routine (ISR) that runs at 400 Hz.

When the PDC runs in one of the velocity control modes, then this ISR will determine the current frame rate and set an additional ISR to run at this rate. This second ISR, upon execution, sets the current frame. A frame fetch is handled as an atomic operation; once the controller begins transmitting a certain frame, it will complete this frame before moving on to another.

The PDC supports two *channels* of pattern control. These are the degrees-of-freedom of the memory buffer that stores the individual frames that make up a pattern. The current frame is set by the current index for both channels. To enable offline reconstruction of the time histories of the pattern indices (i.e., the sequence of displayed frames), the 2 analog outputs encode the frame index for each pattern channel. For each of these channels, several modes of control have been implemented to support a variety of fly flight experimental paradigms:

1. Open-loop: In this mode the current value of the internal function generator, scaled by a gain, and added to a bias, sets the display rate. The gain and bias are set in the PC control program.

2. Closed-loop: The difference in voltage between 2 analog input signals (scaled and offset) sets the frame update rate. In a typical tethered flight experiment, each channel is connected to a signal encoding the amplitude of each of the fly's wings.

3. Closed-loop with bias: This mode is a combination of the first two modes. The pattern update rate is determined by the sum of the input voltage difference (scaled by the gain), the bias, and the current function generator value. This mode is useful for supplying a time-varying bias signal to challenge a fly flying under closed-loop conditions.

4. External position: An input voltage sets the frame index. The gain and bias are now used to specify the mapping of the measured voltage to a frame index. This mode enables the use of an external (arbitrary) waveform generator or a second PC, etc., to set the pattern position.

5. Internal position: The internal function generator is used to set the current pattern frame. This is useful when precise timing of the sequence of presented frames is required.

In the 'velocity control' modes (1, 2, and 3) the PDC determines the update rate (for a certain channel) and then fetches frames sequentially at this rate. In the 'closed-loop' modes (2 and 3) this rate may be varying rapidly while the PDC is running. In the 'position control' modes (4 and 5), the displayed frame is set by an index that is either supplied by the internal software-based function generator (updated from the PC control program) or is decoded from an externally applied signal. Since the channels are updated independently, each channel can run in any one of the five modes.

2.1.4 Display panels

The panels are the display devices of the system. Each panel is a compact package (32 mm × 32 mm × 19 mm) that contains a circuit board with an ATmega8 MCU (Atmel Corp.), an 8-channel Darlington sink driver (ULN2805), an 8 × 8 green LED dot matrix display (BM-10288MI, American Bright Optoelectronics Corp.), and other electronics for driving the LEDs (the complete schematic is shown in Figure 2.3). Each panel is individually addressed and communicated with over the TWI bus (TWI is the name of Atmel's implementation of the I^2C bus, a standard interface for communication between integrated circuits). Each panel runs a compact program whose function is to receive updated pattern data and refresh the display. The brightness of each LED can be set to one of eight intensity levels, and the entire display is refreshed at no less than 372 Hz (the display rates depend on several factors, discussed in §2.1.7). The ATmega8 was selected for its low cost, small size, large number of input/output lines, integrated TWI, and the ability of each output line to directly drive an LED. While there are commercially available integrated circuit devices for driving LED displays, we chose to take a programmable route in the design of our system. The developed system is faster than if it were built using an off-the-shelf LED driver, and is adaptable

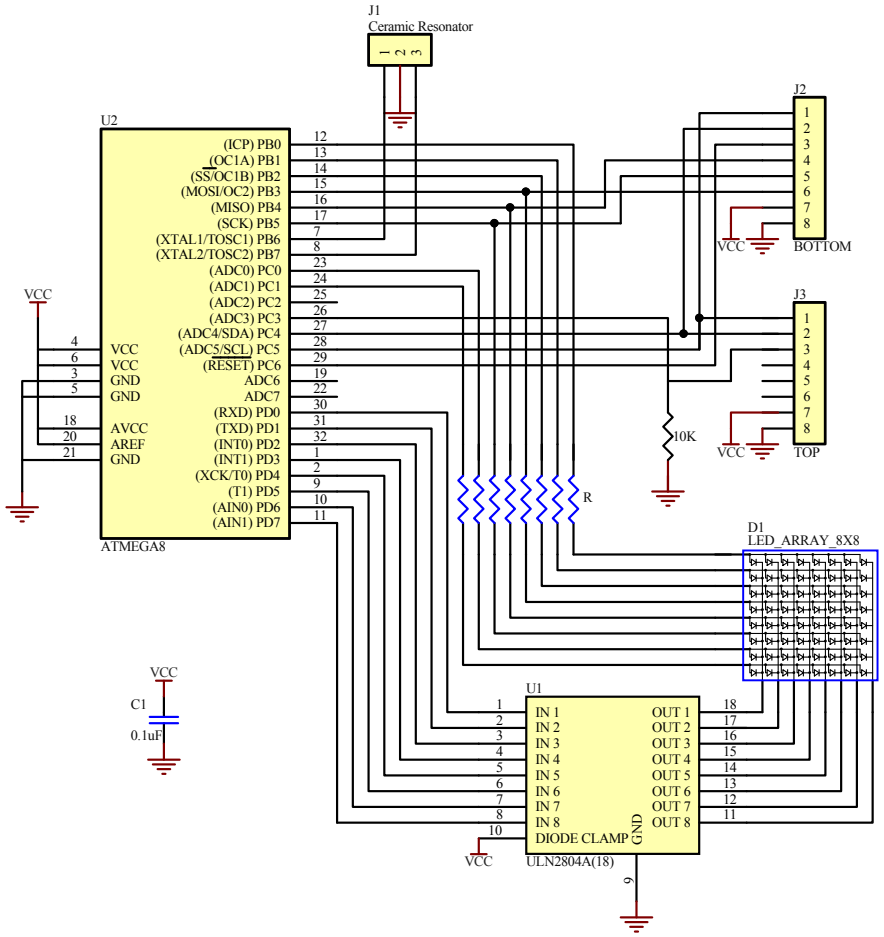

Figure 2.3. Circuit schematic for one display panel. Each panel contains one Atmel ATmega8 microcontroller and an 8-channel Darlington sink driver (ULN2804A). The controller writes the pattern for one column at a time, and enables the corresponding line on the Darlington driver. The entire display is scanned by repeating this for all 8 columns. Resistors (labeled R) are used to limit the current through each row of LEDs, ensuring consistent brightness. The value of R is set to match the electrical properties of the LEDs, for our system, R = 82 Ω. There are two 8-pin connectors, labeled *TOP* and *BOTTOM*; power, ground, and the two TWI signals pass through both connectors. Additionally, the BOTTOM connector carries the 3 signals necessary to program the microcontroller. Also, the 10 KΩ pull-down resistor is used to set the RESET line of the panel connected through the TOP connector. Since the entire circuit board could not be larger than the 32 mm × 32 mm size of the LED display and the current-carrying traces must be adequate to power the display, surface mount components were used wherever possible.

to any number of display tasks.

To activate a single LED, one of the pins of the ATmega8 (configured as an output line) must be turned 'on,' i.e., set to its high value of 5 V. Current is sourced from this pin, and passes through a current limiting resistor and one row of the 8×8 LED display. An individual LED is turned on once the corresponding column line is enabled on the Darlington driver. The driver acts as sink, allowing current to flow. The distinction between the rows and columns of each panel is arbitrary; in this description we use the same convention as in the diagram of the LED matrix in the schematic (Figure 2.3). The entire 64-LED matrix is scanned using 8 row lines and 8 column lines—the 'pattern' for a single column is set as the output, and then that column is enabled on the line driver. Since only one column is active at any instant in time, the LEDs must be scanned quickly to prevent the perception of flicker.

INDIVIDUAL PIXEL INTENSITY CONTROL

Because each panel is continuously scanned, an individual LED that is 'fully on,' is in fact only receiving current during 1/8 of the refresh cycle. One refresh cycle is the time needed to update all of a panel's LED pixels. In the typical implementation, this cycle occurs at approximately 2600 Hz. The panels system implements multiple levels of *greenscale* intensity by using consecutive refresh cycles (each of length 384 μs). Using seven cycles, eight intensity levels are possible, since each LED can be on for anywhere from none to all of the refresh cycles. This scheme yields a remarkably linear control of light intensity, as demonstrated in §2.1.6. The cost of this arrangement is a reduction in the minimum refresh rate to about 372 Hz (see §2.1.7). In the simplest implementation of this intensity control, each frame would require seven copies of an 8-byte sequence, each byte specifying the column 'pattern' of LEDs that should be active during each of the seven refresh cycles. However, by taking advantage of binary decoding, the system requires only 3 bytes for each column of a panel's piece of a *greenscale* pattern. This solution minimizes the size of the data packet that must be sent to each panel, saving communication time at the expense of increasing the computational burden on the MCU. The panel control program extracts the 3 bits that

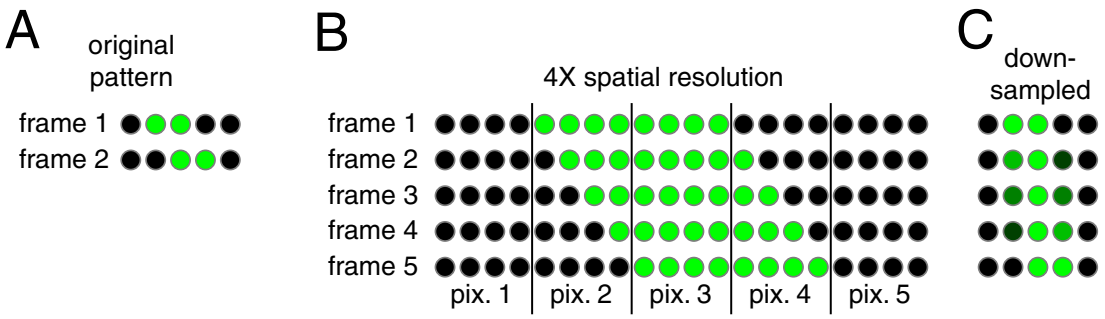

Figure 2.4. (A) An example of a small 5-pixel patch of pattern. To display apparent motion stimuli, the pattern can be advanced by shifting the pattern (to the right in the example). To enable finer control of the pattern's motion, the pattern is designed for a display that is 4 times larger (B), and advanced at a rate of one pixel per frame. The higher resolution pattern (C) is obtained by down-sampling the larger pattern (the intensity values of every 4 consecutive pixels are averaged).

correspond to each pixel and decodes these to obtain a value (0–7) that determines the number of refresh cycles for which the pixel should be active. A 4-level version of this scheme has also been implemented in an analogous manner. The panel controller determines how to treat the incoming packet based on its size: an 8-byte packet is a standard binary pattern, a 16-byte packet is handled as a 4-level *greenscale* pattern, and a 24-byte packet is interpreted to be an 8-level *greenscale* pattern.

2.1.5 Increased pattern resolution using intermediate intensity levels

A simple method for increasing the effective spatial resolution of the display (and hence the effective temporal resolution as well), is to use the panels' ability to display intermediate *greenscale* levels to interpolate the intensity of pattern pixels at transitions from on to off. As an illustration, consider the simple pattern in Figure 2.4A. To provide smooth motion of the pattern, subsequent frames must contain shifted versions of the original image. However, the smallest increment that the pattern can be shifted is one pixel, and thus the display rates must be integers (1, 2, 3, ... fps). A larger display (positioned farther from the viewer) will yield greater effective temporal resolution, since each single pixel increment will correspond to a smaller step. Using a simple trick, it is possible to exchange spatial for temporal resolution. When a pattern

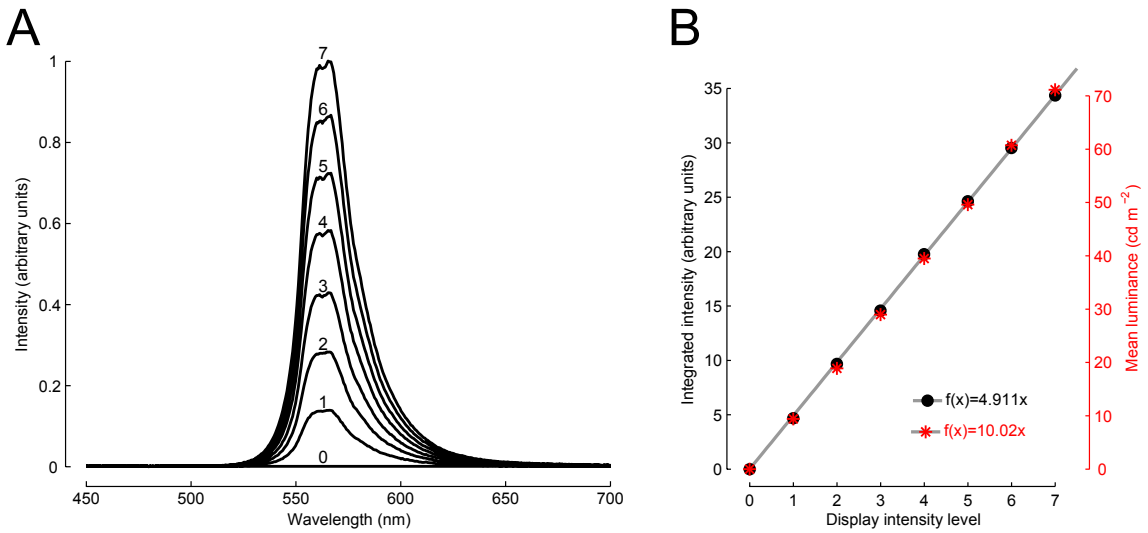

Figure 2.5. The LED-based display implements 8 linearly varying intensity levels. (A) The relative intensity of the display, measured at all 8 intensity levels (numbered above each measurement), reveals that only the magnitude of the measured intensity changes, while the spectral content does not. (B) To test the scaling of the intensity levels, the measured spectral intensity response values were integrated (across wavelength) and are plotted as black circles. These values are compared to independent measurements of the absolute luminance of the surface of the display, plotted as red asterisks. Both data sets are well fit by a straight line (in gray) that passes through the origin (integrated intensity line fit: $R^2 = 0.9999$; absolute luminance line fit: $R^2 = 0.9989$). The ratio of the line-fit slopes is used to scale the ordinate for each set of measurements.

is made, it can be designed as if the display were larger by some factor G ($G = 4$ is used in the example of Figure 2.4B). Then after the patterns are designed for this larger display, the intensity of each group of G adjacent pixels is averaged, to yield an image at the original (spatial) resolution, but with an effective temporal resolution increased by a factor of G. Of course, the panels system currently implements only 8 *greenscale* levels, so $G = 7$ provides the greatest possible increase. In the example of Figure 2.4C, once down-sampled to the original resolution, 4 frame transitions are required to advance the pattern by the angular extent equivalent to 1 pixel of the original pattern.

2.1.6 Validation of display properties

To characterize the optical properties of the display, the spectral intensity and the luminance of the panels were measured. The relative spectral intensity of the display was measured with a spectrometer (USB2000, Ocean Optics Inc.). This device reports the light intensity across wavelength as counts from a sensor array. Much effort and specialized equipment is required to properly convert these counts into radiometry units, so this reading was normalized and is presented in arbitrary units (Figure 2.5A). Slight inaccuracies in the sensor readings appear at all wavelengths. To correct for this, the reading taken when the display was inactive (intensity level of 0) was subtracted from the readings at each intensity level. These measurements show that for the 8 intensity levels that the panels are capable of displaying, only the spectral intensity increases, while the spectral content of the signal does not change. The peak in the LED intensity occurs at approximately 565 nm, corresponding to the yellow-green part of the visible spectrum. By integrating this relative intensity measurement, it is possible to estimate the success of the time-division scheme in implementing a linear set of intensity levels. The results show that the implemented system is quite linear; a least-squares line fit constrained to go through zero ($f(x) = 4.911x; R^2 = 0.9999$) is plotted along with the data (Figure 2.5B). Additionally, a colorimeter (Chroma Meter CS-100A, Konica Minolta, Inc.) was used to measure the absolute luminance produced by the display.

The mean absolute luminance of the display was measured at all 8 intensity levels and is also plotted in Figure 2.5B. These measurements are also strikingly linear and are fit with a straight line constrained to go through zero ($f(x) = 10.02x; R^2 = 0.9989$). Since the integrated relative intensity and luminance data sets are well fit by a straight line passing though zero, they have been plotted on the same plot; the ratio between the slope of the line fits has been used to scale the ordinate for each data set. It is not at all surprising that if one data set is explained by a linear relationship, then the other will also be. Converting from radiometric to photometric quantities requires applying a wavelength-dependent scaling term (the luminous efficiency function for

photopic vision) and integrating across wavelengths (Blevin et al., 1983). However, the relative magnitude between different measurements at the same wavelength will be similarly scaled, and then integrated across wavelength—these operations preserve the original relationship. The results in Figure 2.5B are simply used to show two independent confirmations of the linear scaling of the implemented intensity levels.

One parameter of interest is the maximum contrast of the display. The (Michelson) contrast is defined as the normalized difference between the luminance of the brightest and darkest regions of the display: $(L_{max} - L_{min})/(L_{max} + L_{min})$, where L_{max} and L_{min} are the maximum and minimum luminance, respectively. However, determining the maximum achievable contrast of the display is not a straightforward matter. Since the system is modular, the maximum contrast will largely depend on the geometry of an assembled system and the patterns being displayed. It is important to note that unlike displays built from discrete LEDs, the LEDs that form the 8×8 dot matrix displays that are used in our system are set in an opaque black plastic. This construction virtually eliminates any light bleeding from an active LED to a neighboring pixel, significantly increasing the contrast of the display. For this reason, the contrast of the 30-panel floor display (Figure 5.1) is effectively 100%. For the cylindrical flight arena (Figure 2.2B), the contrast is lower due to light reflected from the opposite side of the curved display. The worst-case maximum contrast was estimated by measuring the luminance of a 16-pixel square region of the arena wall, while this region displayed a 'fully on' and 'fully off' portion of a 30° period striped pattern. This measurement yielded a relative contrast of approximately 93% ($L_{max} = 72$ cd m^{-2} and $L_{min} = 2.7$ cd m^{-2}).

2.1.7 Temporal control of the display

There are two independent rates to consider when discussing the performance of the display in its current implementation. The rate at which an individual panel refreshes all 64 pixels, is called the *refresh rate*, and the rate at which the PDC can send pattern data to the panels is called the *data rate*. Because several components of the

system are programmable, it is very likely that future programming improvement will enable higher performance. In the current system, the refresh rate is determined by an ISR on each panel that is executed at 20,833 Hz. Each time this ISR executes, one column of the display is illuminated according to the activation sequence in the display buffer. Refreshing the entire display requires 8 interrupts, yielding a refresh rate of approximately 2604 Hz. When a panel displays an eight-level *greenscale* pattern, seven consecutive refresh cycles are required for one *refresh* of the display, yielding a worst-case refresh rate of 372 Hz. Even at this much lower rate, the display will redraw the contents of the frame buffer at well above the flicker fusion rate of *Drosophila* (determined by ERG recordings to be no more than 100 Hz in dark-adapted adults), and still well above the rates of most laboratory insects (Miall, 1978). The data rate also varies depending on the size of the display and the complexity of the patterns being sent. Patterns are transmitted to the panels at about 2100 8-byte frames per second per panel. A typical cylindrical flight arena with 11 columns of panels, configured so that the panels in each column have the same address, displays approximately 190 frames per second. For a *greenscale* pattern, the increased frame size results in a data rate of approximately 68 frames per second. Several speed enhancements have been implemented. In many experiments, all rows of a panel display the identical 'pattern,' as in the stripe fixation pattern used in the experiments of §3.1, thus it is possible to send only one byte for a binary pattern and three bytes for a *greenscale* pattern, and have each panel simply repeat the pattern to fill all 8 rows. This approach yields roughly a five-fold speed increase. Another possibility is to buffer the patterns on each panel—there is sufficient storage to buffer 100 frames in the SRAM on each panel's MCU. Then the PDC need only communicate the current frame number to all panels via a general call. This approach is limited in the size of the patterns for which it is appropriate, but 'data rates' of several kHz are possible. Furthermore, the description presented in this paper is for the most general use of the display system. There are many optimizations that could, if necessary, increase the performance of the display for a particular experiment.

2.1.8 Discussion: Suitability of the display for insect visual systems

The new panel-based display system described here has been designed as a stimulus source matched to the requirements of experiments on *Drosophila* vision. The size and resolution of each panel is such that a reasonably sized display can be constructed with a spatial resolution that is well under the interommatidial distance of *Drosophila*. Furthermore, it is possible to artificially increase the spatial resolution of a display by producing subpixel motion between frames, and interpolating the pixel intensities at the points of transition.

It is worthwhile to compare the spectral content of light emitted by the LEDs used in the display (Figure 2.5A) with the spectral sensitivities measured from fly photoreceptors and from behavior. Using the optomotor response of *Drosophila* to a rotating pattern of varying spatial wavelengths, Heisenberg and Buchner (1977) generated a behavioral spectral sensitivity function. This function reveals that the relative sensitivity of the optomotor response is highest for wavelengths between 350 nm and 500 nm, and is reduced, though still present in the greener wavelengths emitted by the panels. A similar function for the spectral sensitivity of the R1-6 photoreceptors has been measured in *Drosophila* (Wu and Pak, 1975) and other flies (Stark et al., 1977). Although the response of the *Drosophila* motion detecting system (thought to be mediated by the R1-6 retinal subsystem (Heisenberg and Buchner, 1977)) is reduced when the stimulus consists of green wavelengths, we are certain that, e.g., the closed-loop stripe fixation responses (Figure 3.1C) provide evidence that the brightness of the panel displays is sufficient to drive the motion detecting system to levels of saturation. Recently, blue and white LEDs have become available in the 8×8 package that is compatible with the panel circuit. Because these LEDs will more efficiently drive the R1-6 photoreceptors, using them in future generations of the display will enable lower power consumption, and thus, larger displays dissipating less heat.

2.2 Tethered flight experiments

2.2.1 Fly preparation

All presented experiments used 3–4-day-old female *Drosophila melanogaster*, from a laboratory culture descended from wild-caught females. The flies were maintained on a 12 h:12 h light:dark cycle, and were tested during the last 5 hours of their subjective day. Flies were anesthetized by cooling (to approximately 4°C) and tethered to a 0.1 mm tungsten rod with UV-activated glue. The details of the tethering procedure are as previously described (Lehmann and Dickinson, 1997; Dickinson et al., 1993). In all experiments, flies were given at least one hour of recovery, but used within 6 hours. All experiments were conducted in a darkened room—the only significant illumination was produced by the panel displays.

2.2.2 Wingbeat measurement

While in flight, *Drosophila* modulate the trajectory of each wing in a constrained, though complex manner (Dickinson et al., 1993). In free flight, even subtle changes to the wingstroke trajectories result in large differences in the forces produced (Fry et al., 2003). A significant and consistent deformation of the wingstroke pattern is observed in tethered flies (Fry et al., 2005) (corresponding to a prominent pitch down moment), but nonetheless, tethered flies do perform significant steering—using their wings—in response to visual (Götz, 1987; Dickinson et al., 1993; Tammero et al., 2004) and other stimuli (Götz and Biesinger, 1983; Frye and Dickinson, 2004). To measure some features of the complex wing kinematics of flying tethered flies, we make extensive use of an optical tracking system, called the *wingbeat analyzer*, that is described in detail by Götz (1987) and Dickinson et al. (1993). In brief: an infrared LED, positioned above the fly, casts a shadow of the beating wings onto a pair of large, rectangular-shaped photodiodes, positioned directly below the fly (one per side of the fly). An IR-pass optical filter is used to ensure that only the light from the IR LED is detected by the photodiodes. A mask with a roughly crescent-shaped cutout, is used as an aperture to occlude the wing shadow, such that maximal occlusion occurs when

the wing is positioned dorsally, and minimal occlusion occurs when the wings are in the ventral position.[3] Thus the signal provides a monotonically increasing signal (proportional to the amount of IR light not occluded by each wing and the mask), that is close to zero when the wing is near the dorsal upstroke to downstroke transition, and largest when the wings are ventrally positioned. If the fly is well positioned above the sensor (so that the shadow of the full sweep of the wing is well matched to the mask), the further the wing is towards the maximal excursion, the larger the signal measured by the photodiode. Analog circuitry conditions the signals from the two photodiodes and provides the wingbeat amplitude on each side (via a peak-detection algorithm), the wingbeat frequency (identical for both wings), and the timing of the ventral flip, for each wing-stroke cycle. The signals provided by this system are a simplification of the wing kinematics, since the complex trajectories (requiring 3 Euler angles, per wing, for an appropriate description) are being projected down to a two-dimensional plane. However, careful experiments have shown that the signals measured by the wingbeat detector are roughly proportional to true (morphological) wingbeat amplitude (Dickinson et al., 1993), and that the difference in the left and right wing stroke amplitudes is highly correlated with torque (Tammero et al., 2004). It is this last feature of the wingbeat analyzer that is most relevant for the presented results, since torque (about the animal's yaw axis) is proportional to the difference between the left and right wingbeat amplitudes. The rotational response of flies in the face of visual stimuli can be studied in an expedient and repeatable manner, and an adequate signal exists for closing a sensorimotor feedback loop with a minimal time delay.

2.2.3 Open- and closed-loop experiments

When conducting the experiments described in Chapters 3–4, tethered flies were positioned, in a hovering posture, in the center of a cylindrical flight arena constructed from 44 of the panels described in §2.1 (Figure 2.2B). The panels were plugged into a

[3]This results in a wave form that is affectionately known as a *hütchen* (diminutive form of hat, in German), for its resemblance to a Prussian hat.

circuit board that aligns 12 panels into a ring (or technically, a regular dodecagon). Eleven columns of 4 panels each were used, with one column unfilled directly behind the fly. The total resolution of this display is 32×88 pixels. Because the display is not uniformly distant from the fly's retina, the angle subtended by each pixel on the retina depends on its height in the cylinder. The maximum size pixel for this arena geometry occurs in the coronal plane that runs through the middle of each of the fly's eyes, and subtends a visual angle of 3.75° on the fly's retina. This maximum pixel size is below the interommatidial distance of *Drosophila* (Heisenberg and Wolf, 1984), so pattern motion is effectively simulated as an apparent motion stimulus; the one-pixel jumps between consecutive frames produce the illusion of continuous motion. The wingbeat analyzer provides an instantaneous measurement of the wingstroke amplitude of the right and left wings of the fly; these signals were connected to the analog inputs of the PDC for use in closed-loop experiments. The difference in the left and right wing stroke amplitudes is highly correlated with torque (Tammero et al., 2004), suggesting that this is an appropriate signal to use in closing a feedback loop around attempted body rotations. With the PDC set in closed-loop mode, the difference between the voltages encoding the wingbeat amplitudes was used to close a negative feedback loop around the angular velocity of a rotating pattern. All flies were positioned such that the wingbeat amplitudes were within a consistent voltage range, and were run with the identical value of gain, setting the coupling between differences in left and right wingbeat amplitudes (corresponding to yaw torque) and the rotational velocity of the display. A relatively high gain was used, one that enabled all flies to readily 'fixate' a stripe within the frontal field of view, but not so large that oscillations of the stripe dominated the orientation behavior.

In open-loop trials, the response of the fly to some controlled sequence of visual input is measured. The data from these experiments are best displayed as the time series of the average response (typically turning) of the group of tested flies to the stimulus (or the mean of the time-averaged responses of all flies during each trial type). In closed-loop experiments, the rotational steering of the fly is used to set the rotational velocity of the displayed pattern in a negative feedback loop. The

presented results typically show the orientation of the pattern with respect to the fly, that is usually best summarized as a histogram (plotted in polar coordinates). Unless otherwise stated, all grouped data are presented as the mean of the per-fly responses, where each fly's response is typically the mean response during several trials. The error bars shown represent the s.e.m. of this mean of mean responses.

A general goal of the experiments presented in this thesis was to test as many visual stimuli conditions as possible, while avoiding a priori decisions about the stimulus conditions that flies *ought* to 'care' about. Simplified laboratory stimuli are a controlled way to assay features of *Drosophila*'s complex visuomotor control system, but it is often unclear where in parameter space the 'best' simple stimuli reside, and the response trend across many stimuli conditions is more informative than the response to some preferred stimulus. Therefore, a main challenge in designing these experiments was to include as many parameter variations as possible, while still testing all variations at least once on each fly. This required keeping the duration of each experiment to under 30 minutes, and ensuring that all flies remain 'engaged' during the course of the experiment. Even in the dark, tethered *Drosophila* will fly and produce varying patterns of yaw torque (Heisenberg and Wolf, 1979). However, most flies will not fly for more than a few minutes in the flight arena while receiving strong visual stimuli under pure open-loop conditions. Further, steering data that are collected during prolonged periods of open-loop flight are often flawed, because the torque produced by flies not receiving any sensorimotor feedback can drift far away from equilibrium (zero). In practice, nearly every fly responds well to closed-loop (stripe fixation) conditions, as indicated by elevated wingbeat frequencies and generally more 'vigorous' flight (Heisenberg and Wolf (1988) report that *Drosophila* 'know' the feedback loop is closed within less than 100 ms). The most effective open-loop experiments are conducted as short trials that are interspersed with closed-loop trials (stripe fixation works well) that are just long enough to keep the fly engaged and ensure that the torque produced is near equilibrium. For experiments that require longer open-loop trials, it is best if the stimulus varies in time in some non-trivial way, such as back-and-forth oscillation. These two strategies have been employed throughout, such that a typical experiment

may consist of 30–50 trial types, presented in random block trials, and interleaved with short bouts of closed-loop stripe fixation. Conceptually, the fly is always in closed loop, except that every so often, the loop is opened, and the fly must respond to some novel stimulus. All trials during which the flies stopped flying were discarded as determined by a check of the wingbeat frequency.

2.2.4 Data acquisition and analysis

During the course of the experiments, the left and right wingbeat amplitudes, the wingbeat frequency, and the analog voltages encoding the instantaneous positions of the 2 pattern channels were sampled at 500 Hz by a Digidata 1320A data acquisition system (Axon Instruments). Because trials were randomly determined during the course of an experiment, a USB-1208LS (Measurement Computing Corp.) was used to send a voltage encoding the current trial type from the PC script that runs each experiment. This signal was acquired along with the above data. All data analysis was performed offline using software written in MATLAB. In preparation for subsequent analysis, a data parsing routine segmented the data by trial type using the recorded signal encoding the trial identities.

For the closed-loop experiments, the data set of interest is the time series of orientations of the fly, which is the rotational position record of the pattern during each trial type. For rotational closed-loop experiments in the cylindrical flight arena (Figure 2.2B), the pattern consists of 96 positions along the azimuth; the recorded analog signal that encodes the position of the pattern was scaled and rounded to accurately recover the instantaneous position index of the pattern. A summary of the orientation time series data during each closed-loop epoch is obtained by collapsing the data into an orientation histogram of 96 bins, one for each position of the pattern.

For the open-loop experiments, the desired quantity is the mean turning response of individual flies to the short period of pattern motion. The turning response was computed as the difference between the left and right wingbeat amplitudes. Although the trials follow a brief closed-loop flight segment, there is, on occasion, some drift in

the torque produced by each fly, and so the mean response during the 100 ms previous to the stimulus onset was subtracted from the subsequent turning response. More complicated data normalization strategies were considered, but rejected, as discussed in §2.2.6.

2.2.5 Quantification of fixation behavior

Under closed-loop conditions, tethered *Drosophila* will vigorously orient towards a prominent vertical stripe (Heisenberg and Wolf, 1979). This behavior, termed fixation, is explored under a variety of contrast and luminance levels. To allow for comparisons across treatments, a simple metric (called the Histogram Width Metric, HWM) was developed, and is described in §3.1. However, many of the paradigms used in later experiments present the flies with conditions under which they may selectively orient towards two positions in the pattern that are separated by 180°: the focus of expansion (FOE) and the focus of contraction (FOC). To quantify behavior in these experiments, it was necessary to employ basic circular statistics. Circular statistics are the appropriate tool for averaging orientation data; linear statistics do not work, because the mean of two orientation positions, one at 1° and the other at 359° should be 0°.

In place of the usual arithmetic mean, we make use of the circular mean, calculated as the vector sum of the orientation data. The mean orientation of a vector, of length n, of instantaneous orientation angles, θ_i is defined by vector addition. The definitions for the circular statistic quantities are based on the development in Fisher (1993) and Batschelet (1981). First we calculate

$$\overline{C} = \frac{1}{n}\sum_{i=1}^{n}\cos\theta_i \quad \text{and} \quad \overline{S} = \frac{1}{n}\sum_{i=1}^{n}\sin\theta_i. \tag{2.1}$$

Then the angle of the mean vector, the *mean direction* is

$$\overline{\theta} = \begin{cases} \tan^{-1}(\overline{S}/\overline{C}) & \overline{C} > 0, \\ \tan^{-1}(\overline{S}/\overline{C}) + \pi & \overline{C} < 0, \\ \pi/2 & \overline{S} > 0, \overline{C} = 0, \\ 3\pi/2 & \overline{S} < 0, \overline{C} = 0, \end{cases} \tag{2.2}$$

and the *mean resultant length*, corresponding to the mean direction $\overline{\theta}$ is

$$r = \sqrt{\overline{S}^2 + \overline{C}^2}, \quad \text{and} \quad 0 \leq r \leq 1. \tag{2.3}$$

The mean direction, $\overline{\theta}$, can be directly computed using the `atan2` function in many programming languages (including MATLAB), that determines the appropriate quadrant of the result. The circular (or angular) *standard deviation* is defined as

$$s = \sqrt{-2\log(r)}, \tag{2.4}$$

or is also alternatively defined as

$$s = \sqrt{2(1-r)}. \tag{2.5}$$

Both definitions of s have properties that are similar to the standard deviation in linear statistics, and are roughly equal for large values of r. The mean resultant length, r is related to the dispersion of the data around the mean heading, but only when the data form a single cluster. When r is close to one, the data must be very tightly clustered; however, $r = 0$ can occur when the data are randomly distributed, or, e.g., in the case of two tight clusters of data that are 180° apart.

Fixation behavior must involve some period of time during which the fly maintains a small range of orientations with respect to the pattern. Therefore, large values of r can be used to identify these sequences in the data. Since fixation behavior must have some non-trivial duration, a window corresponding to 2 seconds of orientation data is

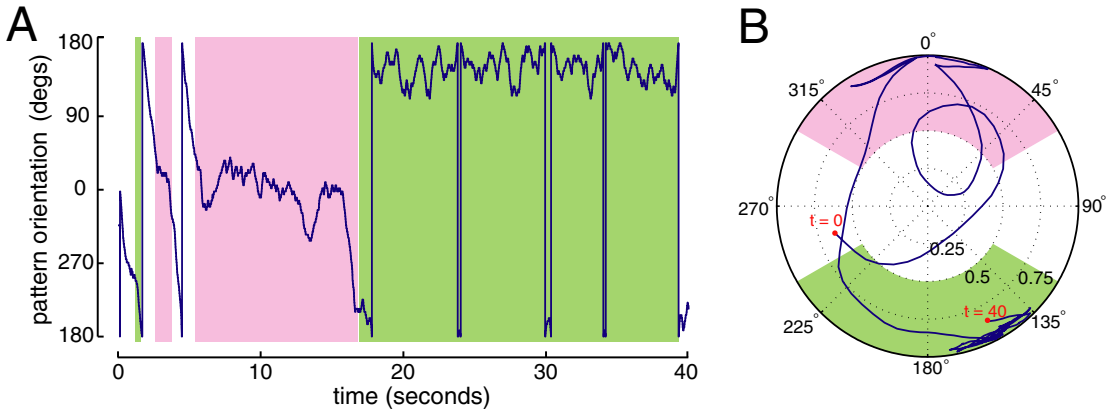

Figure 2.6. Several of the experiments presented in Chapters 2–3, contain stimuli in which *Drosophila*, operating under closed-loop conditions, may selectively orient towards one of two features of the pattern, separated by 180°. (A) A sample segment of orientation data from a single fly, during which the fly shows significant orientation towards both 'poles' (the foci of expansion and contraction) of the pattern. To quantify the orientation preference in this paradigm, a moving 2 seconds window of the circular mean and the mean resultant length, r, is computed (B). If $r_i \geq 0.5$, then the pattern position is treated as stable, and if either the FOC is frontal (area shaded green) or the FOE is frontal (shaded pink), then the window is tagged accordingly.

used to form the vector θ, of length 1000 (data collected at 500 samples per second) for which r and $\overline{\theta}$ are determined. To prevent the arbitrary starting position of the 2-second window from eliminating bouts of fixation from the analysis, the window is moved through the data set in small increments of 100 ms (50 samples). Using this strategy, there are $N = \lfloor (n - w)/inc \rfloor$ total number of windows, where n is the length of the data set, w is the length of the window, and inc is the number of samples per increment of the window. Fixation is considered to be significant when $r_i \geq 0.5$, and the FOC and FOE are considered to be fixated when $\overline{\theta}$ is in the 120° sector centered at the respective pole of the pattern. A sample orientation time series, in which a fly shows significant fixation of both poles of the stimulus is shown in Figure 2.6A. The circular mean in a sliding 2-second window is plotted in Figure 2.6B, showing the regions in the polar plot, corresponding to the time series data, during which the fixation is scored as being orientated towards the FOC or FOE. For each of the N

windows, the fixation behavior is scored as follows:

$$\begin{aligned}
\mathrm{FIX}_{\mathrm{FOC},i} &= \begin{cases} 1, & \text{if } \frac{2}{3}\pi \le \overline{\theta}_i \le \frac{4}{3}\pi \ \text{ and } \ r_i \ge 0.5, \\ 0, & \text{else }, \end{cases} \\
\mathrm{FIX}_{\mathrm{FOE},i} &= \begin{cases} 1, & \text{if } \overline{\theta}_i \le \frac{1}{3}\pi \vee \overline{\theta}_i \ge \frac{5}{3}\pi \ \text{ and } \ r_i \ge 0.5, \\ 0, & \text{else }, \end{cases} \\
\mathrm{FIX}_{\mathrm{NONE},i} &= 1 - (\mathrm{FIX}_{\mathrm{FOC},i} + \mathrm{FIX}_{\mathrm{FOE},i}).
\end{aligned} \tag{2.6}$$

Periods of no fixation can be caused by a failure of the data in the window to meet either the significance cutoff associated with r_i or the sector criteria for the mean orientation direction. For each trial type, the percent of time that each fly's behavior is classified in one of the 3 categories is calculated using the mean of the fixation scores over the length of the trial:

$$\begin{aligned}
\overline{\mathrm{FIX}}_{\mathrm{FOC}} &= \frac{100}{N}\sum_{i=1}^{N}\mathrm{FIX}_{\mathrm{FOC},i}\ \%, \\
\overline{\mathrm{FIX}}_{\mathrm{FOE}} &= \frac{100}{N}\sum_{i=1}^{N}\mathrm{FIX}_{\mathrm{FOE},i}\ \%, \\
\overline{\mathrm{FIX}}_{\mathrm{NONE}} &= \frac{100}{N}\sum_{i=1}^{N}\mathrm{FIX}_{\mathrm{NONE},i}\ \%.
\end{aligned} \tag{2.7}$$

In some cases it is useful to compute the fixation scores as a function of time (or sample), averaged across several trials (for each fly). Suppose there are K repetitions of a certain trial, then fixation scores for each sample i are determined by aligning the data for each repetition and averaging the fixation scores in each ith window:

$$\begin{aligned}
\overline{\mathrm{FIX}}_{\mathrm{FOC},i} &= \frac{100}{K}\sum_{j=1}^{K}\mathrm{FIX}^{j}_{\mathrm{FOC},i}\ \%, \\
\overline{\mathrm{FIX}}_{\mathrm{FOE},i} &= \frac{100}{K}\sum_{j=1}^{K}\mathrm{FIX}^{j}_{\mathrm{FOE},i}\ \%, \\
\overline{\mathrm{FIX}}_{\mathrm{NONE},i} &= \frac{100}{K}\sum_{j=1}^{K}\mathrm{FIX}^{j}_{\mathrm{NONE},i}\ \%.
\end{aligned} \tag{2.8}$$

The use of a 2-second window, a 100 ms window increment, 120° sectors, and a cutoff of $r_i \geq 0.5$, were educated, though largely arbitrary, choices. Several tests have been conducted using a smaller window, both larger and smaller sectors, and different r cutoff values, and tested on relevant data. The choices used here were deemed appropriate for capturing fixation behavior when it occurs, and if anything, are rather conservative, as evidenced by the high (approximately 20 %) value of $\overline{\mathrm{FIX}}_{\mathrm{NONE}}$ occurring during trials with competing, attractive stimuli (example in Figure 4.2).

2.2.6 Fly alignment as a source of noise

There are many sources of noise (broadly defined) that enter the presented data. Probably the most significant contribution is 'operator error,' the precision with which each fly is tethered and then focused above the wingbeat sensor can introduce both bias and variance (among other effects) into the recorded responses. If the fly is positioned too far towards one side of the mask, the distribution of turning responses will contain a left-right asymmetry, because the signal from one wing will typically be much larger then the other. A fly that is too far forward on the mask will typically have a saturated shadow—the signal will be large, but the complete range of the steering generated by the animal will not be projected onto the sensor. Similarly, a fly that is too far back will yield small signals that feature a dead zone—large excursions of the wing are well projected, but smaller ones are not. Alignment and tethering also contribute to the variance of the response from an individual fly by altering the dynamic range of the measured signal. The orientation of the body around the pitch axis also affects the size of the projected shadow. To minimize these effects, every effort is made to tether all flies in as consistent a manner as is possible.[4] Also, when each fly is introduced into the flight arena, all experiments begin with a period of closed-loop stripe fixation that is used to assess the fly's alignment. Under closed-loop conditions, flies can compensate for small misalignments, but a badly tethered and aligned fly will always struggle to fixate a stripe. This condition is corrected by repositioning the flies until they can fixate a stripe for at least 10 seconds; only then

[4]All data in this thesis were generated by flies tethered by the author.

do the experiments begin. Even with these precautions, small asymmetries in the responses to symmetric conditions do arise. Many of the experiments presented herein consist of a large number (30–50) of distinct trial types, presented as random block trials. Because many of the open-loop experiments contain stimuli that should elicit a bilaterally symmetric response, (e.g., expansion from the right or expansion from the left), this mirror symmetry in the responses is assumed during the data analysis. After a visual inspection to confirm that the data are approximately symmetric, the responses for each fly are combined with responses during the mirror symmetric trials (with the appropriate sign inversion). Wherever this averaging is used, it is explicitly mentioned in the following chapters.

To demonstrate the effects of misalignment on the 'hütchen' signal, it is instructive to consider a toy example where the amplitude measurement from each wing is taken to be a normally distributed random variable. Consider the example of a certain visual stimulus that will cause a fly to turn right with some 'intensity,' and the same stimulus in the opposite direction will cause a turn of equal strength to the left (the classical syndirectional optomotor stimulus and a laterally positioned expansion stimulus will yield this type of response). The idealized case of a fly's turning response in such a case, where expansion is presented from the right and left of the animal, is shown in Figure 2.7a. In this case, the fly turns with perfect symmetry, producing a 1 V difference between the outer and inner wing for the two turns. Several disturbances to the idealized case in (a) are considered and shown in Figure 2.7: (b) a constant bias (0.5 V), whereby the right wing is favored; (c) the gain on the right wing is 35% higher then on the left wing; (d) the variance on right wing has doubled; (e) the mean of the right wing is reduced by half; (f) the fly has some inherent asymmetry that causes clockwise turns to one direction that are larger than turns in the opposite direction. The turning response to expansion from both sides is simply the difference between the left and right wingbeat amplitudes and is shown in the third row of Figure 2.7. The combined PDFs for the L - R signal are plotted in the bottom row of Figure 2.7. Each of these plots also lists the mean and standard deviation for each PDF. Although many perturbations were simulated, it is instructive to note that the mean

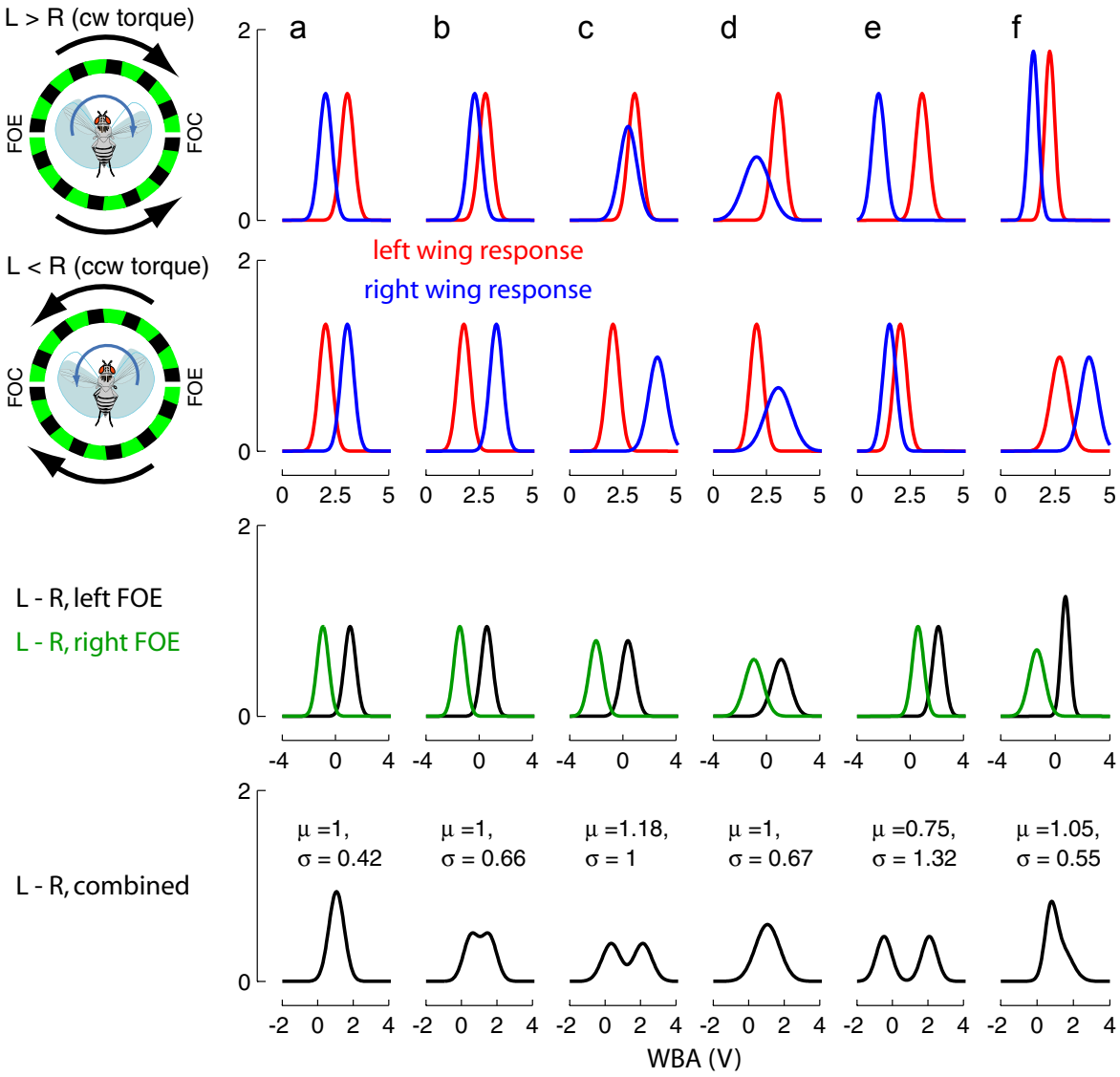

Figure 2.7. Several factors contribute 'noise' to the measurement of wingbeat amplitudes. We consider a toy data set for a fly responding to a strong expanding pattern, where the focus of expansion (FOE) is positioned on one side of the fly. The fly will turn away from this focus of expansion by producing a turning torque, generated by modulating the difference in wingbeat amplitude between the left and right wing (Tammero et al., 2004). A useful experimental method is to separately present stimuli with mirror symmetry—such as the expansion emanating from the left and right of the fly—and then combine the response to these symmetric stimuli during the data analysis. To clearly demonstrate some of these signal degrading factors, the measured wingbeat amplitude (a voltage) from each wing is modeled as a normally distributed random variable. The probability density function (PDF) for the left and right wing in response to the left FOE and the right FOE are shown in the top two rows. In the third row, the PDF of the instantaneous L - R signal (a proxy for the torque the fly is producing), is shown for both cases. Finally, in the last row, the averaged PDF for the mirror symmetric cases is plotted.

of each distribution, is indeed quite close to the idealized case (a), with a 1 V mean. The compensation is perfect for the case where there is a constant bias added to the responses (this approximates what occurs when the fly is slightly off center with respect to the mask), and when the variances of the wings are different, but the means are as in the ideal case. It is important to note that this 'flip and average' method essentially posits that each fly is producing symmetric responses, and somehow, operator error has interfered with their detection. The upshot is that the method yields cleaner results, with less data. Of course, the compensation could be done at the level of the entire set of flies in the data set, but often the factors degrading the symmetry of the measured responses act on both wings in some complicated, but not independent way. Thus, correcting for this degradation on a per-fly basis is preferred.

To demonstrate how the toy data considered above relate to distributions of fly data in actual experiments, we show (in Figure 2.8) the corresponding distributions for 7 flies in response to laterally positioned FOEs, taken from the data set presented in Figure 3.7. The 7 (of 15) flies were selected to demonstrate the range of wingbeat amplitude distributions that are observed in a typical data set; several of the flies that are not shown yielded distributions that are remarkably similar to those of flies 1 and 3. Each fly was presented with multiple presentations (at least 3) of expansion form the right and left for 3 seconds (along with 23 other trial types, presented in random order, results not shown). All of the amplitude data for each wing during the multiple presentations are combined to form the histograms in the top two rows of Figure 2.8. Note that these histograms reveal no information about the (certainly important) temporal correlations in the left and right wing activity. The third row of Figure 2.8, shows the distribution histograms for the instantaneous L-R values. Since the left and right wingbeat amplitudes are correlated, it is expected that the L-R distributions, appear less erratic (with fewer peaks) than the distributions for the individual wings. Several of the included distributions reveal similar perturbations to the factors considered in the toy examples: the distributions for fly 1 show both the slight bias effect (b) and some variance difference (c) between the wings. The histograms of fly 4 are rather symmetric, but with higher variance on both wings.

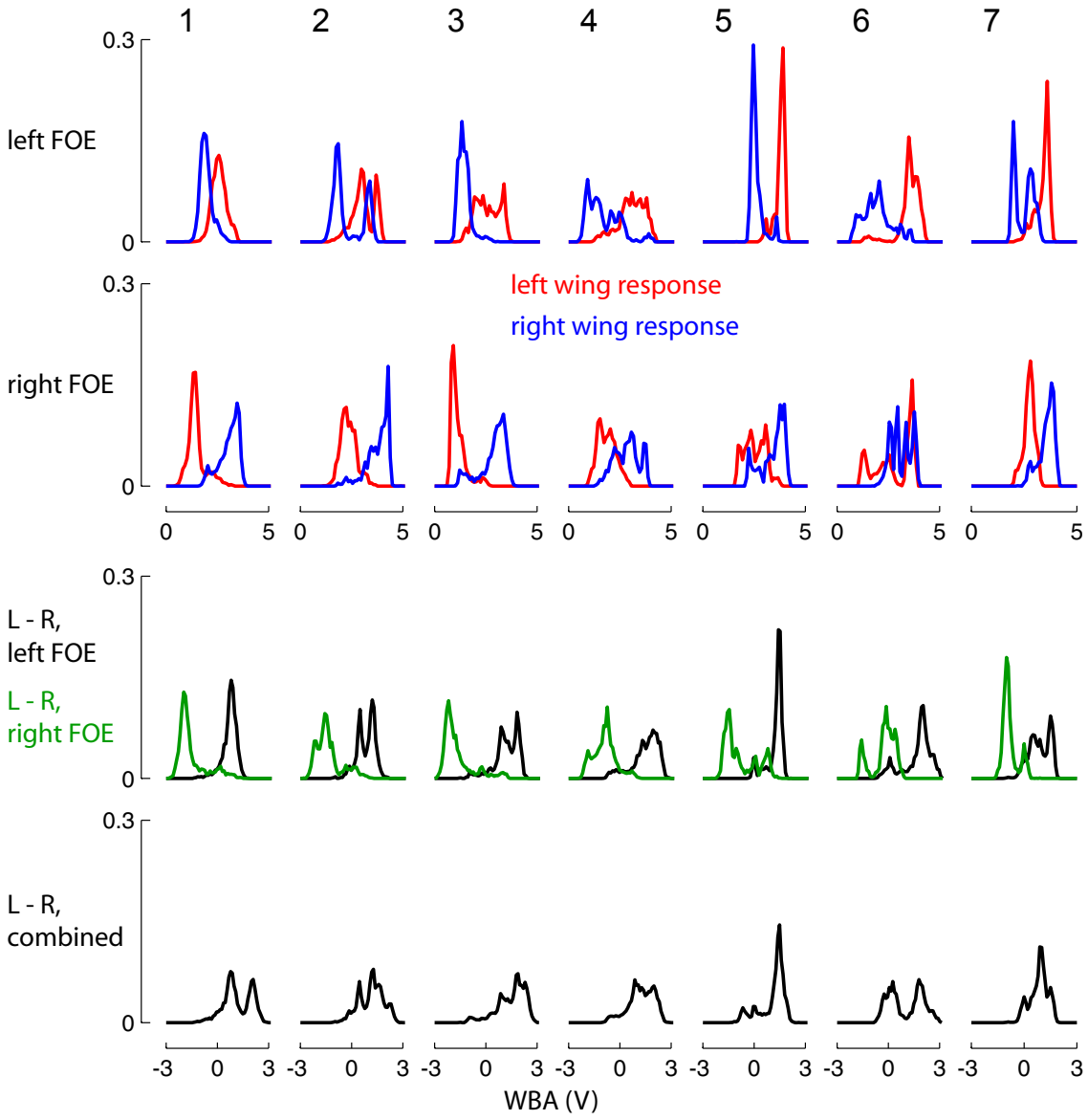

Figure 2.8. As a comparison to the toy data in Figure 2.7, the response distributions for several individual flies are shown. Each column (1–7) represents data taken from an individual fly. The data are organized as in Figure 2.7. The distributions for each wing in response to the left FOE and the right FOE are shown in the top two rows. In the third row, the distribution of the instantaneous L - R signal (a proxy for the torque the fly is producing), is shown for both cases. Finally, in the last row, the averaged distributions for the mirror symmetric cases are plotted.

Fly 5's data resemble case (f)—the fly is clearly turning more in response to one stimulus than the other. Some flies seem to exhibit an innate preference for turns in one direction, although this 'preference' is simply caused by significant rolling and yawing of the body relative to the ideal tethering orientation, such that the animal's visual experience is rather different than the intended one. These data demonstrate the effectiveness of combining mirror symmetric data. Although the response of each fly to each presented expansion direction can be quite different, the histograms in the last row of Figure 2.8 (the combined L-R distributions), are much more consistent than would be expected from the per-wing histograms at the top of the Figure. Even in the case of fly 6—this fly essentially does not turn away from the rightward FOE stimulus—the 'flipped and averaged' distribution yields a mean turning response that is close to the mean response of the entire group.

One final note: a careful inspection of these data suggest why many sophisticated data normalization schemes do not work—the data are not well approximated by a Normal distribution, so any compensations based on normalizing the data to some standard distribution should not be an effective method to align data from different flies. Several linear data normalization schemes (shifting and scaling only), applied per fly, were attempted:

1. Zero-mean each fly—the mean L-R calculated over the entire experiment was subtracted from each trial (equivalent to subtracting the mean per-wing amplitude from each wing).

2. The L-R amplitude was set close to zero at the start of each trial by subtracting the mean L-R value during the 100 ms immediately preceding each trial.

3. Each wing was normalized to the mean mean and standard deviation of both wings for all flies in the data set.

4. L-R was directly normalized to a zero mean and to the standard deviation of all flies. This is not identical to the scheme above.

5. L-R during each trial was normalized by subtracting the mean L-R value during the 100 ms immediately preceding each trial, and the standard deviation of the data snippet (from one trial) was scaled using the ratio of the mean standard deviation (over the whole data set) to the standard deviation during the 100 ms prestimulus L-R.

6. L and R were separately normalized by subtracting the mean amplitude for each wing during the 100 ms immediately preceding each trial, and the standard deviation during each trial was scaled using the ratio of the mean standard deviation (over the whole data set) to the standard deviation of the 100 ms pre-stimulus per-wing wingbeat amplitude.

In practice, these methods prove useful for small data sets; in any data set with 10 or more flies, there is no improvement (as determined by comparing the standard deviations of the grouped multi-fly data) supplied by these 'histogram normalization' schemes. Therefore, all the open loop data presented here has been scaled in a simple manner—using strategy 2 above—the responses shown are the difference between the L-R signal during the stimulus presentation and the mean value during the 100 ms before stimulus onset. Why normalize at all? In pure open loop, with any visual feedback removed, flies do not steer in a very consistent way. This is the reason for using the strategy of performing all open-loop experiments with short, interleaved closed-loop trials. Thus the bouts of closed-loop behavior tend to keep the flies generating nearly symmetric wingbeats.

2.2.7 Head motion analysis

To investigate the role of head motion in the expansion-avoidance reflex, video recordings of the flies' heads were made during open-loop presentations of expansion stimuli. A firewire CCD camera (Basler A602f-2) with a telephoto lens (Infinity Proximity series InfiniMini) was mounted such that the image plane was as close to orthogonal with the fly's tether as the ergonomics of the flight arena allow (approximately 10° off). The lens was focused such that the fly's head was in the center of the field of

view and formed an image of approximately 200 × 200 pixels. The Basler camera was configured to capture images when triggered by an external signal, that was supplied by the Panel Display Controller. All image acquisition was handled by the Fview program (courtesy of Andrew Straw, Dickinson Lab, Caltech). Subsequently, the image, wingbeat, and flight arena data were then temporally aligned and analyzed in MATLAB. During experiments, the cameras were triggered at 50 Hz, such that head motion was easily recorded, though we lack the temporal resolution to distinguish the sequencing of sudden small movements by the head and wings.

2.3 Notations and conventions

Every effort has been made to ensure that the descriptions of the presented data are consistent throughout the document. Some general notes on the nomenclature and conventions that are used in the thesis are provided:

- The difference between left and right wingbeat amplitudes of the fly is used as the turning response. This quantity will be abbreviated as either ΔWBA or simply as 'L - R' (units of volts). As indicated in Figure 2.7, $\Delta\text{WBA} < 0$ corresponds to counterclockwise torque, and $\Delta\text{WBA} > 0$ corresponds to clockwise torque.

- The sum of wingbeat amplitudes is also presented as an important steering response. This quantity is abbreviated as either ΣWBA or as 'L + R' (units of volts).

- The wingbeat frequency of the fly (identical for both wings) is referred to as WBF (units of Hz).

- In Chapters 3–5, the speed of pattern motion is often described in terms of the temporal frequency of the pattern. Conceptually, the temporal frequency is the rate at which one cycle of a moving, period pattern passes by one (any) position in space, in units of cycles/second, or Hz. Historically, this term has often been referred to as *contrast frequency*. The term *contrast frequency* was used because *temporal frequency* was reserved for the speed of the moving pattern, though of

course the quantity has nothing to do with contrast, per se. When the speed of the moving pattern is referred to as frame rate, or angular velocity, (units of degrees/second), there is no need to use the potentially confusing term. The temporal frequency (abbreviated as f_t) is given by the ratio of the pattern's angular velocity to its spatial period (V/λ).

- The label *fly* or *flies* is used quite casually throughout the thesis. Approximately 100,000 species of flies (insects of the order Diptera), have been described. Unless referring to previous work, in which the tested species are explicitly given, all other uses of the terms refer to the humble fruit (or vinegar or pomace) fly, *Drosophila melanogaster*, and in particular to the Dickinson lab strain.

Chapter 3

Interaction between Object-Orientation and Expansion-Avoidance Behaviors

Under closed-loop conditions, tethered *Drosophila* will vigorously orient towards a prominent vertical stripe (Heisenberg and Wolf, 1979). This behavior, termed fixation (first established in the housefly *Musca domestica* (Reichardt and Wenking, 1969), is so robust that in a remarkable experiment, Götz (1987) observed sustained object orientation during a nearly continuous 32-hour period. In a second, much newer finding, it has been established that the strong avoidance of the focus of expansion (FOE) of a panoramic expansion pattern by tethered *Drosophila*, yields an equally robust closed-loop paradigm wherein flies will actively orient towards the focus of contraction (FOC) (Tammero et al., 2004). These two experimental paradigms exploit very different behaviors. In the case of object-orientation, the behavior relates to the animal's control of orientation over some distance—a fly orients towards an attractive object, presumably with the intention of exploring it as a possible landing site (though later in this chapter, I will argue that perhaps orientation towards prominent vertical objects in the environment is a generally sensible navigation strategy). The expansion-avoidance behavior is likely to serve as an *escape response*, a large and fast (and non-adapting) response to an imminent collision. Clearly, the paradox discussed in §1.9 is just that, paradoxical, as it is difficult to conceive of the frontal fixation of visual contraction as a useful long-term navigation strategy. Since these two behaviors serve very different purposes, it is interesting (and feasible) to investigate the relative

contributions of these two responses to various combinations of the two stimuli.

The experiments described in this chapter were designed to address the first and second hypotheses discussed in §1.11. The first two results presented in this chapter were conducted to establish that the modification necessary to combine the stimuli do not significantly affect the two robust behaviors being examined. One set of experiments was conducted to determine whether flies are able to fixate a stripe under a wide range of luminance and contrast levels. Further, the expansion-avoidance behavior was examined at different contrast levels, a necessary test for the second hypothesis of §1.11, that relates to the use of the 'high' contrast expansion patterns in the original experiments of Tammero et al. (2004). Once the contrast dependence of the two behaviors was explored, several combinations of the object-orientation and expansion-avoidance evoking stimuli were tested. Many experiments were conducted to establish the most significant effects and to ensure that the protocols used were sensible—only the most consistent, well-controlled, and informative results are included.

3.1 Effect of contrast on open-loop object orientation

3.1.1 Experimental design

We sought to assess the effect of pattern intensity and contrast on the strength of stripe orientation under visual closed-loop conditions. The display's 8 intensity levels make it possible to display 56 combinations of stripe and background patterns. However this proved too large a test set to allow for multiple repetitions with each fly, so instead 21 combinations were tested. A 30° wide vertical stripe with intensities of 0 (stripe consists of inactive LEDs), 3 (intermediate intensity level), and 7 (the brightest possible stripe consisting of maximally active LEDs), were used in combination with all background levels other than the stripe's intensity. Each combination of stripe and background intensity level is described by the *stripe contrast* of the pattern. This

Table 3.1. Experimental conditions used to test the effect of pattern contrast and intensity on closed-loop stripe fixation behavior

Stripe IL	Background IL	Stripe contrast (%)
0	1	-100
0	2	-100
0	3	-100
0	4	-100
0	5	-100
0	6	-100
0	7	-100
3	0	100
3	1	50
3	2	20
3	4	-14.3
3	5	-25
3	6	-33.3
3	7	-40
7	0	100
7	1	75
7	2	55.6
7	3	40
7	4	27.3
7	5	16.7
7	6	7.7

term is defined to be the relative contrast between the stripe and the background:

$$\text{stripe contrast} = \frac{\text{stripe intensity - background intensity}}{\text{stripe intensity + background intensity}}. \tag{3.1}$$

A positive value corresponds to a stripe that is brighter than the background, and a negative value to a background that is brighter than the stripe. The stripe contrast (SC) values for the 21 tested combinations are listed in Table 3.1. Each combination was presented to tethered flies during 40-second closed-loop trials, interspersed with a 3-second pause, during which the entire display was set to a uniform, intermediate intensity value. These stimulus conditions were presented as random block trials. In total, 22 flies completed between 1 and 2 15-minute repetitions of this protocol.

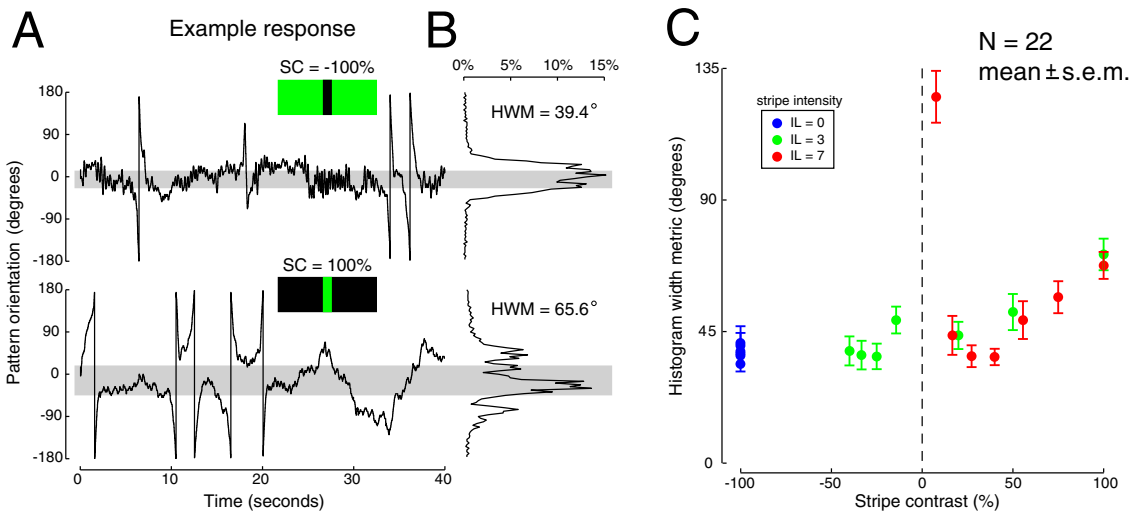

Figure 3.1. Effect of pattern luminance and contrast on the closed-loop orientation behavior of *Drosophila*. (A) Example periods of orientation behavior: in the top trace the pattern is a dark stripe on a bright background (stripe contrast, SC = -100 %), in the lower trace the fly was presented with a bright stripe on a dark background (SC = 100 %). The fly controls the azimuthal position of the single-stripe pattern by modulating the difference between left and right wingstroke amplitudes. When the stripe is in front of the fly, the position of the pattern is near zero. (B) For each 40-second trial, the percentage of time that the flies orient towards any single position of the pattern is represented as a histogram. The gray bars correspond to the Histogram Width Metric (HWM), defined as the minimum position band that must include zero and contain 50% of the histogram area. (C) The mean (± s.e.m.) HWM for 21 levels of stripe contrast is plotted against stripe contrast. The values are grouped by the intensity level (IL) of the stripe: blue for the lowest stripe IL, green for an intermediate stripe IL of 3 (out of 7), and red for the highest IL, corresponding to the brightest stripe. Over most of the tested range, fixation performance is nearly constant. For positive, increasing stripe contrast levels fixation degrades, evidenced by the trend towards a larger HWM. Also, clear deficits in fixation arise for the trials conducted at the lowest positive stripe contrast level.

3.1.2 Results

In the results presented here (Figure 3.1), flies have active control over the rotational velocity of a 30° stripe. The position sequences of the stripe for two *typical* trials for an individual fly (Figure 3.1A), reveal that for most of each trial, the stripe is actively positioned in front of the fly, even under inverted luminance conditions. For each 40-second trial, a histogram is used to represent the percentage of time that a fly orients

towards any position of the pattern (Figure 3.1B). Sustained orientation towards the stripe is reflected by a large area under the histogram curve around the zero (frontal) position. By inspection, it might seem reasonable to fit the orientation histograms with a Normal distribution. However, this (or a similar) strategy is inappropriate for these data. When flies do not fixate the stripe, the pattern will often 'spin' around them. This spinning, when collapsed into the orientation histogram, essentially contributes a uniform distribution of stripe positions for some component of the data set. The flat tails that result from this are not well captured by a Gaussian fit. Thus, we quantify the dispersion of the orienting behavior by computing the minimum position band that includes zero, and contains 50% of the histogram area (shown as the gray bar for the two data sequences and histograms in Figures 3.1 A and B).

The mean values (± s.e.m.) of the 50% histogram width metric (HWM) for the 21 tested levels of stripe contrast are shown in Figure 3.1C, revealing that flies fixate stripes with nearly constant performance over a large contrast range. Further, in all cases flies truly *fixate* the stripe, that is, the orientation behavior is significantly different than random orientation (HWM = 180°). The blue cluster of points at -100% contrast corresponds to the trials with a stripe of intensity 0 and the full range (1–7) of background intensity levels. For these seven conditions the fidelity of stripe fixation is essentially constant. On the right-hand side of the plot, corresponding to trials where the background is darker than the stripe, there is a noticeable trend of reduced performance with increasing stripe contrast. The one condition under which flies show clear fixation deficits (though performance still differs from random orientation), is the case of stripe intensity 7 and background intensity 6; this condition represents the highest intensity pattern with the lowest contrast (7.7%) of those tested.

The two example traces in Figure 3.1A were selected because the HWM values calculated for each trial are very close to the mean for the entire set of flies. Of course, many flies do better than this mean value, and many perform worse. Because the HWM is defined to include zero, a small HWM value can only indicate that robust fixation occurs—most of the time the stripe is in front of the fly. However, several factors can contribute to a larger HWM, and large amounts of raw data must be scrutinized to

determine these effects. Phenomenologically, either the pattern is spinning quickly (and thus there are insufficient motion cues to allow for stable fixation), or at other times, many flies show bouts of what has been termed 'anti-fixation' (Heisenberg and Wolf, 1984); the pattern is fixated for just a few seconds and then sent behind the fly, only to come up on the other side and remain in front for a few seconds, eventually alternating sides again. A short period of 'anti-fixation' can be seen during the lower orientation times series in Figure 3.1A (during t = 8–20 seconds). In the conditions where fixation degrades, the orientation time series will often exhibit periods of either spinning or 'anti-fixation' interspersed with fixation. Additionally, asymmetries in tethering and fly alignment make the stripe fixation task more difficult. However, the HWM does capture the fact that for most of the tested contrast and luminance combinations, the stripe is actively positioned in front of the flies for the majority of the closed-loop trial.

3.2 Effect of contrast on closed-loop expansion-avoidance

3.2.1 Experimental design

A series of experiments were conducted to assess the effect of pattern contrast on the closed loop expansion-avoidance response. In these experiments and others that follow,[1] the standard expansion pattern used consisted of 4-pixel-wide bars of active and inactive pixels, or a spatial frequency of 30°/cycle. The pattern is designed with two degrees-of-freedom: the first contains the 8 frames required for one cycle of expansion, and the second contains the 96 positions around the arena from which expansion can emanate. This expansion-rotation (ER) pattern allows the rate of expansion to be set as an open-loop parameter (one that the fly has no control over), and the rotational component of the pattern is controlled by the fly in closed-loop, such that the fly can selectively orient with respect to the foci of the pattern. To test the effect of pattern contrast on the closed-loop expansion-avoidance behavior, four patterns were constructed with the same mean luminance, but with varying contrast,

[1]Except in the experiment that explicitly tested different spatial frequencies §4.1.

Table 3.2. Contrast of patterns used to test expansion-avoidance behavior

Condition name	CL 1	CL 2	CL 3	CL 4
Intensity level, dark bar	3	2	1	0
Intensity level, bright bar	4	5	6	7
Contrast (%)	14.3	42.9	71.4	100

as summarized in Table 3.2. The rate of open-loop expansion was 30 fps, corresponding to a temporal frequency of 3.75 Hz, a speed at which the expansion-avoidance response was shown to be robust. Each pattern (at one of four contrast levels) was presented to tethered flies during 30-second closed-loop trials, interspersed with an additional 30-second closed-loop stripe-fixation trial,[2] presented in random block trials. In total, 13 flies completed between 2 and 8 repetitions of this protocol, with each repetition lasting 4 minutes.

3.2.2 Results

Flies were given active control over the rotational velocity of the focus of expansion of the ER pattern, at one of four contrast levels. The results of the closed-loop expansion-avoidance experiments (Figure 3.2) reveal that lowering the contrast of the ER pattern does not significantly alter the flies' behavior, as was found for most of the tested levels of contrast in the case of the stripe-fixation paradigm. The orientation histograms of Figure 3.2A, are the mean histograms obtained by averaging the histograms from each fly's orientation data during each of the 4 trial types. The histograms contain 48 bins, each corresponding to 2 adjacent locations of the FOE around the cylinder. A useful comparison for these data is the case of random orientation, which yields a flat distribution of (100/48)% at all positions. The gray disk in Figure 3.2A represents this distribution for random orientation. To further quantify the orientation behavior,

[2]The interleaved experiments consisted of stripe fixation stimuli of several different contrast levels, serving as a pilot study for the data presented in §3.1. These initial studies revealed that there is likely an interaction effect between the stripe fixation trials that were used in between the closed-loop expansion-avoidance trials. In general these initial experiments revealed that short time trial experiments (30 seconds or less) were unreliable, in that the data averaged over the entire trial were too strongly dependent on the initial condition of the trial.

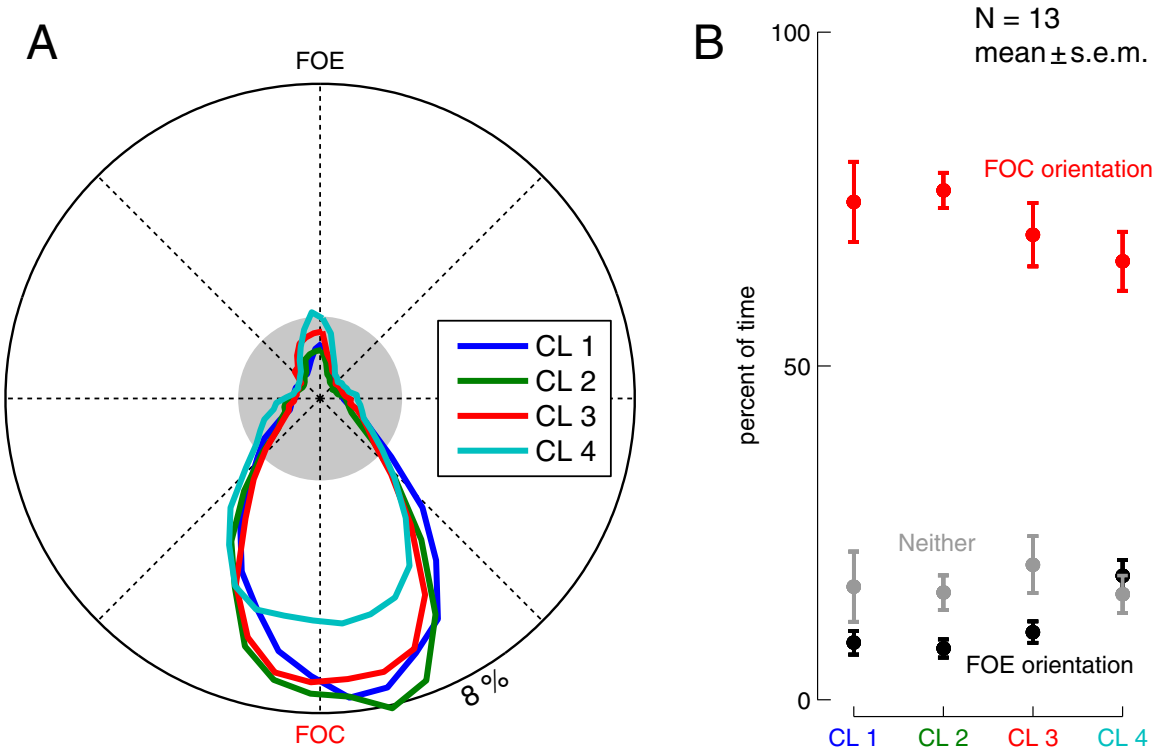

Figure 3.2. Effect of pattern contrast on the closed-loop expansion avoidance behavior of *Drosophila*. (A) The mean orientation histograms (plotted in polar coordinates), show the percentage of time that the flies orient towards any single position of the FOE, for each of the four tested levels of pattern contrast. The gray disk represents random orientation. The fixation metrics (B) reveal the percent of time that the flies actively regulate the position of either the FOE or the FOC in front. The data show that the strong preference for orienting towards the focus of contraction is largely unaffected by the contrast of the pattern.

the methods described in §2.2.5 were applied to each 30-second trial. The mean (± s.e.m.) fixation scores for each condition are obtained by averaging each fly's mean scores as computed using equation 2.8, and are plotted in Figure 3.2B. The flies fixate the FOC for the vast majority of the time during all four trial types.

To test the null hypothesis—that the tested contrast levels have no significant effect on the orientation towards the focus of contraction—a one-way, balanced, ANOVA was performed on the percent of time of FOC fixation, $\overline{\mathrm{FIX}}_{\mathrm{FOC}}$, for the 13 flies in the data set (the red points in Figure 3.2B). The ANOVA confirms the null hypothesis, that the sample means for these 4 contrast levels are essentially the same ($p = 0.3601$). When

an ANOVA was performed on the percent of time that each fly oriented towards the FOE (the black points in Figure 3.2B), the null hypothesis was rejected ($p = 0.0003$). A multiple comparisons test revealed that the means for CL 1–3 are not significantly different, but the mean percent of time orienting towards the FOE is significantly different between CL 4 and the other three levels, even at $\alpha = 0.01$ (corresponding to 99% confidence level). This data set shows a surprising dependence on the tolerance of the FOE at the highest tested contrast level, though this heightened tolerance only achieves the level of random orientation (indicated by the gray circle in Figure 3.2A). Results from additional experiments (not shown), suggests that this tolerance is likely due to an interaction effect between this paradigm and the stripe fixation trial that preceded it. During the first few seconds of the closed-loop expansion-avoidance trial immediately following a stripe fixation trial, stronger than average FOE tolerance is exhibited (and apparently more so at the highest contrast level).

3.3 Compound stimuli I: Closed-loop expansion-avoidance vs. object orientation

3.3.1 Experimental design

To further explore the fixation of the focus of contraction that occurs under closed-loop conditions, a series of experiments were conducted using several compound stimuli patterns containing combinations of the expansion-avoidance (ER) pattern and a moving object. To test the hypothesis that the focus of expansion may be tolerated if flies are undergoing directed flight, a modified version of the CL 1 (lowest contrast) ER pattern was created, containing a 30°-wide high-contrast stripe embedded at the focus of expansion (this pattern is the Expansion-Rotation-Stripe, ERS pattern). This experimental condition essentially places two attractive stimuli in direct opposition, testing the relative attractiveness of both. In the first set of experiments closed-loop behavior of flies was tested with the ER and ERS pattern, with two rates of open-loop pattern expansion, 10 and 30 frames per second, corresponding to $f_t = 1.25$ and $f_t = 3.75$ Hz. The experimental series consisted of 30 seconds of closed-loop stripe fixation

(stripe IL 0, background IL 3), followed by 90 seconds of closed-loop control over one of the two patterns at one of the two speeds of expansion, presented in random block trials. The initial starting position of the ER and ERS patterns was alternatively either the FOE or the FOC.[3] Flies that could not complete at least 8 trials (1 each of the 2 patterns at 2 speeds with 2 initial conditions) were discarded from the data set. In total, 16 flies completed between 1 and 2 repetitions of the 8 trial protocol, each repetition required 16 minutes.

The most 'interesting' case in the above experiment was found to be the ERS pattern with the slower temporal frequency (1.25 Hz) of expansion (Figure 3.3). To assess the longer term fixation behavior of flies in response to this treatment, 6-minute long trials were conducted. The first experiment consisted of 30 seconds of closed-loop stripe fixation (stripe IL 0, background IL 3), followed by 6 minutes of the ERS pattern (CL 1, expansion at 10 fps). For all trials the FOE was the initial condition. In total 15 flies completed between 1 and 5 repetitions of this protocol. A final experiment testing the long term closed-loop behavior was performed using the identical protocol as above, except that half of the trials had a strong bias added to the fly's turning response (for the entire 6 minute trial). Thus the rotational velocity of the pattern is given by: $\omega(t) = G \cdot \Delta\text{WBA} + B + b(t)$, where G is the constant gain, B is the constant bias (set to zero in these experiments), and $b(t)$ is a time-varying bias of $\pm 150^\circ/s$, that alternates direction every 5 seconds. A small data set of 5 flies was collected, with each fly completing at least one trial each of the bias and no bias conditions.

3.3.2 Results

Flies were given active control over the rotational velocity of the focus of expansion of the low contrast ER pattern, as well as the ERS pattern (stripe embedded at the FOE). The results of the closed-loop expansion-avoidance experiments are shown in Figure 3.3; the data are plotted using the organization as the previous results of §3.2.2.

[3] At the time this experiment was conducted, there was some concern about the validity of identical experiments, but with shorter trials, so these longer trials were performed with the alternating initial condition to assess this effect.

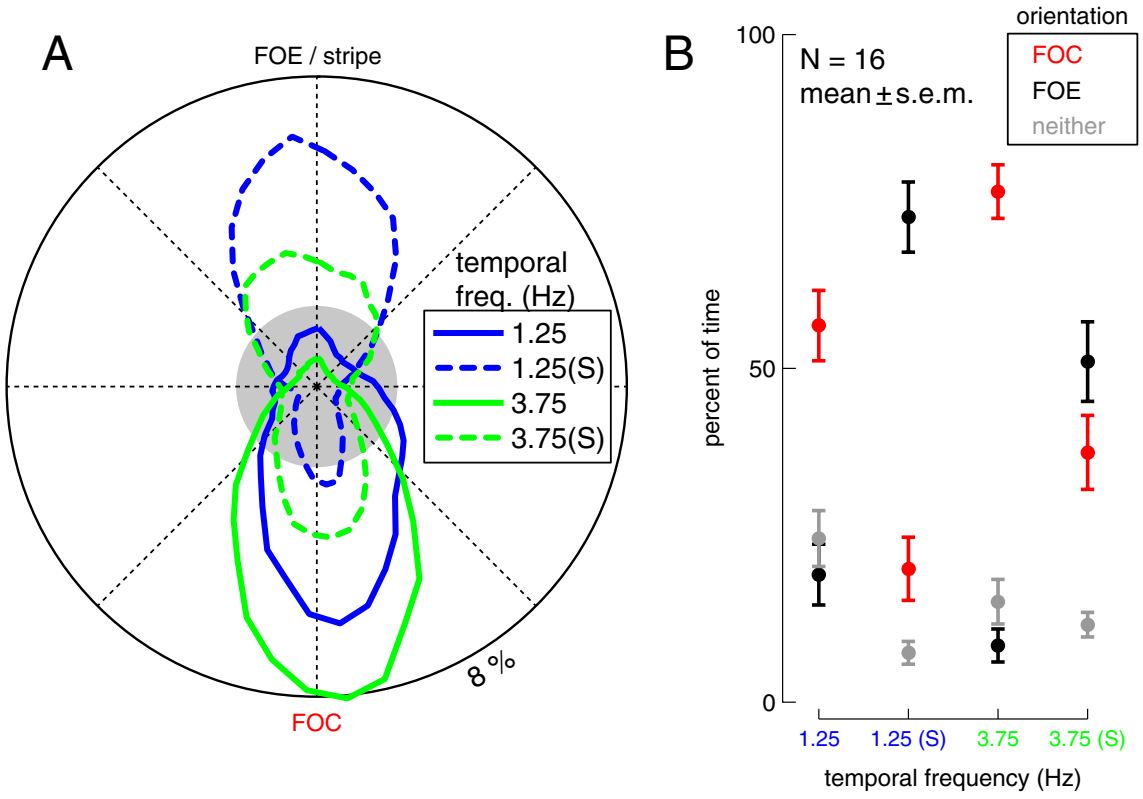

Figure 3.3. Tethered *Drosophila* exhibit fixation/tolerance of the focus of expansion while fixating a stripe. Plotting conventions follow those of Figure 3.2. (A) The polar mean orientation histograms for the ER and ERS patterns under closed-loop conditions. The pattern was expanded at two speeds presented with and without a dark 30° stripe at the FOE. The trials labeled with an (S), and plotted with dashed lines, correspond to the mean orientation of flies to the compound stimulus. (B) The mean fixation scores during these four conditions, reveal that the strong preference for the FOC is reduced when the stripe is present, and instead, the flies spend most of their time fixating the FOE even at the higher expansion rate.

The orientation histograms (Figure 3.3A) show the mean of each fly's orientation behavior, for all four trial types (but grouped across the two initial conditions). The orientation histogram confirms the previous findings, flies orient towards the FOC of the expansion-rotation pattern, and do so with a tighter distribution at the higher (3.75 Hz) expansion rate. Placing a stripe at the FOE significantly effects the orientation preference. In the ERS trials, the fixation scores (Figure 3.3A) show that flies fixate the FOE for longer than the FOC, at both temporal frequencies. It is clear that in response to the compound stimuli, especially at the higher expansion rate, the flies

exhibit behavior that appears bistable, both the FOE and FOC can be fixated for some period of time. Therefore, it is necessary to examine the effect of the initial condition on the behavior of the flies during the 90-second trial. How important is the first thing they see?

To examine the effect of the initially presented orientation of the pattern on the 'long-term' behavior, the percent of time that the flies orient towards the FOE and the FOC for each of the 4 treatments in Figure 3.3, is plotted as a time series in Figure 3.4, calculated using equation 2.9. To produce the data plotted in Figure 3.4, the fixation scores in every 5 consecutive sliding windows (either a 0 or 1 in each) is averaged, and then averaged again across repetitions. The effect of the initial orientation of the pattern (either the FOE or the FOC) becomes negligible after about 7 seconds, as the fixation score time series converge to the values averaged over the entire trial length. Therefore, it is reasonable to ignore the effect of the initial condition for experiments that are at least 40 seconds in length, although for much shorter experiments this effect can indeed be significant.

Earlier experiments had suggested an interaction effect with the 'pure' stripe-fixation trials that were interspersed with the closed-loop expansion-avoidance trials, whereby the inclusion of the stripe fixation trial yielded higher FOE tolerance. Therefore the orientation behavior of flies in the most interesting case from above, the slower expansion pattern with the stripe embedded at FOE, was tested during even longer, 6 minute trials. The fixation behavior was again scored using equation 2.9, and the results from every 5 consecutive sliding windows were averaged. The time-dependent fixation behavior (Figure 3.5) shows a slight enhancement of the FOE preference initially, followed by a sustained level of stripe fixation/FOE tolerance.

A final variation on this protocol was to test the long term fixation of the slow expansion ERS pattern while a time varying bias was added to the flies' turning response. The bias is used as a disturbance added to the flies' steering; the inability to compensate for such a bias would be an indication that the fixation behavior is rather fragile. The results of this experiment are shown in Figure 3.6; the data are plotted using the same organization as the previous results of §3.2.2. Comparing the behavior

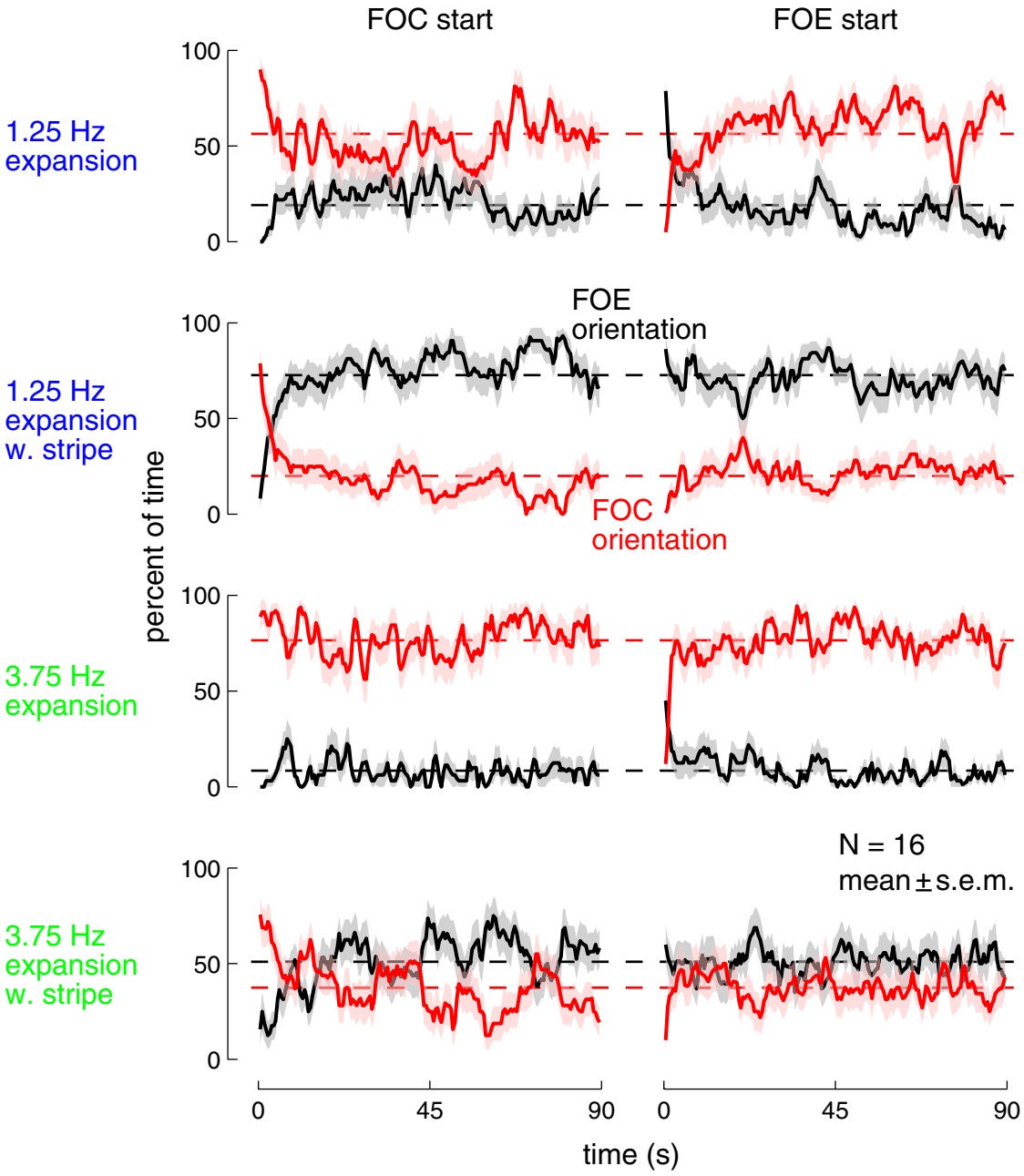

Figure 3.4. Effect of initial condition on the closed-loop behavior in the expansion-rotation-stripe paradigm. The fixation scores in the four conditions from Figure 3.3B are plotted as functions of time. The dashed red and black lines show the mean fixation scores (combining the 2 initial conditions), that are the data points shown in Figure 3.3B. These data suggest that within the first 7 seconds of the 90-second trial, the scores converge to their average values.

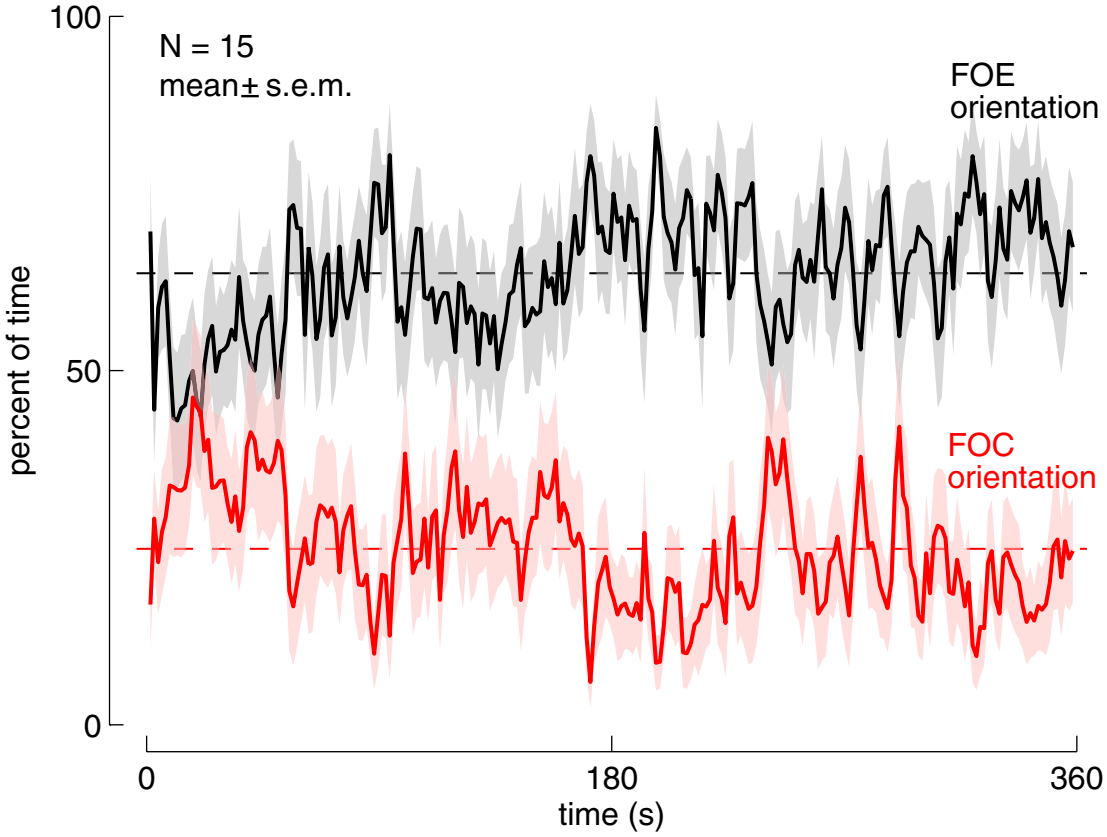

Figure 3.5. The longer term fixation behavior is assessed by conducting experiments of the low temporal frequency pattern with the stripe embedded in the FOE for a period of 6 minutes. The plot shows the fixation performance metric plotted over time. The FOE preference increases slightly at first and is then essentially constant.

during the trials with the bias applied to those with no bias, the orientation histograms (Figure 3.6A) reveal a looser distribution of stripe positions and the fixation scores (Figure 3.3B) show a reduction in the percent of FOE orientation. The effects of the small sample size used in this experiment can be seen in the result—the data set included 2 flies that oriented towards the FOC for longer than the mean response of §3.2.2. Thus the orientation histogram reveals a pronounced percent of time towards the FOC, and the mean fixation scores feature large error bars. Nonetheless, these data show that even with this very large bias, the FOE is still fixated approximately 50 % of the time.

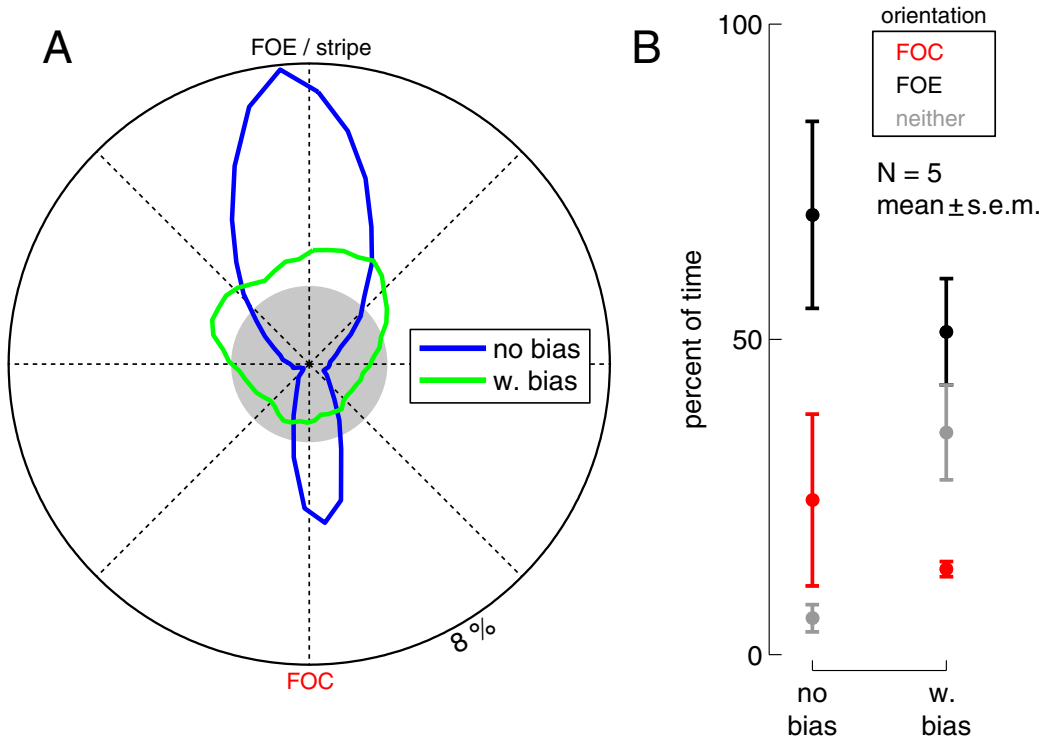

Figure 3.6. The closed-loop behavior of *Drosophila*, while controlling the orientation of the expansion-rotation-stripe pattern at the 1.25 Hz expansion rate, with and without the addition of a time-varying bias of $\pm 150°/s$. Plotting conventions follow those of Figure 3.3. Even with the addition of the large bias, the FOE tolerance/stripe fixation occurs approximately 50% of the time.

3.4 Compound stimuli II: Open-loop object motion superimposed on open-loop visual expansion

3.4.1 Experimental design

To further explore the interaction between the expansion-avoidance response and the stripe-fixation behavior, a laterally positioned, low contrast, expansion pattern was presented, while a 30° dark stripe was rotated around the fly at a constant angular speed. Constant speed rotation of a stripe around the fly is a technique that has been used to rapidly determine the position- and direction-dependent response to an attractive stimulus (Reichardt and Poggio, 1976; Heisenberg and Wolf, 1979). The compound stimuli used in this experiment allow a simple comparison of the response to the combined presentation and the open-loop responses to either pattern motion

Table 3.3. Experimental conditions for open-loop stripe motion and open-loop lateral expansion

Right expansion trial		Left expansion trial	
Expansion rate (Hz)	Stripe speed (°/s)	Expansion rate (Hz)	Stripe speed (°/s)
3.75	0	-3.75	0
3.75	-60	-3.75	60
3.75	60	-3.75	-60
3.75	-120	-3.75	120
3.75	120	-3.75	-120
1.25	0	-1.25	0
1.25	-60	-1.25	60
1.25	60	-1.25	-60
1.25	-120	-1.25	120
1.25	120	-1.25	-120
0	60	0	-60
0	120	0	-120
0	0		

presented independently. The experiment tested 2 expansion rates (temporal frequency of 1.25 and 3.75 Hz), with the expansion positioned laterally and from both sides, and rotations of the pattern at 60°/s and 120°/s in both directions. Additionally, the experimental series included trials where the lateral expansion was presented alone, and trials where the stripe was rotated, while the low contrast striped pattern remained stationary 'behind' the stripe. The experiment was designed to use the 'flip and average' technique discussed in §2.2.6. Table 3.3 lists the 25 experimental conditions used in this experiment, where every row shows the pair of trials combined in the analysis (after an inspection to ensure that the data were indeed nearly symmetric). The open-loop experiments lasted 3 seconds for the faster rotating stripe, and 6 seconds for the slower one, and were interspersed with a 5-second closed-loop stripe fixation trial (same pattern with the expansion turned off, stripe position determined in closed loop). The 25 trial types were presented in random block trials. In total, 15 flies completed between 3 and 5 repetitions of this protocol, each repetition lasted approximately 4 minutes.

3.4.2 Results

The response to the laterally-positioned expansion (presented in isolation) is shown in Figure 3.7. As expected, flies turn away from the expansion;, in this grouped case the turns are counterclockwise, away from the FOE on the animals' right. The mean data are fit with a single exponential function of the form $f(t) = \alpha(1 - \exp(-t/\beta))$; this fit is plotted as the black line in Figure 3.7. The exponential fit to the turning response, agrees quite well with the mean data. This fit is only used to compare to the responses with the compound stimuli in further analysis (Figures 3.8 and 3.9), and not to make any claims about the nature of the responses.[4] It is noteworthy that the flies' mean response to low contrast, slow expansion shows a remarkable level of phase locking to the discrete (single frame) advances of the pattern, as emphasized by the gray lines in Figure 3.7.

The mean of the response time series to the compound stimuli are presented in Figure 3.8. The time axis has been scaled so that the 3 and 6 second trials are easily comparable. The center row shows (in green) the position of the stripe during the experiment—at the start of the trial the stripe is behind the fly and then it rotates a full 360° around the fly. Because the stripe rotates at constant speed, the time axis also specifies the position of the stripe. As the stripe rotates from the rear of the display in the clockwise direction, the response to the stripe motion is small and slightly increases as the flies attempt a small turn towards the stripe while it is on their left. As the stripe nears the midline, the mean response changes sign, as the flies attempt to now turn clockwise to follow the stripe. The response is largest when the stripe is in front of the fly and moving progressively on the retina. Note that the mean response changes sign before the stripe actually crosses the midline, suggesting that the flies implement a strategy whereby they 'anticipate' the stripe. In the top 2 rows of Figure 3.8, the stripe rotates in the opposite direction as the front-field portion of the expansion stimulus (and with the rear field expansion); in the bottom 2 rows, the opposite occurs—the stripe rotates with the front field motion and against the rear

[4] In other words, the specific values of α and β are not particularly important.

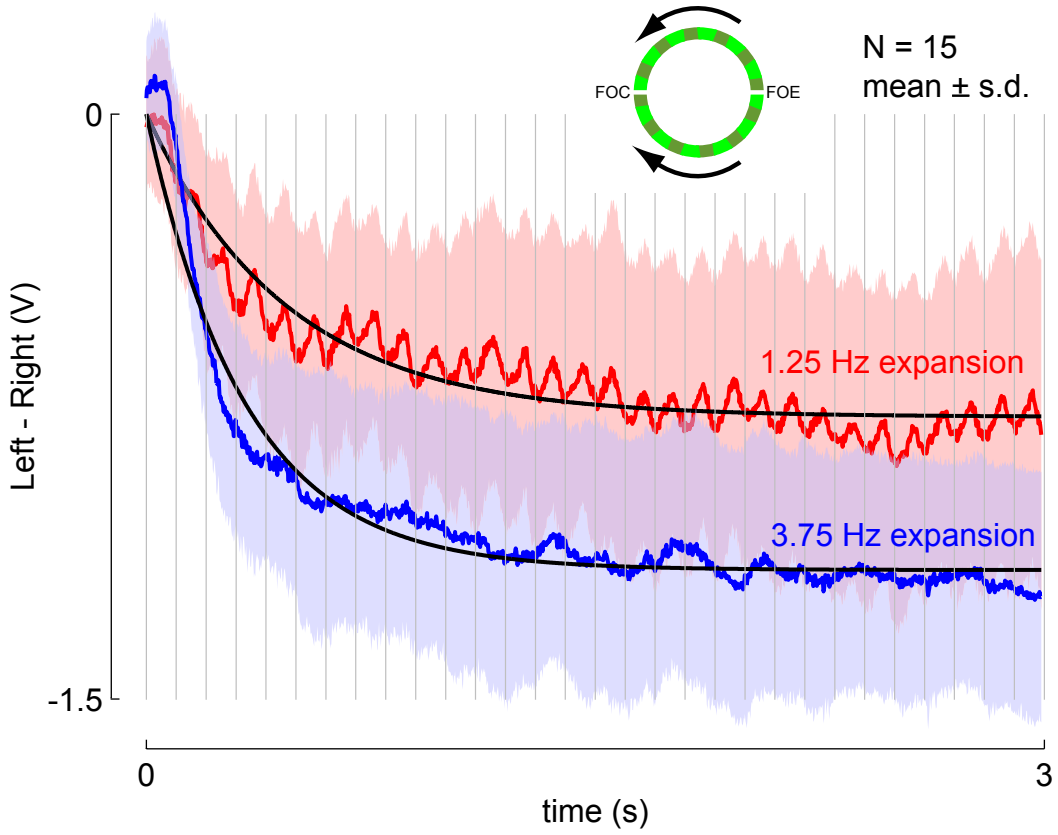

Figure 3.7. Open-loop turning response to lateral expansion (presented from right-to-left), for two different rates of expansion. The mean (± s.d.) turning response, shows that flies will produce a sustained turn away from a laterally positioned (low contrast) focus of expansion, and turn with larger amplitude away from the stronger expansion stimulus (of the two tested). The black lines show the result of an exponential fit (constrained to pass through 0) to the data. This fit is used for comparison with the subsequent results. At the slower expansion rate, the data show a remarkable level of synchronicity with the advances of the pattern. The 1.25 Hz expansion corresponds to 10 frames per second, the gray lines mark the times at which the pattern was updated with a one frame advance.

field motion (we shall refer to the first case as FF^- and the second as FF^+). To aid the comparison of the individual responses, along with the averaged response of the fly in each of the compound stimulus trials (in blue), each plot shows the response to the stripe, presented in the absence of expansion (in red), and the exponential fit to the expansion presented in the absence of the stripe (in black). It can generally be seen that the responses reveal a hybrid strategy, in some cases the mean response is more stripe-like, while at other times it is more expansion-like, and occasionally

looks like a nearly perfect compromise. To make these observations more concrete, the residuals—remaining when the mean response to the compound stimuli is subtracted from the response to either stimuli presented alone—are plotted in Figure 3.9.

The residuals plot (Figure 3.9) is to be interpreted as follows: when either the black line ($\text{resp}_{compound} - \text{resp}_{expansion}$) or the red line ($\text{resp}_{compound} - \text{resp}_{stripe}$) is close to zero, the corresponding response to the individual stimulus is close to the response to the compound stimulus. For example, in the first 3 seconds of (a) and (c), the black line is nearly zero, indicating that $\text{resp}_{compound}$ is nearly identical to $\text{resp}_{expansion}$. At other times, as in the second half of the plot in (b), or the last part of (h), when the residual lines are roughly equidistant from zero, the mean behavior can be interpreted as compromising between the two stimuli, not being closer to either one. At the lower expansion rate (second and fourth rows), the flies exhibit more of a stripe-following response than in the higher expansion cases, as evidenced by the red curves being closer to zero. Clearly there is a difference in the shape of the responses curves for the FF^- and FF^+ conditions. In the FF^- case, the flies respond as if only expansion were presented during the start of the trial, and then right before the stripe crosses the midline, the flies transition to more of a stripe-only response. In the slower expansion trials (c, d) the stripe-only residual is nearly zero; in the faster expansion cases (a,b) flies seem to compromise between the two responses (and almost produce the stripe-only response for the slowly moving stripe). In the FF^+ case, the flies compound response is dominated by the expansion-only response. However, when the stripe is in the region where it would (if presented alone) produce the largest response (to the left of center), the mean response is actually a larger turn than would be produced in the expansion-only case. This is evidenced by the drop in the black curve and the rise in the red curve that can be seen in all four cases (g, h, i, j), but is especially prominent in the cases where the stripe is moving faster.

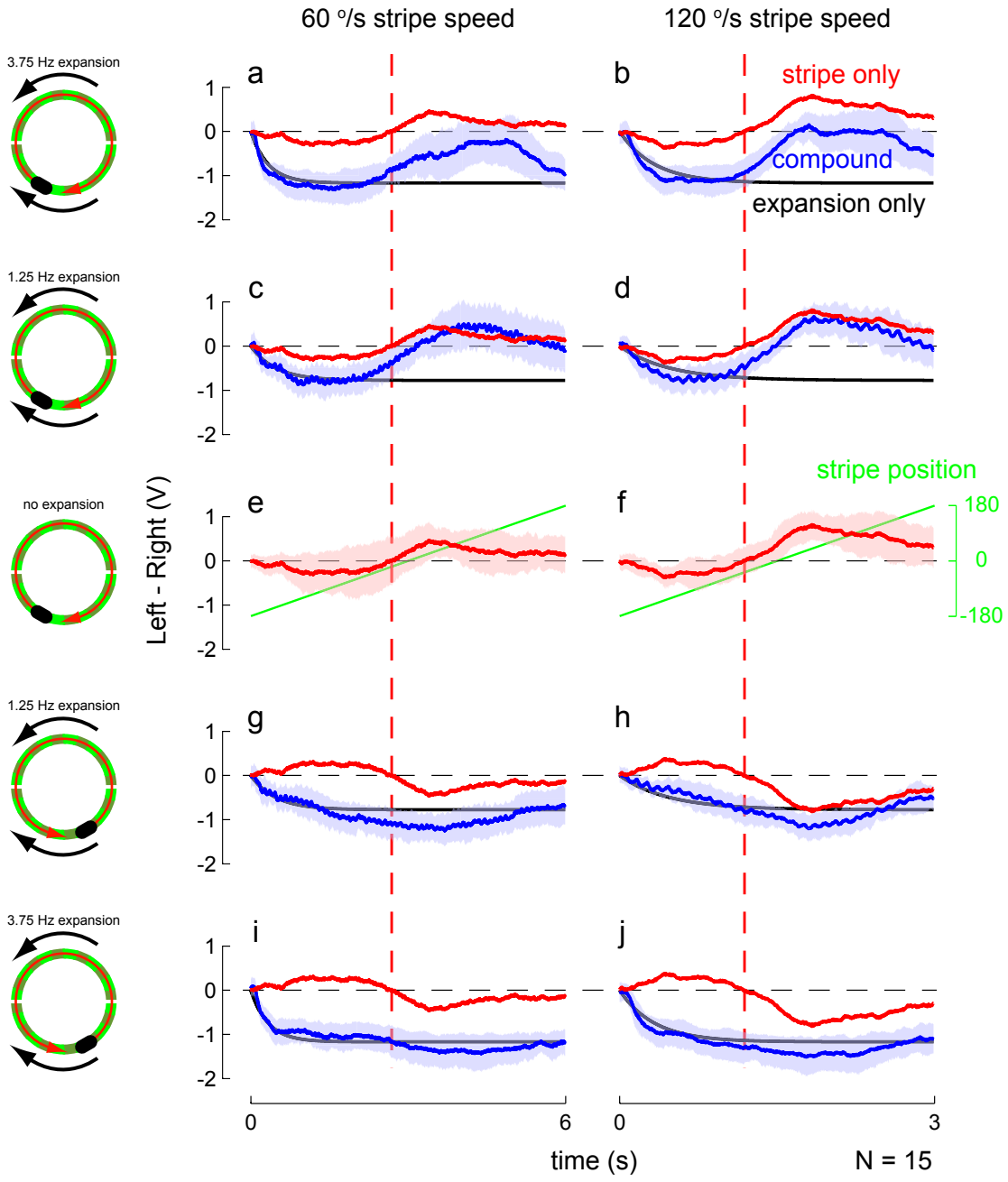

Figure 3.8. Open-loop turning response to compound stimulus consisting of a laterally positioned focus of expansion and a stripe rotating at constant velocity. In the center row, (e, f) the response to the stripe rotating on a stationary background is shown. In the other plots, the response to the compound stimulus is shown in blue, while the response to the stripe is plotted in red (reproduced from e,f), and the exponential fit to the response to the expansion-only stimulus is plotted in black. The dashed red lines show the locations of the zero crossing of the stripe response, which precede the time when the stripe actually crosses the midline.

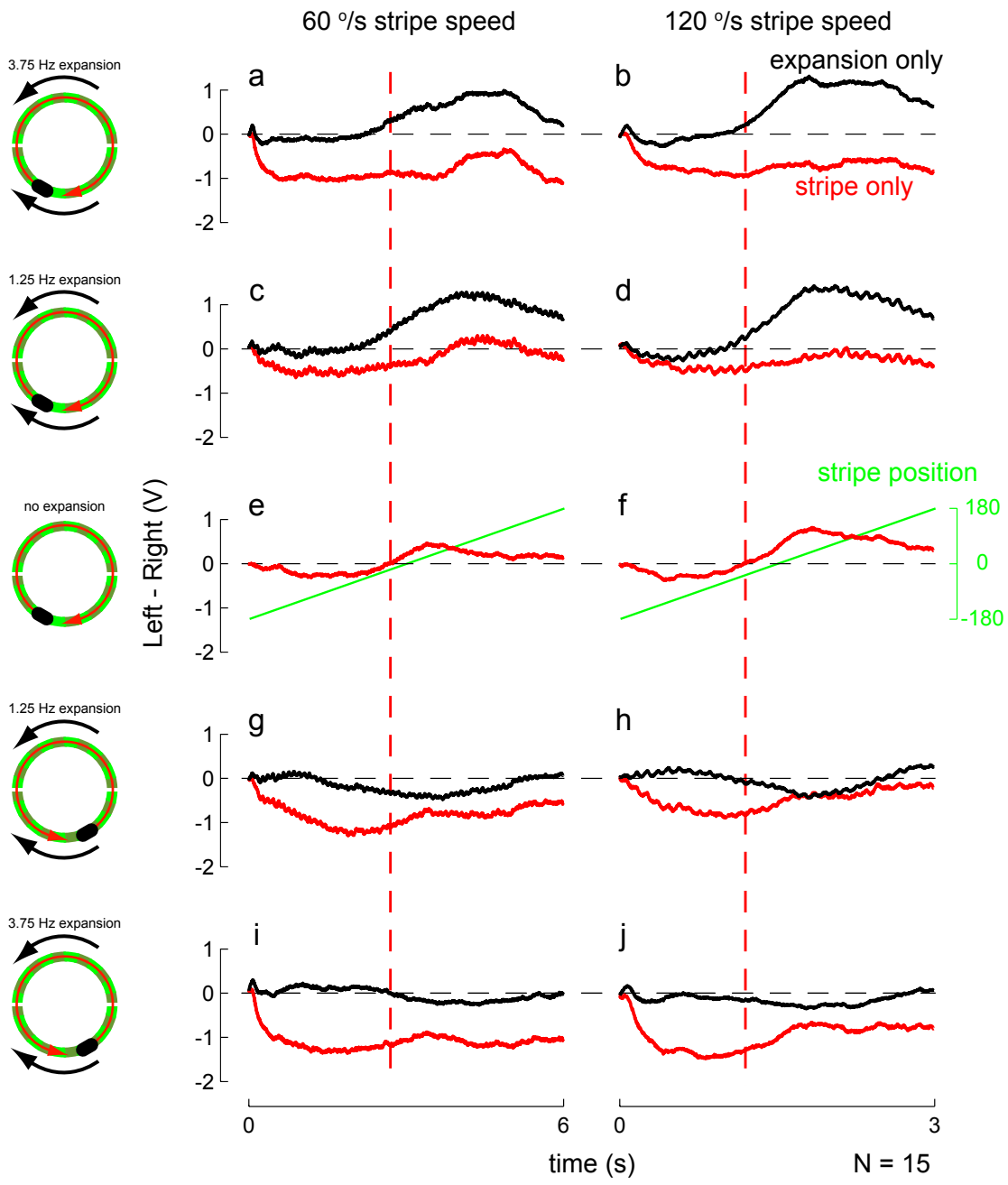

Figure 3.9. Residuals of the open-loop turning response to the compound stimuli. The (signed) difference between the mean compound stimulus response and the responses to either stimulus presented in isolation is shown to provide insight into this complex phenomenology. The trial types are organized to correspond to the data presented in 3.8. The 'distance' to the expansion-only response is shown in black, and the difference with the stripe-only response is in red. Small values for one of the residuals indicate that the response to the compound stimulus is quite close to the response obtained when that stimulus was presented alone.

3.5 Compound stimuli III: Closed-loop object orientation superimposed on open-loop visual expansion

3.5.1 Experimental design

The results of the previous section show that while presented with a considerably aversive stimulus (strong lateral expansion), the turning behavior of *Drosophila* is influenced by the position and direction of motion of a prominent vertical object. However, can they fixate this object in the face of such a strong stimulus? In a further experimental manipulation, the fly is given closed-loop control of the rotational velocity of the 300° dark stripe, while the low-contrast laterally centered expansion occurs in open-loop at a set speed. The experiment tested 2 expansion rates (temporal frequency of 1.25 and 3.75 Hz) and a no-expansion case, with the FOE positioned laterally and from both sides, while the fly controls the position of the stripe in closed-loop. Each of the 5 closed-loop trials was presented for 40 seconds in random block trials. Interspersed with the closed-loop trials were 20-second open-loop trials whose results are not presented. In total, 9 flies completed between 2 and 4 repetitions of this protocol, each repetition lasting 5 minutes.

3.5.2 Results

In the results presented in Figure 3.10, flies had active control over the rotational velocity of a 30° stripe, while a laterally centered expansion occurs in open-loop. For these experiments, the orientation histograms for each treatment and the corresponding distributions of the flies' steering responses (the left – right wingbeat amplitudes) are shown. The distributions plotted in red, correspond to the data from the pure stripe fixation trials—the rate of expansion was 0. As expected, the mean distribution of stripe positions shows that the stripe is fixated frontally with high probability. Also the distribution of steering responses is tightly distributed around 0 V; the flies only produce occasional, small turns of alternating sign to keep the stripe in front. The results in Figure 3.10 suggest that the lateral expansion acts much like a turning bias. When expansion is presented from the right (blue and green curves), the flies (on

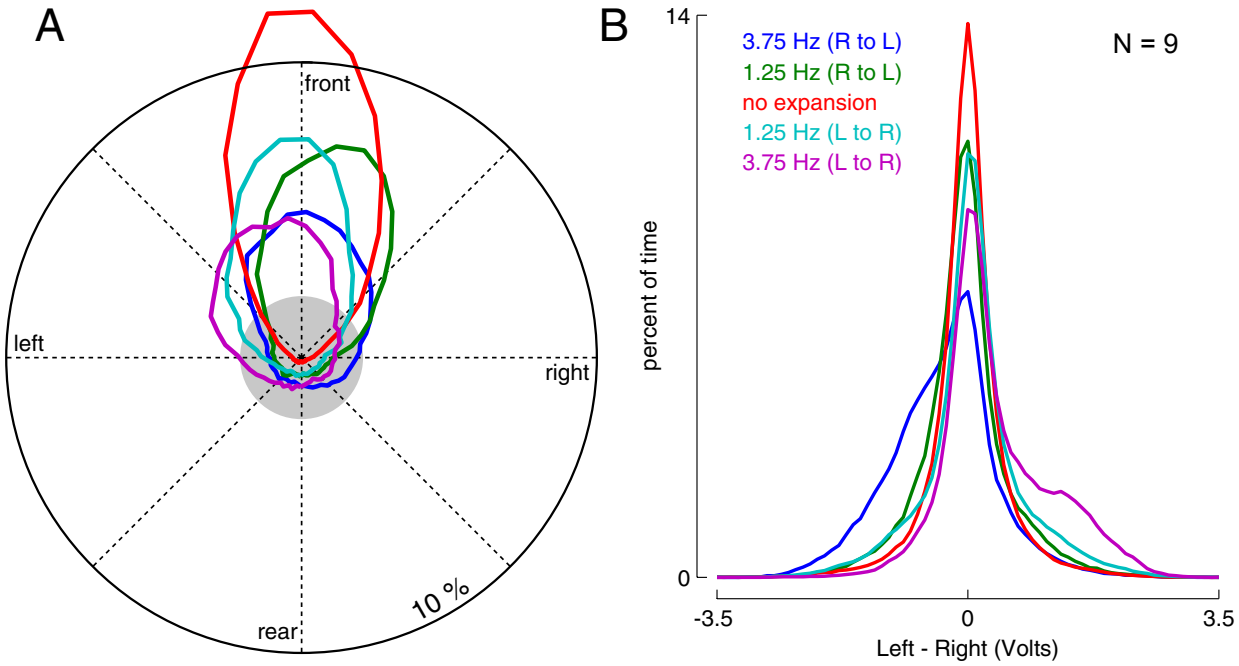

Figure 3.10. Flies are able to orient towards a stripe in the face of a constant lateral expansion disturbance. (A) The orientation histograms (mean of each fly's orientation histogram) show that frontal fixation of the stripe is tightest when no expansion is presented. For the trials where expansion is presented, the corresponding orientation distributions flatten and shift slightly to one side, indicating that the position of the stripe is still controlled in front of the fly for much of the time, but is not as tightly regulated. (B) The distribution (averaged over 9 flies) of all instantaneous turning (the left – right wingbeat amplitudes), as measured in the presence of the 5 treatments. When lateral expansion is presented, there is a shift away from the roughly symmetric distribution obtained in the no-expansion case (red curve). The direction of the shift is consistent with the fly's attempt to both fixate the stripe and turn away from the presented expansion.

average) fixate the stripe frontally, but the turning distribution shows a shift towards a negative ΔWBA value, indicating that (on average) the flies turn away from the expansion. Similarly, when the expansion emanates from the left (cyan and magenta curves), the distribution of turning response is skewed towards positive ΔWBA values, indicating that flies turn away from the expansion by generating more clockwise torque in response to the left-to-right expansion. The orientation histograms show a similarly biased distribution—when the expansion emanates from the right, the blue and green curves show greater probability on the right, and for the expansion emanating from

the left, the cyan and magenta curves show a leftward bias in probability. The shift is in the expected direction—as the flies attempt to turn away from the FOE, the negative feedback causes the stripe to move in the opposite direction, towards the FOE.

A more complete presentation of the data in Figure 3.10 is provided by considering a two-dimensional histogram—a tabulation of the distribution of the flies' turning responses at each position of the pattern. Two versions of this histogram have been computed and are presented in Figure 3.11. The histograms in the left column of Figure 3.11 show proper probability distributions, the probability that a sample (of stripe position and turning response) will reside in each bin is assigned a color value, that is related to percentage by the scale bar at the top of Figure 3.11. The histograms in Figure 3.10 can be obtained from the 2D histograms by integrating over one dimension—the orientation histograms are recovered by integrating over ΔWBA, and the ΔWBA distributions are recovered by integrating over position. In the pure stripe fixation case (third row) the position distribution is tightly clustered around the origin, and the orientation distributions are shifted slightly towards the focus of expansion, in the trials where lateral expansion is presented (as is seen in the orientation histograms of Figure 3.10A). In these data, it can be difficult to see the relationship between stripe position and turning response because the animals are in behavioral closed loop, and thus, most of the time, the stripe is very near the midline and the flies engage in small-amplitude turns. Therefore, the occurrence frequency in bins near the origin is very large, obscuring the quick, but important corrective responses that are produced in response to stripe positions that are away from the front. To address this problem, the 2D histograms on the right of Figure 3.11 show the result of normalizing the original distribution data such that the distribution at each position of the pattern (each column of the histogram) sums to 1/48 of 100% (there are 48 position bins). Thus the rare, but presumably important large turns made in response to the stripe at positions away from the midline are emphasized.

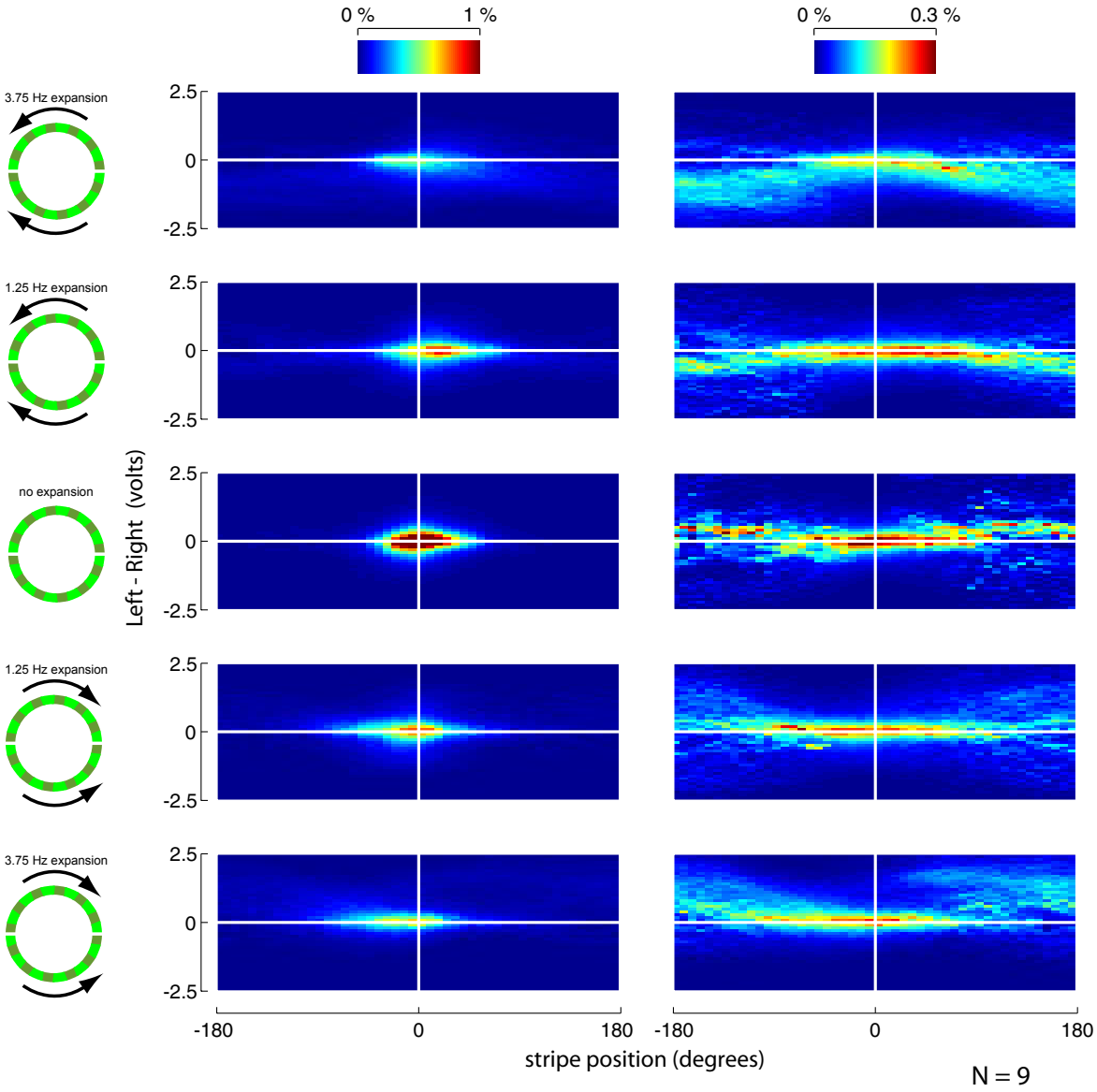

Figure 3.11. The relationship between the position of the stripe and the flies' turning response is quantified as a 2D histogram, showing the distribution of instantaneous turning (left – right, or ΔWBA) at each position of the stripe. Color is used to represent the percentage of recorded samples that are grouped into each bin; color axis scale bars (for each column) are at the top. Two versions of the same distributions are shown. On the left the histograms represent the true frequency counts of the occurrence of a particular turn amplitude while the pattern is at a particular position. The histograms on the right show these same distributions, but they have been normalized for each position of the pattern such that each column accounts for (1/48)% of the total probability. In the normalized histograms it is possible to resolve the response of flies to positions of the stripe that are only rarely encountered.

3.6 Discussion

3.6.1 Contrast dependence of object-orientation and expansion-avoidance behavior

In general, the absolute luminance of regions of the visual world are of little interest to the fly's visual system. It is the difference between the luminance values of objects, the contrast, that is locally encoded by the photoreceptors and the lamina before entering the motion detecting pathway (Laughlin, 1994). Furthermore, identified motion-sensitive interneurons (in the lobula plate of the blowfly *Calliphora*) show a saturating response to motion stimuli of increasing contrast (Egelhaaf and Borst, 1989). This locally applied saturation of the contrast signal has been shown to significantly improve the accuracy of velocity estimation by models of fly Elementary Motion Detectors (EMDs; Dror et al., 2001). The performed experiments were motivated by the presumed need of flies to perform similar navigation tasks and be able to distinguish prominent objects in various environments under a variety of light levels. The results presented show that for most tested combinations of stripe and background luminance, the object-orientation performance of *Drosophila* is essentially constant. The closed-loop expansion-avoidance behavior showed a similar invariance to the 4 tested contrast levels. These findings are entirely consistent with the notion that a contrast saturation is applied to the sampled visual world, prior to the motion processing system. This saturating non-linearity enhances the contrast present in the stimulus, such that at the level of the EMDs, the stimuli are similar. However, this enhancement is not without limits: when little contrast is available in a bright scene, the motion energy caused by the moving edges that define the stripe is greatly reduced, and phase-locked turning is seen in response to discrete advances of the expansion stimulus (Figure 3.7).

Our results are not without precedent. Heisenberg and Buchner (1977) recorded the closed-loop orientation behavior of tethered *Drosophila* towards a single stripe, while varying the background luminance. Their findings suggest that for increasing background luminance the frontal fixation of the stripe improves (based on the

percent of the histogram contained in the 30° band centered in front of the fly, a metric for orientation 'tightness' that is very similar to the HWM). The results presented here (Figure 3.1C) do not demonstrate this effect—the HWMs for all conditions corresponding to stripes that are darker than the background are essentially equal. The simple reason for this disparity is that in the result of Heisenberg and Buchner (1977), the major improvement in the orientation behavior occurs between a background intensity of approximately 0.01 cd m^{-2} and a background intensity that is 10, 100, and 1000 times higher. However, there is only a small difference between the orientation towards a dark stripe superimposed on the two brightest backgrounds tested (approximately 1 cd m^{-2} and 10 cd m^{-2}). The lowest (non-zero) background intensity level that we tested has a luminance of approximately 10 cd m^{-2}, which corresponds to the brightest background in the original experiment. To repeat the experiment of Heisenberg and Buchner (1977) would require implementing dimmer background intensity levels (or using a neutral density filter).

In other related work, Heisenberg and Wolf (1979) show a surprising result—in open-loop experiments with tethered *Drosophila*, a black stripe on a white background and white stripe on a black background elicit responses of opposite polarity, suggesting that flies would orient towards the dark stripe on a bright background and away from a bright stripe on a dark background. Our results confirm that, on average, the orientation histograms of flies presented with stripes that are darker than the background (negative stripe contrast) have a higher HWM than the histograms corresponding to positive stripe contrast patterns. However, in all cases we observe that for much of the trials, flies orient towards the stripe. Of course, when the data are presented as histograms, we collapse the temporal dimension, so this finding can only be inferred from the HWM data shown in Figure 3.1. It is worth noting that bouts of 'anti-fixation' are occasionally observed (as in lower orientation sequence of Figure 3.1A) during positive stripe contrast trials. A large part of the seeming discrepancy between our results and those of Heisenberg and Wolf (1979), owes to the differences in the way these experiments were conducted. Our experiments were conducted under closed loop, where the instantaneous speeds of the pattern are often quite high. In the

open-loop experiment of Heisenberg and Wolf (1979), the stripe was spun around the fly at a very slow rate (20 seconds per revolution). Further, much of the difference in orientation towards the two stimuli is seen via the turning direction implied by a train of torque spikes—short bursts of torque in one direction, thought to be the tethered flight analog of free-flight body saccades. In high-gain, closed-loop, object-orientation experiments, torque spikes are almost entirely absent from the behaviors we record. Since the open-loop turning responses of flies are dependent on the speed, position, and direction of the stripe (Reichardt and Poggio, 1976; Heisenberg and Wolf, 1979), it is not surprising that open-loop results obtained for slow, unidirectional rotations of a stripe do not predict the behavior of flies in high-gain, closed-loop conditions.

3.6.2 Compound stimuli I: High-contrast object at the FOE

The results of §3.3 confirm the first hypothesis of §1.11: in the presence of a prominent vertical object to direct flight, *Drosophila* tolerate a level of image expansion that would otherwise induce strong avoidance. These results suggest that the object-orientation response may serve an important role in the control of translatory flight by *Drosophila*. By inhibiting the expansion-avoidance response, orientation towards a stationary object guarantees straight flight, a strategy that should serve to regulate other visually controlled behaviors and enhance information from other sensory systems.

It is not surprising that flies exhibit a bistable orientation preference while controlling the rotational velocity of the ERS pattern, the compound stimulus used in the experiments of §3.3. This pattern contains two attractive stimuli that are separated by 180°. The expansion-contraction pattern is a large-field stimulus that excites nearly all of the eye, thus there is sufficient 'signal' for the animal to respond to the pattern in virtually any orientation (as is clear from the position-dependent response in Figure 1.4E). However, the high-contrast stripe, which is a small field stimulus, is not visible when it is behind the fly, and generates only a small response when it is visible by more than 90° away from the midline (Figure 3.8e,f). Since the stripe is embedded in the FOE, it is highly likely that in many cases the fly might fixate the FOC of the

pattern and never encounter the stripe (since it would remain directly behind the fly). This scenario was the concern that the longer term experiments and the repeated trials with different initial conditions sought to address. The results summarized in Figures 3.4 and 3.5, show that the effect of the initial condition persists for no more than 7 seconds into the trial, and that there is an initial improvement in FOE orientation after about 40 seconds; beyond this time, the mean orientation behavior is achieved and sustained. There is no evidence for any learning or habituation occurring over the 6-minute trial, which is a sufficient period of time for flies to show learning in the visual pattern conditioning protocol (Guo and Guo, 2005; Liu et al., 2006). The addition of a strong time-varying bias to the 6-minute experiments with closed-loop control over the compound ERS stimulus, confirms that the stripe fixation is vigorous. However, since the expansion component of the pattern is created by motion, it is possible that the strong rotatory bias would render the perception of the expansion stimuli to be weaker.

3.6.3 Open- and closed-loop variations on the theme, compound stimuli II and III

The compound stimuli tested in §3.4 and §3.5, were designed to test the interaction between two independent behaviors that are robustly exhibited by tethered *Drosophila*. The combined fixation with expansion patterns present the flies with laboratory idealizations of circumstances that have some intuitive reality, such as the case when a fly is flying towards an object and must tolerate some significant amount of frontal expansion (which occurs precisely because she is flying towards that object), or when a fly is flying towards a prominent object while some other objects or surfaces loom on another part of the retina.

The stripe and expansion interaction experiments can also be thought of as a type of sensor fusion experiment, though confined to a single sensory modality. The notion that the animal must fuse two disparate types of visually processed information is strengthened by the initial observation that expansion avoidance and stripe fixation

serve very different purposes. Thus it is not surprising that at times one dominates the other, and at times a compromise is struck between the two responses. One important note, these kinds of experiments are not simple, the interactions can be complex and it is important to characterize the response to each modality in isolation. Further the complexities of comparing open- and closed-loop versions of similar experiments necessitated some interesting analysis.

In the experimental treatment that combined open-loop stripe rotation with open-loop expansion (§3.4), tethered *Drosophila* respond with a more stripe-like response when the stripe motion is directed against the expansion motion in the front hemifield (FF^- condition). In these cases (top two rows of Figure 3.8), when the stripe is in front of the fly (the region where the stripe responses are largest), the stripe produces a strong relative motion cue against the background. The fact that this stripe 'pop out' yields a turning response that is stripe-like is consistent with previous results (Kimmerle et al., 1997, 2000), in which female *Lucilia* were shown to exclusively orient towards objects that were simulated to be nearby, that is the motion of the objects was faster than the 'distant' background. In the FF^+ conditions (bottom two rows of Figure 3.8), the stripe response and the expansion response are in favor of a turn in the same direction. In this case the mean response of the flies is a larger turn than is produced in response to either stimulus presented in isolation. These findings suggest that even with the strong expansion, the flies also respond to the stripe, seemingly able to respond to either stimulus or both, depending on their strength and their relative configuration.

In the experimental treatment that combined closed-loop object-orientation with open-loop lateral expansion (§3.5), tethered *Drosophila* respond to the compound stimulus as if it were a stripe-fixation paradigm with the addition of a rotatory bias. Stripe-fixation is exhibited, but with a bias towards the side from which the expansion emanates. The expansion-avoidance response causes the animal to turn away from the FOE, perturbing the stripe towards the FOE's side, at which point the stripe-fixation response would presumably bring the stripe back to the center. Thus it is expected that the stripe would mostly reside between the FOE and the midline. Further insight

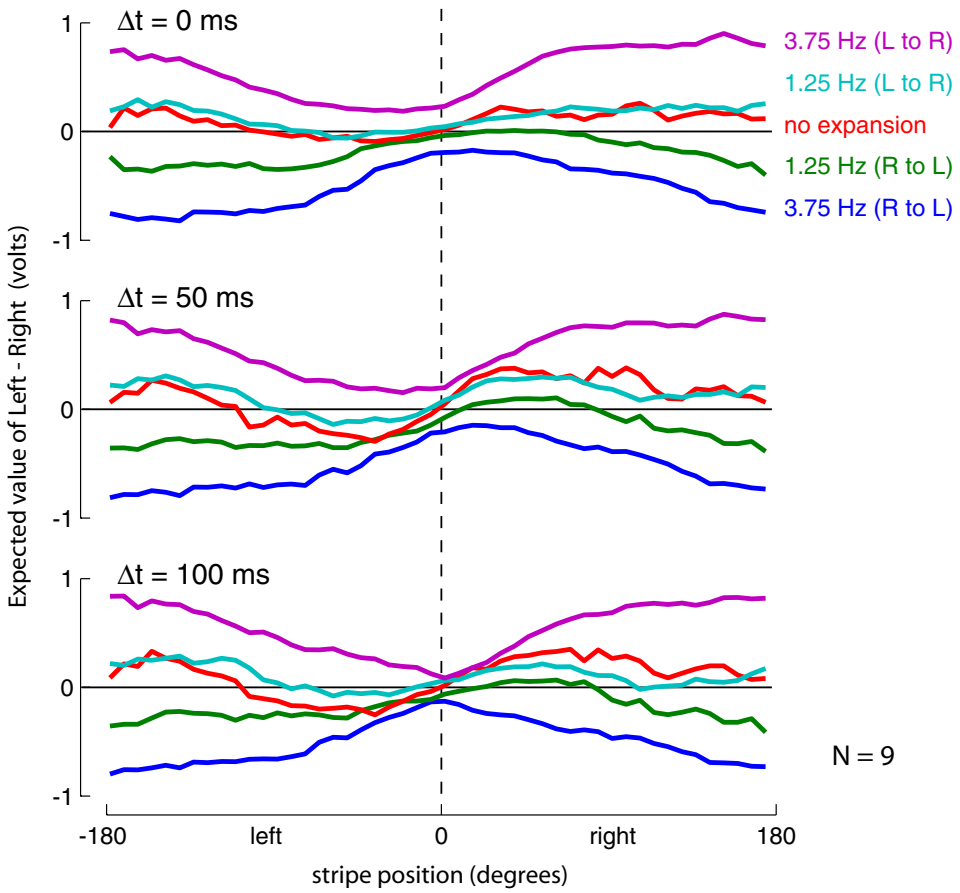

Figure 3.12. A useful comparison between the open-loop(§3.4) and closed-loop (§3.5) versions of a similar experiment can be obtained by computing the expected value of the turning response at each position of the stripe. The Δt value on each of the four plots indicates the amount of time that the turning (ΔWBA) response was advanced relative to the object position. The expected values of the response show the shift in turn magnitude that is appropriate for each trial (e.g., for the blue and green curves, $\Delta\text{WBA} < 0$). Also much of the position-dependent shape as seen in the open loop trials (Figure 3.8) is also recovered.

into this behavioral pattern can be obtained by comparing these data to the responses of the open-loop experiment data presented in §3.4.

The histograms of Figure 3.11 provide an opportunity to address the relationship between the open-loop (§3.4) and closed-loop (§3.5) versions of a similar experiment. Since the histograms capture the turning behavior of the fly in response to each position of the stripe, it is possible to compute the position-dependent mean response, the exact quantity shown in Figure 3.8. From either version of the histograms, it is a simple matter to calculate the expected value of the turning response at each

position of the stripe. At each position the turning probabilities are normalized so that they sum to 1, the expected value is then computed as the sum of all of the products of the probability at each ΔWBA bin with the ΔWBA value of that bin center ΔWBA. The results of this calculation on the histograms of Figure 3.11 are shown in Figure 3.12. The response of flies to stripe motion is not instantaneous, as there is some delay between visual motion and a motor response. Heisenberg and Wolf (1988) show this delay to be in the range of 50–100 ms; tethered *Drosophila* respond to the displacement of a bar with a latency of 50 ms, and this behavior of flies will reflect whether or not a feedback loop is closed within 100 ms. To account for this time delay, the expected value of a time-advanced version of the turning response (ΔWBA) relative to the object position is computed for time delays, Δt, of 50 and 100 ms. The expected value of the turning response at the 50 and 100 ms time delay are probably the most appropriate data set for comparison with the open-loop experiments of §3.4. These plots show many similar features. In fact, the expected values (with $\Delta t = 50$ ms) of the turning response curves look remarkably similar to the open-loop traces in a–d of Figure 3.8. When the stripe is behind the flies, the response is a turn away from expansion (ΔWBA < 0 for the right FOE, blue and green traces, and ΔWBA > 0 for the left FOE, cyan and magenta traces), but when the stripe is in the area where the open-loop data show the most stripe-like response, in the frontal quadrant towards the FOE, the responses are close to 0 for the faster expansion cases, and actually show a sign change for the slower expansion case, indicating that the flies orient towards the stripe.

These experiments should not, a priori, be comparable since the response of a fly to a stripe depends not only on the stripe's position, but also on the speed and direction of motion, and on these quantities for some short period into the past. The expected value of the turning response should therefore be dependent on more then one variable, but there are simply not enough data in this set to further condition this calculation. The fact that they are comparable, and show strong similarity to the open-loop trials in which the response to the compound stimulus is much more stripe-like suggests that in the closed-loop experiments of §3.5, the stripe is more 'salient' and controls

the behavior much more so than in the open-loop trials. This is consistent with the results that the stripe remains fixated, but with a bias towards the FOE. However, this finding is at odds with the previous results of Heisenberg and Wolf (1988, Figure 4) that show that the response to a moving stripe is fundamentally different under open- and closed-loop conditions. This difference is attributed to the difference in methodology; here the open-loop responses are compared with the position-dependent expected value of the stripe-fixation response during closed-loop trials. In the previous study the displacements during a closed-loop trial were replayed to flies in open-loop and the responses were found to diverge. The currently-employed method allows a more sensible comparison of open- and closed-loop experiments, when the stimulus conditions are roughly the same, the responses are also roughly the same, independent of the 'loop status.' An additional result is that the turning response values in Figure 3.12 are somewhat smaller than those observed in the related open-loop experiment. This finding is consistent with the idea that much of fly steering is actually quite subtle, and flies steer with larger turns in open-loop experiments (in which they are unable to affect the stimulus), than in the counterpart closed-loop trials which are a better approximation of real flight.

3.6.4 Synchronicity of open-loop turning response to low contrast expansion

The level of phase-locking between the turning response and the discrete one-frame advances of the expansion pattern shown in Figure 3.7 have thus far only been seen for the slow expansion speed and low contrast pattern. This response is almost certainly a motor readout of the activity of some gain control mechanism that is acting to produce large behavioral responses to what must be a very weak signal. The stimulus induces a negative turn, so the up-peaks correspond to decays in the turning response. The increase in the turns (towards more negative values) are in response to the frame advance represented by the gray line—revealing a delay of approximately 60 ms from stimulus advance to the start of the motor response, and roughly 100 ms to the peak

motor response. These observations are useful for the identification of parameters in the motion processing and gain-control pathways. A similar result has perhaps been shown in the response to expansion restricted to a small region in front and behind the fly (Tammero et al., 2004, Figure 3B). It is not clear if these repeatable ripples in this response are an example of the same phenomena, since the stimulus in these experiments consisted of pattern motion at a very high temporal frequency (10 Hz). The motion detector example data of §6.2 reveal two types of phase locking that may be transduced as motor output. The phase-locked ripple seen in Figure 3.7 is an example of the faster modulations that follow the discrete advances of the stimulus, which can only occur when the motion detectors are being weekly driven.

Chapter 4

Spatial and Temporal Dissection of the Expansion-Avoidance Behavior

The desire to integrate the results of Tammero et al. (2004) with the emerging picture of *Drosophila*'s flight control system has motivated much of the work in this thesis. This chapter documents further manipulations of the stimuli that elicit the robust expansion-avoidance response in tethered *Drosophila*. The experiments pursued in this effort seek to test the second and fifth hypotheses of §1.11: that either the stimuli used in the original experiments of Tammero et al. (2004) are somehow too strong, or that the crude approximation of a real translatory optic flow field does not induce appropriate flight responses. As the expansion-avoidance paradigm has only recently been established, there is little in the literature aside from Tammero's body of work (2002b; 2002a; 2004) to provide context for these experiments. As discussed in §1.8, the literature contains a few significant results from the free flight behaviors of flying insects, but does not contain any explanations of the visual control of translatory motion that are suitable for, e.g., a model of insect flight or a robotic implementation.

The forward-flight paradox stems from tethered flight results that fail to cohere with intuition and free-flight results. One approach would be to abandon tethered flight experiments altogether. However, we believe that the tethered flight preparation allows a tremendous opportunity to assay an intact sensorimotor system with high degree of control over the animal's sensory experience. Careful use of the method must result in a better understanding of *Drosophila*'s flight control system.

The experiments in this chapter were conducted in the same cylindrical flight arena that was used in Chapter 3. The first experiments reported in this chapter are modeled after several important previous efforts in which methodical modifications of the parameters of visual stimuli were used to constrain the computational underpinnings of robust navigation behaviors (Götz and Wenking, 1973; Heisenberg and Buchner, 1977; Buchner, 1984; Borst and Bahde, 1986; Srinivasan et al., 1991). The application of this approach has yielded a novel insight—the expansion-avoidance behavior exhibits a speed-dependent inversion. The later experiments documented in this chapter are attempts to further constrain the properties of this presumably important visuomotor computation.

4.1 Effect of pattern spatial and temporal frequency on closed-loop expansion-avoidance

4.1.1 Experimental design

The experiments in this chapter all involve a manipulation of the basic expansion pattern introduced in Chapter 3, referred to as the expansion-rotation (ER) pattern. This pattern is an approximation of a translatory optic flow field, the translational component is provided by bars that drift at the same rate, symmetrically about some point, called the focus of expansion. A closed-loop assay is formed by allowing the fly to control the position of the FOE by simple negative feedback of the ΔWBA turning response. The standard expansion pattern used in Chapter 3, consisted of 4-pixel-wide bars of active and inactive pixels for a spatial frequency of 30°/cycle. This spatial frequency was selected because it is in the range that has been shown to yield maximum stimulation of *Drosophila*'s optomotor reactions (based on results of Buchner (1976), where Figure 8 shows peak turning reactions to vertical stripe motion of 1.3 Hz temporal frequency with a spatial wavelength in the range of 20°–40°).

A stated objective of the experiments presented in this thesis is to avoid a priori determination of the most behaviorally appropriate stimuli. Therefore, a large set of spatial and temporal frequencies of the expansion motion were tested in the closed-loop

Table 4.1. Experimental conditions for closed-loop expansion-avoidance. The table entries are the temporal frequency for each combination of expansion frame rate and spatial wavelength of the pattern.

	Spatial wavelength		
Frames/s	15°	30°	60°
0	0 Hz	0 Hz	0 Hz
5	1.25 Hz	0.625 Hz	0.3125 Hz
10	2.5 Hz	1.25 Hz	0.625 Hz
20	5 Hz	2.5 Hz	1.25 Hz
40	10 Hz	5 Hz	2.5 Hz
80	20 Hz	10 Hz	5 Hz
120	30 Hz	15 Hz	7.5 Hz

expansion-avoidance paradigm. Patterns of 3 spatial wavelengths were created, and advanced at 7 different frame rates, yielding the 21 experimental conditions listed in Table 4.1. As indicated in the table, each pattern is expanded at 0 fps; this treatment is pure optomotor closed-loop, included as a control. In order to successfully complete these experiments, it was necessary to reduce the closed-loop gain used during these optomotor trials to 60% of the gain value used for all other trials. Without this reduction in closed-loop gain, most flies would stop flying before the end of the 40-second trial. Each of the three patterns was presented to tethered flies during 40-second closed-loop trials, during which expansion occurred at one of the 7 speeds; these trials were interspersed with 5 seconds of closed-loop (high contrast) stripe fixation, in random block trials. In total 16 flies[1] in the data set completed between 1 and 2 repetitions of this protocol, each repetition lasting for 15.75 minutes.

4.1.2 Results

Flies were given active control over the rotational velocity of the focus of expansion of the expansion-rotation pattern, at one of 3 spatial wavelengths while the open-loop expansion occurs at one of 7 expansion rates. The orientation histograms of Figure

[1]As an indication of the difficulty in conducting this experiment, 30 flies were tested with this protocol but only the 16 presented flies completed at least one trial of each type.

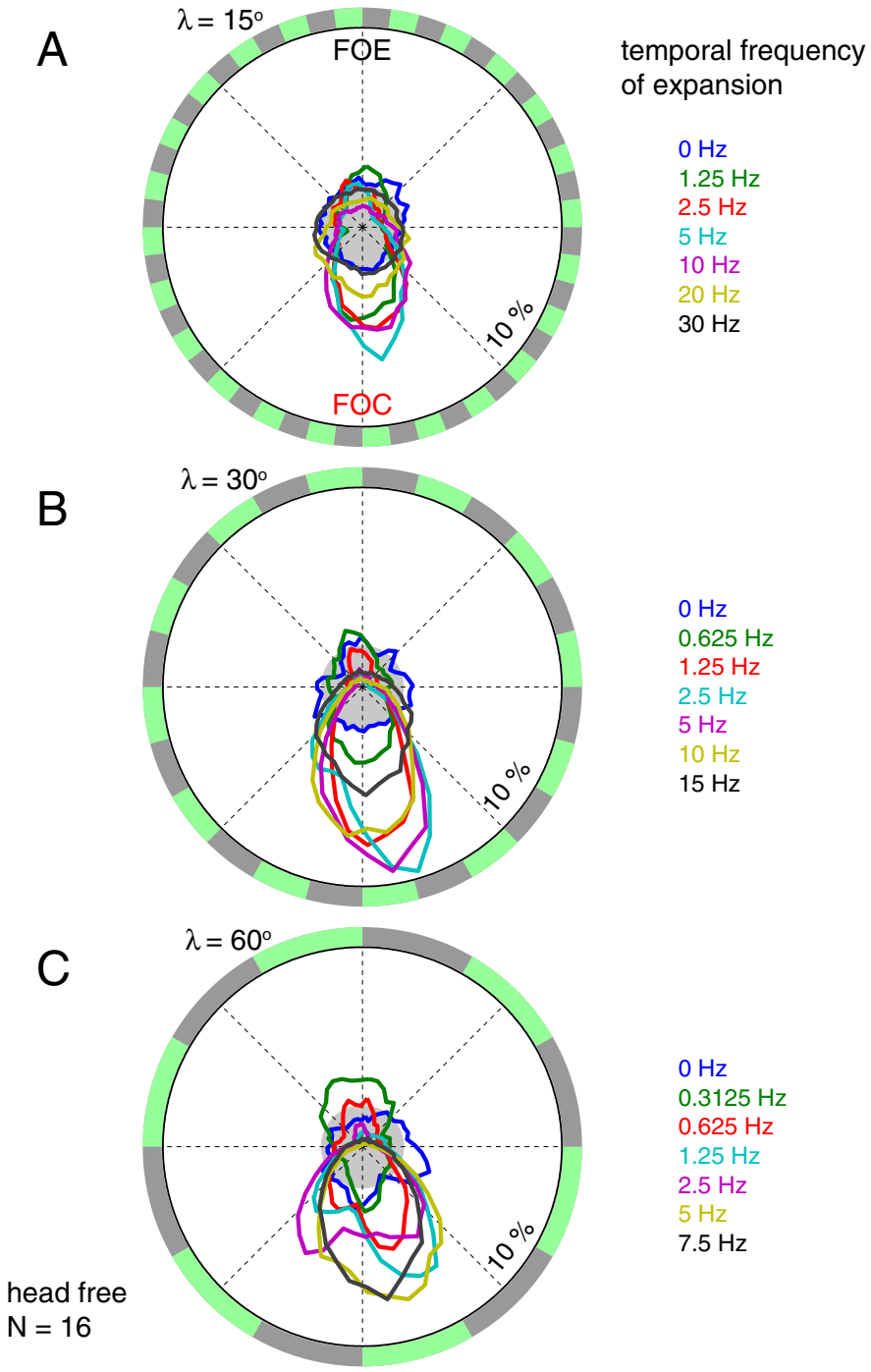

Figure 4.1. The orientation histogram for flies flying in rotational closed-loop while a pattern at one of the three different spatial wavelengths expands at one of 7 speeds. The plotting conventions follow those of Figure 3.2, orientation towards the FOE is plotted at the top of the polar plot and the gray circle indicates the distribution associated with random orientation. In all cases the optomotor trials (plotted in blue) reveal no orientation preference. Otherwise most trials feature prominent fixation of the FOC, with some greater than random probability for orienting towards the FOE at the slower temporal frequencies.

4.1 are the mean histograms obtained by averaging the histograms from each fly's orientation data during each of the 21 trial types. The histograms contain 48 bins, each corresponding to 2 adjacent locations of the FOE around the cylinder. As before, the distribution of random orientation is represented with the gray disk. The three trials of rotational optomotor (0 Hz) closed-loop flight, plotted in blue, reveal the expected result of no orientation preference towards any feature of the pattern. Most of the remaining 18 trials feature significant orientation towards the FOC. Qualitatively, it appears as if there is some intermediate range of expansion temporal frequencies for which the fixation of the FOC is most tightly regulated in front of the animal. Additionally, at slower rates of expansion, most prominently seen in the 0.3125 Hz histogram of Figure 4.1C, there is significant orientation towards the FOE.

To further quantify the orientation behavior, the method described in §2.2.5 was applied to each 40-second trial. The mean (± s.e.m.) fixation scores for each of the 21 condition are obtained by averaging each fly's mean scores as computed using equation 2.8, and are plotted in Figure 4.2. The results of the closed-loop expansion-avoidance experiments (Figures 4.1 and 4.2) reveal that at lower temporal frequencies the flies selectively orient towards the FOE, while the originally observed behavior of robust FOC fixation (Tammero et al., 2004) only occurs at higher temporal frequencies. The fixation behavior in the expansion-avoidance trial with patterns consisting of bars with $\lambda = 30^\circ$ and $\lambda = 60^\circ$ is virtually identical. The closed-loop orientation behavior with the highest spatial frequency pattern, $\lambda = 15^\circ$, shows an attenuated fixation response, largely due to the higher percent of time during which the pattern is *spinning*, as captured by the 'no fixation' category. Since the fixation scores and orientation histograms are devoid of most temporal information, it is informative to consider an example orientation sequence (Figure 4.3) in which the rate of expansion is switched from a temporal frequency of 3.75 to 0.25 Hz every 10 seconds. As clearly demonstrated, the orientation preference switches rapidly from FOC orientation at the faster speed to FOE preference at the lower speed.

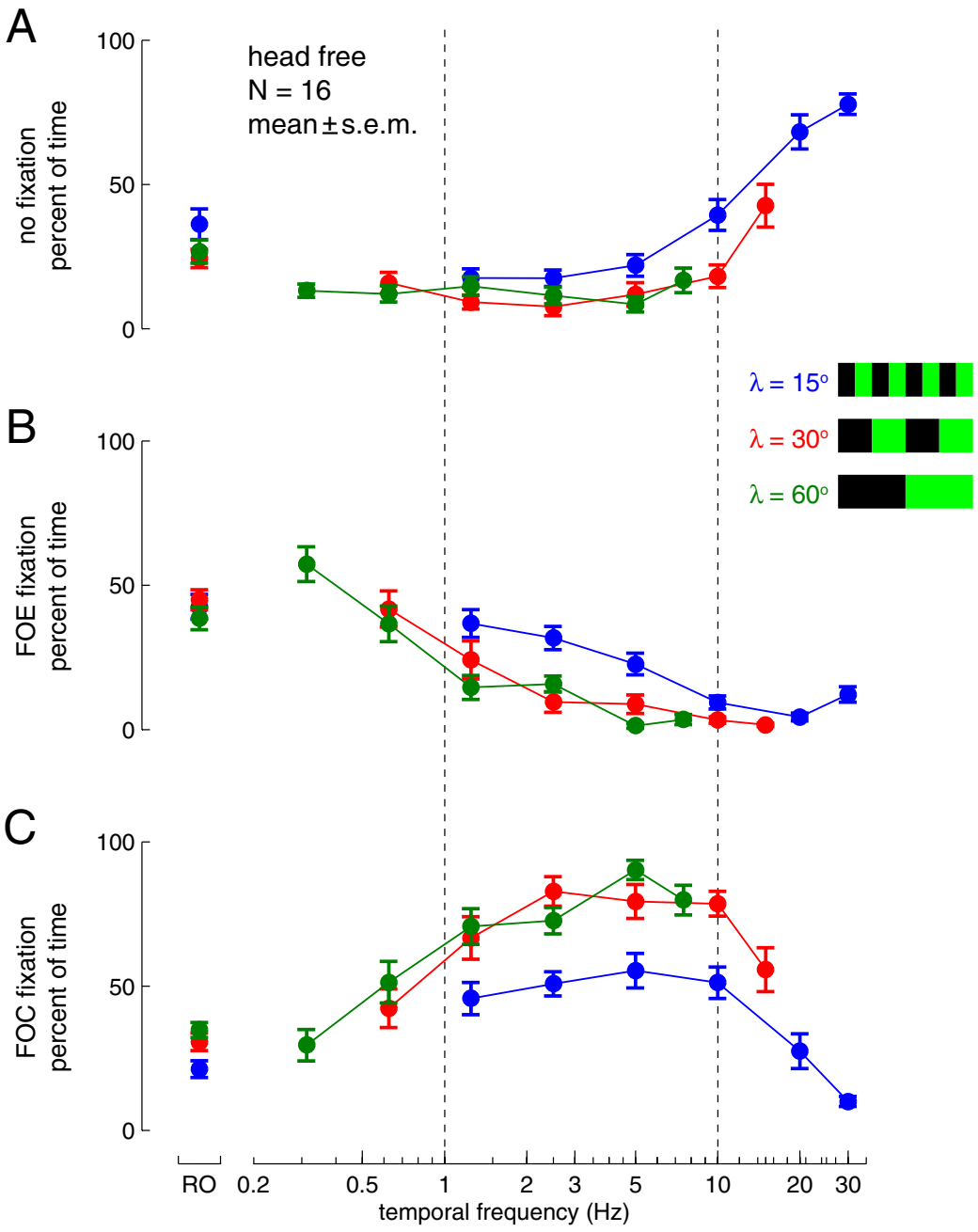

Figure 4.2. The percent of time that flies spend orienting towards the FOE (B) or the FOC (C), or neither (A), have been determined using the fixation scoring procedure outline in §2.2.5. The mean (± s.e.m.) scores for the 21 tested combination of spatial wavelength (λ of 15°, 30°, and 60°), and frame rate, are plotted on a log scale of temporal frequency (Table 4.1). As a control, 1 trial of each spatial wavelength was not expanded, this trial corresponds to rotational optomotor closed-loop, and the fixation scores for this case (plotted at the position labeled RO) are near the ideal value of (100/3)%. The dashed lines emphasize the fixation behavior at the 1 Hz and 10 Hz temporal frequency of expansion. The data show that the strong preference for orienting towards the FOC is replaced by FOE fixation at low temporal frequencies.

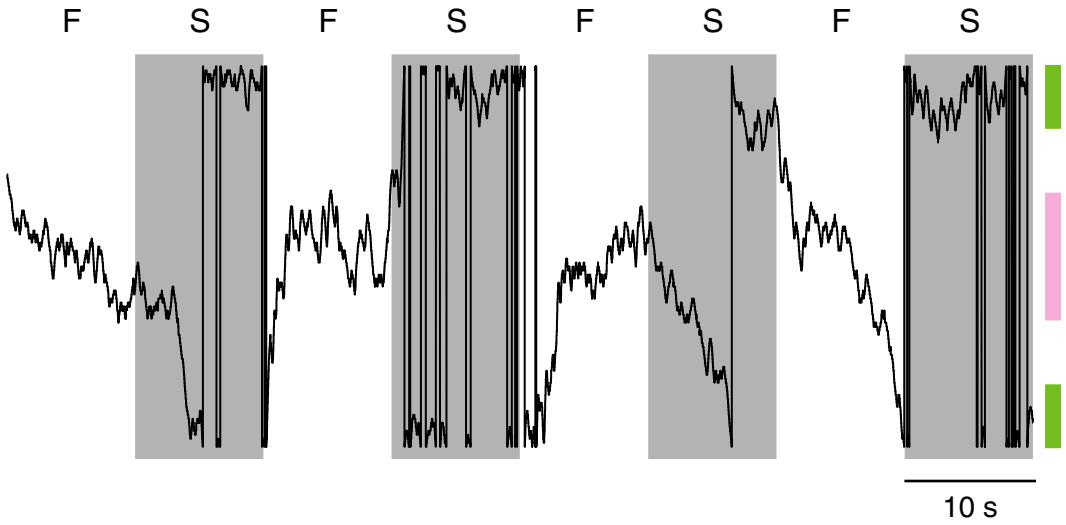

Figure 4.3. The orientation preference of *Drosophila* flying in the expansion-avoidance paradigm under closed-loop conditions can be quickly altered by changing the rate of pattern expansion from the faster temporal frequency of 3.75 Hz (noted by F in the figure), to 0.25 Hz (S). The example orientation behavior of an individual fly is shown, while the temporal frequency is alternated every 10 seconds (gray bars). The pink bar on the far left shows the region that is tagged as FOC orientation, and the green bars indicate the region tagged as FOE orientation, by the binning procedure described in §2.2.5, and illustrated in Figure 2.6. The orientation data show that under both speed conditions, transient fixation of either focus can occur after the change in expansion rate.

4.2 Effect of temporal frequency on open-loop expansion-avoidance

4.2.1 Experimental design

To further explore the speed-dependent inversion of the expansion-avoidance response found in the closed-loop experiments of §4.1, an open-loop version of these experiments was conducted. Two versions of this experiment were conducted, one with head-fixed flies (a dap of UV-activated flue binds the back of the head to the thorax), and one with head-free flies. The head-free fly experiment used the expansion-rotation pattern with $\lambda = 30°$, and tested at 5 expansion rates (temporal frequency of 0.125, 0.25, 0.5, 1, and 8 Hz), with the FOE located at 10 positions around the fly. The experiment was designed to sample the expansion rates close to the critical value at which the

inversion occurs, and to favor the frontal position of the FOE. The positions of the FOE tested were: 0°, ±30°, ±60°, ±90°, ±135°, and 180°. For all of the rates of expansion except the fastest (8 Hz), the pattern used required 24 (as opposed to 8) frames to complete one 8-pixel cycle, taking advantage of the display's intermediate intensity values to achieve smoother stimulation at low speeds (as discussed in §2.4). The experimental series consisted of a 4-second test phase of open-loop expansion, followed by a 5-second interstice of closed-loop stripe fixation. The 50 stimulus conditions (10 positions, 5 temporal frequencies) were presented in random block trials. In total, 36 flies completed between 2 and 3 repetitions of this protocol, each repetition lasting nearly 7.5 minutes.

A second version of this experiment, conducted with flies with fixed heads, made use of a similar protocol: 6 expansion rates were tested (temporal frequency of 0.25, 0.5, 1, 2, 4, and 8 Hz), with the FOE located at 8 positions around the fly. The positions of the FOE tested were: 0°, ±45°, ±90°, ±135° and 180°. This experiment made use of the standard expansion-rotation pattern with $\lambda = 30°$ that required 8 frames to complete one 8-pixel cycle. The experimental series consisted of a 4-second test phase of open-loop expansion, followed by a 5-second interstice of closed-loop stripe fixation. The 48 stimulus conditions (8 positions, 6 temporal frequencies) were presented in random block trials. In total, 23 flies completed between 2 and 3 repetitions of this protocol, each repetition lasting 7.2 minutes.

4.2.2 Results

One goal of the experiments described in the section was to produce a tuning curve for the turning response to large-field expansion that could be directly compared with the results of Tammero et al. (2004), and reproduced here in Figure 1.4E. Tethered (head-free) *Drosophila* were presented with the large-field expansion stimulus centered at 10 positions on the retina and at 5 different temporal frequencies of expansion. To gauge the flies' turning behavior in response to the stimuli, the desired quantity is the mean left minus right wingbeat amplitude during the short periods of pattern motion.

For each trial, the mean response during the 100 ms previous to the stimulus onset was subtracted from the subsequent turning response. For each fly, the mean turning response was determined by first using the 'flip and average' technique discussed in §2.2.6 to combine the data for the symmetric presentations[2] of motion (after an inspection to ensure that the data were indeed nearly symmetric).

The speed- and position-dependent mean (± s.d.) turning responses are shown as a time series in Figure 4.4. The mean (± s.e.m.) over the entire 4-second trial is plotted in Figure 4.5. Although the data have been grouped across symmetric presentations, the data are plotted in the form of a tuning curve to enable the comparison with the previous results. The data are generally in agreement with the closed-loop results of §4.1; at speeds below 1 Hz, deviation from a frontally centered FOE towards the right side of the flies elicits a counterclockwise turn, an attempt to orient towards the FOE. At higher speeds, and at lateral and rearward positions of the FOE, the turning response resembles the tuning curve reproduced in Figure 1.4E. The time series data in Figure 4.4 reveals several interesting features of the temporal mechanism for motion integration. The expansion-avoidance response to the 8 Hz expansion stimulus with the FOE at the ±30° position shows a very slow accumulation of the response, suggesting that this stimulus only weakly drives the expansion-avoidance 'filter.' Also the time series data shows phase locking to the discrete pattern advances of the expansion stimulus. This phase locking can clearly be seen in the mean response to 0.125 Hz expansion (3 fps), and is also present in the responses to the 0.25 and 0.5 Hz expansion, but is not at all seen at the faster rates. The presence of this ripple has been used to determine an appropriate 'visuomotor' time constant in §6.2.2.

As discussed in §1.6, increases in thrust produced by *Drosophila* are well correlated with an increase in the bilateral sum of wingbeat amplitudes (Götz, 1964). Additionally, the wingbeat frequency along with the wingbeat amplitude determine the mechanical power of the flight muscles (Lehmann and Dickinson, 1997). These two important measurements of flight performance, in response to the open-loop presentation of the

[2]The frontal and rear FOE presentation were only presented once per trial block, and as such there is no symmetric version of these trials.

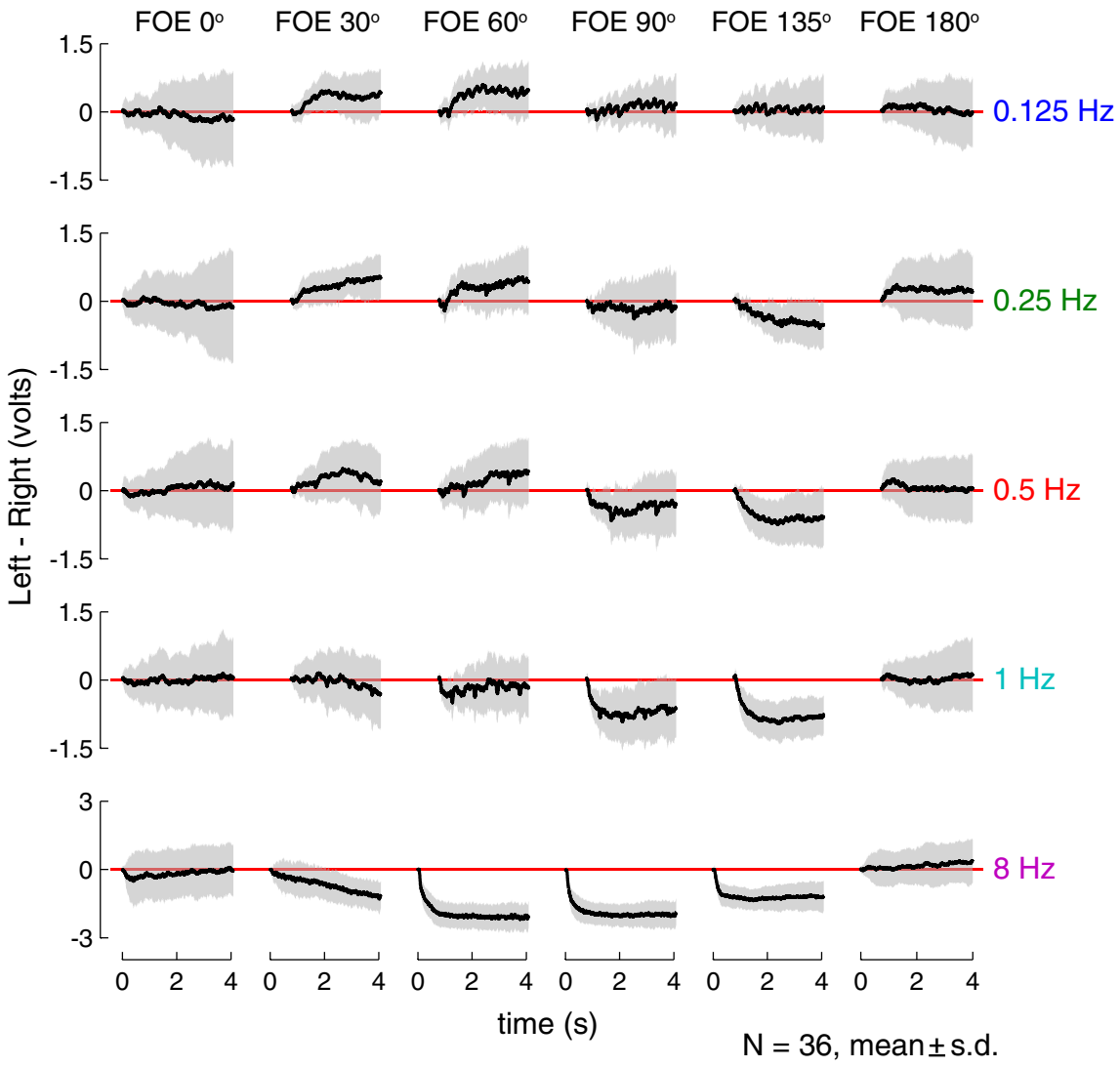

Figure 4.4. The steering response of *Drosophila* to large-field expansion of varying speeds and orientations, presented under open-loop conditions. The mean (± s.d.) turning responses (difference between left and right wingstroke amplitudes) to the expansion emanating from 6 locations (mirror symmetric presentation on the left of the animal have been averaged with the presented data), at 5 temporal frequencies, are displayed. The responses to the 0.125, 0.25, and 0.5 Hz expansion show phase locking to the advances of the expansion pattern.

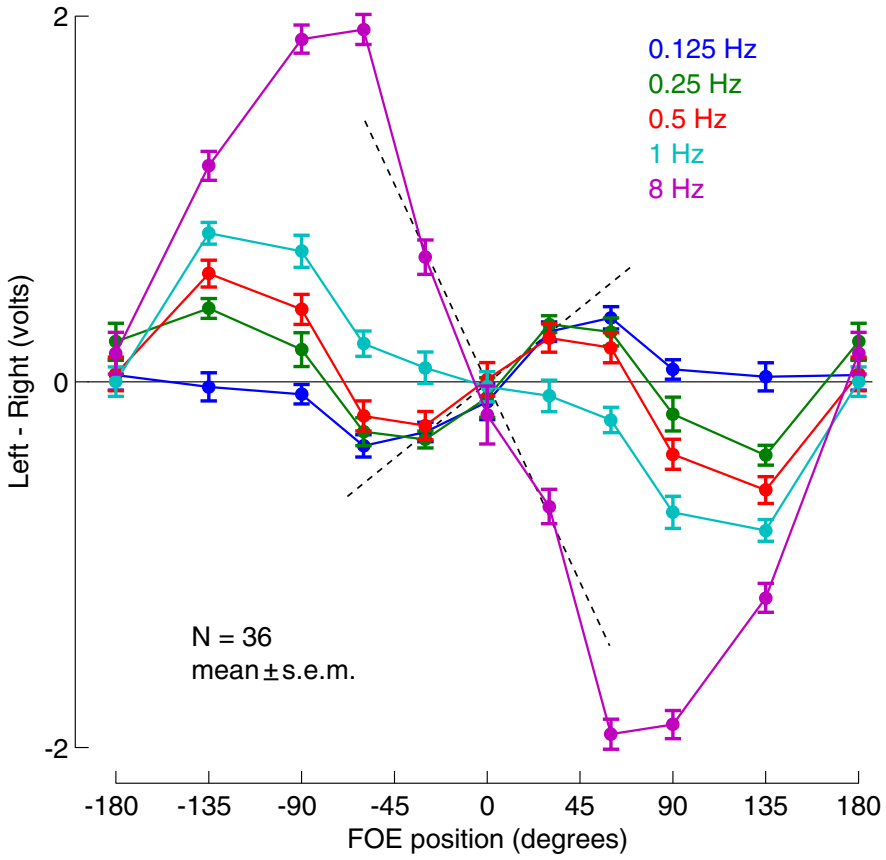

Figure 4.5. Open loop turning response to expansion presented at 10 positions around the fly, for five different rates of expansion. The mean (± s.e.m.) turning response, shows that flies turn away from expansion at all speeds when it is positioned laterally and rearward. However, at lower rates of expansion, the turning directions is opposite—the flies turn so as to orient towards the FOE. The dashed lines are drawn to emphasize that the slope of the response curve near the origin to expansion of different speeds changes sign, predicting that the FOE should be frontally stable at slower speeds, but unstable at the higher rates of expansion.

expansion stimuli, are shown in Figure 4.6. For the test of speed- and orientation-dependent effects on the 'thrust' response, the desired quantity is the mean left plus right wingbeat amplitude (ΣWBA) response of individual flies to the short period of pattern motion. The mean value of ΣWBA during the 100 ms prior to the onset of each open-loop trial was subtracted from the subsequent ΣWBA response, so that the change in the 'thrust' signal is being reported. The mean (± s.e.m.) for the change in ΣWBA and the mean (± s.e.m.) of the wingbeat frequency are plotted. A large reduction in both the ΣWBA and WBF signals is seen in response to the fast

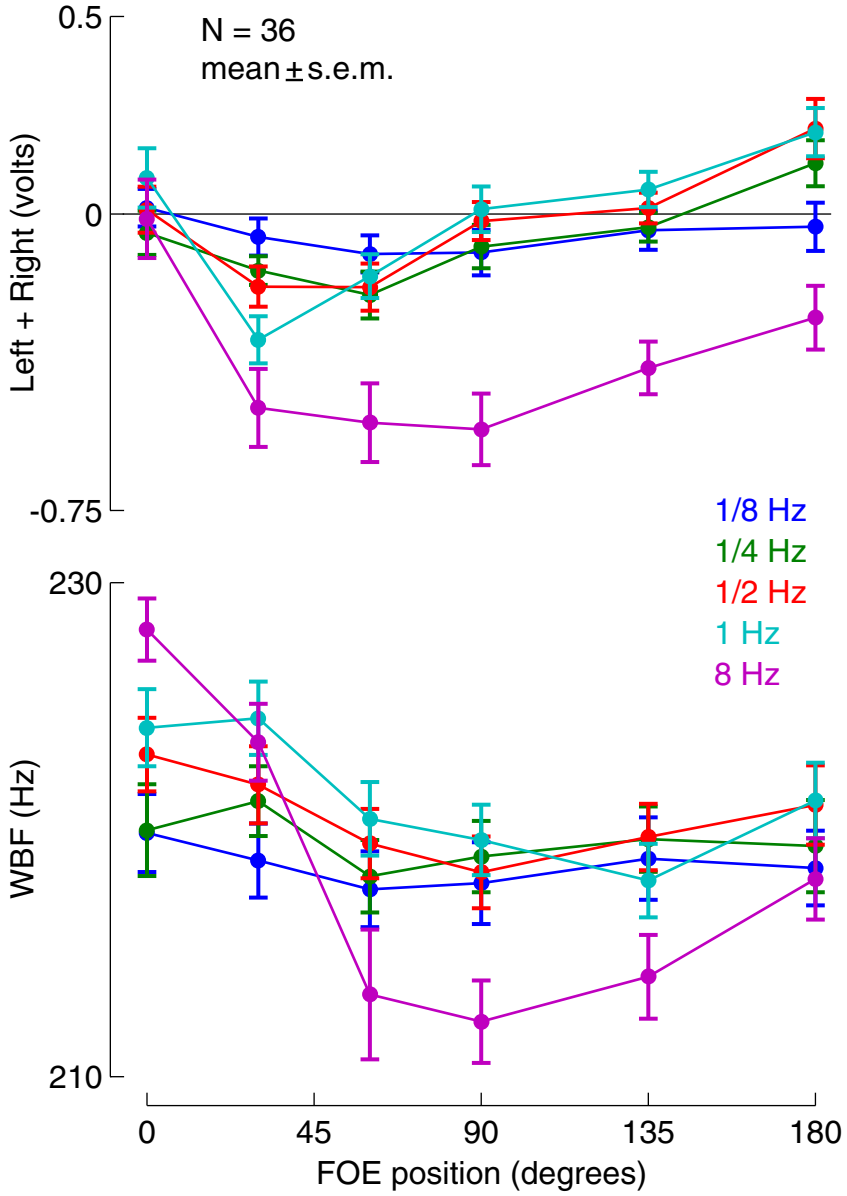

Figure 4.6. Open-loop WBF and ΣWBA (proxy for thrust) responses to expansion presented at 10 positions around the fly, for five different rates of expansion. Since symmetry has been used to combine data presented from both sides, the data are shown as if all expansion was presented on the right side of the animals. The data are plotted so that the colors correspond with the turning response data in Figures 4.4 and 4.5.

expansion trials (in magenta) that induce large turns. Of course, ΣWBA and ΔWBA are not independent, the summed stroke amplitude is reduced when the flies produce a turning response (the bilateral changes tend to results in a decrease in the mean wingbeat amplitude). The shape of the WBF response curve matches well with WBF responses to an expanding square pattern—the largest increase occurs in response to frontal expansion, and declines as the expansion moves towards the rear (Tammero and Dickinson, 2002a). It is interesting to note that at all speeds the frontal FOE yields virtually no change in ΣWBA, but the frontal FOC induces a ΣWBA increase. This is suggestive of a velocity control mechanism as discussed in §5.3.4.

A similar experiment has been repeated with head-fixed flies. The intention of conducting this experiment was to obtain a 'cleaner' result; fixing the heads of the flies ensures that the visual stimuli are experienced by all flies in a more uniform manner. The speed- and position-dependent mean (± s.e.m.) turning, 'thrust,' and wingbeat frequency responses of the head-fixed flies are shown in Figure 4.7. All data have been processed in an identical manner to the head-free experiments, and so the details are omitted. There is a striking difference between the head-fixed and head-free responses—the centering response that occurs at lower temporal frequencies is absent. At all tested speeds and lateral FOE positions, the head-fixed flies respond by turning away from the FOE.

One possible cause for the discrepancy between the head-fixed and head-free turning responses is that the mean response data averaged over the duration of a 4-second trial may obscure important features of the flies' response. Many visually mediated responses in flies are evoked within no more than 200 ms of stimulus onset (David, 1985; Heisenberg and Wolf, 1988; Tammero and Dickinson, 2002a; Bender and Dickinson, 2006b). Therefore, it is possible that only the flies' response in the first few hundred milliseconds represents behavior that is relevant to free-flight conditions. To test this possibility, the first 0.75 seconds of the mean turning response data of head-free and head-fixed flies is shown in Figure 4.8. The FOE positions where the turning response inversion occurs in the head-free flies, and might occur in the head-fixed flies are shown. This expanded view of the turning responses does not reveal

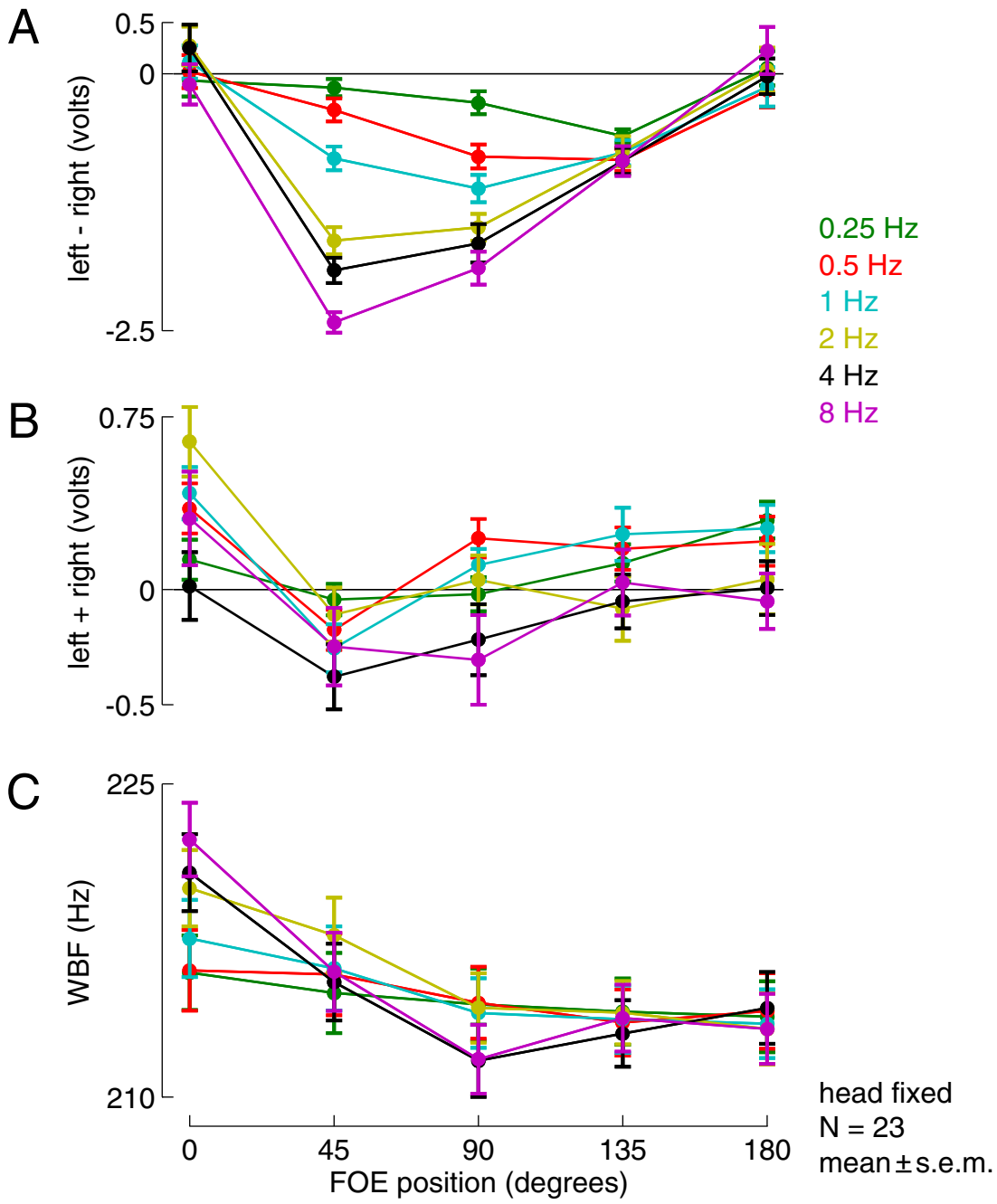

Figure 4.7. Open-loop expansion avoidance in head fixed-flies. The mean (± s.e.m.) turning (A), 'thrust' (B), and WBF (C) responses of head-fixed flies to large-field expansion presented at 8 positions around the fly, for 6 different rates of expansion. The data are shown as if all expansion was presented on the right side of the animals, combining the symmetric presentations. The data are plotted so that the colors correspond with the head-free responses, for the 4 temporal frequencies that are the same across the 2 experiments. The turning response shows that gluing the flies heads eliminates the centering response; the flies always respond by turning away from the FOE.

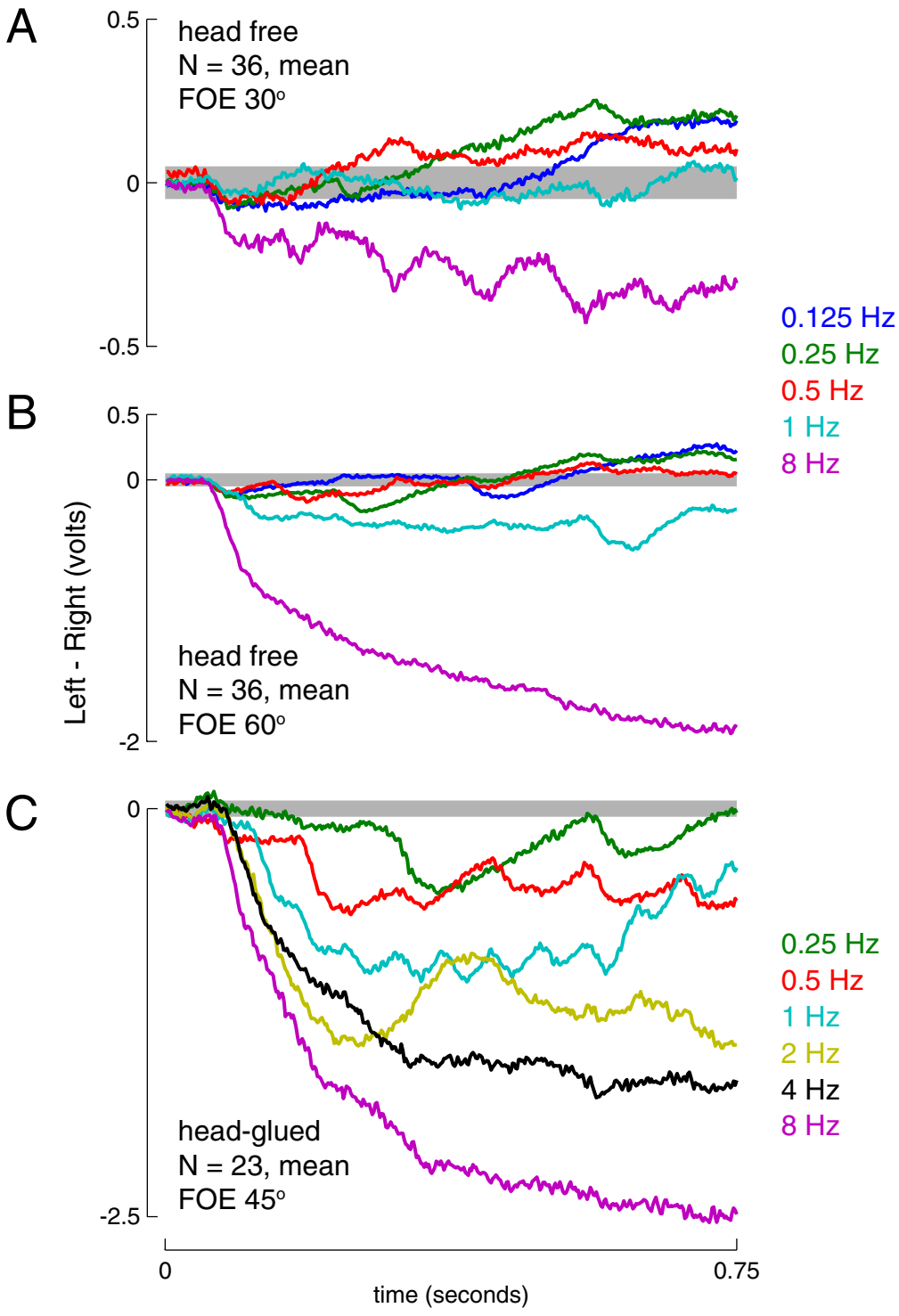

Figure 4.8. The mean turning responses during the first 750 ms of open-loop expansion trials. The turning response of head-free flies to expansion centered at 30° (A), and 60° (B). For comparison, the turning response of head-fixed flies to large-field expansion centered at 45° (C). The gray bars indicate the ±50 mV range.

any centering-like response in the head-fixed data. The head-free turning response to the FOE at 30° shows the expected sequence of increasing response amplitudes, the response to 0.125 Hz, the slowest stimulus, is the last to increase above the zero baseline (gray box), followed by the 0.25 Hz response and then the 0.5 Hz response. This indicates some form of motion integration underlies the centering response.[3] A comment on the phase locking present in the responses of Figure 4.8: the ripple seen in the magenta response of (A) is locked to the 8 Hz cycles of the stimulus, while the ripples seen in the green, red, and cyan responses of (C) are locked to the discrete (1-frame) advances of the pattern. In a model of a fly motion detector (§6.2.2) both types of ripple are also observed.

4.3 Closed-loop expansion-avoidance with restricted spatial extent

4.3.1 Experimental design

To address the fifth hypotheses of §1.11, that the crude approximation of a real translatory optic flow field may be responsible for the expansion-avoidance behavior, an experiment was conducted to test the closed-loop expansion-avoidance behavior while the spatial extent of the pattern was restricted to lateral portions of the eye. This configuration approximates the optic flow seen while flying down an infinitely long tunnel, in which the motion across lateral regions of the eye is nearly constant. The patterns used were based on the standard (spatial wavelength of 30°) expansion-rotation pattern from §4.1, with smoother motion (24 frames per cycle) provided by using intermediate intensity levels. To display motion restricted to the lateral portions of the arena, two patterns were designed with all pixels in the front and rear 60° and 120° of the arena set to an intermediate intensity (IL = 3). Experiments were performed at 3 temporal frequencies of expansion: 0.25 Hz, a rate at which FOE fixation is prominent; 0.625 Hz, a rate near the critical value for the inversion

[3]This is hardly a surprising result, as even low-pass filtering, which is known to exist in the motion processing pathway, is a type of integration.

of orientation preference; and 5 Hz, a speed at which FOC orientation dominates. The experimental series consisted of 40-second closed-loop trials, during which one of 3 patterns (180°, 120°, and 60° extent per side) was expanded at one of the three temporal frequencies. These trials were interspersed with 5 seconds of closed-loop (high contrast) stripe fixation, in random block trials. In total, 13 flies completed between 2 and 3 repetitions of this protocol, each repetition lasting for 6.75 minutes.

4.3.2 Results

Flies were given active control over the rotational velocity of the FOE of the three different expansion-rotation patterns, with 180°, 120°, and 60° visible extent per side. The stimulus can be thought of as virtually painting out frontal (and rear) regions of the fly eye (with the usual caveats about head motion). The orientation histograms of Figure 4.9A, are the mean histograms obtained by averaging the histograms from each fly's orientation data during each of the 9 trial types. Each polar plot groups the orientation histograms corresponding to the trials using the 3 patterns, at one of the 3 temporal frequencies of expansion. The histograms corresponding to complete stimulation agree with the previous results; significant FOE orientation is observed at f_t=0.25, the behavior at f_t=0.625 shows orientation towards both foci, and the behavior at f_t=5 is dominated by FOC orientation. Because no motion is presented in front, the pattern must rotate beyond the blind zone before the location of the foci can be determined. Therefore, it is expected that the histograms of the orientation data corresponding to the trials in which the expansion pattern is displayed in a restricted region will be flatter than those corresponding to the unrestricted stimulus trials. This flattening is seen in all cases, but is most prominent in the histograms corresponding to the 5 Hz expansion. The orientation histograms are a useful measure of the flies' behavior, but since all temporal information is removed, it is difficult to analyze the effect of the restricted pattern extent beyond the observation regarding the expected flattening.

To further quantify the orientation behavior, the method described in §2.2.5 was

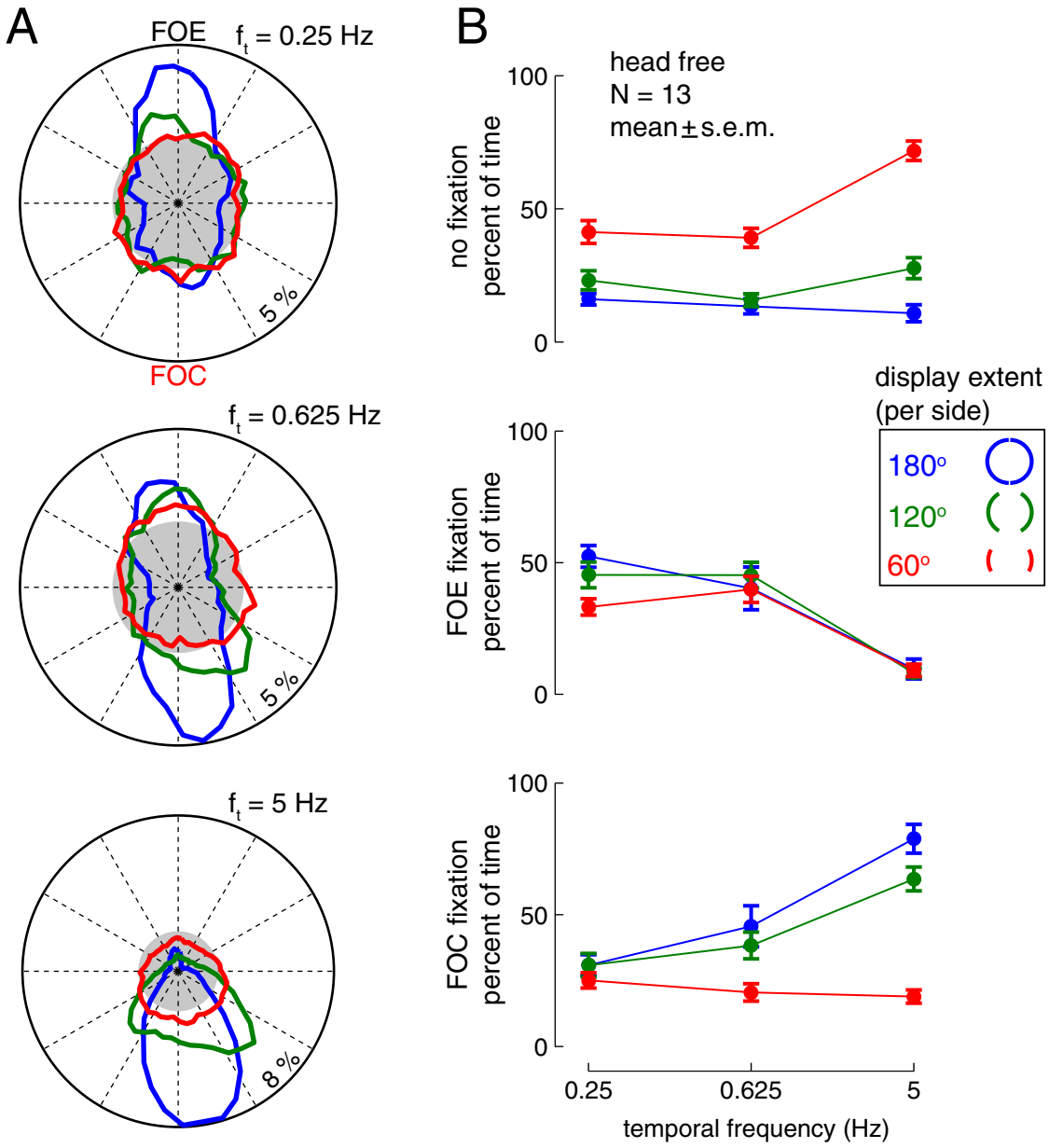

Figure 4.9. The closed-loop orientation behavior under the expansion-avoidance paradigm with laterally restricted motion. The orientation histograms (A) for flies flying in rotational closed-loop are shown, following the plotting convention used throughout—orientation towards the FOE is plotted at the top of the polar plot and the gray circle indicates the distribution associated with random orientation. Each polar plot (A) shows the orientation histograms grouped by the temporal frequency (f_t) of expansion. The fixation scores (B) show the mean (± s.e.m.) percent of time that flies spend orienting towards the FOE, FOC, or neither.

applied to each 40-second trial. The mean (± s.e.m.) fixation scores for each of the 9 condition are plotted in Figure 4.9B. The trends in the fixation scores reveal that the orientation behavior is largely unchanged between the original (180°, in blue) pattern and the 120° (in green) version. However, the orientation preference in response to the expansion stimulus restricted to a lateral 60° region shows little difference in FOE orientation from the 180° and 120° cases, but significant differences in FOC orientation. The increase in the percent of time during which the flies are not fixating, seen in the red trace, is almost entirely accounted for by the decline in FOC orientation. A tunnel stimulus restricted to a (bi)lateral 60° region appears to only minimally diminish the FOE orientation behavior, as if the centering-like response does not make use of frontal visual motion. There is even weak evidence that the FOE orientation is actually enhanced in the case of the 60° tunnel stimulus with $f_t = 0.625$ Hz expansion.

4.4 Closed-loop expansion-avoidance with asymmetric expansion

4.4.1 Experimental design

The fixation of the FOE at lower temporal frequencies shares many properties with the centering response of bees (Srinivasan et al., 1991). The optic flow seen during straight flight (with little sideways motion) will feature a focus of expansion that is roughly in front, though the side of the eye that is closest to a textured surface will receive stronger flow. If indeed the FOE orientation is the result of balancing the motion seen by the right and left eyes, then there should be a predictable shift in the orientation preference (away from the side observing faster motion) if the expansion occurs with different speeds on both sides of the fly. To test this hypothesis, several patterns were created capable of displaying asymmetrical expansion (with expansion rate ratios of 0:1, 1:2, and 1:20). The patterns used were based on the standard (spatial wavelength of 30°) expansion-rotation pattern from §4.1, with smoother motion (24 frames per cycle) provided by using intermediate intensity levels. Experiments were performed using 14 combinations of expansion rates, listed in Table 4.2. The combinations were

Table 4.2. Median pattern orientation for closed-loop expansion-avoidance with asymmetric expansion

left f_t (Hz)	right f_t (Hz)	median orientation	comments
0	5	$156.00° \pm 11.66°$	P val vs. 5:5, 0.0922
0.25	5	$154.06° \pm 3.73°$	P val vs. 0:5, 0.8374; vs. 5:5, 0.0031
2.5	5	$165.31° \pm 2.79°$	P val vs. 5:5, 0.0853
2.5	2.5	$173.75° \pm 4.14°$	—
5	5	$176.88° \pm 5.78°$	—
5	2.5	$191.25° \pm 5.12°$	P val vs. 5:5, 0.0761
5	0.25	$203.44° \pm 4.57°$	P val vs. 5:0, 0.7897; vs. 5:5, 0.0016
5	0	$201.00° \pm 8.68°$	P val vs. 5:5, 0.0375
0	0.25	$-3.00° \pm 8.33°$	P val vs. 0.25:0.25, 0.8314
0.25	0.5	$-13.13° \pm 5.45°$	P val vs. 0.5:0.5, 0.0914
0.25	0.25	$-0.94° \pm 5.08°$	—
0.5	0.5	$1.56° \pm 6.29°$	—
0.5	0.25	$-3.13° \pm 5.14°$	P val vs. 0.5:0.5, 0.5695
0.25	0	$5.25° \pm 2.81°$	P val vs. 0.25:0.25, 0.4625

selected to test asymmetries at the lower temporal frequencies where 'centering' occurs, at the higher temporal frequencies where FOC orientation dominates, and in cases of extreme asymmetry. The experimental series consisted of 30-second closed-loop trials, during which one of the 14 trial types was expanded. These trials were interspersed with 5 seconds of closed-loop (high contrast) stripe fixation, in random block trials. In total, 12 flies completed between 1 and 2 repetitions of this protocol, however only 5 of the 12 flies were presented with the patterns consisting of no motion on one side (0:1 ratio). Each repetition lasted approximately 6 minutes (10 trials) or 8 minutes (all 14 trials).

4.4.2 Results

Flies were given active control over the rotational velocity of the FOE of the expansion-rotation pattern, with several asymmetries of expansion. The resulting orientation histograms are shown in Figure 4.10. The orientation histograms are grouped to allow comparison of orientation behavior for fast asymmetric expansion (A), slow asymmetric

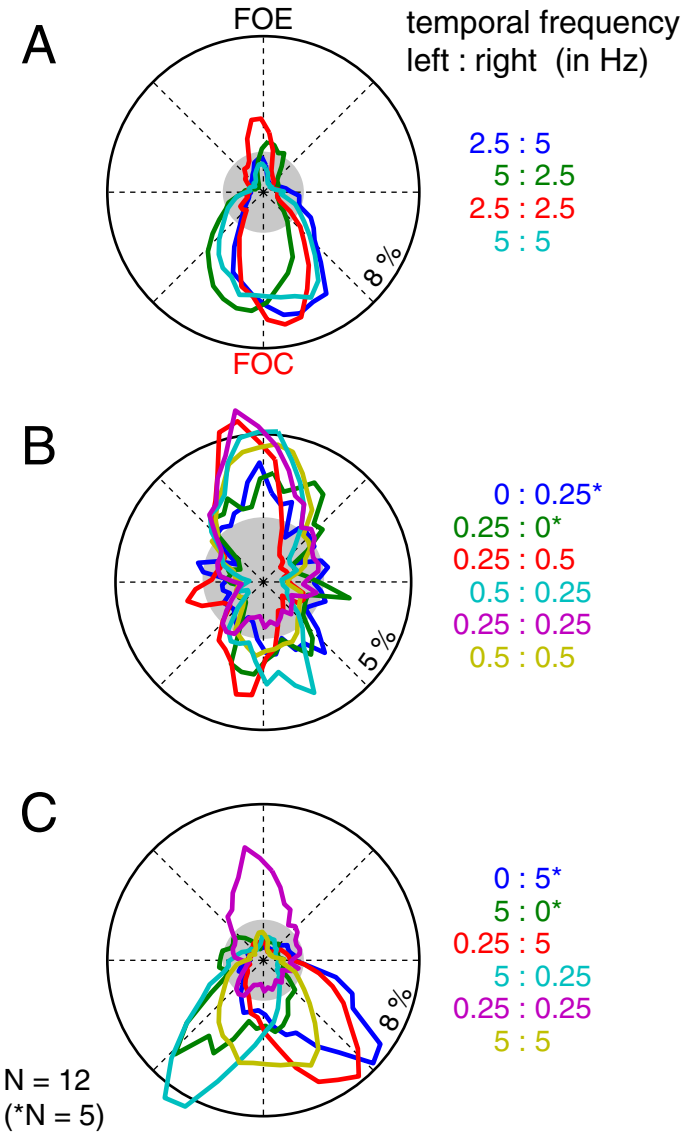

Figure 4.10. The closed-loop orientation behavior under the expansion-avoidance paradigm with asymmetric motion on the right and left side of the fly. The orientation histograms for flies flying in rotational closed-loop are shown, following the plotting convention used throughout—orientation towards the FOE is plotted at the top of the polar plot and the gray circle indicates the distribution associated with random orientation. The orientation histograms are grouped to allow comparison of orientation behavior for fast asymmetric expansion (A), slow asymmetric expansion (B), and large asymmetries (C). In general there is a shift in the preferred orientation directions towards the slower side.

expansion (B), and large asymmetries (C). In general, it can be seen that there is a shift in the preferred orientation directions towards the side of slower expansion, corroborating the findings of a similar experiment performed with a 1:2 asymmetry of a fast expansion pattern (Tammero et al., 2004, Figure 7). To further quantify the shift in orientation preference, we compute the median orientation direction. The standard circular median cannot be used for these data, because the distributions are multi-modal, therefore, the median values computed are restricted to the hemisphere in which the majority of the orientation data reside. For the 14 tested trial types, the median orientation directions are listed in Table 4.2.

The median orientations in Table 4.2 are listed in FOE-centric coordinates, the same as used in (among others) Figure 4.5; negative positions indicate that the FOE is on the animal's left (FOC on the right), positive angles correspond to the FOE positioned on the right, zero corresponds to a frontal FOE and $\pm 180^\circ$ to the FOE positioned behind, and the FOC in front. The table also contains the results of statistical tests between the median orientations. Also comparisons were done using a t-test, and the relevant comparison is with the median orientation of symmetric motion at the faster speed. The table shows that when at least half of the pattern contains high temporal frequency motion, the flies position the FOC in front. However, when there is a large asymmetry in the temporal frequency of the pattern, the preferred orientation is biased towards the slower side of the pattern. The shift in the median orientation is approximately 25° when the asymmetry is large (either 0.25 or 0 Hz on one side, and 5 Hz on the opposite side). There is no statistical difference between the shift in orientation for the complete (0:5 Hz) and the large (0.25:5 Hz) asymmetry trials. The shifted median orientation positions seen in the 0.25:5 Hz and 5:0.25 Hz trials are significantly different from the FOC orientation seen in the symmetric 5 Hz trial. The orientation behavior at the complete asymmetry of 5:0 and 0:5 Hz is not as tightly regulated, and thus the median orientations are only significantly different from the FOC orientation at the $\alpha < 0.1$ level. The shift in median orientation corresponding to the 2.5:5 Hz asymmetry is approximately 13°; this median orientation shift is only significantly different from the FOC orientation at the $\alpha < 0.1$ level.

At the low expansion speeds, the flies selectively orient towards the FOE. When asymmetric pattern motion is presented, the shifts in preferred orientation are much smaller but generally follow the same trend—they are away from the side of faster motion, towards the slower motion side. However, only one of the 4 trials, the 0.25:0.5 asymmetry, is significantly different from the FOE orientation at the $\alpha < 0.1$ level. Although the small data set does not prevent this conclusion to be made with strong statistical rigor, it appears that the response to asymmetric expansion is a centering-like response, the flies turn towards the side of less motion.

4.5 Closed-loop expansion-avoidance with accelerating expansion

4.5.1 Experimental design

Contrary to a long-standing assumption (put forth by Reichardt and Poggio (1976), based on data from Land and Collett (1974)), the recent results of Fry et al. (2003) have demonstrated that the dynamics governing rotational motion of flies are dominated by inertia rather than friction. Since the physical basis for rotational and translational inertia is essentially the same, it is almost certain that the dynamics of forward flight are also governed by inertial forces. For this reason, increases in forward thrust will correlate with acceleration, not velocity, of the body. To our knowledge there have been no attempts to stimulate a fly with an accelerating translatory flow field. We have approximated the constant acceleration of the temporal frequency of an expanding flow-field with a velocity ramp, that drives expansion at a constant velocity for one second, and then increases (or decreases) at a constant rate. The pattern used was the standard (spatial wavelength of 30°) expansion-rotation pattern from §4.1, with smoother motion (24 frames per cycle) provided by using intermediate intensity levels. Four trial types were tested consisting of a 20-second closed-loop expansion-avoidance trial during which the temporal frequency of expansion was either accelerated or deceleration at 0.125 Hz/s (3 fps/s) or 0.25 Hz/s (6 fps/s; these units are used to emphasize the fact that the stimulus is actually driven by a velocity ramp). In total,

8 flies completed between 4 and 5 repetitions of this protocol, consisting of the 4, 20-second closed-loop trials, interspersed with 10 seconds of closed-loop stripe fixation, presented as random block trials.

4.5.2 Results

Flies were given active control over the rotational velocity of the FOE of the expansion-rotation pattern, while the rate of expansion was either accelerated or decelerated. The results of this experiment can be used as a quick test for the critical value of the FOE/FOC orientation preference inversion, and can further be used to see if this value depends on the time-history of expansion accelerations (and velocities) of temporal frequency. The results of the experiment are shown in Figure 4.11. In response to the temporal frequency ramps (B) driving the rate of expansion, a typical time series of the flies' orientation is shown (A). In the cases of acceleration (in blue), the flies originally orient towards the FOE, and then switch to FOC fixation midway, or later, through the trial; for the decelerating stimulus, the opposite occurs.

To quantify the orientation preference, the method described in §2.2.5 was applied to the orientation data during each 1 second of constant temporal frequency expansion. The mean (± s.e.m.) fixation scores (computed using equation 2.8) during each 1-second bin, for all four cases, are plotted in Figure 4.11C. From the previous open-loop (§4.2) and closed-loop (§4.1) results, the critical value above which FOE orientation becomes unstable was shown to be between 0.625 and 1 Hz. The orientation preference in the face of expansion values in this range is as likely to be towards the FOE or the FOC. During the closed loop trials with a constant expansion rate of 0.625 Hz, the FOE and FOC are both 'fixated' for about 45% of the time (see Figure 4.2). To compare this preference with the behavior that is measured while the expansion rate is changing, the 40% FOE fixation is (arbitrarily) taken as a cutoff for a 'strong' FOE preference in Figure 4.11C. Except in the case of the last 6 seconds of the faster acceleration data, the mean FOE orientation percent never declines below 20%. In general, when the rate of expansion varies, the strength of FOE orientation increases.

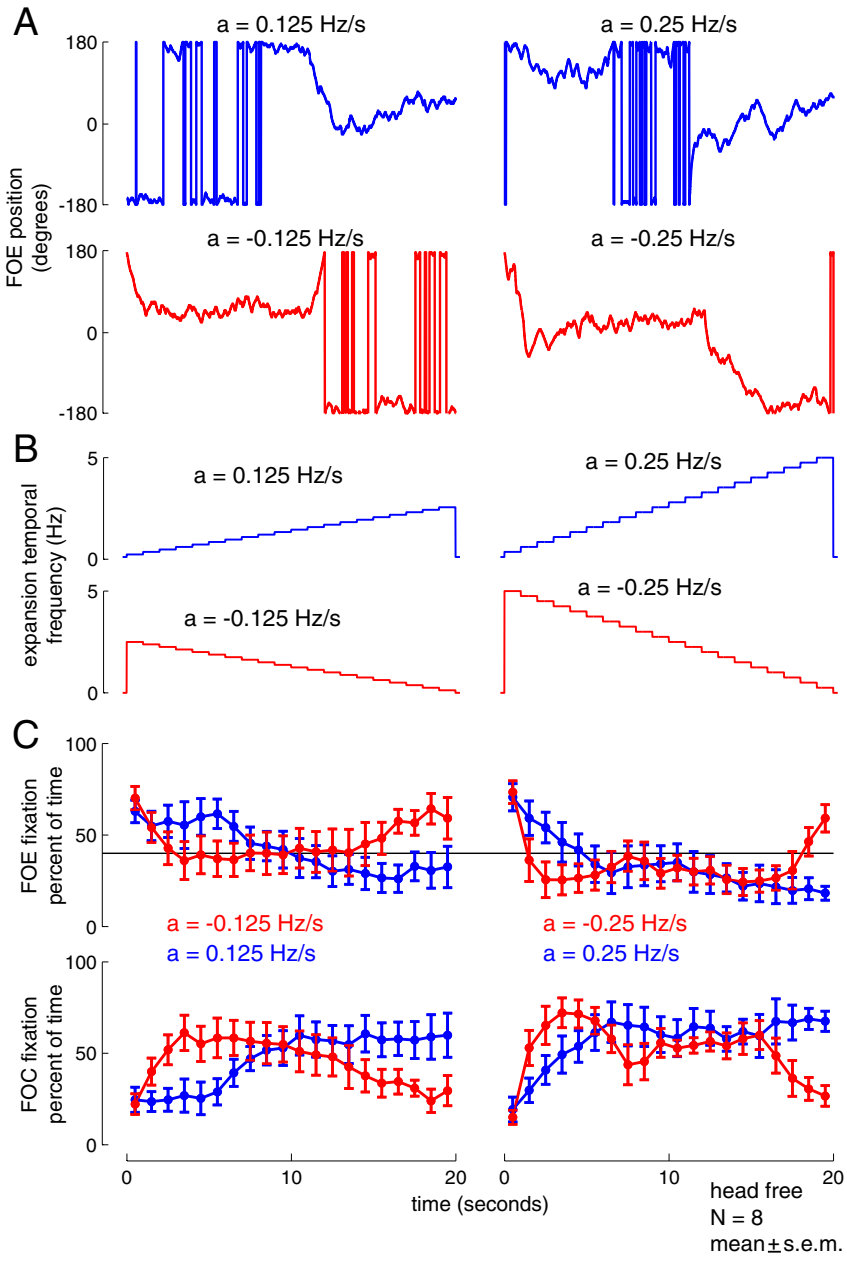

Figure 4.11. The closed-loop orientation behavior of *Drosophila* presented with constant accelerating (in blue) and deceleration (in red) temporal frequency of expansion. (A) Typical orientation time series during the 20 seconds trials (from one fly), during which the fly had closed-loop control of the position of the FOE, while (B) the expansion rate was increased and decreased at a constant rate (one velocity step per second). (C) The mean percent of time, during each 1 second of constant temporal frequency expansion, that the flies oriented towards either the FOE or FOC. The solid black line marks the 40% level of FOE orientation. In the case of slow deceleration, a strong preference towards the FOE is exhibited throughout the sequence of temporal frequency changes.

Further the mean percent of time orientation curves are not mirror-symmetric, the orientation preference depends on whether the fly encounters expansion of a certain rate during either acceleration of deceleration. The critical value, below which FOE orientation exists at or above the 40% level, is 1.625 Hz during the -0.125 Hz/s deceleration, 1.25 Hz during both the 0.125 and 0.25 Hz/s acceleration trials, and 0.5 during the -0.25 Hz/s deceleration trial. Thus the temporal frequency critical value for the centering response, collected under constant f_t conditions, is likely to be an underestimate of the behaviorally relevant value, which may be twice as large when determined under varying expansion speeds.

4.6 Discussion

The open- and closed-loop results of this chapter shed new light on the findings of Tammero et al. (2004); the expansion-avoidance behavior of *Drosophila* appears to reside on a continuum, where at the slower speeds, flies exhibit a centering response that gets weaker and yields to expansion-avoidance at higher speeds.

4.6.1 Do the expansion-avoidance results agree with predictions of fly motion detectors?

Ignoring the inverted responses that occur at low temporal frequencies, the open-loop expansion-avoidance results (Figures 4.4 and 4.7) are generally in agreement with properties of fly motion detectors. The responses are larger at increasing temporal frequencies, beyond which saturation is expected to occur (and was observed with 16 Hz expansion stimuli in pilot studies not shown), in accordance with the response properties of insect motion detectors (Buchner, 1976). The most striking evidence for the expansion-avoidance behavior being mediated by an array of Hassenstein-Reichardt (HR) Elementary Motion Detectors (EMDs) is provided by the fixation scores for the closed-loop experiment in Figure 4.2. The percent of time of FOC orientation, qualitatively resembles the typical shape seen for a system that is mediated by an HR-like motion detector—there is a temporal frequency optimum, and the optima for

this behavior under each of the three different spatial frequencies align at the same value. There are numerous examples of curves with these similar properties; originally found in the turning response of a walking beetle (Hassenstein and Reichardt, 1956; Reichardt, 1961), also observed in behavioral responses of walking and flying flies (Götz and Wenking, 1973; Heisenberg and Buchner, 1977; Buchner, 1984), in triggering the landing response in houseflies (Borst and Bahde, 1987), and in recordings of lobula plate tangential neurons (Hausen, 1982b; Haag et al., 2004). It is important not to overemphasize this similarity, because the curves in Figure 4.2C are not obtained from open-loop turning responses, rather they are the percentage of time that the flies orient towards the FOC. Nonetheless, the similarity does suggest that at the very least an array of HR-like (or modified HR motion detectors (Dror et al., 2001; Lindemann et al., 2005) underlies the expansion-avoidance behavior.

In Chapter 6, the expansion-avoidance response is modeled by an array of HR EMDs. From this effort, the predictions of the model can be compared to the behavioral data. A typical HR EMD designed to match the temporal frequency optimum relevant to flying *Drosophila* (§4.6.2) predicts that the $\lambda = 30^\circ$ pattern should produce a weaker motion signal than the pattern at $\lambda = 60^\circ$ expanded at an equivalent temporal frequency (as shown in Figure 6.4). Because the percent of time that flies carry out a particular orientation behavior, is identical for $\lambda = 30^\circ$ and $\lambda = 60^\circ$, this suggests that the expansion avoidance mechanism is not strictly dependent on the magnitude of the motion detector response, but rather is mediated by some form of bilateral comparison. The attenuated fixation observed with the $\lambda = 15^\circ$ pattern is likely due to the optical prefiltering of these narrower stripes (which at 7.5° each, are just at the threshold of no significant attenuation by the point-spread function of the *Drosophila* lens optics (Buchner, 1984). Thus, the signal does not enter the motion detectors as effectively as do the large-field cues generated by the lower spatial period patterns. However, the enhanced FOE orientation observed with the $\lambda = 15^\circ$ (seen as a rightward shift in Figure 4.2B, suggests that the magnitude of the motion detector response does affect the centering response more so than the expansion-avoidance response.

4.6.2 Temporal frequency optimum of Drosophila expansion-avoidance

To our knowledge, the only published value for the temporal frequency optimum (TFO) in a *Drosophila* optomotor behavior is from the work of Götz and Wenking (1973) on stationary walking flies. The peak turning is measured in response to rotatory motion of a 28° spatial wavelength pattern at a temporal frequency of 3 Hz (although the error bars suggest the 2-4 Hz range is the 'optimum'). The closed-loop FOC orientation data presented in Figure 4.2C obtains the highest percentage at a temporal frequency of 5 Hz (at the largest spatial wavelength). An ideal HR motion detector yields a TFO that is independent of spatial frequency (for sine or square intensity patterns) (Zanker et al., 1999); this is clearly the case in Figure 4.2C. A preliminary version of the open-loop expansion-avoidance experiments of §4.2 showed that the response to 15 Hz expansion was only slightly reduced from the response level at 8 Hz expansion (results not shown), suggesting that either the 8 Hz and 15 Hz responses straddle the TFO, or that the response gradually declines at temporal frequencies beyond the optimum, so that both 8 Hz and 15 Hz are just beyond a broad peak.

These new results suggest that the TFO of *Drosophila* motion detectors during flight is in the 5–8 Hz range. This new TFO value for *Drosophila* agrees with the TFO of HSE cells in Blowflies (Hausen, 1982b, Figure 5), also found to be approximately 5 Hz. This correspondence is somewhat surprising because the visual system of larger flies is often presumed to be optimized for faster motion. This value is considerably higher than the one reported for walking flies, but is this a difference between flight and walking or between expansion and pure rotational stimuli? Recent results from tethered flies in an identical experimental apparatus (Duistermars et al. in prep.) show that the TFO of *Drosophila* turning responses to rotation and expansion are the same, but that at each temporal frequency, the expansion stimulus induces larger magnitude turns than the rotational stimulus. Further, these experiments yield a TFO in a band that covers 5–10 Hz. Also the simultaneous investigation of the optomotor and landing responses of house flies (Borst and Bahde, 1987) reveals that the TFO for these two very different behaviors is the same (4 Hz). To obtain this result, Borst

and Bahde (1987) lowered the contrast of the landing stimulus to account for the differences in the transient responses of the motion detectors due to the differences in the dynamics of stimulation. It is unlikely that such a correction would change the results of §4.1, 4.2, but the observation does suggest that the open-loop stimuli may yield a higher TFO, which is consistent with our results. The recent results with freely flying *Drosophila* in a novel 'virtual open-loop' paradigm (Fry et al. in prep.) yield a TFO of around 8–10 Hz. Taken together these results strongly suggest that in flight the TFO for *Drosophila* motion detectors is approximately 5–8 Hz (but not likely to be much higher due to the distinction between steady-state and transient stimulation of the motion detectors (Borst and Bahde, 1987; Egelhaaf and Borst, 1989)). The discrepancy between the TFO in flight and in walking may be attributed either to parallel motion detection pathways with differing time constants (as observed by O'Carroll (2001)), some form of motion adaptation (Maddess and Laughlin, 1985; de Ruyter van Steveninck et al., 1986), or to some tuning that occurs downstream of the motion detectors.

4.6.3 Do the properties of fly motion detection predict the speed-dependent inversion?

One tantalizing suggestion is that the bell-shaped response curve predicted by HR-type motion detectors and observed in a wide variety of behavioral and electrophysiological studies (Srinivasan et al., 1999; Egelhaaf et al., 1989) in some way explains the speed-dependent inversion of the expansion-avoidance response (and of the ground motion response of Chapter 5). There is little evidence to support this idea. One difficulty is that *Drosophila*'s TFO is now believed to be at least 5 Hz, and the critical value governing the speed-dependent inversion is less than 1 Hz. Further, the fact that the monotonicity of the motion detector response (increasing temporal frequency yielding increasing EMD response) reverses beyond the TFO can only explain changes in response amplitude, not a sign inversion. The expansion-avoidance response is mediated by a system that in some way compares the motion seen by the right and left

eyes—since in all of the experiments both eyes receive motion of the same temporal frequency, the reversal of monotonicity is irrelevant to this behavior. Rather than the shape of the HR EMD response curve producing the speed-dependent inversion, it is far more likely (to this author) that subtle navigation occurs at lower values of image motion (monotonically increasing), while at higher speeds the strong, escape-like (e.g., expansion-avoiding) responses dominate the flies' behavior.

4.6.4 Hypothesis for role of head motion

The difference between the open-loop turning responses of head-free (Figure 4.5) and head-fixed (Figure 4.7) flies was certainly an unexpected result—the centering response disappears. At this point we can present no comprehensive explanation of this curiosity. It is entirely clear that fixing the head of *Drosophila* has an effect on tethered flight behaviors—when the closed-loop expansion-avoidance behavior of head-fixed flies was tested, the flies only showed transient fixation of the FOC. The long-lasting, robust, and repeatable orientation towards the FOC (Tammero et al., 2004) seems to also depend on head motion. To our knowledge, these are the first examples of significant behavioral differences caused by fixing the head of a tethered *Drosophila*.

In a series of experiments that are not documented in this thesis, the head motion of (head-free) flies was recorded (method outlined in 2.2.7) while they were presented with the open-loop expansion stimuli used in §4.2. A detailed analysis of head motion is required, but in brief, changes in head motion appear to be highly correlated with changes in wing motion. In response to high speed expansion presented at 45° to the animal's right, the flies generate counterclockwise torque (right WBA > left WBA), turning away from the FOE, while the head rotates to the left. When slow expansion is presented from this same position, the flies produce clockwise torque (right WBA < left WBA) to orient towards the FOE and the head rotates to the right. In general it appears that head rotation is coordinated with body rotation (other evidence for coordinated motor activity in flies is provided by Zanker et al. (1991), Hengstenberg

(1991), and Van Hateren and Schilstra (1999)).

One possibility is that the head motion simply rotates the location on the retina at which the FOC occurs. In order for the position of the FOE to cross the midline the head must rotate by more than the angular distance of the FOE from the midline (since at low speeds the head rotates towards the FOE). This is unlikely because orientation towards the FOE exists for FOE displaced by as much as 60° (or more) away from the midline, and the head of *Drosophila* is unable to rotate by this amount due to morphological constraints. Further, the expanded turning response time series shown in Figure 4.8, shows that the turn appears to accumulate rapidly, and that there is little time for the head to move and reposition the FOE. Lastly, it is not at all clear why head motion would alter the visual experience of a fly during slow expansion and not during faster expansion (especially considering that the head motion is largely mirror symmetric).

The head motion videos do show a surprising 'neutral' position of the head. As a tethered fly begins to fly, the head pitches forward considerably and remains in this position throughout flight. The head fixing procedure employed in the presented data aims to fix the head in the position now known to approximate the non-flight posture. The significant pitching of the head in tethered flight (not measured, but it may be as much as 30° or more) would considerably alter the regions of the eye that perceive the expansion stimuli. Since the head is fixed at an increased pitch angle, the direction of expanding motion that will be perceived as roughly parallel to the eyes of a head-free fly, will contain a significant component of upwards motion. It is possible that the system mediating the centering response is inhibited by this upward motion, which has been shown to initiate a 'thrust' response (Götz, 1968; Götz and Wandel, 1984). There is actually very strong evidence that this affects the behavior we report. A comparison of the ΣWBA responses in head-free flies (Figure 4.6), with the ΣWBA of head-fixed flies (Figure 4.7A) reveals that in response to the frontal FOE of all tested expansion rates, the head-free flies produce virtually no increase in ΣWBA, however head-fixed flies produce a massive increase in ΣWBA. This suggests that at the very least the pitch angle of the fixed heads used in these experiments is a significant effect,

although without further experiments we can not conclude that this is responsible for the disappearance of the centering response. Finally, it is not clear that fixing the heads of flies is a better way to conduct these experiments; the visual stimuli can be more reliably presented, but an important sensorimotor feedback loop is interrupted.

Based on the videos of the head motion of flying flies, our working hypothesis is that the role of head motion in *Drosophila* flight is to compensate for the inertial difference and an imperfect transmission mechanism (the neck) between the thorax and the head. The head turns towards the direction that the body is also turning, such that the head remains in line with the direction of flight. This hypothesis has the potential to explain why head motion relative to the body has not been detected in high speed video of freely flying *Drosophila* (G. Card, personal communication, 2005; Fry et al., 2003). We currently do not have video of the head motion of *Drosophila* with sufficient temporal resolution to compare it to the well-studied yaw motion of the heads of freely flying blowflies, which appear to show a motor pattern that minimizes the rotations of the head relative to the body (Van Hateren and Schilstra, 1999; Kern et al., 2006).

4.6.5 Closed-loop results with modified expansion-avoidance stimuli

Once the inversion of the expansion-avoidance behavior was established, several subsequent experiments were conducted to further characterize the behavior by placing constraints on the computational underpinnings of the centering and expansion-avoidance responses.

LATERALLY RESTRICTED EXPANSION

The orientation histograms and fixation scores for these experiments (Figure 4.9), demonstrate that reducing the motion to lateral regions of the eye significantly affects the orientation towards the FOC, but does not affect the FOE orientation (centering response). The centering response does not appear to make use of motion information from the frontal region of the eye and is most sensitive to motion at the sides. This finding further confirms that the FOE orientation is similar to the centering response

in bees, which is also thought to depend on motion perceived at 90° to the direction of flight (Srinivasan et al., 1991, Figure 8).

ASYMMETRIC EXPANSION

As has been demonstrated repeatedly, at low temporal frequencies of expansion, tethered *Drosophila* selectively orient towards the FOE. When slow, asymmetric pattern motion is presented, there is a small (barely significant) shift towards the side of slower motion. This constrains the sensitivity of the centering response—presumably flies will tolerate some small amount of asymmetry. This is evidenced by experiments with both walking and flying *Lucilia* that were blinded in one eye, in which Kern and Egelhaaf (2000) show only extremely small differences (biased towards the seeing eye) in locomotion when compared to untreated flies. In contrast to the low speed centering response, FOC orientation is strongly preferred at high temporal frequencies of expansion, but the response to asymmetric motion also shows a shift towards the side of slower motion. Is this also some kind of centering response? The shift in orientation seen with the 0:5 Hz and 0.25:5 Hz expansions asymmetries, are on the order of 25°, just slightly larger than half the size of *Drosophila's* rear blind spot. Presumably, once the fast motion side is rotated behind the fly by more than this amount, a portion of this fast motion stimulus is seen by the contralateral rear quarter field, which has been shown to elicit a counter-turn (Figure 4 of Tammero et al. (2004)). In the high-speed case, this apparent centering is complicated by the fact that once the turn towards the slower side is too large, expansion-avoidance dominates the response—thus this is probably not true centering, as occurs in the case of FOE orientation. As will be seen in the computational modeling of expansion-avoidance, it is possible to construct a system that yields both FOE orientation and centering, but a system that yields FOC fixation produces turns of precisely the opposite sign as the centering response. The weak centering response observed with low speed asymmetrical expansion is consistent with the free-flight behavior of *Drosophila* in between saccades, where flies were found to turn slightly away from the closer side of the arena (Tammero and Dickinson, 2002b).

ACCELERATING EXPANSION

The experiments of §4.5, were conducted as a way to introduce an accelerating visual stimulus into the simulations of translatory flight. Since increases in flight thrust are likely to result in body accelerations, the constant accelerations of the expansion may affect the flies' orientation preference. To some extent, this is observed in the fixation scores of Figure 4.11C. The critical value above which FOE orientation becomes unstable was shown to be between 0.625 and 1 Hz (§4.1, §4.2). In all trials of the acceleration assay except for fast deceleration, the critical value is found to be 1.25 Hz or higher. Thus, the temporal frequency critical value for the centering response, collected under constant f_t conditions, is likely to be an underestimate of the behaviorally relevant value, which may be twice as large when determined under varying expansion speeds. In response to the slower deceleration of expansion, flies maintain significant FOE orientation at all tested speeds. This suggests that if the flies perceive they are 'slipping' by either moving backwards or not moving forward quickly enough, then they respond by vigorously flying forward, towards the FOE. This suggestion is a modification of the 'preferred groundspeed' velocity control model suggested by Kennedy (1940), but one that is based on a dynamic comparison[4] of speed estimated by lateral regions of the eye. As a final note about the critical value of the centering response, the recent results with freely flying *Drosophila* in a novel 'virtual open-loop' paradigm (Fry et al. in prep.) show that the preferred flight speed of *Drosophila* in a tunnel lined with a sine wave grating corresponds to a laterally perceived temporal frequency of approximately 1 Hz. This result provides a methodologically independent corroboration of the behavioral relevance of the described inversion that governs the transition from a centering response to expansion avoidance.

[4]By a dynamic comparison, I mean that the fly does not simply compare the measured EMD response to some preferred level, otherwise there would be no difference in the critical value between the accelerating and constant velocity expansion experiments.

Chapter 5

Flight Responses to Ground Motion

In this chapter we investigate some responses of flies to motion of the ground below them. This line of investigation was pursued to address the third hypothesis of §1.11: the absence of visual motion below the flies in cylindrical arena experiments may contribute to the paradoxical preference for frontal contraction. In the typical range of free flight body postures of *Drosophila*, large parts of the eye are pointing downwards (David, 1979, 1978); these eye regions are drastically under-stimulated in most tethered flight assays. There is good evidence that visual estimation of ground motion is a crucial component of the *Drosophila* flight control system (David, 1978, 1979, 1982b). To test the role of ground motion on the steering response of tethered *Drosophila*, we built a planar display for presenting flies with patterns from below (Figure 5.1).

5.1 Turning responses to open-loop ground motion

5.1.1 Experimental design

Once tethered and rested, flies were positioned in a hovering posture 6 cm above a planar configuration of the display panels, as depicted in Figure 5.1. The display was constructed from 29 panels, arranged as a 6 × 5 grid (192 mm × 160 mm), with one panel (directly below the fly) removed to allow for the projection of the wingbeat shadow onto the wingbeat analyzer sensor. The fly was positioned such that there was one more row of the display in front than behind her. To prevent reflections of

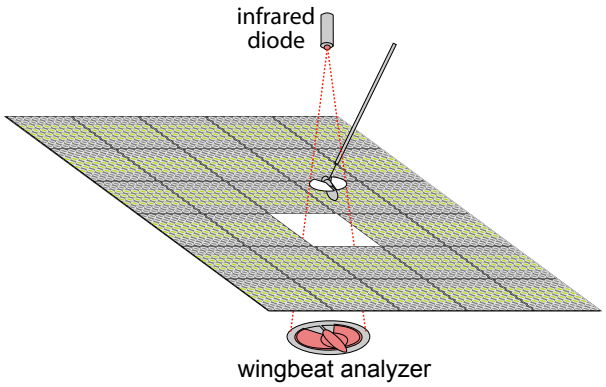

Figure 5.1. A 6 × 5 display (192 mm × 160 mm) of panels was constructed to evaluate the effect of ground motion on the visual control of flight. One panel, directly below the tethered fly, is removed to allow the wingbeat shadow to project onto the sensor.

the moving pattern from creating inadvertent motion stimuli on objects surrounding the experiment, a box lined with light-absorbing flock paper was placed around the display.

To assay the turning response to ground motion, the designed pattern consisted of alternating 4-pixel-wide bars of active and inactive pixels. In this geometry, the display is not uniformly distant from the fly retina. Therefore, it is sensible to define the spatial frequency of such a pattern for a hypothetical ommatidium with an optical axis pointing straight down. Directly below the fly, the pattern has a spatial frequency of approximately 30°. The pattern was advanced at 5, 10, 20, and 40 frames per second, corresponding to temporal frequencies of 0.625, 1.25, 2.5, and 5 Hz, respectively. Multiple orientations of the pattern were generated by rotating the original pattern frame using the Image Processing toolbox in MATLAB. Upon rotation, pixel values were determined by rounding the local intensity to force a binary-valued pattern. The experimental series consisted of a 5-second test phase of ground motion, followed by a 3-second pause with no motion, during which the entire display was set to a uniform, intermediate intensity value. During the test phase, the pattern was displayed at one of the 8 orientations (cartooned along the abscissa of Fig. 5.2B), advancing at one of

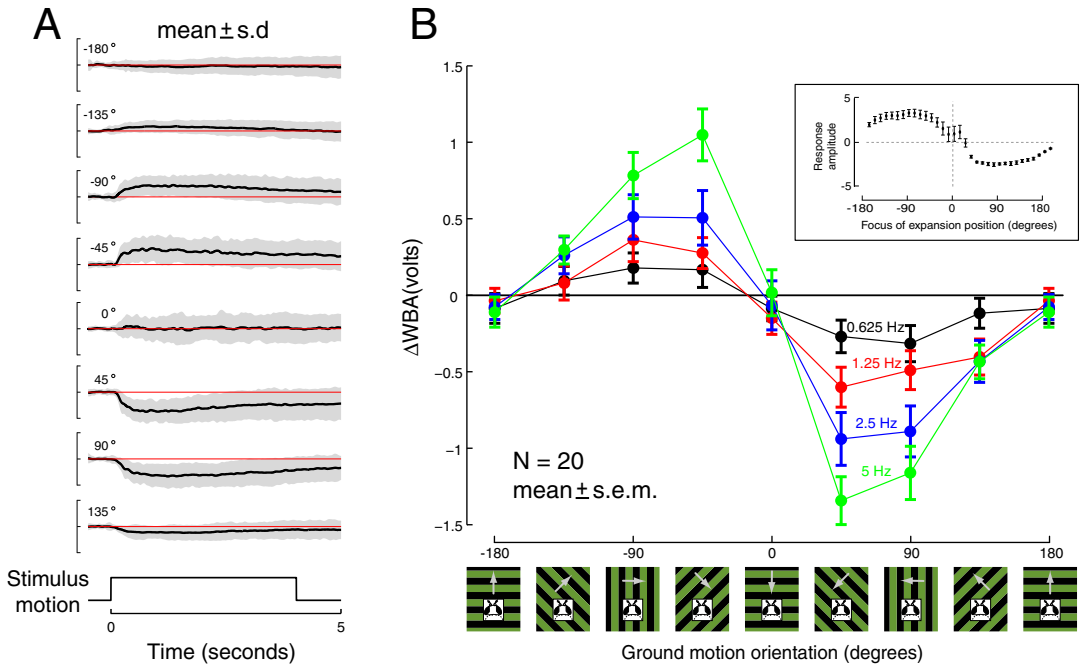

Figure 5.2. The steering response of *Drosophila* to ground motion of varying speeds and orientations, presented under open-loop conditions. When presented with visual motion from below, tethered flies attempt to turn with bilateral changes in wingstroke amplitudes. (A) The turning response (difference between left and right wingstroke amplitudes) to 8 directions of ground motion, for a temporal frequency of 2.5 Hz, is displayed as mean ± s.d. (N = 20). The annotation on each plot corresponds to the direction of motion. The ordinate is shown as a scale reference, range is -2V–2V. (B) The mean turning response to the 4 tested temporal frequencies of ground motion is plotted against the direction of image motion (N = 20; plotted as mean ± s.e.m.). The response curves reveal a trend that is very similar to the previous result obtained in a cylindrical arena while varying the spatial position of the focus of a panoramic stimulus of expanding stripes (inset, reproduced from Tammero et al. (2004)). For the temporal frequencies tested, the responses are progressively larger for increasing temporal frequencies. The 'tuning curve' suggests that flies turn so as to minimize the perceived displacement of the ground beneath them.

the four speeds in the direction orthogonal to the orientation of the stripes. The 32 stimulus conditions were presented in random block trials. In total, 20 flies completed between 1 and 5 repetitions of this protocol, each repetition lasting approximately 255 seconds.

5.1.2 Results

For these open-loop ground motion experiments, the desired quantity is the mean turning response of individual flies to the short period of pattern motion. The wingbeat amplitude data was low-pass filtered (4th-order Butterworth filter, 10 Hz cutoff), and the turning response was computed as the difference between the left and right wingbeat amplitudes. For each trial, the mean response during the 250 ms previous to the stimulus onset was subtracted from the subsequent turning response. For each fly, the mean turning response was determined for each of the 32 trial types (8 directions at 4 speeds), and is shown in Figure 5.2). The animal's *turning response* was monitored by the optical recording of the wingbeat amplitudes on both sides of the fly. The traces in Figure 5.2A show the mean (± s.d.) turning response of flies to coherent translatory motion (at a temporal frequency of 2.5 Hz) of the striped pattern below them. Flies turn so as to minimize the visually-perceived displacement below them, e.g., when the ground is drifting from right to left (orientation of 90°), the flies try to turn leftward, by producing counterclockwise torque. Therefore, the steering response to ground motion is consistent with the classically observed syndirectional optomotor turning response—when presented with a rotating environment, flies will turn so as to reduce the imposed retinal motion (Götz, 1964). A 'tuning' curve for the flies' orientation behavior (Figure 5.2B) has been constructed from the aggregate mean of the per-fly mean turning responses during the first 2 seconds after stimulus onset, for each of the 32 trial types. For the four motion speeds that were tested, the response of flies increases with temporal frequency. Presumably, the response would saturate, and eventually decline at even higher temporal frequencies, as predicted by the response properties of insect motion detectors (Buchner, 1976).

5.2 Speed-dependent orientation response to open-loop ground motion

The striking similarity between the ground motion turning response of Figure 5.2 and the open-loop expansion-avoidance turning response (originally measured by Tammero

et al. (2004), and also explored further in Chapter 4), suggested an investigation into the response to ground motion of slower temporal frequencies—would ground motion also exhibit a speed-dependent inversion? To address this question a variant of the experiment in §5.1 was conducted. This new experiment allowed the analysis of an additional long-standing question—is there a measurable signal that correlates well with translatory velocity, something that could be used to close a feedback loop around the speed of translation? Strong evidence suggests that flying insects adjust their airspeed to maintain a preferred level of visually transduced groundspeed (originally proposed by Kennedy, see the discussion §1.8). As discussed in §1.6, increases in thrust produced by *Drosophila* are well correlated with an increase in the bilateral sum of wingbeat amplitudes (Götz, 1964). Although the relationship between true thrust and ΣWBA is complex, the sum of wingbeat amplitude is clearly related to the control of flight speed, and is an important motor readout of a system that is clearly in need of further investigation.

5.2.1 Experimental design

Flies were positioned above the floor display as in the experiment of §5.1. As with the experiment of the previous section, the designed pattern consisted of alternating 4-pixel-wide bars of active and inactive pixels, however this pattern required 24 (as opposed to 8) frames to complete one 8-pixel cycle, taking advantage of the intermediate intensity values to achieve better temporal resolution (as discussed in §2.4). The pattern was advanced at 3, 6, 12, 24, and 120 frames per second, corresponding to temporal frequencies of 0.125, 0.25, 0.5, 1, and 5 Hz, respectively. As with the pattern used in §5.1, multiple orientations of the pattern were generated by rotating the original pattern frame. The experimental series consisted of a 4-second test phase of ground motion, followed by a 6-second period of closed-loop stripe orientation (discussion below). During the test phase, the pattern was displayed at one of 4 orientations (front-to-back, back-to-front, and 45° to the right and left of the fly), advancing at one of the 5 speeds in the direction orthogonal to the orientation of the stripes. The 20

stimulus conditions were presented in random block trials. In total, 13 flies completed between 2 and 5 repetitions of this protocol, each repetition lasting approximately 200 seconds.

To aid in conducting these experiments several stripe-fixation paradigms were attempted. David (1982b) reports that freely flying *Drosophila* will adjust their flight trajectories to fly in the direction of a stationary stripe on the floor. Several closed-loop patterns were tested: a striped (8-pixel spatial period) pattern rotating about the fly's position or moving side-to-side, a full 8-pixel-wide stripe directly below the fly, and a shortened bar (only on one side of the fly, not in front and behind—so that the fly need not choose when both ends of the bar are visible). But none of these closed-loop paradigms proved to be successful, resulting in anything like fixation. Nonetheless, it appeared that flies were (badly) controlling the pattern motion, and so the full 8-pixel wide bar pattern was used in the closed-loop assay interspersed with the open-loop tests (using a closed-loop gain that is half the size of the typical gain used in the cylindrical arena experiments).

5.2.2 Results

Tethered *Drosophila* were presented with open-loop ground motion at 5 temporal frequencies, moving along 4 directions, front-to-back, back-to-front, and ±45°. For the test of speed-dependent effects on the turning response (the ±45° motion), the desired quantity is the mean left minus right wingbeat amplitude response of individual flies to the short period of pattern motion. For each trial, the mean response during the 100 ms previous to the stimulus onset was subtracted from the subsequent turning response. For each fly, the mean turning response was determined by first using the 'flip and average' technique discussed in §2.2.6 to combine the data for the two directions of motion (after an inspection to ensure that the data were indeed nearly symmetric). The mean turning response (± s.d.) to the 45° motion (moving front-to-back and right-to-left) is shown as a time series in Figure 5.3A. The mean (± s.e.m.) over the entire 4-second trial is plotted in Figure 5.3B. At the 4 lower speeds, the flies turn

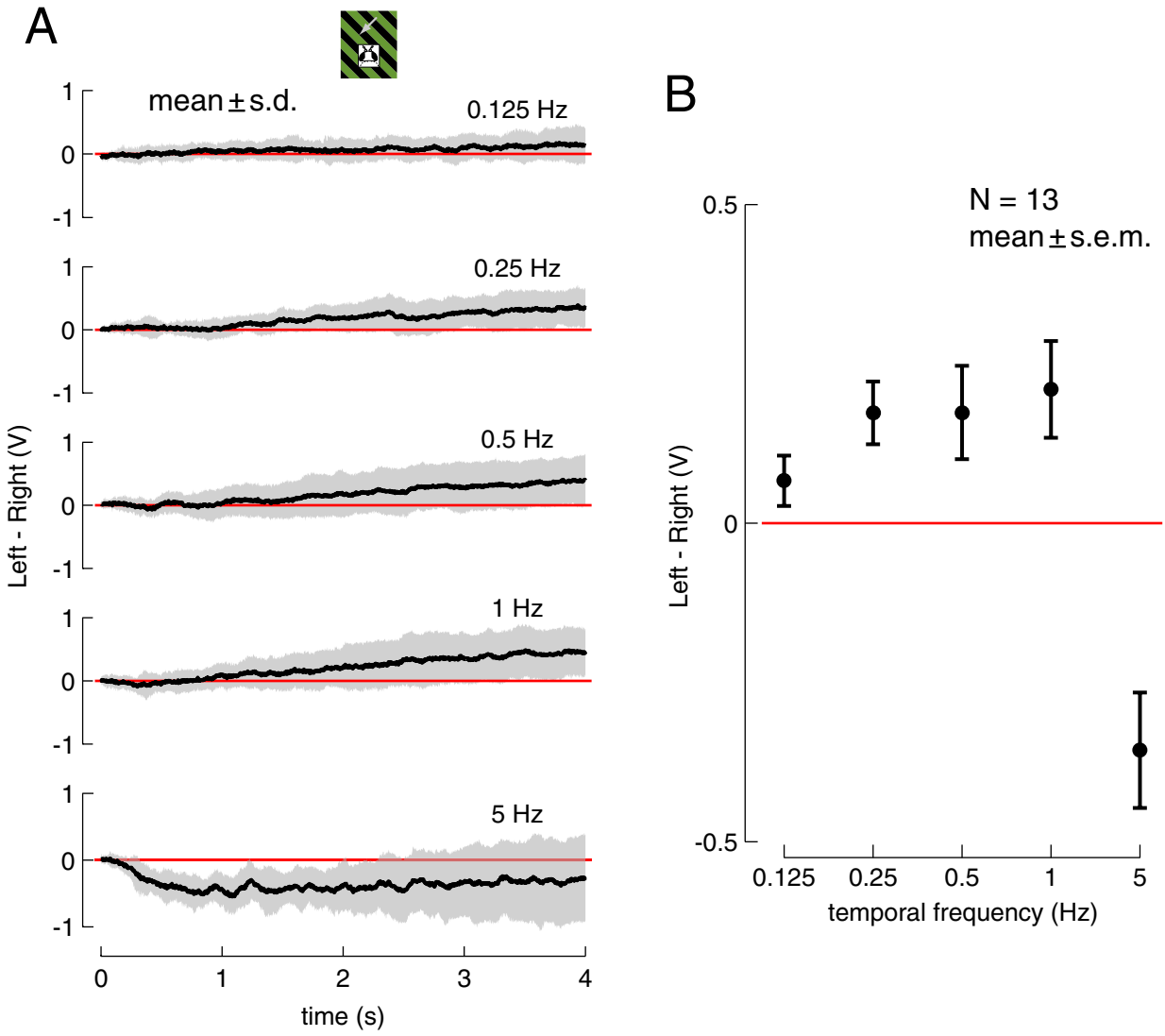

Figure 5.3. The steering response of *Drosophila* to open-loop ground motion of varying speeds (presented at ±45°, but averaged and displayed as if the motion is from in front and to the right). (A) The time series of the mean (± s.d.) turning response (difference between left and right wingstroke amplitudes) to 5 speeds of ground motion along the 45° direction. (B) The mean (± s.e.m.) turning response (averaged over the entire 4-second trial) to the 5 tested temporal frequencies of ground motion. As with the expansion-avoidance reflex (compare to Figure 4.5), the turning response to ground motion exhibits a speed-dependent inversion. At slower speeds, the turning response will orient the fly towards progressive (front-to-back) motion, while at higher speeds, the response is an attempt to orient the flies towards regressive ground motion.

clockwise, towards the source of translatory motion to their right, while at the highest speed the turning response is in the opposite direction. These results confirm that as with the expansion-avoidance response (Chapter 4), the ground-motion steering responses of *Drosophila* also feature a speed-dependent inversion.

The experimental series contained trials of front-to-back and back-to-front at the 5 speeds. For the test of speed-dependent effects on the 'thrust' response, the desired quantity is the mean left plus right wingbeat amplitude (ΣWBA) response of individual flies to the short period of pattern motion. Unlike the wingbeat amplitude difference (ΔWBA), the sum of amplitudes does not possess a convenient zero crossing. Largely as a result of tethering and fly alignment (§2.2.6), individual flies may produce drastically different values of the ΣWBA signal in response to the same stimulus.[1] Therefore, the mean value of ΣWBA during the 100 ms prior to the onset of each open-loop trial was subtracted from the subsequent ΣWBA response, so that the change in the 'thrust' signal is being reported. The mean (± s.d.) of this change in ΣWBA response to progressive (front-to-back) and regressive (back-to-front) ground motion is shown as a time series in Figure 5.4. The corresponding mean (± s.e.m.) over the entire 4-second trial is plotted in Figure 5.5A. The ΣWBA to progressive motion (in blue) is not significantly different from zero at the four lower speeds (t-test, in increasing order of f_t; P values are: 0.704, 0.0756, 0.2586, 0.1389, and 0.0002), but the response to regressive motion (in green) does differ from zero at all 5 speeds (t-test, P values of 0.0114, 0.0063, 0.0064, 0.0001, and 0.0003). To assess if the small (approximately zero) change in ΣWBA in response to the slower progressive motion is indicative of straighter flight, with less turning, the mean (± s.e.m.) absolute value of ΔWBA for these 10 conditions is plotted in Figure 5.5B. The absolute value is used, because the flies are likely to turn in either direction since the pattern presents no lateral motion. In all cases turning reaction are quite different from zero, and the (Δabs(WBA)) response to progressive and regressive motion was only found to be significantly different at the $f_t = 5$ Hz (t-test, in increasing order of f_t P values are:

[1] Although it is tempting to think that with the appropriate feedback signal much of this variability will go away, in analogy to the relatively arbitrary turning signals generated by flies operating under open-loop conditions that are rapidly made precise once a rotational feedback loop is closed.

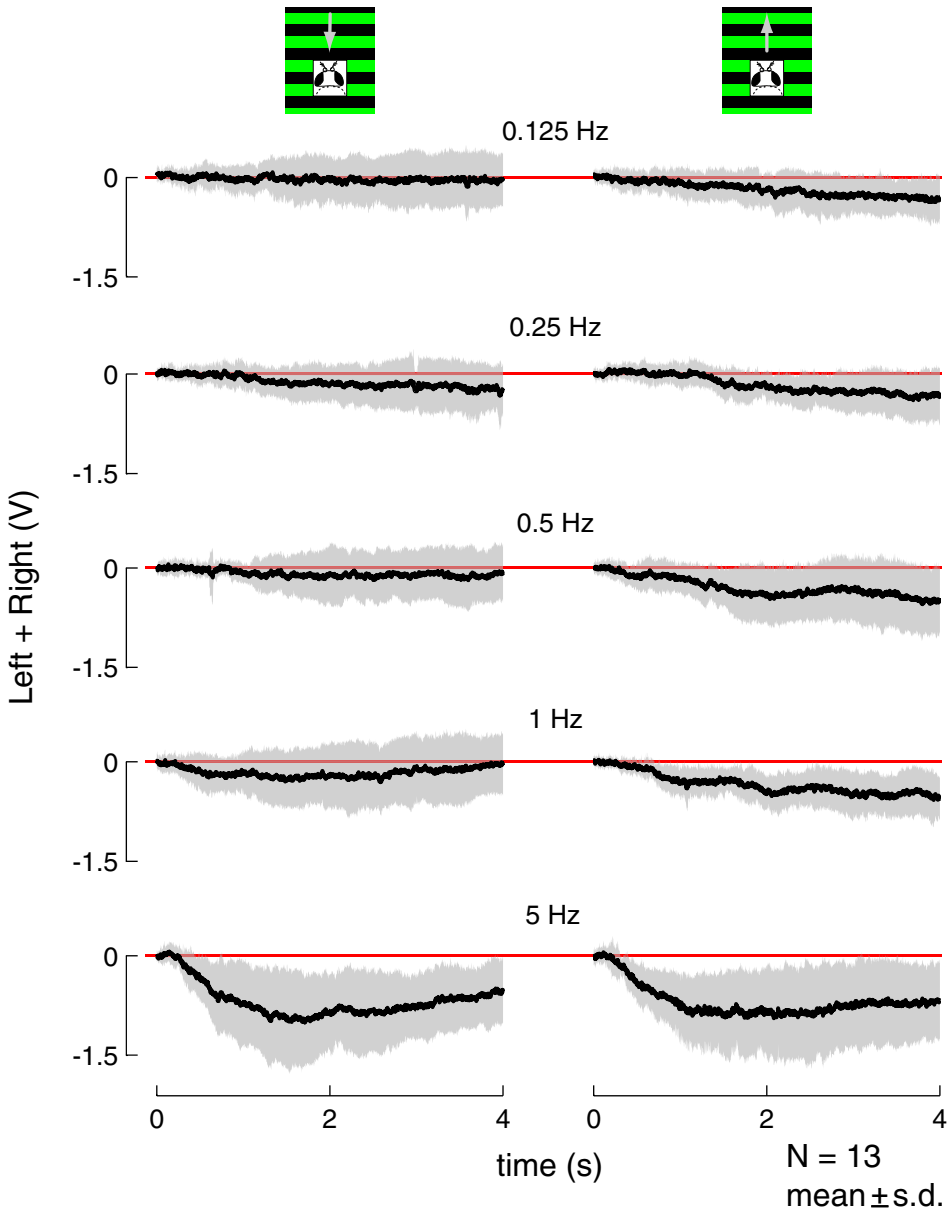

Figure 5.4. The mean (± s.d.) time series for the sum of left and right wingbeat amplitudes (a proxy for thrust force) to open-loop presentation of progressive and regressive ground motion at varying speeds. The quantity plotted is the change in the sum of wingstroke amplitudes after the onset of the open-loop trial. In all cases, there is either little change or a decrease in the left plus right signal.

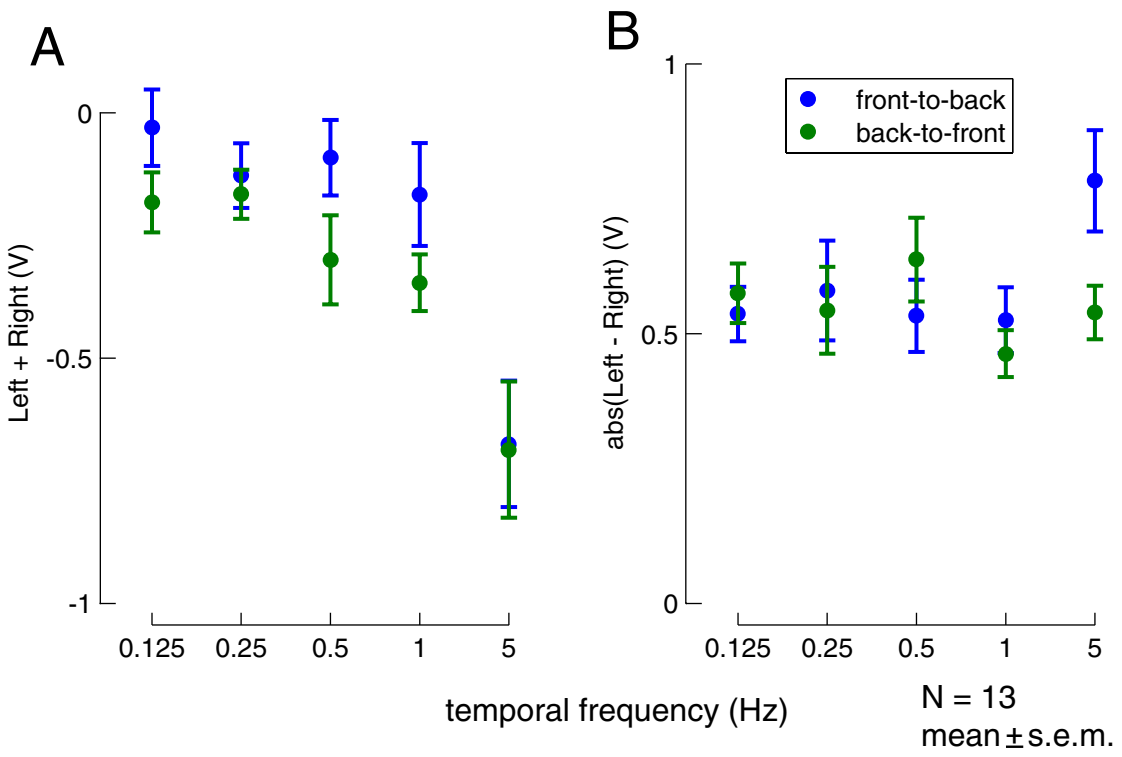

Figure 5.5. The mean change in the 'thrust' (sum of left and right wingbeat amplitudes), and the absolute value of the change in turning (difference between left and right wing) to open-loop translatory ground motion (both progressive and regressive). (A) The mean change in the 'thrust' response, corresponding to the time series data of Figure 5.4, either does not change or decreases during the open-loop trial. At the four slower speeds the response to progressive motion (blue) shows a smaller decrease than the response to regressive motion (green). (B) The absolute value of the turning response, used as a proxy for general steering, does not reveal large differences between speeds.

0.6113, 0.768, 0.3198, 0.4171, and 0.0308). At the four slower temporal frequencies tested ($f_t < 1$ Hz), there is no evidence that the onset of regressive motion causes a change in the modulation of the summed wingbeat amplitudes, though this is not accompanied by a decrease in attempted steering.

To conduct these experiments it was useful to include a closed-loop stimulus interspersed with the open-loop trials. As mentioned above, none of the tested closed-loop stimuli were very successful. The mean orientation histogram (± s.e.m.) during the 6-second closed-loop stripe fixation trials is shown in Figure 5.6A. The orientation of the stripe at 8 positions is cartooned along the perimeter of the plot.

In comparison to the random orientation percentage (indicated by the gray circle in the orientation histogram), it is clear that the flies are not fixating the stripe. The increased probability of the position of the stripe indicated at the top of plot is due to the initial position of the stripe at the start of the pattern. If true fixation occurred, then there would also be an increased probability associated with 180° opposite stripe position, in which the display shows the identical image. From the initial experiments with the ground motion paradigm (§5.1), it was apparent that flies respond in a robust and repeatable fashion to visual stimuli presented from below, but experiments were difficult to conduct because flies would not fly for very long during these experiments. Perhaps this is a more extreme, though similar situation as occurs during cylindrical arena open-loop experiments—most flies are not likely to fly for more than 10 minutes or so without any periods of closed-loop control (unless their flight motivation is altered by, e.g., prolonged starvation or the presentation of odors). Therefore, even though it does not appear that the flies are actually 'fixating' the stripe during the closed-loop trials presented in Figure 5.6A, this paradigm is extremely useful in that flies respond with increased WBF (Figure 5.6B) during these trials (preventing flies from ceasing to fly), and has enabled longer experiments.

Since the mean change in the 'thrust' data in Figure 5.5, show very similar responses for progressive and regressive motion, one possible hypothesis is that the downward-looking motion detector system that regulates groundspeed is primarily sensitive to non-direction motion. A simple test of this hypothesis is to stimulate the flies with a sinusoidally varying ground motion stimulus, as shown in Figure 5.7. The pattern was oscillated through a sine wave of ±50 frames at 0.2 Hz (an analysis of the collected data show the oscillations, commanded to run at 0.2 Hz did in fact run closer to 0.205 Hz). The mean data in this figure do not show a frequency doubling, in either the ΣWBA or the WBF response—overall there is a trend towards reduced ΣWBA and WBF, which is typical in longer open-loop trials. Both ΣWBA and WBF increase during front-to-back motion, and decrease during back-to-front motion. The changes in ΣWBA and WBF occur (on average) within approximately 250 ms of the change in direction of the stimulus. The response to oscillating ground motion shows no

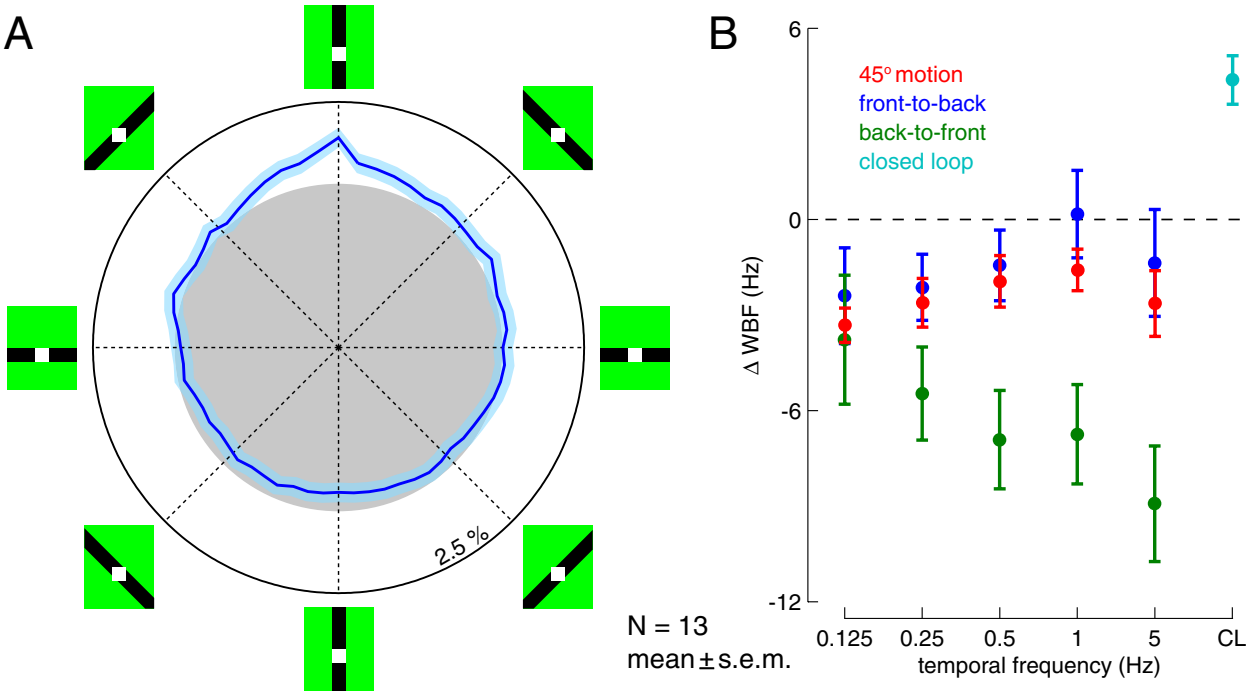

Figure 5.6. The search for a robust closed-loop paradigm using the ground display was not successful. However, flies certainly responded to a large (8-pixel wide) stripe, rotating about the fly's position. The mean (± s.e.m.) orientation histogram (A), does not reveal a strong preference for any position of the stripe other than the initial orientation (gray circle indicates percentage for random orientation). (B) The change in wing beat frequency during a trial for the data presented in Figures 5.3, 5.4, and 5.5 and during the closed-loop epochs, is shown. During the short closed-loop trials, wing beat frequencies are elevated, indicating that, at the very least, the flies fly 'harder' in response to the closed-loop stimulus.

evidence for a non-directional response. While these experiments were conducted, the head motion of the tethered flies was also recorded (§2.2.7), revealing that the head also passes through some oscillations about the pitch axis. This provides additional evidence for the idea that the head moves to compensate for rotations of the body, as modulations of ΣWBA will certainly affect the pitch angle of the body (with a roughly 80 ms time delay (David, 1985)).

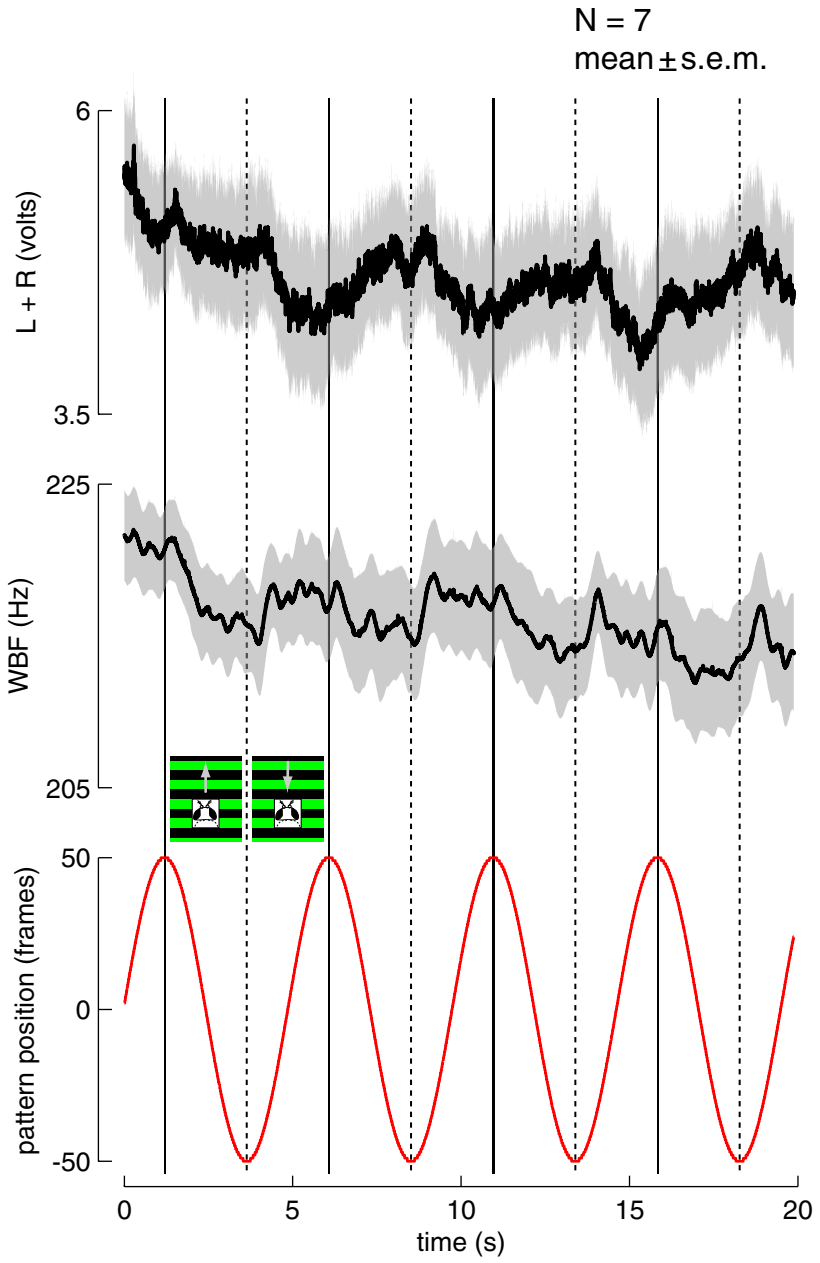

Figure 5.7. The mean (± s.e.m.) WBF and ΣWBA responses to oscillating translatory ground motion. These traces do no show evidence of frequency doubling, indicating that the WBF and ΣWBA respond to the directional motion of the pattern and not the direction-independent temporal frequency. The dashed vertical lines show the transitions to front-to-back motion. In general the WBF and ΣWBA increase during progressive motion and decrease during regressive motion.

5.3 Discussion

5.3.1 Turning responses to ground motion

The observed steering response of *Drosophila* when stimulated with ground motion is consistent with both the classically observed syndirectional optomotor turning response and the expansion-avoidance reflex. At all speeds, the mean response of flies to the moving bars oriented at 0° and 180° are close to zero. However the sign of the slope of the tuning curve through these points is opposite. This suggests that the regressive, or back-to-front motion, is the stable configuration. The stability of regressive motion predicts that flies apparently 'prefer' *backwards* flight. The shape of the tuning curve, and the predictions for stable backwards flight are highly analogous with the recently observed expansion-avoidance response (Tammero et al., 2004). For comparison, this previously published tuning curve has been replicated as an inset in Figure 5.2B. As has been done with the expansion-avoidance paradigm, the current results suggest that it should be possible to close a feedback loop around the direction of a translating floor stimulus.

The response of *Drosophila* to visual motion simulating a translating flow field revealed that flies selectively orient towards the contracting pole of an expanding pattern (Tammero et al., 2004). This paradoxically suggests that flies seem to prefer flying backwards. The ground motion experiments were motivated by a desire to test the hypothesis that the lack of ground motion, known to be a critical component of the flight control system, may contribute to these paradoxical findings. This did not prove to be the case—the ground motion results are entirely consistent with the avoidance of panoramic visual expansion. In an experiment simulating side-slip, a tethered fly in a cylindrical flight arena, presented with an expansion cue to their right, will try to turn leftwards (Tammero et al., 2004). The corresponding global side-slip stimulus would consist of right-to-left ground motion, from which we show that flies would also turn leftwards. It is almost certain that the combined stimulus (presented in a hypothetical cylindrical flight arena above a floor display) would elicit responses of the same direction.

To our knowledge, these experiments were the first attempt to measure the response of a tethered fly to pattern motion presented from below the animal. With freely flying *Drosophila* in a wind tunnel, David (1979) showed that for strong ground motion stimuli, most flies exhibit floor-following speed changes. If the floor is accelerated below them, then flies modulate their airspeed to move in the direction of the ground motion. However, in these results, flies maintained their upwind orientation, and moved relative to the ground motion by modulating their production of forward thrust. In a separate experiment, flying *Drosophila* in still air were found to orient in the direction of moving stripes presented in a square opening in the floor of a square chamber (David, 1982b). While our results show a type of floor-following behavior, the tuning curve presented in this paper predicts that flies should orient so that they receive a regressive ground cue. David (1979, 1982b) does not report this behavior. There are two, not necessarily mutually exclusive explanations for this difference—either the visual speed on the retina of the freely flying flies was much lower than the range of speeds tested here, and/or the role of wind, or some other sensory stimulus not present under tethered conditions, is sufficient to bias the flies' orientation towards progressive motion.

5.3.2 Speed-dependent turning response

The turning response of tethered *Drosophila* in response to a translating ground motion exhibits a speed-dependent inversion as was found with the expansion-avoidance paradigm. The analogy with the results of Chapter 4 is apt; at higher speeds both the ground motion and the expansion-avoidance responses are turns away from the direction of motion, presumably an aggressive course correction of some sort, while at the slower speeds the flies turn so as to maximize progressive motion. The confirmation of this finding in two very different paradigms suggests that this previously unreported feature of vision-based *Drosophila* navigation may be a significant component of the flight control system.

The turning response to ground motion shown in Figure 5.3 disagrees with the

tuning curve obtained in the earlier experiment (Figure 5.2). The newer results show that at all temporal frequencies below and including 1 Hz, the turning response is towards progressive motion, while the previous results show a response of the opposite sign at 0.625 Hz and 1.25 Hz. Every effort was made to maintain similar conditions between these experiments that were conducted 2 years apart, but the results in Figure 5.3 were obtained using a newly built display of slightly improved panels that are brighter and faster. Additionally, the stimulus used in the experiments of Figure 5.3 was generated using much smoother motion (method discussed in §2.4), and the newer experiments were interspersed with epochs of closed-loop control. A subsequent experiment (not shown) has suggested that the smoothness of the ground motion at low speed is necessary to show the centering-like (inverted) response. The significant methodological improvements in the newer experiments were probably the cause of this discrepancy.

5.3.3 Differences in the critical value of inversion across the eye

As demonstrated by the results of §5.2, the downward looking regions of the *Drosophila*'s eye encode motion that yields a speed-dependent inversion of the turning response to ground motion. The critical value at which the response inverts is not easily established with the current data—it can only be bounded as greater than 1 Hz and less than 5 Hz. Even if uncertain, it is likely that this critical value is higher than the similar value found with the expansion-avoidance paradigm in Chapter 4. One possible explanation is that different regions of the eye have different temporal frequency optima of the motion detectors. Götz and Wenking (1973) show optomotor responses of walking flies to motion at 3 positions on the retina at different orientation; the temporal frequency tuning curves show differences in the response amplitude that depend on the position on the eye of motion and the motion direction, but show no significant differences in the temporal frequency optima at the different eye regions. To our knowledge, only the very recent work of Straw et al. (2006) has explicitly tested local properties (temporal, spatial, and contrast sensitivities) of motion detection on the eye and found

a modest temporal frequency enhancement in the frontal eye regions of *Eristalis*. This tuning for faster motion is presumed to assist in aerial chasing, and so is not likely to relate to *Drosophila* motion processing. Alternatively, the as-yet unknown system that mediates the speed-dependent inversion simply does so with different speed tuning. A final hypothesis is that the critical value obtained in the ground motion assay may be closer to the relevant value for translatory flight. The ground motion assay presents the flies with a much less ambiguous implementation of a visual motion stimulus approximating translation, rather than the cruder expansion-based version of translatory flow presented in the experiments of Chapter 4. The fast, high-gain expansion-avoidance reflex that is ideally stimulated by the FOE-FOC stimulus (most likely a quick coarse correction), may dominate the centering response and result in a lowered critical value for the response inversion.

5.3.4 Search for a velocity control signal

When flying on a rigid tether, *Drosophila* produce a downward pitching moment (Sugiura and Dickinson in prep.; Fry et al., 2005). Because the control of steering about this axis is as yet not fully understood, it is not clear how to correlate changes in ΣWBA with steering forces. It is entirely possible that the signals obtained using the wingbeat analyzer are simply too heavily 'filtered' to recover enough of the complexity of the full wing kinematics to make such predictions. One aim of the experiments of §5.2 was to find a signature of velocity control in the measurable wingbeat signals. It was hoped that the plot of the changes in ΣWBA in response to progressive and regressive motion of various temporal frequencies (Figure 5.5) would reveal a zero crossing, indicating that whatever modulation of the coupled lift-thrust-pitch control the flies generate was passing from one sign to another, transitioning from pitch up or increased thrust to a pitch down or decreased thrust. Such a signal could be exploited in a closed-loop velocity control experiment, which would all but enable the much sought after double closed-loop assay in which the thrust signal controls forward motion, and the yaw signal is used for turning. Unfortunately, the results of Figure 5.5

do not reveal such a zero crossing. At best the responses show no change in ΣWBA as the experiment transitions from the (poor) closed-loop rotational control of a stripe to slow progressive motion. Presuming that during this entire experimental series the flies are producing a pitch down moment, then at the onset of slow progressive motion, since the ΣWBA signal is unchanged, the flies do not produce any velocity control signal at all. This either indicates that the stimulus motion is too low to induce a compensatory reaction (though this is unlikely because the same speed of motion with a component of side slip is sufficient to generate a turning response), or is evidence that the progressive motion is in the range of *Drosophila*'s preferred groundspeeds (the Kennedy theory discussed in the introduction to §5.2) and therefore, does not necessitate further wingbeat adjustments. This issue is far from resolved; further experiments are necessary and stimulation of additional sensory systems must be considered.

Chapter 6

Computational Modeling of Expansion-Avoidance and Centering Behavior

The modeling effort described in this chapter was undertaken to provide a 'proving ground' for many of the ideas that emerged in the interpretations of the behavioral data in Chapter 4. The behavioral data is treated as providing a set of constraints for the properties of the computational model. It is worthwhile to emphasize that a black-box style of modeling is employed herein,[1] the goal of which is to understand the algorithmic basis for the observed behaviors. I make no claims about any particular component of the model mapping to a specific set of neurons—however the search for the neural circuits underlying these behaviors can only be aided by a more complete description of their function. This work is motivated by the conceptual hierarchy laid out by Marr (1982), and shown in Figure 6.1. If the ultimate goal is to understand the complex behavior underlying the visual control of flight (or any information processing system), Marr (1982) claims that this understanding must occur at three distinct, interacting levels—the top level concerns the goal of the computation being carried out, the intermediate level concerns the algorithm being implemented, and the bottom level concerns the physical realization of the algorithm. This hierarchy provides a useful context for studies of the flight behavior of *Drosophila*, which can be thought of as a

[1] An interesting discussion of the ways in which modeling can be used to describe behavior is provided by Webb (1999).

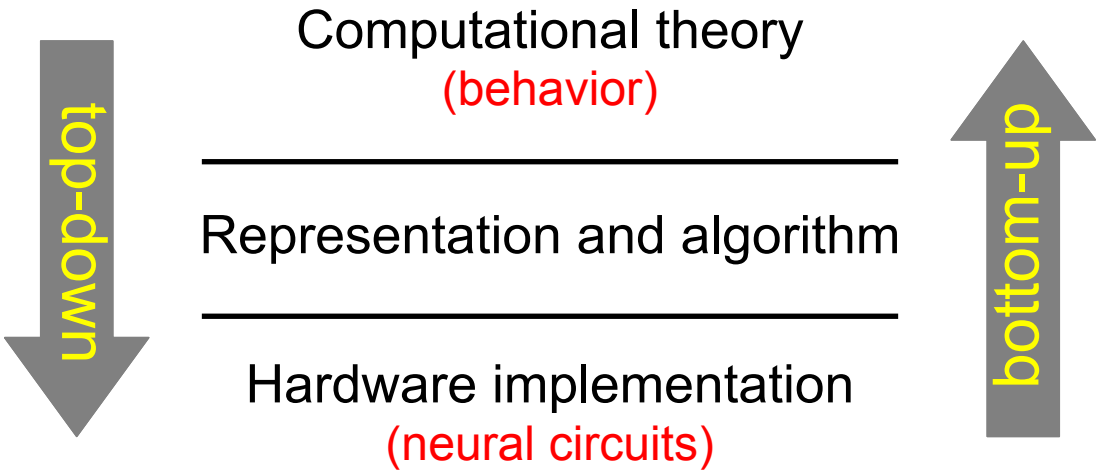

Figure 6.1. The conceptual hierarchy for understanding information processing systems as outlined by Marr (1982). The experiments presented in this thesis are an example of the top-down approach to unraveling complex behavior. The goal of the computational modeling is to use the behavioral results (top level) and the known properties of fly visual processing (bottom level) to study the algorithmic basis for the flight navigation behaviors.

readout of the animals' computations, that are ultimately implemented by circuits of motion-processing and motor-control neurons. In this context, the behavioral approach employed in this thesis is clearly seen as a top-down strategy, as investigations of behavior are used to constrain the algorithmic and circuit levels below. Methods rooted in physiology, genetics, and imaging represent the complementary, bottom-up approach. As a final comment, the simulation effort in this chapter stems from a belief that models of animal behavior are of little value without any attempt at their validation (Webb, 2006).

6.1 Methods: Modeling the fly visual system

The motion detection system of flies has an extensive history of detailed investigation (§1.3). The image-forming and motion-detection pathways of the fly visual system are well modeled with a simple compound eye optics model above a photoreceptor array feeding an array of Hassenstein-Reichardt (HR) Elementary Motion Detectors

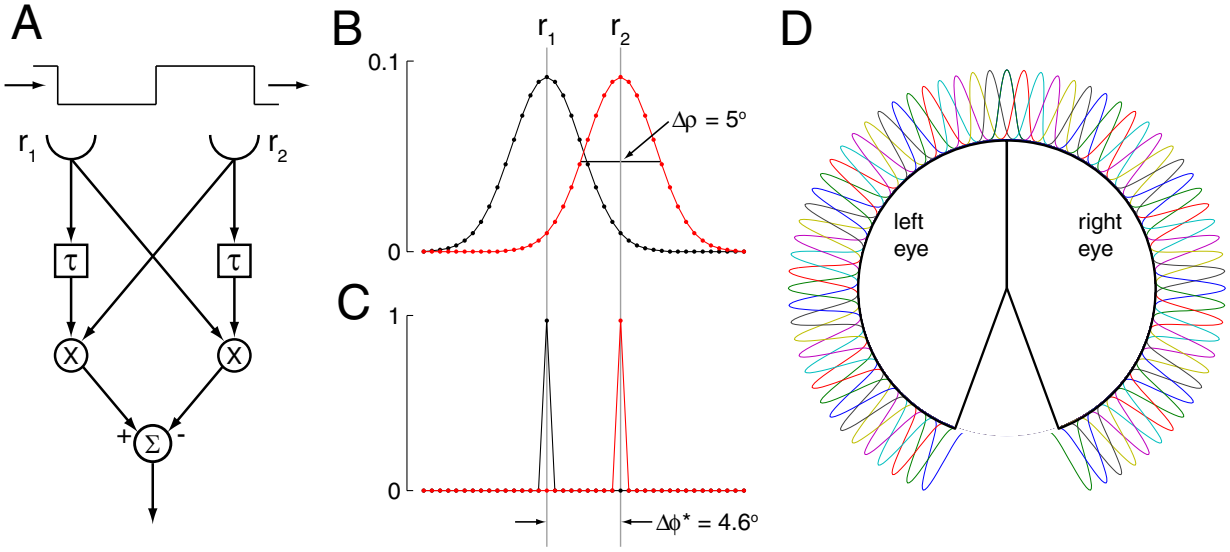

Figure 6.2. (A) The basic Hassenstein-Reichardt motion detector, composed of a 'delay and correlate' mechanism. As some time varying intensity sweeps across the two photoreceptors, (from left to right) first stimulating r_1 and then r_2, the delayed version of signal from r_1 will exhibit some temporal coincidence with the signal from r_2, yielding a positive response. (B) Two models for the visual system front end. The historical model was simply the needle-like sampling function, shown in C. The Gaussian sampling function models the point-spread function of the ommatidia of *Drosophila*'s compound eye. (D) The simulated 2-D retina, in which the equatorial plane through the eye is modeled as an array of bell-shaped sampling functions, with a uniform spacing. There is a one-receptor overlap in the front and approximately a 40° blind spot in the rear.

(EMDs). Since the experiments discussed in this thesis primarily rely on rotational responses of the animal to motion presented on a cylindrical display, a planar retina, representing an equatorial cross-section through the fly's eye, makes an appropriate model. In *Drosophila*, the photoreceptor array is distributed with near uniformity throughout the eye. Along the equatorial region of the eye, there is an overlap of approximately 5°–10° in the front, and a blind spot of roughly 40° directly behind (to our knowledge, the only *Drosophila melanogaster* eye map was done by E. Buchner, and reprinted in Heisenberg and Wolf (1984)). The components of the simulated fly eye are shown in Figure 6.2. The basic HR EMD (A) reveals the 'delay and correlate' mechanism; the inputs to each paired motion detector are the signals from adjacent ommatidia (Buchner, 1976). In the original modeling of the HR EMD,

the photoreceptors were modeled as needle-shaped (delta) functions that sample the intensity signal at one point in space (C). Significant realism is provided by including the point-spread function of compound eye optics, which act as a spatial low-pass filter (B). This point-spread function of the compound eye optics, $L(\Theta)$, is modeled as a Gaussian (bell-shaped) sampling functions of the form

$$L(\Theta) = k \exp\left[-\frac{4 \ln 2}{\Delta\rho^2}\Theta^2\right], \tag{6.1}$$

where k is the normalization constant, $\Delta\rho$ is the acceptance angle of the photoreceptor, and Θ is the vector of positions around the eye. This fit for the compound eye optics is based on equation B.5 of Snyder (1979), but using the notation of Burton and Laughlin (2003). In the simulations of *Drosophila*, we use $\Delta\rho = 5^\circ$ (after Figure 18 of Buchner (1984)), and Θ is sampled at increments of 0.375° for 960 positions on the retina. The circular retina is modeled as an array of 72 such photoreceptors, with a binocular overlap of 1 photoreceptor in the front, and a blind spot of approximately 20° per side in the rear (Figure 6.2D). Buchner (1984) specified that the interommatidial angle, $\Delta\phi^*$, for *Drosophila* is 4.6°; in order to accommodate a simple discretization, the implemented retina uses $\Delta\phi^* = 4.5^\circ$. The retinal image is formed by the convolution of the intensity signal $I(\Theta, n)$, a function of angular position and the discrete sample time, n, with the acceptance function of the photoreceptors:

$$R(n) = L(\Theta) \otimes I(\Theta, n). \tag{6.2}$$

In the simulated retina presented here, the 72 $L(\Theta)$ functions are concatenated as a matrix, and the retinal image $R_j(n)$, where j is index of ommatidia, is obtained by matrix multiplication.

Ray tracing is used to simulate the view of the fly in a virtual environment,[2]. The simulated environments used thus far are either a circular arena or a corridor. A lookup table is created that specifies the boundaries of patches of bright and dark

[2]The method used is not the sophisticated ray tracing common in modern computer graphics, but is the simpler version, often called *ray casting* that does not account for reflections, refraction, or absorption of the light rays.

intensity on the walls of the environment. At each simulation time step, n, the intersection of the rays emanating from the 960 positions of Θ is determined by the equations for line-circle intersection (in the circular arena) or for the intersection of two lines (in the corridor simulated as a long rectangle). Once the intersection values are determined, the lookup table is used to determine the intensity values at each location along Θ, yielding the intensity signal, $I(\Theta, n)$. To implement rotations of the simulated eye, the orientation of the 960 rays is rotated relative to the environment. The choice of sampling the environment at 960 positions was a deliberate one that enables a very simple integration of the simulated eye into a simulated flight arena. The standard cylindrical flight arena used in the experiments of Chapters 3–4 consists of a circumference of 96 pixels; a simple factor of 10 up-sampling of the identical patterns used in the flight arena experiments yields the 960 samples of the visual world required for determining $I(\Theta, n)$.

The array of Hassenstein-Reichardt motion detectors is used to compute the optic flow field from the retinal image $R_j(n)$, where j indexes the 72 ommatidia, and n is the discrete time step number. A first-order low-pass filter (with time constant τ) is used to accomplish the delayed intensity signal required for the EMD computation. The temporal frequency optimum (TFO) of the HR EMD response curve is entirely determined by low-pass filter time constant τ: TFO $= 1/2\pi\tau$. We use $\tau = 30$ ms, which yields TFO $= 5.3$ Hz, in agreement with the TFO of the expansion-avoidance behavior (§4.6.2). We define two digital filter coefficients, $A = \exp(-h/\tau)$ and $B = 1 - \exp(-h/\tau)$, where h is the sampling interval, 1/1000 s. The delayed intensity function is:

$$D_j(n+1) = B * R_j(n) - A * D_j(n). \tag{6.3}$$

Finally, the response of the HR EMD array is computed by multiplying the delayed signal at each position with the current value at the neighboring position and subtracting the resulting value of the mirror symmetric pair. In contrast to previously implemented HR EMD arrays where the retina was treated as a single uniform structure (Tammero

and Dickinson, 2002b; Reiser and Dickinson, 2003), in the current results the motion for each eye is computed separately. Because the motion is computed between pairs of photoreceptors, if there are J elements in $\mathbf{R}(n)$, where $J = 72$ in the current simulation, there will be $J - 1$ elements in the motion detector array output, which leads to a right-left asymmetry in the EMD response array if the retina is treated as a single 'input.' The right and left halves of the retina are treated as separate inputs, resulting in EMD responses that are symmetric in the case of, e.g., frontal expansion. The responses of the motion detector array on the right, MR, and left, ML, sides are computed as:

$$ML_k(n) = D_k(n) * R_{k+1}(n) - D_{k+1}(n) * R_k(n), \quad (6.4)$$

$$MR_k(n) = D_{36+k}(n) * R_{37+k}(n) - D_{37+k}(n) * R_{36+k}(n), \quad (6.5)$$

where k indexes the motion detector array output from the right and left eye. Because the motion in each eye is treated separately, there are 35 elements in each of ML and MR.

6.2 Simulation results

6.2.1 Response properties of the modeled motion detectors

Before examining the response of the full motion detector array, the response properties of the HR EMD to several stimuli are considered. The implemented HR EMDs receive inputs from a photoreceptor array with optics modeled after the *Drosophila* compound eye, and the time constant in the motion detection pathway has been selected to match the experimental results of Chapter 4. To aid in the analysis of the expansion-avoidance behavior, the response of the modeled EMD to the motion of patterns with the three spatial periods used in the experiments of §4.1 is explored in some detail. The time series of $t_f = 5$ Hz (near the TFO) motion stimuli and the corresponding EMD responses are shown in Figure 6.3. Because of their historic importance as

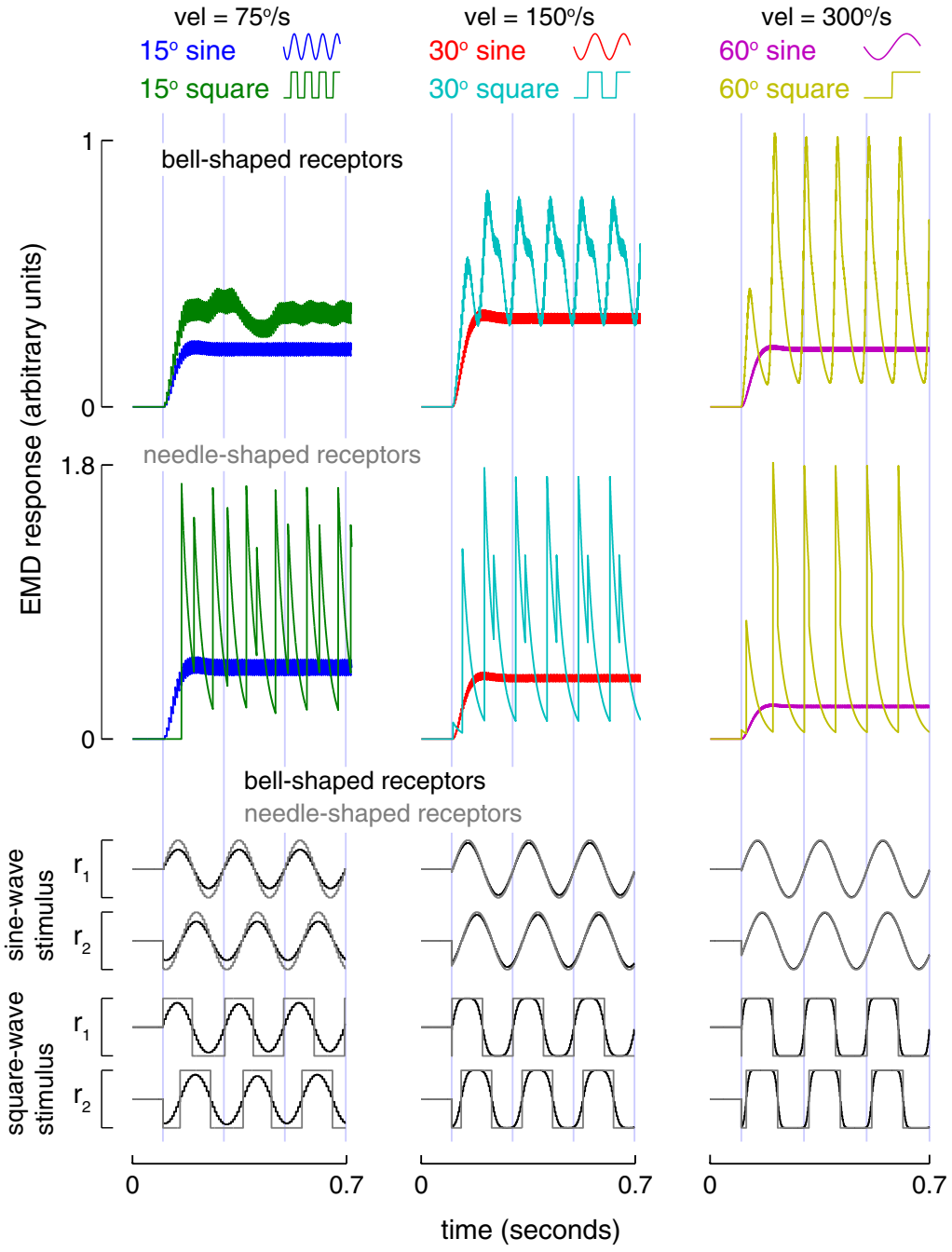

Figure 6.3. The response of a single motion detector unit (receiving input from the photoreceptor pair r_1 and r_2, as in Figure 6.2A) to motion of sine-wave and square-wave intensity patterns of 3 spatial frequencies, moving at the same temporal frequency of 5 Hz (close to the temporal frequency optimum of the HR detector). The responses signals from both needle-shaped and bell-shaped receptors are shown, as well as the stimulus intensity transduced by the two photoreceptors, r_1 and r_2, for both needle- and bell-shaped receptor sampling functions. The EMD responses are colored to match the mean data in Figure 6.4.

stimuli in studies of fly motion detection, the model EMD has been stimulated with square- and sine-wave gratings of the three temporal frequencies, and for completeness, both needle- and bell-shaped photoreceptors have been simulated. The motion begins at t = 0.1 seconds, and continues until 0.7 seconds, during which 3 cycles of the stimuli pass by the photoreceptors. Because the three patterns have different spatial wavelengths ($\lambda = 15°, 30°, 60°$), the angular velocity of the patterns is adjusted to yield the same temporal frequency (75°/s, 150°/s, 200°/s, respectively). The bottom row of Figure 6.3 shows the time series of the stimulus intensity filtered by the photoreceptors. In comparison to the needle-shaped sampling (data in gray), the photoreceptors using the Gaussian optical sampling act as spatial low-pass filters, significantly attenuating the intensity transduced in response to the $\lambda = 15°$ stimulus. The top row of Figure 6.3 contains the response of the EMDs receiving inputs from the bell-shaped receptors. The EMD response to the motion of the sine-wave grating stimuli is essentially constant; the ripples seen in these responses are due to the transient responses associated with the discrete advances of the pattern. The EMD responses to square wave stimuli show prominent transient responses (ripple) at twice the stimulus frequency. In general, the higher spatial frequencies present in the square-wave stimuli generate larger instantaneous differences between the two photoreceptors, resulting in larger transient (and mean) responses.

The mean EMD responses to the motion of patterns containing the three spatial periods used in the experiments of §4.1, over a large range of temporal frequencies are shown in Figure 6.4. In this simulation, the bell-shaped receptors are used, and as with the example time series of Figure 6.3, the receptors have been stimulated with sine-wave and square-wave intensity motion. The curves show the expected shape of the HR EMD response—for increasing temporal frequencies the EMD response features a monotonically increasing response that peaks at the TFO, beyond which increasing temporal frequency of stimulus yield a monotonically decreasing response. A further complication is that the EMD response does not report the true velocity of the pattern, and the responses are dependent on the spatial and temporal frequency of the pattern. The EMD responses are also dependent on the spectral content of

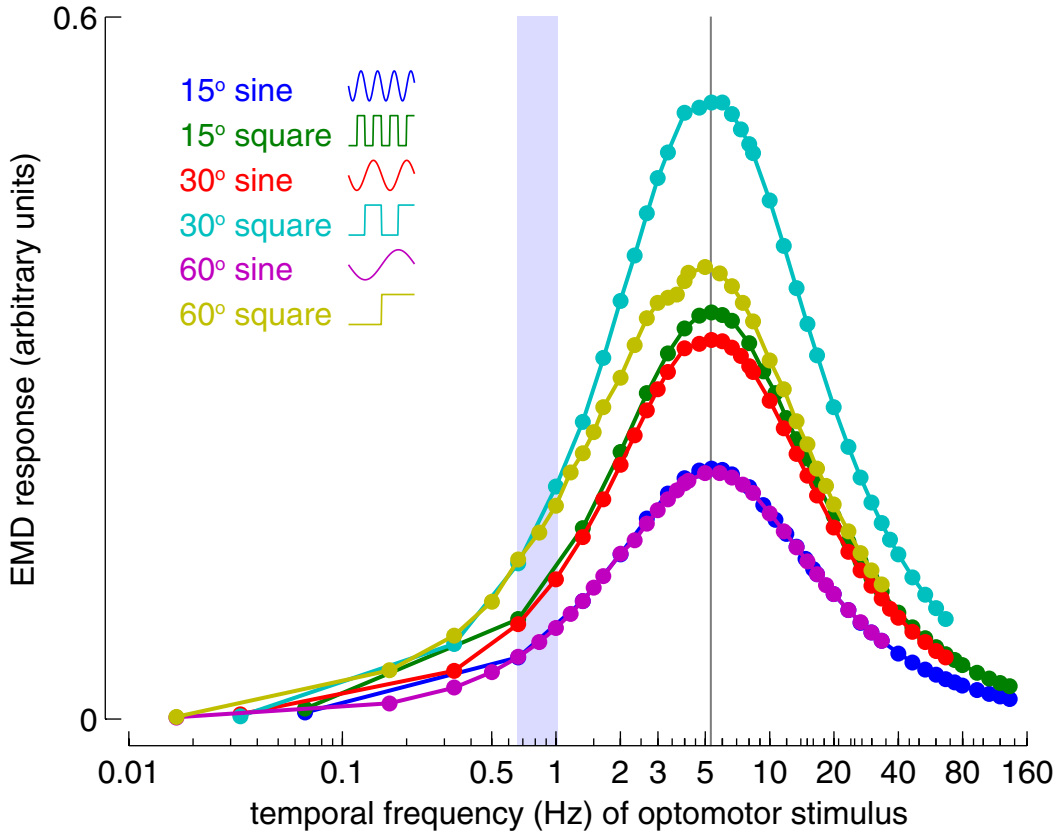

Figure 6.4. The response curve for an HR EMD unit with parameters selected to model the expansion-avoidance response of *Drosophila*, plotted against temporal frequency (log scale). The EMD response depends on the spatial and temporal frequency of the pattern, and on the pattern's spectral content. Each circle shows the result of a single simulation—the mean EMD output in response to stimulation with sine and square wave intensity gratings of the three spatial periods used in the experiments of §4.1. The temporal frequency optima of the six curves coincide at the theoretically predicted value, indicated by the vertical line. The gray vertical bar shows the 2/3–1 Hz band, in which the critical value for the centering response is likely to reside.

the pattern, which is why the response to a square-wave and a sine-wave version of patterns of the same temporal frequency can be so different. Each dot in Figure 6.4 represents the mean response of a single simulation. The TFO of all six response curves coincide at the theoretically predicted value of 5.3 Hz, which is indicated by the vertical line. The gray vertical bar is added to emphasize the 2/3–1 Hz band, the temporal frequency range that is relevant for the critical value of the centering response. At every temporal frequency, the response to square-wave motion is highest,

and the spatial frequency dependence reveals a tuning whereby the response to the $\lambda = 30^\circ$ pattern is closest to the spatial frequency optimum. The spatial frequency dependence can be seen in the time series examples of Figure 6.3, where at the lower spatial frequency, the EMD response reaches larger transient output, but then drops to a lower baseline level. A type of aliasing can be seen in response to the 15° and 60° sine-wave patterns. The EMD output curves in response to these two patterns are essentially identical, but for very different reasons; the 15° stimulus is heavily attenuated by the low-pass optical filtering, while the phase difference between the two photoreceptors seeing the 60° pattern is small, minimizing the temporal coincidence in the motion detector.

6.2.2 Spatial integration and filtering of EMD outputs

A commonly proposed model for the optomotor response of flies consists of an HR EMD array, whose outputs are spatially integrated and then temporally low-pass filtered (Borst and Bahde, 1986; Warzecha and Egelhaaf, 1996). Warzecha and Egelhaaf (1996) simulate such a system to model the syndirectional optomotor control system of a blowfly. In this simulation, a first-order low-pass filter with a time constant of 750 ms is used. The low-pass filter is a black-box model for the delays and 'smoothing' that occurs between the motion processing pathways and the motor output. A similar model has been implemented (shown for one eye in Figure 6.5A), and was stimulated with constant rotation, which could occur either during an optomotor stimulus, or during frontal expansion, where each eye receives constant rotation. The simulations have been carried out using the method for simulating the *Drosophila* eye and the flight arena stimuli discussed in §6.1.

The open-loop time series data of Figures 4.4 and 4.8 provide a useful comparison to the simulated responses of the 'visuomotor' control system. The open-loop turning responses to slow expansion stimuli exhibit a prominent 'ripple' that is phase locked to the discrete advances of the pattern. This ripple is seen in the mean response to 0.125 Hz expansion (3 fps), and is also present in the responses to the 0.25 and 0.5 Hz

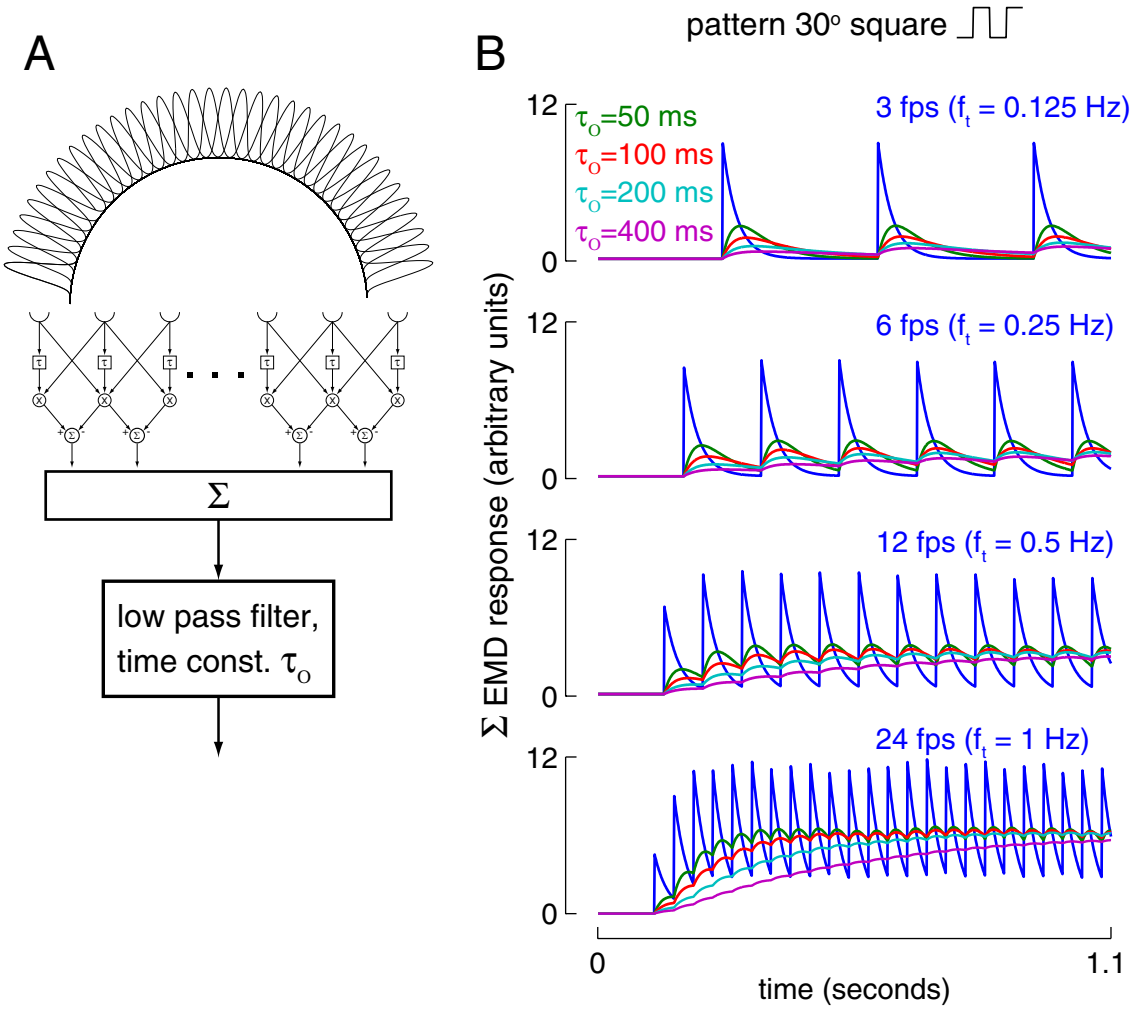

Figure 6.5. (A) A simple model for the integration and filtering of the EMD responses in one eye. After all EMD outputs are summed, a first-order low-pass filter (time constant τ_o) is applied. This time constant models the delays and 'smoothing' that occurs between the EMDs and motor output. (B) To facilitate direct comparison with the results of Figure 4.4, the same pattern (30° square wave with smoothing), was rotated (or expanded in front of the fly) at 3, 6, 12, and 24 fps. The blue traces show the summed EMD response, and the additional traces are this quantity once filtered by the first-order low-pass filter with the specified time constant. A value of $\tau_o = 200$ ms provides a qualitative agreement with the open-loop response data.

expansion, but is virtually absent in the 1 Hz expansion responses. These qualitative observations were used to determine an appropriate visuomotor time constant. The identical pattern used in the experiment of §4.2, the expansion-rotation pattern with square-wave intensity of $\lambda = 30°$, and smooth motion provided by intermediate intensity levels, was simulated at the slower temporal frequencies used in Figure 4.4. The low-pass filter was implemented using the difference equation in 6.3, for time constants of 50, 100, 200, and 400 ms. The results of the simulation are shown in Figure 6.5. The HR responses show two types of ripple, one is triggered by the discrete, one-frame advances of the simulated pattern, and the other slower ripple, is locked to cycles of the pattern. The slower ripple is almost imperceptible in these responses, but is strongly seen in the local responses (as in Figure 6.3), but since different parts of the eye image a different part of the pattern, the summed response across one eye has only a small remainder of this effect. The summed EMD responses of Figure 6.5B, shown in blue, are low-pass filtered with four different time constants, and the results of the filtering are shown color coded to the labeled time constant value. The results of filtering with $\tau_o = 200$ ms provide a qualitative agreement with the open-loop data summarized above; there is a prominent ripple in the responses to the expansion at temporal frequencies of 0.125, 0.25, and 0.5 Hz, that is largely attenuated in the response to $f_t = 1$ Hz expansion.

6.3 What metrics best describe *real* expansion?

In this section we set out to answer a relatively straightforward question—what does a fly see when in flight? This question is of particular importance given the results of Chapter 4. We wish to determine if the critical value governing the speed-dependent inversion of the expansion-avoidance response occurs in a range of behaviorally relevant temporal frequencies. One approach to quantifying the behaviorally relevant expansion is to simulate the free flight behavior of *Drosophila*. Unfortunately, there are only a few cases of substantial data on the free flight behavior of *Drosophila* while the visual conditions are well controlled. The most appropriate free-flight data that can serve

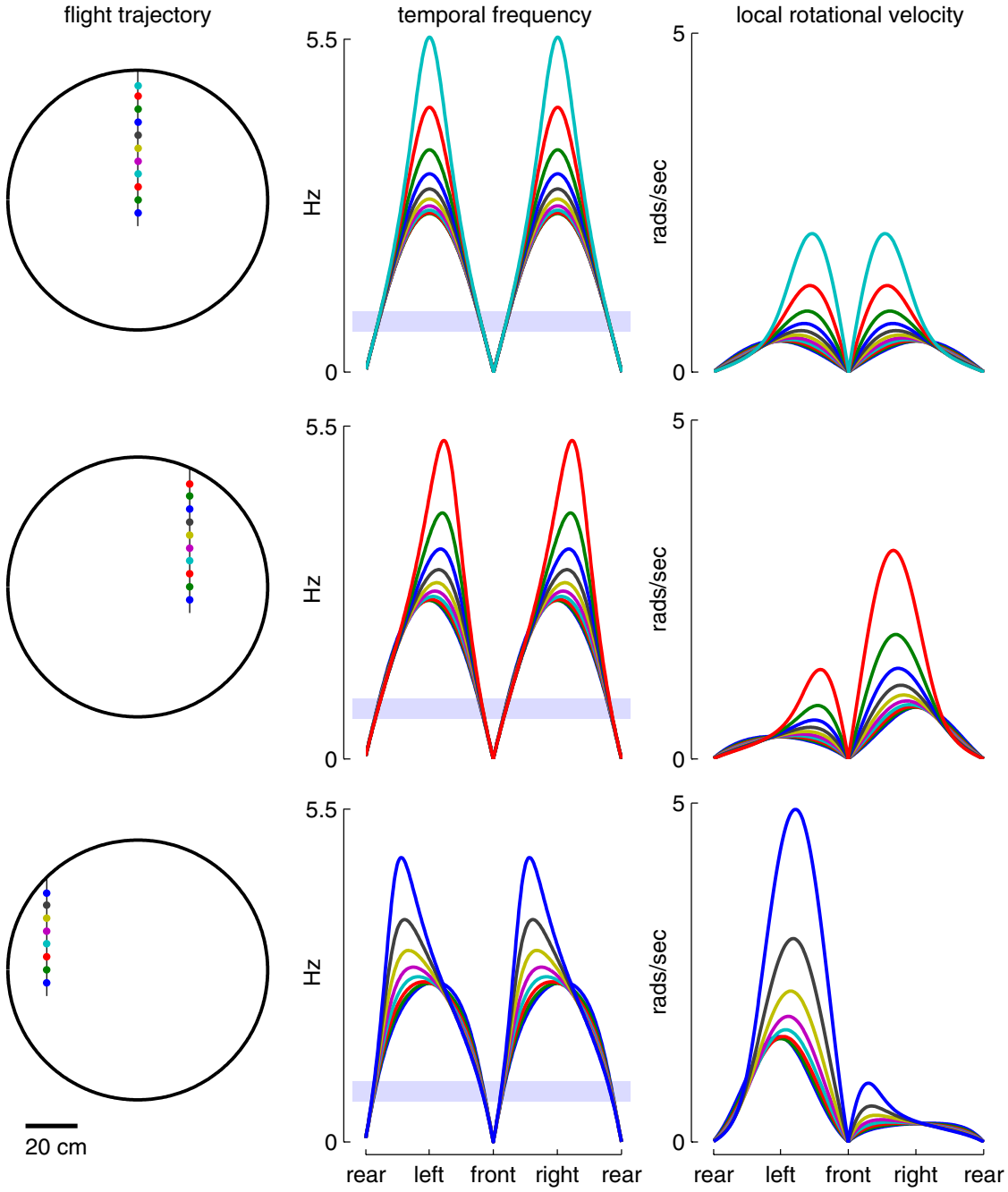

Figure 6.6. Geometric metrics of image motion of a virtual fly. These metrics are two ways to account for the type of motion impinging on the retina of a fly moving in a 1 m diameter environment while translating at 23 cm/s. Each trace shows the motion metric at each position on the retina, while the fly is at the position along the trajectory indicated by the matching color. In the right column, the local rotational velocity at each position on the retina is shown—this is a purely geometric quantity, and is independent of the patterns on the wall. The left column shows the corresponding temporal frequency calculated at each point on the retina assuming that the walls are lined with a 5° (from the center) uniform checkerboard pattern.

as a 'ground truth' for the simulation results is provided by Tammero and Dickinson (2002b). In these experiments, flies were tracked in free flight in a 1 m diameter cylinder, while the walls of the environment were either white (or untextured, but with a prominent horizon cue) or while covered with a random checkerboard pattern (each square of the checkerboard covers a $5^\circ \times 5^\circ$ patch when viewed from the center). In this environment flies maintain nearly straight flight that is interspersed with rapid body saccades. Several basic features of the flies' straight flight in this environment have been extracted for the purpose of comparison with simulated work. The mean speed of free flight is estimated to be around 23 cm/s in the textured background, and approximately 30 cm/s in the uniform background (estimated from Figure 5 of Tammero and Dickinson (2002b)). Also, the flies do slow down just slightly before a saccade, which is suggestive of the 'clutter' response of bees (Srinivasan et al., 1996). Although flies appear to exhibit some visually mediated velocity control, this is not included in the simulated results that follow.

The virtual fly was translated (in open-loop) along straight paths in the 1 m diameter circular environment at 23 cm/s. The view of the fly was obtained using the ray-tracing procedure outlined in §6.1. The paths of the virtual fly can be seen in the left column of Figure 6.6. The first attempt to measure the fly's perceived expansion used geometric quantities to describe the visual motion. For the geometric metrics of motion, the walls of the arena contain a uniform (one-dimensional) checkerboard pattern with boxes of size 5° (as seen from the center). The geometrically determined temporal frequency 'seen' by each part of the eye during the flight along the three paths is shown in the center column of Figure 6.6. The temporal frequency was found by simply 'edge counting,' to determine the rate at which each of the 960 rays emanating from the eye would transition from a dark to a bright patch. To obtain the smooth curves in the figure, several hundred simulations were run (with incremental orientation differences) and averaged together. The gray horizontal bar in these plots indicates the 2/3–1 Hz band, in which the critical value for the centering response is likely to reside. The second geometric measurement of visual motion is simply the local rotational velocity experienced by each ray during flight along the three paths.

The results of this are shown in the right column of Figure 6.6. The local rotational velocity is determined by forming the angle between the current intersection point of each ray and the previous intersection of the same ray; division by the sampling time (and the small angle approximation) then yields the rotational velocity.

Both of the metrics in Figure 6.6 capture some of the relevant features of motion perceived during the flight along these paths. Both metrics show a frontal focus of expansion at which no motion is measured, and show increased values as the fly approaches the wall. The temporal frequency metric shows perfect (π) periodicity, which is expected considering the geometry of line-circle intersection, but conflicts with an intuition that the motion of the farther side should be reduced. The local rotational velocity measurement does show this property; there is little relative motion seen by the side of the eye that is farthest from the wall. As purely geometric quantities, these metrics fail to account for the responses of biological motion detectors. [3] However, both quantities are typically thought of as inputs to the HR EMD; the HR EMD with needle-shaped receptors would indeed respond to these geometric temporal frequencies. The HR EMDs are often thought of as estimating the 'true' rotational velocity, which is the quantity plotted in the left column of Figure 6.6.

A more realistic simulation was conducted in which the response of the EMD array to visual motion experienced along straight flight trajectories was computed. As before, the virtual fly was translated (in open-loop) along straight paths in the 1 m diameter circular environment at 23 cm/s, and the view of the fly was obtained using the ray-tracing procedure outlined in §6.1. The walls of the arena contain a random checkerboard pattern with boxes of size 5° (as seen from the center). The EMDs were simulated using the spatial and temporal filtering properties selected to match the *Drosophila* motion detecting pathways, and the motion detector output is filtered using a low-pass filter with $\tau_o = 200$ ms, established in §6.2.2.[4] The simulation

[3]The distinction between the velocity field and the optic flow field is worth repeating. The velocity field is a geometric measure of motion projected onto the retina, or the local rotational velocities shown here. The optic flow field is the pattern of intensity motion across the retina, transduced by a motion detecting system.

[4]The results are not spatially integrated so that the responses at all retinal positions can be seen, but the individual values were filtered with the $\tau_o = 200$ ms filter so that a better comparison to the

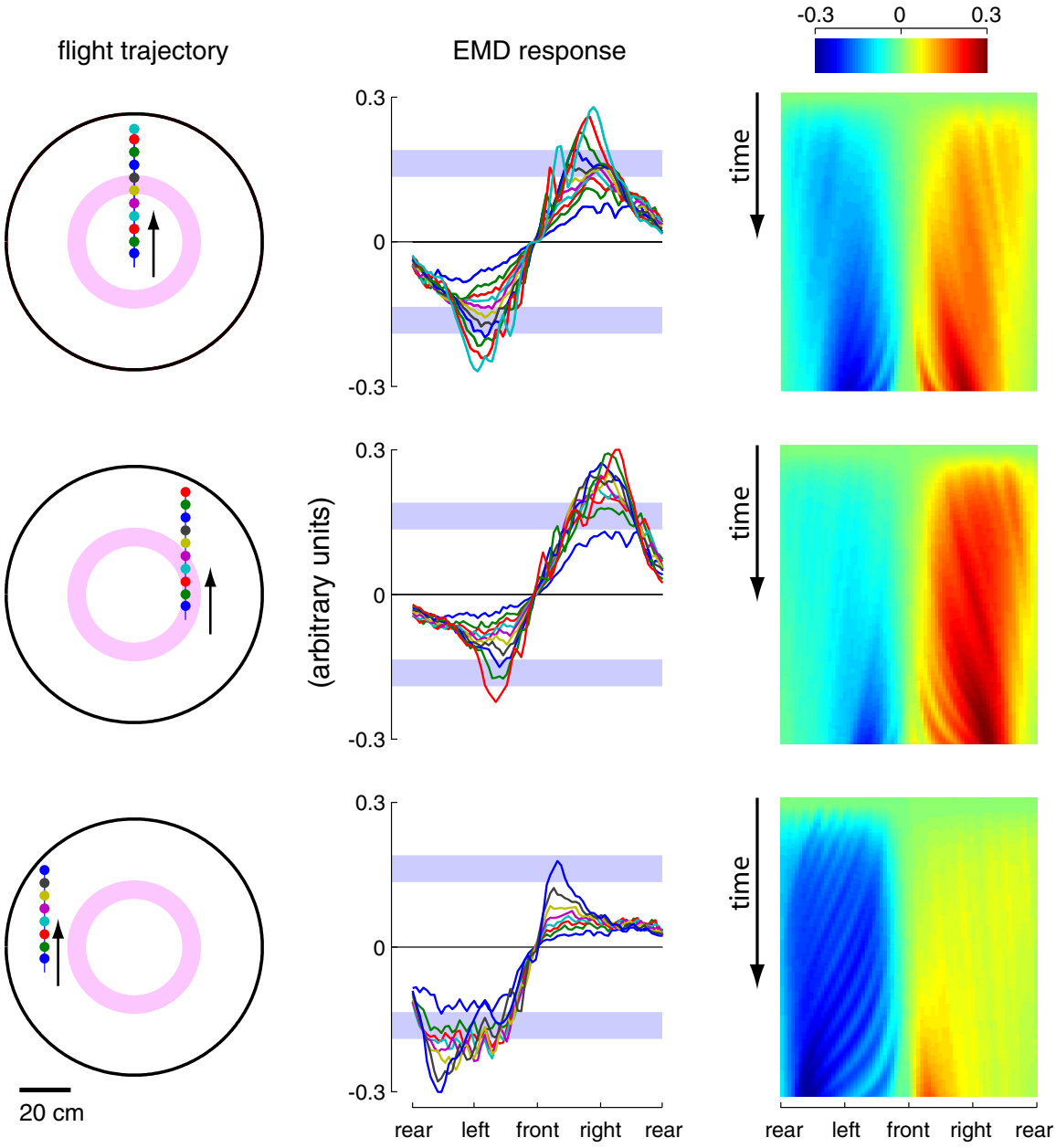

Figure 6.7. The response of the HR motion detector array while the virtual fly is translated at 23 cm/s along straight flight trajectories in a 1 m diameter environment. In the middle column, each trace shows the mean EMD array response at each position on the retina, while the fly is at the position along the trajectory indicated by the matching color. In the right column, the EMD response at each position on the retina for the duration of the trial is shown using pseudocolor to represent magnitude. The trial lengths are not identical, the arrows serve as 1-second scale bars.

results are shown in Figure 6.7, and correspond to the trajectories shown in the left column. The EMD responses (center and right columns) shown were obtained as the mean responses of 50 runs along each trajectory, where in each case the orientation of the fly, and the pattern on the wall was randomized. The gray horizontal bars indicate the magnitude of EMD responses to square-wave intensity pattern motion in the range of 2/3–1 Hz (the top and bottom of the range were obtained by averaging the very similar response magnitudes to the 30° and 60° square wave patterns in Figure 6.4). The concentric circles in the arena figures (in pink) indicate the distances from the center of the arena inside of which 50% and 75% of saccades take place (18.8 cm and 26.1 cm, respectively). These distances were determined by forming the cumulative probability distribution from the saccade distance histogram in Figure 8 of Tammero and Dickinson (2002b). Although the responses shown are from averaged data that have been low-pass filtered, it should be noted that the responses of the EMD array in individual simulations have the same general shape, but with large deviations that are dependent on the locations of specific high contrast edges that differ across simulations.

6.4 Upwind flight via expansion avoidance

This section explores the possibility of using the fly's visual system as the means of counteracting the effect of wind disturbances during upwind flight. To establish the feasibility of visually guided upwind orientation, a detailed closed-loop flight simulation has been implemented.[5] The model was developed to test the hypothesis suggested by the data on expansion-avoidance (reproduced from Tammero et al. (2004) as Figure 1.4)—that the movement of the visual focus of contraction could be used to detect wind direction, since upwind flight induces a frontally centered focus of the visual motion field.

behavior data can be made.

[5]The work documented in this section is based on a class project (as part of for CDS 270), that has been previously published as Reiser et al. (2004).

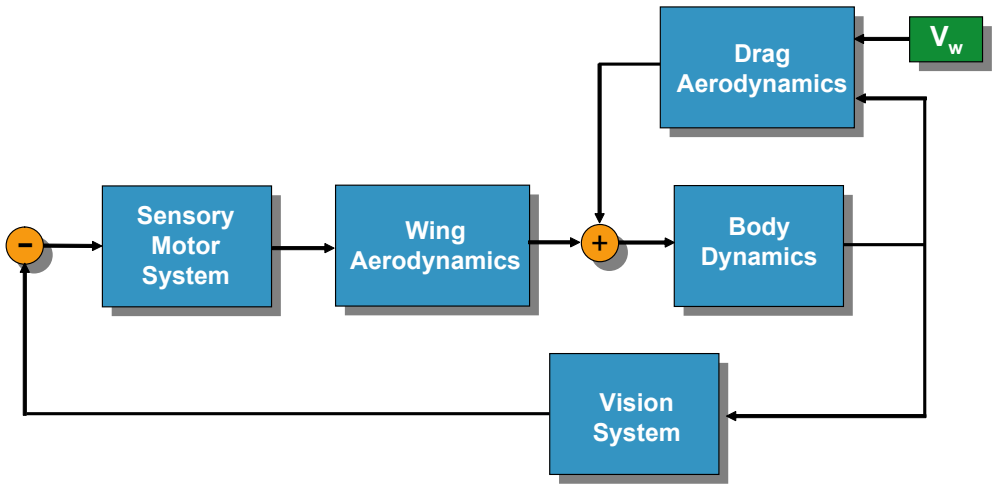

Figure 6.8. Closed loop model used for study of upwind flight. V_w is the wind disturbance, a vector quantity.

6.4.1 Closed-loop model of upwind flight

A closed loop representation of the fly's control system (Figure 6.8) is divided into several blocks including body dynamics and body aerodynamics (plant), the wing aerodynamics (actuator), the vision system (sensor) and the sensorimotor system (controller). The function of the body dynamics block is to take as inputs the forces and torques from the wing and body aerodynamics blocks and produce the resultant translational and rotational motion of the insect body. In the body aerodynamics block the inputs are the wind velocity magnitude and direction, the body velocity and the body rotational position, and the outputs are the resultant aerodynamic forces on the body. The left and right wing kinematics are the inputs to the wing aerodynamics block, which outputs the resultant aerodynamic forces on the body due to wing motion. The function of the vision system block is to take as inputs the inertial translational and rotational velocity and output an estimate of the visual focus of contraction location (error). The loop is closed through the sensorimotor block, which generates parameterized values for controlled wing kinematics from the estimate of the visual focus of contraction location.

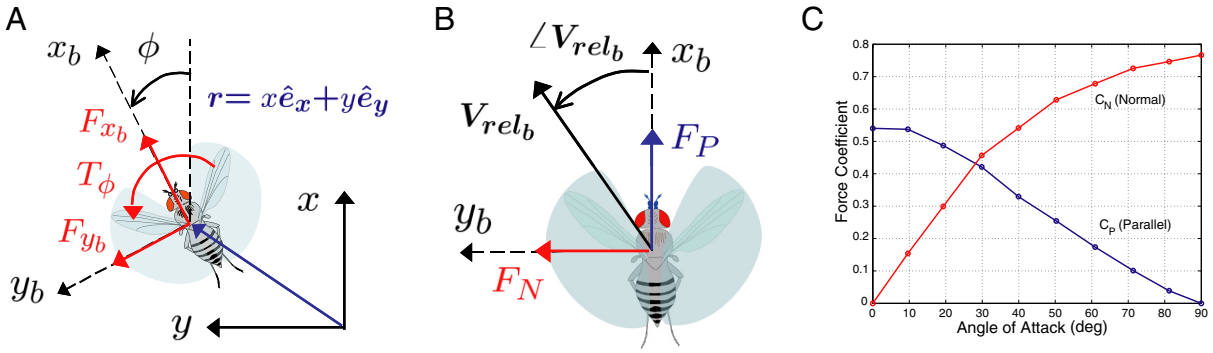

Figure 6.9. (A) Insect coordinate frames showing body forces and torques; (B) Force directions acting on the insect body; (C) Force coefficients for parallel and normal aerodynamic forces.

6.4.2 Body dynamics

We close the loop in our model around a single axis of rotation. Therefore, we have restricted the dynamics of the insect body to planar translatory motion along a single axis of rotary motion (Figure 6.9A). In our simulation we ignore out-of-plane forces, however the forces generated from our wing kinematic model are of the order required to balance the weight of the insect. The translational position, $\boldsymbol{r}$, and rotational position, $\boldsymbol{\phi}$, are defined by $\boldsymbol{r} = x\hat{\boldsymbol{e}}_{\boldsymbol{x}} + y\hat{\boldsymbol{e}}_{\boldsymbol{y}}$ and $\boldsymbol{\phi} = \phi\hat{\boldsymbol{e}}_{\boldsymbol{z}}$, where $\hat{\boldsymbol{e}}_{\boldsymbol{z}} = \hat{\boldsymbol{e}}_{\boldsymbol{x}} \times \hat{\boldsymbol{e}}_{\boldsymbol{y}}$. The map from inertial coordinates, $\boldsymbol{r}$, to body fixed coordinates, $\boldsymbol{r_b}$, is given by:

$$\boldsymbol{r_b} = \begin{pmatrix} \cos\phi & \sin\phi \\ -\sin\phi & \cos\phi \end{pmatrix} \boldsymbol{r}.$$

We assume the the insect has mass, m, rotational inertia about the ϕ axis, J, and experiences applied force $\boldsymbol{F} = F_{x_b}(t)\ \hat{\boldsymbol{e}}_{\boldsymbol{x_b}} + F_{y_b}(t)\ \hat{\boldsymbol{e}}_{\boldsymbol{y_b}}$, and torque $\boldsymbol{T} = T_\phi(t)\ \hat{\boldsymbol{e}}_{\boldsymbol{z_b}}$. The equations of motion under these assumptions are given by Newton's second law:

$$\begin{bmatrix} m\ddot{x} \\ m\ddot{y} \\ J\ddot{\phi} \end{bmatrix} = \begin{bmatrix} F_{x_b}\cos\phi - F_{y_b}\sin\phi \\ F_{x_b}\sin\phi + F_{y_b}\cos\phi \\ T_\phi \end{bmatrix}.$$

The resultant applied force $\boldsymbol{F}$ and torque $\boldsymbol{T}$ are due to the aerodynamic forces on

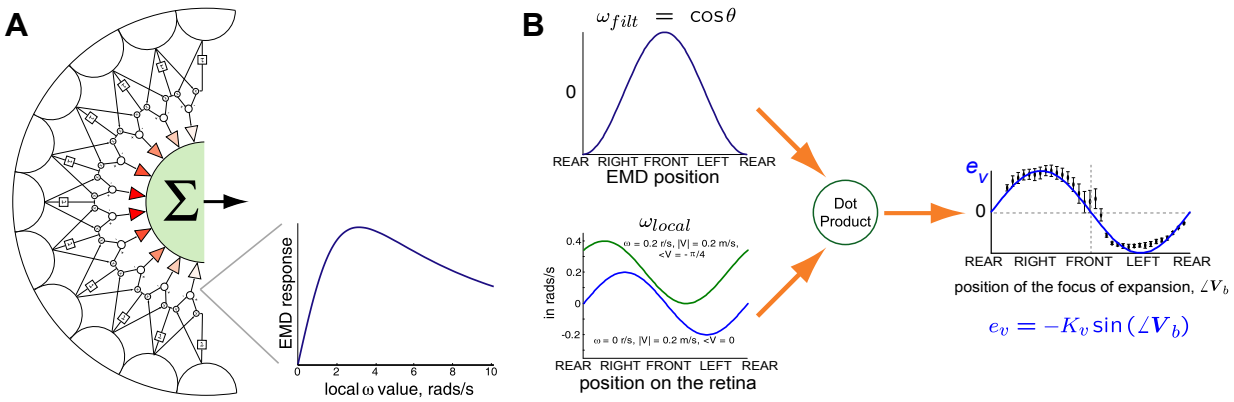

Figure 6.10. Two representations of the visual system modeling. (A) Schematic diagram of the retina and the motion processing and matched filter circuitry. A typical EMD response is also shown. (B) The operations of the matched filter on the velocity field vector. The filter is minimally responsive to the upwind flight profile of local velocities. The filtering process is a projection (dot product). The data superimposed on the filter result is excerpted from Tammero et al. (2004), showing the open loop turning response of *Drosophila* to the location of the focus of expansion. This simple model of open-loop visual response agrees well with data from tethered *Drosophila*.

the wings and body (§6.4.4). Wing motion generates unsteady lift and drag, which is well-approximated with a quasi-steady model. The body aerodynamic forces result from the relative velocity of the body with respect to the free stream (wind), and the drag associated with rotation of the body about the z-axis:

$$\begin{aligned} F_{x_b}(t) &= F_{Aero,x_b}(t) + F_{Wind,x_b}(t) \\ F_{y_b}(t) &= F_{Aero,y_b}(t) + F_{Wind,y_b}(t) \\ T_\phi(t) &= T_{Aero}(t) - C\dot{\phi}(t). \end{aligned}$$

Fry et al. (2003) measured the rotational inertia, J, and damping, C, about the morphological yaw axis (normal to the insect body). As we intend to use the functional axis of rotation (Figure 6.9A) for this simulation, we assume that the differences in these constants about the two axes are negligible.

In order to characterize the aerodynamic forces on the insect body during flight, we analyzed data from experiments performed with robofly, a dynamically scaled physical model of a flapping insect. An insect-shaped body was subjected to a range of forward

velocities in an oil tank at various angles of attack, with the resultant forces recorded and reduced to parallel and normal force coefficients (Figure 6.9C). The size of the body was scaled so that the Reynolds number ($Re \approx 200$) matches what a typical insect sees during nominal flight ($0.1 - 0.3\ m/s$).

The relative velocity of the insect with respect to the air (Figure 6.9B) is determined by the wind direction and magnitude, the body velocity, and the orientation (all specified in inertial coordinates): $\boldsymbol{V}_{rel} = \boldsymbol{V}_{wind} - \dot{\boldsymbol{r}}$. Since the aerodynamic forces will be computed in the body frame, we need the relative velocity in body coordinates:

$$\begin{pmatrix} V_{rel,x_b} \\ V_{rel,y_b} \end{pmatrix} = \begin{pmatrix} \cos\phi & \sin\phi \\ -\sin\phi & \cos\phi \end{pmatrix} \begin{pmatrix} V_{rel,x} \\ V_{rel,y} \end{pmatrix}.$$

The magnitude and phase in body coordinates are then

$$\begin{aligned} \mid \boldsymbol{V_{rel_b}} \mid &= \sqrt{V_{rel,x_b}^2 + V_{rel,y_b}^2}, \\ \angle \boldsymbol{V_{rel_b}} &= \texttt{atan2}\left(V_{rel,y_b}, V_{rel,x_b}\right). \end{aligned}$$

Now we can compute the resultant aerodynamic forces:

$$\begin{aligned} F_{Wind,x_b} &= \frac{1}{2}\rho A \mid \boldsymbol{V_{rel_b}} \mid^2 C_P(\angle \boldsymbol{V_{rel_b}}), \\ F_{Wind,y_b} &= \frac{1}{2}\rho A \mid \boldsymbol{V_{rel_b}} \mid^2 C_N(\angle \boldsymbol{V_{rel_b}}), \end{aligned}$$

where ρ is the density of air, A is the projected cross-sectional area of the insect, $\mid \boldsymbol{V_{rel_b}} \mid$ and $\angle \boldsymbol{V_{rel_b}}$ are the magnitude and phase of the relative velocity in body coordinates, and C_N, C_P are the normal and parallel force coefficients that have been reduced from the experimental force data.

6.4.3 Visual system model

The model for the compound eye of *Drosophila* used in this simulation study is slightly simpler than the newer version described in §6.1. In the simulation presented, the fly's retina is modeled as a circular array of 90 receptor/EMD units, with 4° spacing

between receptors. In general, the response of an EMD is dependent on the visual system structure, i.e., the time delay and the spacing of the receptors in the retina, and also on properties of the visual input, such as image contrast and spatial frequency content. Figure 6.10A shows an EMD array, as well as a typical response curve for an EMD corresponding to the environment statistics used in the presented simulations. In the simulations, the computed EMD response curve is used as a look-up table to convert local velocities on the retina to EMD signals.

The simulated visual makes use of a 'matched filter' inspired by the hypothesis derived from studies of lobula plate neurons in flies (discussed in §1.4). Applying these ideas to the simulated planar world, the optic flow field is a vector spanning the field of view. For flight oriented in the direction of the wind, there cannot be a sideslip component to the local velocities measured by the EMDs. Flies exhibit a preference for orienting towards the focus of contraction of the velocity field, which means they can only orient upwind if they are flying slower than the wind. This suggests a simple strategy for visual wind detection—fly slowly and seek out foci of contraction. We designed a filter that is minimally responsive to the desired profile of local velocities (the equilibrium condition). Because these responses are (roughly) sinusoids, the reasonable filter is simply the profile itself but phase shifted by 90°, and the filtering process is the dot product of the two curves. This interpretation of matched filters agrees with some of the LPTCs, which give cosine-like response to stimulation in various directions (with a peak in the so-called locally preferred direction). An example of the filtering process and some typical velocity field vectors are shown in Figure 6.10B. Since the EMD array produces an estimate of the velocity field, it is instructive to analyze the filtering process on the velocity field (true optic flow):

$$\omega_{local} \;=\; \omega_o - \frac{|\,\boldsymbol{V}_b\,|}{R}\sin\left(\theta - \angle\boldsymbol{V}_b\right),$$

where ω_o is the instantaneous rotation, $\mathbf{V}_b$ is the instantaneous absolute velocity in body coordinates, θ is the angular coordinate in the body frame, and R is an arbitrary fixed distance to the environment. The matched filter is $\omega_{filt} = \cos\theta$, and the filtering operation is a dot product,

$$\begin{aligned} e_v &= \langle \omega_{local}(\theta), \omega_{filt}(\theta) \rangle \\ &= \frac{1}{2\pi} \int_0^{2\pi} \omega_{local} \cdot \omega_{filt} \, d\theta \\ &= -K_v \sin(\angle \boldsymbol{V}_b), \end{aligned}$$

where K_v is the gain used in the visual system. As we can see in Figure 6.10B, this open loop result agrees well with the experimental data from Tammero et al. (2004). In our simulation we use the EMD array's estimate of the velocity fields, which does not alter the fundamental shape of this response curve, but is not amenable to simple analysis.

6.4.4 Wing aerodynamics and sensorimotor control

The flight forces generated by the simulated fly's wings are implemented as a quasi-steady, semi-empirical model (details of this model are given in Sane and Dickinson (2002)). In general, the instantaneous force produced by a wing is the sum of several effects: translation, rotation, added mass, and other unsteady effects. All of these forces act normal to the wing, which rotates, translates, and deviates continuously throughout a single wing stroke (the parameterization of the wing kinematics is shown in Figure 6.11A). The translational force is the dominant term, accounting for roughly 90% of the force generated by the wing. In our simulations, we only use the translational component of the aerodynamic forces. To further simplify matters, the fly is assumed to hover, thus operating at an advance ratio of zero. Although not strictly valid, the hovering model provides a reasonable force estimate for a fly moving slowly (advance ratios under 0.3). Figure 6.11B shows the performance of this simplified model in comparison to the forces measured when the same wing kinematics

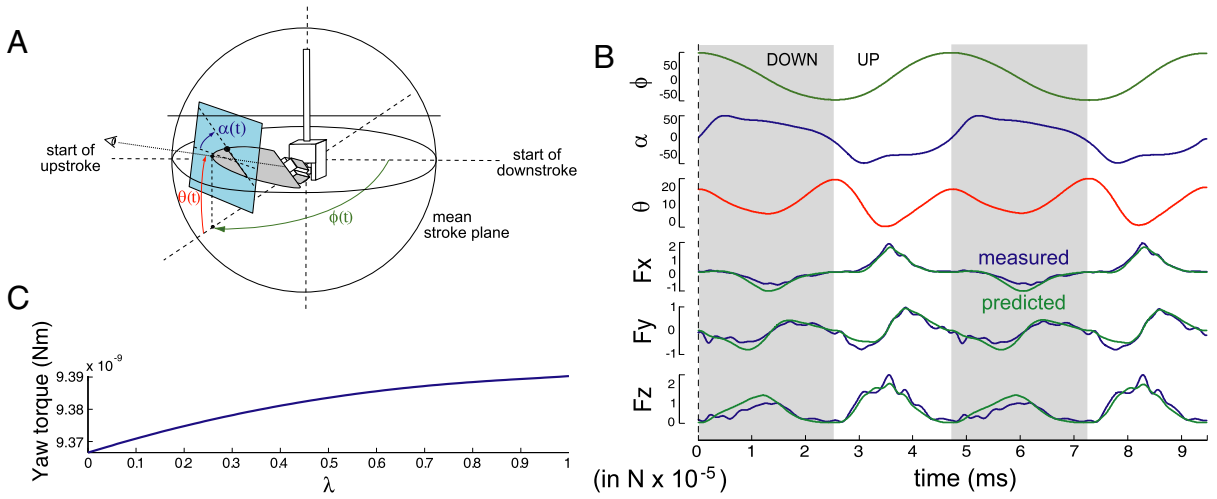

Figure 6.11. The sensorimotor control system interpolates between captured wing kinematics to generate yaw torques. (A) Wing angle parameterizations for the robotic apparatus used to measure aerodynamic forces. (B) Two wing strokes captured from *Drosophila* in free flight and the corresponding flight forces measured on the robot and computed via a quasi-steady model. (C) Torque about the fly's yaw axis produced by one wing as a function of the control parameter.

are run on the robotic model. The torque produced by each wing about the fly's yaw axis is determined directly from the force vector predicted by the aerodynamic model. The right and left wings often take on distinct wing kinematics. The net force and torque generated by the wings combines the contributions from right and left wings appropriately:

$$\begin{aligned} F_{Aero,x_b} &= F_{x,left} + F'_{x,right} \\ F_{Aero,y_b} &= F_{y,left} - F'_{y,right} \\ F_{Aero,z_b} &= F_{z,left} + F'_{z,right} \\ T_{Aero} &= T_{yaw,left} - T_{yaw,right}. \end{aligned}$$

Wing kinematics were selected from an existing database of wing stroke patterns that correspond to actual insect kinematics (the collection of these data is detailed in Fry et al. (2003)). We choose wing kinematics using two selection criteria: the force in the x-direction should result in forward flight not exceeding velocities of

30 cm/s (advance ratio of approximately 0.3) and yaw torques must correspond to realistic angular rotations. Since the model uses only the relatively slow visual system, it is necessary to limit torque about the yaw axis, effectively limiting the rate of angular rotation the insect experiences. The yaw torque requirement stipulates that the difference in torque between the right and left wing should be on the order of 10^{-11} Nm. Two sets of wing kinematics were selected that met the criteria discussed above, one corresponding to low torque kinematics and the second to kinematics generating higher torque. We define a parameter, λ, to span the range of wing stroke kinematics between the low and high torque patterns. The parameter λ ranges smoothly between 0 and 1, defining a linear weighting between the two endpoint kinematics. Figure 6.11C shows the torque about the fly's yaw axis produced by one wing as a function of λ. We have found that linearly interpolating between two sets of kinematics gives a smooth transition between the forces produced by these endpoint kinematics. In our simulation we refer to the sensorimotor block as the control system that couples the sensory information from the visual system to the flight muscles. This system takes the error from the visual system as an input and generates the control values for each wing: $\lambda_R = 1 - k|e_v|I_{[0,\infty)}(e_v)$, and $\lambda_L = 1 - k|e_v|I_{(-\infty,0]}(e_v)$, where k is the control system gain, and $I_{(-\infty,0]}(e_v)$ is an indicator function whose value is 1 when $e_v \in (-\infty, 0]$, and 0 otherwise. Furthermore, e_v is restricted to the range [-1 , 1] to ensure that λ_R and λ_L are in the range [0 , 1].

6.5 Results

The stated goal of the project is to modulate upwind flight, and so our controller sets the torque about the fly's yaw axis. To test the ability of the closed loop system to orient the fly in the upwind direction, we presented 'step inputs' to the control system, where the fly was given an initial velocity and orientation and the wind was set at a fixed magnitude and direction. In the experiments presented, the fly's initial orientation is set in the positive x (forward) direction, with some small (0.1 m/s) velocity in the same direction. The wind magnitude is set at 0.4 m/s, which is always

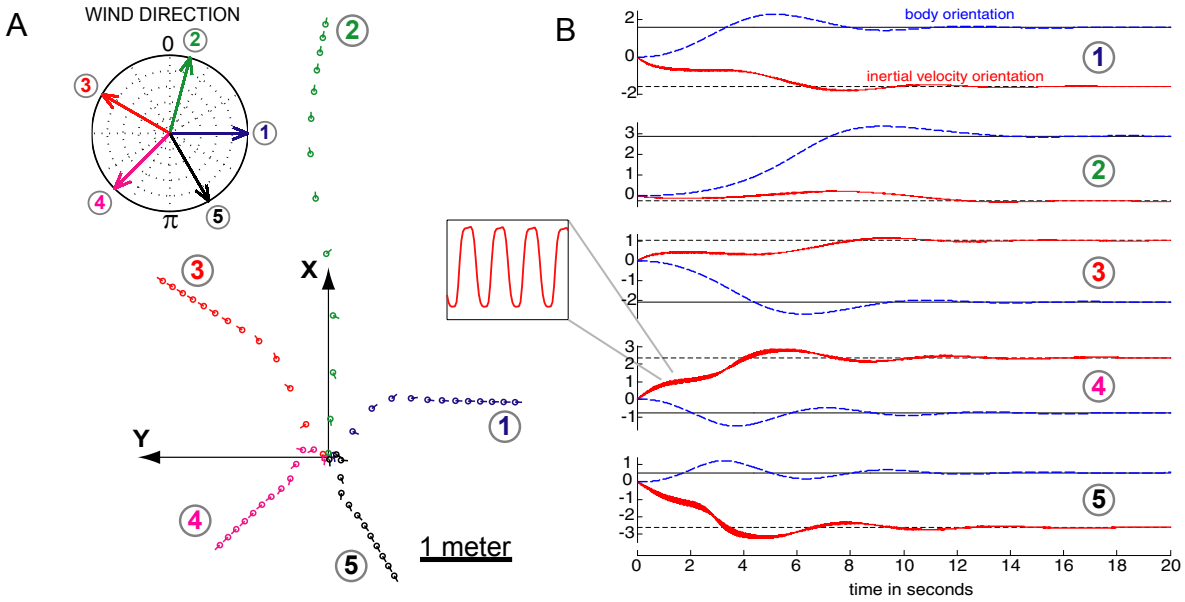

Figure 6.12. Two equivalent representations of responses to step changes in wind direction are shown: (A) simulated 20-second flight trajectories, with fly positions plotted every 1.5 seconds. All trajectories start at the origin, and the wind direction is shown in the compass. (B) Step responses in wind direction, showing zero steady-state error. The high frequency oscillations shown correspond to the subtle perturbations on the fly's instantaneous velocity induced by the wing stroke cycle. All measurements are in radians.

faster than anything the fly could achieve. Five different wind directions are then introduced.

Two equivalent ways of displaying the results are shown in Figure 6.12. In each plot of Figure 6.12B, the dashed horizontal line shows the wind direction set point; the solid horizontal line shows the desired body orientation angle for upwind flight; the solid trace corresponds to the orientation of the inertial reference frame velocity; the dashed trace corresponds to the body orientation angle. The numbered markers on the right side of each response plot correspond to the numbered trajectories and wind directions in Figure 6.12A. It is clear from both representations of the step responses that the tracking works, in the sense that the steady state error is driven to zero, resulting in upwind orientation.

From the step response and frequency response data (Figure 6.13) it is clear that the closed loop system is stable. Stability of this system corresponds to orientation

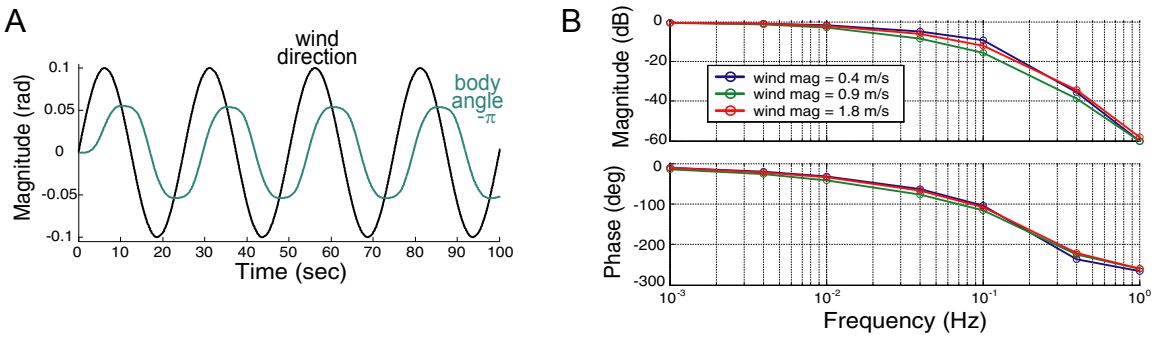

Figure 6.13. Closed loop frequency response. (A) Time domain response to a small signal disturbance of fixed frequency. (B) Small signal frequency response to disturbances in wind heading for several wind magnitudes.

upwind, evidenced by the zero steady state error in the step response plots. Cast as a tracking problem, the tracking error is the amount of sideslip the fly experiences, which is the difference between the inertial velocity orientation and the orientation of the fly's body (these are the two step responses plotted in Figure 6.12). For (backwards) upwind flight this difference should be π, which is achieved at steady state, so the tracking error is zero. Interpreting the frequency response data shown in Figure 6.13 in terms of tracking the mean wind direction, we can see the system is insensitive to disturbances, except at very low (less than 0.01 Hz) frequencies. Furthermore, the frequency response is not significantly affected by changing wind speeds.

6.6 Discussion

6.6.1 Modeling procedure

The procedure in this section demonstrates a simple method for fitting two time constants to the orientation behavior of *Drosophila*. The first time constant governs the response properties of the motion detecting system. This time constant is selected to match the temporal frequency optimum obtained from mean responses of open- and closed-loop behavioral data. We use a time constant of 30 ms for the low-pass filter delay in the HR correlator. This value was selected to yield a TFO that is slightly larger than 5 Hz, as suggested by the behavioral data (§4.6.2). A second time constant, τ_o, is selected to match the transient open-loop turning responses of *Drosophila*. The

ripple that can be seen in the turning responses to slowly moving patterns was used to determine an appropriate time constant for the visuomotor pathway. The 200 ms time constant selected is much lower than the 750 ms value used by Warzecha and Egelhaaf (1996), but it provides strong agreement with the open-loop data of §4.2. Measurements of response latency in *Drosophila* reveal that many visually mediated responses are evoked within no more than 200 ms of stimulus onset (David, 1985; Heisenberg and Wolf, 1988; Tammero and Dickinson, 2002a; Bender and Dickinson, 2006b), with latencies as low as 50 ms reported during free flight. A time constant of 200 ms agrees well with these observations. If the stimulus is thought of as a step input into the low-pass filter, within 100 ms the filter output will reach 39% of the steady state value (63% after 200 ms). By comparison, the output of a filter with a time constant of 750 ms will reach 12% of the steady state value after 100 ms.

6.6.2 What 'speeds' are behaviorally relevant?

One challenge to our understanding of the visual control of flight is the non-trivial response properties of the HR motion detectors. There is no consensus about what part of the HR input-output curve is actually used during typical behavior. Götz (1975) suggests that the entire range is behaviorally relevant. A simple control system based on an array of HR detectors would presumably require a monotonic relationship between local speed on the retina and the response of the motion detection system. This view may be simplistic—there could be a strategy that flies employ that exploits the non-monotonicity of motion detection. One intriguing suggestion is that the shape of the HR response curve provides some stability (Warzecha and Egelhaaf, 1996), since the motion during very rapid turns is attenuated. This claim is almost certainly true; the visual system has little influence during the very rapid turning that occurs in *Drosophila* saccades (Bender and Dickinson, 2006a).

The centering behavior that has been the focus of much of this thesis relates to visual control of flight at the other velocity extreme, where stability is not an issue. Since it is very unlikely that the behavioral inversion of expansion-avoidance is

somehow caused by the shape of the HR response curve (§4.6.3), the centering-like response provided by the low speed inversion, seems to suggest that many interesting behaviors 'live' on the monotonic portion of the HR response curve corresponding to lower temporal frequencies. This idea is strengthened by the new results suggesting that the TFO of *Drosophila* motion detection is higher than previously thought (§4.6.2). It is noteworthy that at no point do the EMD responses during the simulated flight of Figure 6.7 exceed 0.31 (in these arbitrary units), only about half of the peak response of the EMD obtained in the simulations of Figure 6.4. This is further evidence suggesting that during much of *Drosophila* behavior the EMDs respond on the monotonically increasing part of the HR response curve. *Drosophila* are clearly capable of flight speeds above 23 cm/s (David, 1978; Budick and Dickinson, 2006), but flight speeds are not set in open-loop, and are reduced in the presence of a highly textured background (Tammero and Dickinson, 2002b). Therefore, it is unlikely that during faster flight a fly would encounter visual motion that is considerably stronger than in the simulations of Figure 6.7.

The magnitude of EMD responses during simulated translatory flight show strong correspondence to the magnitude of EMD responses simulated with the stimuli that elicit the centering response in *Drosophila*. The peak responses of the EMD array during flight segments that are outside of the 'saccade zone' (pink ring in Figure 6.7), are almost all in excess of the range identified as containing the critical value of the centering response (depicted with the gray bars in Figure 6.7). This finding suggests that the centering response is indeed relevant to the free flight data of Tammero and Dickinson (2002b), and probably accounts for the weak centering tendency observed in between saccades, where flies were found to turn slightly away from the closer side of the arena. An inspection of the EMD responses in Figure 6.7 suggests that the hypothesized retinal sensitivity of the centering response is sensible—little motion is seen by frontal eye regions during forward flight, while the lateral regions exhibit the asymmetry that occurs during non-centered flight. The simulated results may explain why more centering is not seen in the free flight data of Tammero and Dickinson (2002b). If the centering behavior is indeed a response to left-right asymmetry, then

the visual conditions in the flight arena were such that only large deviations from a centered trajectory would result in the asymmetry of retinal motion required to produce a strong centering response. The results of §4.4 suggest that flies tolerate a small amount of motion asymmetry (tested with a 1:2 ratio) while centering. When flies were flown in a cylindrical environment lined with horizontal stripe—the flight trajectories are curved, faster, and much closer to the walls (Frye et al., 2003). It is likely that in the absence of strong horizontal motion cues the saccadic response is suppressed, while the centering response dominates flight. These observations suggest that the centering response, the expansion-avoidance reflex, and the saccadic system are in fact separate, parallel systems.

6.6.3 Upwind flight model

The upwind flight model is presented to demonstrate that through a faithful model of the fly's behavior, it is possible to provide some context within which controlled behavioral assays can be interpreted. The model has used the improved understanding of the aerodynamics of insect flight, the force production of realistic wing kinematics, and the higher-level processing in the insect visual system, to 'shrink' the black boxes in earlier models (such as the classic work of Reichardt and Poggio (1976)). The results presented demonstrate the feasibility of visually guided upwind orientation, and have yielded strong agreement with experimental results. These results cannot prove a causal link between the expansion-avoidance response and upwind flight in *Drosophila*, but the simulation makes a strong argument for the plausibility of this relationship. A proper accounting of *Drosophila* upwind flight behavior is critically dependent on well-modeled dynamics. The simulation presented provides evidence that the effect of wind changes on body motion produces a sufficient change in the animal's visual experience to induce compensatory steering. The model answers some questions and raises others. Can a model of the speed-dependent inversion of the expansion-avoidance response enable the virtual fly to transition from backwards to forwards flight in the upwind direction?

Chapter 7

Concluding Remarks

The previous three chapters document the significant results of experimental work conducted in pursuit of understanding the algorithmic basis for the visually mediated control of flight in *Drosophila*. The successful design and implementation of the modular display system documented in Chapter 2, enabled the variety of experimental paradigms presented in the thesis. The significant results from each chapter are summarized below.

7.1 Significant results

7.1.1 Chapter 2: Experimental methods

- A modular display system has been designed to address the challenges of conducting experiments on insect vision. The system has proven to be a robust experimental instrument; it is currently in use in 8 laboratories worldwide, and has even withstood the abuse of intense usage during a two-week laboratory cycle as part of the Neural Systems and Behavior course at the Marine Biological Laboratory over the past two summers.

- The new display system is easily adaptable to many experimental protocols. The scripting interface has been used to conduct all of the *Drosophila* tethered flight experiment presented in this dissertation. In particular, two methods have been used throughout: (1) many open-loop trial types can be rapidly presented while

interspersed with short segment of closed-loop control, and (2) experiments are designed to feature mirror symmetric stimuli; by averaging the responses to these stimuli, many of the measurement errors that typically occur are significantly reduced.

7.1.2 Chapter 3: Interaction between object-orientation and expansion-avoidance behaviors

- The closed-loop behavior of *Drosophila* under two robust paradigms, object-orientation and expansion avoidance, is invariant to large changes in the contrast of the pattern. This finding suggests that contrast saturation is applied to the visually perceived stimulus prior to the motion detection system.

- Several compound stimuli were created to test the response of *Drosophila* to the combination of stimuli that independently elicit robust orientation behavior. The compound stimuli present the flies with a laboratory idealizations of realistic circumstances—when a fly is flying towards an object, she must tolerate some significant amount of frontal expansion.

- The compound stimuli trials demonstrate that in the presence of a prominent vertical object to direct flight, *Drosophila* tolerate a level of image expansion that would otherwise induce strong avoidance.

- Further combinations of the stimuli reveal that flies respond to both stimuli in a context-dependent manner; object orientation dominates when the object is positioned frontally and is undergoing progressive motion, otherwise expansion-avoidance dominates. When both stimuli indicate a turn in the same direction, the response is a larger turn than is produced in response to either stimulus presented in isolation.

- These results suggest that the object-orientation response may serve a much more important role in the control of translatory flight by *Drosophila* than

previously thought. By inhibiting the expansion-avoidance response, orientation towards a stationary object guarantees straight flight.

- In contrast to previous attempts, the experimental protocol and data analysis employed in this Chapter allows a sensible comparison of open- and closed-loop experiments, in which the responses, under similar conditions, are demonstrated to be similar.

7.1.3 Chapter 4: Spatial and temporal dissection of the expansion-avoidance behavior

- The expansion-avoidance behavior is mediated by a motion detection system with many (but not all) of the properties predicted by the Hassenstein-Reichardt motion detector. The temporal frequency optimum of the *Drosophila* motion detection system is reported to be at least 5 Hz, a value that is higher than previously published, but is in agreement with several very recent findings.

- A centering response dominates the orientation behavior at low temporal frequencies and gradually gives way to the expansion-avoidance response at some critical value. The smooth nature of this transition suggests that the centering response and expansion-avoidance systems are either two extremes of some behavioral (single parameter) continuum, or they exist in parallel, and the turning response can be explained as the sum of the responses of the 2 systems.

- Closed-loop and open-loop experiments confirm the behavioral switch from centering to expansion. The critical value for this inversion was found to be approximately 0.75 Hz during constant velocity expansion, but is possibly twice as high during accelerating and decelerating motion.

- When presented with asymmetrical motion, flies respond as if they are centering, by orienting towards the side of slower motion. This orientation bias is more prominently seen during closed-loop expansion-avoidance in response to asymmetric high speed motion. However, since the flies are experiencing regressive

motion, this correction is not likely to be an example of centering. When flies are centering, orienting towards an asymmetric slow speed stimulus, they appear to tolerate a small amount of motion asymmetry.

- The centering response does not make use of motion information from the frontal region of the eye and is most sensitive to motion at the sides, while the expansion-avoidance response depends heavily on frontal motion. This finding further confirms that the centering response seen in *Drosophila* is similar to the well-established centering response in bees.

- The difference between the open-loop turning responses of head-free and head-fixed flies was certainly an unexpected result—the centering response disappears. At present this result cannot be explained, but there is evidence that the head orientation of the fixed-head flies may cause this discrepancy. Based on videos of the head motion of flying flies, our working hypothesis is that the role of head motion in *Drosophila* flight is to keep the head in line with the direction of flight. To our knowledge, these are the first examples of significant behavioral differences caused by fixing the head of a tethered *Drosophila*.

7.1.4 Chapter 5: Flight responses to ground motion

- The observed steering response of *Drosophila* when stimulated with high speed ground motion is consistent with both the classically observed syndirectional optomotor turning response and the expansion-avoidance reflex.

- The turning response of tethered *Drosophila* in response to translating ground motion exhibits a speed-dependent inversion as was found with the expansion-avoidance paradigm. The confirmation of this finding in two very different conditions suggests that this previously unreported centering-like feature of vision-based *Drosophila* navigation is likely to be an important component of the flight control system.

- The downward looking regions of the *Drosophila* eye encode motion that yields

a speed-dependent inversion of the turning response to ground motion, with a critical value that is higher than the similar value found with the expansion-avoidance paradigm in Chapter 4. This difference may be due to different temporal frequency optima in different eye regions. It is also possible that the critical value obtained in the ground motion assay may be closer to the relevant value for translatory flight.

- An attempt was made to find a signature of velocity control in the measurable wingbeat signals that could be used to develop a new forward flight closed-loop assay. A lack of steering was found in response to progressive motion at speeds below the critical value, possibly evidence that these speeds are in the range of *Drosophila*'s preferred groundspeeds. This issue is far from resolved; further experiments are necessary and stimulation of additional sensory systems must be considered.

7.1.5 Chapter 6: Computational modeling of expansion avoidance and centering behavior

- A model of the *Drosophila* compound eye and motion detecting system was implemented. Simulations were conducted either in a virtual environment or in a simulation of the flight arena used for the experiments of Chapters 3–4.

- A simple two step method has been demonstrated for fitting the properties of the Hassenstein-Reichardt model to the behavioral data from Chapter 4. The simulated responses of the model provide qualitative agreement with behavioral data.

- By simulating the responses of the modeled motion detectors during translatory flight, a strong correspondence is seen between the magnitude of motion detected under observed conditions of *Drosophila* free flight and the simulated responses to the stimuli that elicit the centering response in tethered fight. It is unlikely that this correspondence could have been established by an alternative approach

due to the non-invertability of the Hassenstein-Reichardt motion detector input-output behavior.

- The possibility that the expansion-avoidance reflex serves to counteract the effect of wind disturbances during upwind flight was tested. A closed-loop flight simulation was constructed based on realistic models of the physics and biology, demonstrating the feasibility of visually guided upwind orientation.

7.2 Emerging view of visually based flight control in *Drosophila*

With just a few exceptions, the literature on tethered flight control experiments is based on the control of rotational motion. This line of work has suggested that the optomotor equilibrium hypothesis accounts for much of fly flight control. However there are several behavioral and conceptual counterexamples that this strategy cannot explain (§1.7). Much of the effort documented in this dissertation has sought to bridge the gap between tethered and free flight studies in providing some model for the visual processing of translatory motion. Rather than providing a unifying view of visually mediated flight control in *Drosophila*, the results presented suggest that multiple behaviors are in operation concurrently:

1. The newly established centering response that is exhibited when visual motion is not *too strong*. This behavior is demonstrated by the low-speed inversion of the expansion-avoidance response (seen in open- and closed- loop experiments), the weak wall avoidance seen in the free flight data of Tammero and Dickinson (2002b), in the curved flight paths flown in response to the horizontal striped cylindrical environment (Frye et al., 2003), and the axial flight distributions of freely flying *Drosophila* in a wind tunnel (Budick and Dickinson, 2006). Although not fully explored, this behavior has many similarities to the centering response of bees.

2. The expansion-avoidance response, a counterturn away from high-speed expansion that is laterally positioned on the retina. The modeling effort in §6.3

demonstrates that the visual conditions in forward flight maintain a centered focus of expansion. Only with significant motion that is not in line with the flight direction, or high speed rotations of the body, will the focus of expansion move away from the center of the retina. Therefore it is unlikely that the collision avoidance in free flight experiments (Tammero and Dickinson, 2002b) can be explained by the expansion-avoidance response. As validated by the upwind model presented in Chapter 6, the expansion-avoidance behavior is most likely used for side-slip compensation, either due to wind, or as a correction for self-motion. A fast, strong response, that does not adapt seems appropriate for these corrections, as a saccadic strategy might actually be detrimental, especially in shifting winds.

3. The integration of expansion preceding a saccade (as suggested by Tammero and Dickinson (2002b)), is likely to be a separate mechanism from the expansion-avoidance reflex. Under the closed-loop expansion-avoidance paradigm, flies robustly orient towards contraction, exhibiting smooth control, with no evidence for saccade initiation.

4. The object orientation response is used to direct flight over some long distance towards a prominent object. Straight flight is achieved by keeping an object in the center of the retina. This behavior may explain most straight segments observed in *Drosophila* flight. Especially when considering the curved flight paths observed in the absence of vertical edges (Frye et al., 2003), it seems likely that straight flight over long distances requires some object orientation, and not simply haltere feedback.

5. Ground motion has some control on orientation and the pitch/thrust/altitude loop, and also exhibits a speed-dependent orientation. Additional experiments are required to further constrain these behaviors.

6. The classic, syndirectional optomotor response may exist as a separate system, and not as an artifact of the expansion-avoidance response (as suggested by

Tammero et al. (2004)). Some evidence for this is the low gain required to close a behavioral feedback loop around an optomotor equilibrium experiment, and the differences in the dynamic properties of these two systems (Duistermars et al. in prep.).

This list is not exhaustive and does not include the unknown velocity control behaviors that are sure to exist. Rather than calling each of these modules a behavior, it is more appropriate to refer to each response as some input-output relationship that cannot be currently explained by a model that accounts for other behaviors as well. Some modules clearly are independent, such as expansion-avoidance and object orientation, as evidenced by the responses to the compound stimuli of Chapter 3. It must be emphasized that the notion of a *behavior* as a discrete unit is overly anthropomorphic. Suppose that the lobula plate tangential cells acting as matched filters will explain much of visually based flight control. Then there is some highly interconnected network of neurons that each respond to some combination of features in the optic flow field, and the network produces some reduced set of signals that ultimately lead to motor output. That such a network would produce different motor patterns is response to different inputs is not surprising. What may be surprising is that such a network could generate speed dependent behavior, or something as seemingly 'cognitive' as object orientation.

7.3 Future directions and open questions

- The mechanism of the newly discovered speed-dependent inversion of the expansion-avoidance (and ground motion) response must be pursued. It is possible that the inversion is generated by parallel systems, integrating motion from different parts of the eye, that operate with very different time constants. Are there local differences in the temporal frequency optima across the *Drosophila* eye?

- The role of head motion in *Drosophila* flight. The working hypothesis suggested in Chapter 4 should be followed up with more detailed experiments.

- How can the growing body of knowledge about the flight control system of *Drosophila* be integrated into a comprehensive model, such as the Grand Unified Fly Model (Dickson et al., 2006)? If all of the behaviors listed above are indeed independent, and all are implemented by *Drosophila*, will a successful model of fly navigation require the implementation of all modules?

- Are there some general principles that govern the interactions of multiple, parallel behavioral modules? The rules for the interactions must depend on context; for example, the expansion-avoidance behavior must, at some point, give way to a landing behavior.

- *Drosophila* are capable of both saccadic and smooth steering. Under what conditions is one motor pattern preferred?

- Are we in a position to pursue the large neural circuits underlying some (any) of these behaviors, or must the reverse engineering of *Drosophila* flight control remain a top-down enterprise?

References

Baird, E., Srinivasan, M. V., Zhang, S. W., and Cowling, A. (2005). Visual control of flight speed in honeybees. *J. Exp. Biol.*, 208(20):3895–3905. 14

Barron, A. and Srinivasan, M. V. (2006). Visual regulation of ground speed and headwind compensation in freely flying honey bees (*Apis mellifera L.*). *J. Exp. Biol.*, 209(5):978–984. 14

Batschelet, E. (1981). *Circular Statistics in Biology*. Academic Press, New York. 40

Bender, J. A. and Dickinson, M. H. (2006a). A comparison of visual and haltere-mediated feedback in the control of body saccades in *Drosophila melanogaster*. *J. Exp. Biol.*, 209(23):4597–4606. 10, 166

Bender, J. A. and Dickinson, M. H. (2006b). Visual stimulation of saccades in magnetically tethered *Drosophila*. *J. Exp. Biol.*, 209(16):3170–3182. 10, 99, 166

Blevin, W. R., Kessler, K., Mielenz, K. D., and Wyszecki, G. (1983). Principles governing photometry. *Metrologia*, 19(3):97–101. 32

Borst, A. and Bahde, S. (1986). What kind of movement detector is triggering the landing response of the housefly. *Biol. Cybern.*, 55(1):59–69. 88, 148

Borst, A. and Bahde, S. (1987). Comparison between the movement detection systems underlying the optomotor and the landing response in the housefly. *Biol. Cybern.*, 56(4):217–224. 113, 114, 115

Borst, A. and Egelhaaf, M. (1989). Principles of visual-motion detection. *Trends Neurosci.*, 12(8):297–306. 5, 6

Borst, A. and Haag, J. (2002). Neural networks in the cockpit of the fly. *J. Comp. Physiol. A*, 188(6):419–437. 1, 5

Buchner, E. (1976). Elementary movement detectors in an insect visual system. *Biol. Cybern.*, 24(2):85–101. 88, 112, 124, 141

Buchner, E. (1984). Behavioural analysis of spatial vision in insects. In Ali, M., editor, *Photoreception and Vision in Invertebrates*, pages 561–621. Plenum, New York. 1, 13, 88, 113, 142

Buchner, E., Buchner, S., and Hengstenberg, R. (1979). 2-deoxy-d-glucose maps movement-specific nervous activity in the second visual ganglion of *Drosophila*. *Science*, 205(4407):687–688. 5

Budick, S. A. and Dickinson, M. H. (2006). Free-flight responses of *Drosophila melanogaster* to attractive odors. *J. Exp. Biol.*, 209(15):3001–3017. 14, 167, 174

Burton, B. G. and Laughlin, S. B. (2003). Neural images of pursuit targets in the photoreceptor arrays of male and female houseflies *Musca domestica*. *J. Exp. Biol.*, 206(22):3963–3977. 142

Chan, W. P., Prete, F., and Dickinson, M. H. (1998). Visual input to the efferent control system of a fly's "gyroscope". *Science*, 280:289–292. 3

Chapman, R. F. (1998). *The Insects: Structure and Function*. Cambridge University Press, Cambridge, 4^{th} edition. 3

Collett, T. and Land, M. (1975). Visual control of flight behaviour in the hoverfly *Syritta pipiens*. *J. Comp. Physiol. A*, 99(1):1–66. 10

David, C. T. (1978). Relationship between body angle and flight speed in free-flying *Drosophila*. *Physiol. Entomol.*, 3(3):191–195. 9, 18, 121, 167

David, C. T. (1979). Optomotor control of speed and height by free-flying *Drosophila*. *J. Exp. Biol.*, 82:389–392. 18, 121, 135

David, C. T. (1982a). Compensation for height in the control of groundspeed by *Drosophila* in a new, barbers pole wind-tunnel. *J. Comp. Physiol. A*, 147(4):485–493. 12

David, C. T. (1982b). Competition between fixed and moving stripes in the control of orientation by flying *Drosophila*. *Physiol. Entomol.*, 7(2):151–156. 18, 121, 126, 135

David, C. T. (1985). Visual control of the partition of flight force between lift and thrust in free-flying *Drosophila*. *Nature*, 313(5997):48–50. 10, 99, 132, 166

de Ruyter van Steveninck, R., Zaagman, W. H., and Mastebroek, H. A. K. (1986). Adaptation of transient responses of a movement sensitive neuron in the visual system of the blowfly *Calliphora erythrocephala*. *Biol. Cybern.*, 54(4-5):223–236. 115

Dickinson, M. H. (1999). Haltere-mediated equilibrium reflexes of the fruit fly, *Drosophila melanogaster*. *Phil. Trans. R. Soc. Lond. B*, 354:903–916. 2

Dickinson, M. H., Lehmann, F. O., and Götz, K. G. (1993). The active control of wing rotation by *Drosophila*. *J. Exp. Biol.*, 182:173–189. 35, 36

Dickson, W. B., Straw, A. D., Poelma, C., and Dickinson, M. H. (2006). An integrative model of insect flight control. In *Proc. of the 44th AIAA Aerospace Sciences Meeting and Exhibit*, pages 1–19. 177

Dror, R. O., O'Carroll, D. C., and Laughlin, S. B. (2001). Accuracy of velocity estimation by Reichardt correlators. *J. Opt. Soc. Am. A*, 18(2):241–252. 6, 78, 113

Duistermars, B. J., Chow, D., and Frye, M. A. (in prep.). Acute spatial, temporal, and contrast sensitivity of translational optomotor responses in *Drosophila*. 114, 176

Egelhaaf, M. (1987). Dynamic properties of two control systems underlying visually guided turning in house-flies. *J. Comp. Physiol. A*, 161(6):777–783. 11

Egelhaaf, M. and Borst, A. (1989). Transient and steady-state response properties of movement detectors. *J. Opt. Soc. Am. A*, 6(1):116–127. 78, 115

Egelhaaf, M. and Borst, A. (1992). Is there a separate control-system mediating a centering response in honeybees? *Naturwissenschaften*, 79(5):221–223. 14

Egelhaaf, M., Borst, A., and Reichardt, W. (1989). Computational structure of a biological motion-detection system as revealed by local detector analysis in the fly's nervous system. *J. Opt. Soc. Am. A*, 6(7):1070–1087. 6, 115

Egelhaaf, M. and Kern, R. (2002). Vision in flying insects. *Curr. Opin. Neurobiol.*, 12(6):699–706. 5

Egelhaaf, M., Kern, R., Krapp, H. G., Kretzberg, J., Kurtz, R., and Warzecha, A. K. (2002). Neural encoding of behaviourally relevant visual-motion information in the fly. *Trends Neurosci.*, 25(2):96–102. 1, 7

Fisher, N. I. (1993). *Statistical Analysis of Circular Data*. Cambridge University Press, Cambridge, UK. 40

Franz, M. O., Neumann, T. R., Plagge, M., Mallot, H. A., and Zell, A. (1999). Can fly tangential neurons be used to estimate self-motion? In *Proc. of the 9th International Conference on Artificial Neural Networks*, CP 470, pages 994–999, London. IEE. 8

Fry, S. N., Rohrseitz, N., Straw, A. D., and Dickinson, M. H. (in prep.). 14, 115, 120

Fry, S. N., Sayaman, R., and Dickinson, M. H. (2003). The aerodynamics of free-flight maneuvers in *Drosophila*. *Science*, 300(5618):495–498. 1, 8, 9, 35, 109, 118, 158, 162

Fry, S. N., Sayaman, R., and Dickinson, M. H. (2005). The aerodynamics of hovering flight in *Drosophila*. *J. Exp. Biol.*, 208(12):2303–2318. 10, 35, 137

Frye, M. A. and Dickinson, M. H. (2001). Fly flight: A model for the neural control of complex behavior. *Neuron*, 32(3):385–388. 1

Frye, M. A. and Dickinson, M. H. (2004). Motor output reflects the linear superposition of visual and olfactory inputs in *Drosophila*. *J. Exp. Biol.*, 207(1):123–131. 35

Frye, M. A., Tarsitano, M., and Dickinson, M. H. (2003). Odor localization requires visual feedback during free flight in *Drosophila melanogaster*. *J. Exp. Biol.*, 206(5):843–855. 14, 15, 168, 174, 175

Gibson, J. J. (1950). *The perception of the visual world*. Houghton Mifflin, Boston. 5

Gopfert, M. C. and Robert, D. (2002). The mechanical basis of *Drosophila* audition. *J. Exp. Biol.*, 205(9):1199–1208. 3

Götz, K. G. (1964). Optomotorische untersuchung des visuellen systems einiger augenmutanten der fruchtfliege *drosophila*. *Kybernetik*, 2(2):77–91. 8, 95, 124, 125

Götz, K. G. (1968). Flight control in *Drosophila* by visual perception of motion. *Kybernetik*, 9:159–182. 8, 9, 11, 12, 16, 117

Götz, K. G. (1975). Optomotor equilibrium of *Drosophila* navigation system. *J. Comp. Physiol. A*, 99(3):187–210. 11, 166

Götz, K. G. (1987). Course-control, metabolism and wing interference during ultralong tethered flight in *Drosophila Melanogaster*. *J. Exp. Biol.*, 128:35–46. 8, 10, 35, 53

Götz, K. G. and Biesinger, R. (1983). Wind-controlled selection of motion detectors in the eyes of *Drosophila melanogaster*. *Dros. Inf. Serv.*, 59:39. 3, 35

Götz, K. G. and Wandel, U. (1984). Optomotor control of the force of flight in *Drosophila* and *Musca*. II. Covariance of list and thrust in still air. *Biol. Cybern.*, 51:135–139. 9, 117

Götz, K. G. and Wenking, H. (1973). Visual control of locomotion in walking fruitfly *Drosophila*. *J. Comp. Physiol. A*, 85(3):235–266. 88, 113, 114, 136

Guo, J. and Guo, A. (2005). Crossmodal interactions between olfactory and visual learning in *Drosophila*. *Science*, 309(5732):307–310. 81

Haag, J., Denk, W., and Borst, A. (2004). Fly motion vision is based on Reichardt detectors regardless of the signal-to-noise ratio. *Proc. Natl Acad. Sci.*, 101(46):16333–16338. 113

Hassenstein, B. and Reichardt, W. (1956). Systemtheoretische analyse der zeit, reihenfolgen und vorzeichenauswertung bei der bewegungsperzeption des russelkafers *Chlorophanus*. *Z. Naturforsch.*, 11(9-10):513–524. 5, 113

Hausen, K. (1982a). Motion sensitive interneurons in the optomotor system of the fly. 1. The horizontal cells: Structure and signals. *Biol. Cybern.*, 45(2):143–156. 7, 9

Hausen, K. (1982b). Motion sensitive interneurons in the optomotor system of the fly. 2. The horizontal cells: Receptive field organization and response characteristics. *Biol. Cybern.*, 46(2):67–79. 7, 113, 114

Hausen, K. (1984). The lobula-complex of the fly: structure, function and significance in visual behaviour. In Ali, M. A., editor, *Photoreception and vision in invertebrates*, pages 523–559. Plenum, New York. 7

Heisenberg, M. and Buchner, E. (1977). Role of retinula cell-types in visual behavior of *Drosophila Melanogaster*. *J. Comp. Physiol. A*, 117(2):127–162. 34, 78, 79, 88, 113

Heisenberg, M. and Wolf, R. (1979). On the fine-structure of yaw torque in visual flight orientation of *Drosophila melanogaster*. *J. Comp. Physiol. A*, 130(2):113–130. 10, 38, 40, 53, 67, 79, 80

Heisenberg, M. and Wolf, R. (1984). *Vision in Drosophila*. Springer Verlag, Berlin. 5, 10, 37, 58, 141

Heisenberg, M. and Wolf, R. (1988). Reafferent control of optomotor yaw torque in *Drosophila melanogaster*. *J. Comp. Physiol. A*, 163(3):373–388. 10, 38, 84, 85, 99, 166

Hengstenberg, R. (1991). Gaze control in the blowfly *Calliphora*: A multisensory two-stage integration process. *The Neurosciences*, 3:19–29. 1, 2, 3, 116

Karmeier, K., Krapp, H. G., and Egelhaaf, M. (2003). Robustness of the tuning of fly visual interneurons to rotatory optic flow. *J. Neurophysiol.*, 90(3):1626–1634. 7

Karmeier, K., Krapp, H. G., and Egelhaaf, M. (2005). Population coding of self-motion: Applying Bayesian analysis to a population of visual interneurons in the fly. *J. Neurophysiol.*, 94(3):2182–2194. 8

Kennedy, J. S. (1940). The visual responses of flying mosquitoes. *Proc. Zool. Soc. Lond. Ser. A*, 109:221–242. 12, 120

Kennedy, J. S. (1951). The migration of the desert locust (*Schistocerca-Gregaria Forsk*) .1. Behaviour of swarms .2. Theory of long-range migrations. *Philos. T. Roy. Soc. B*, 235(625):163–290. 12

Kern, R. and Egelhaaf, M. (2000). Optomotor course control in flies with largely asymmetric visual input. *J. Comp. Physiol. A*, 186(1):45–55. 119

Kern, R., van Hateren, J. H., and Egelhaaf, M. (2006). Representation of behaviourally relevant information by blowfly motion-sensitive visual interneurons requires precise compensatory head movements. *J. Exp. Biol.*, 209(7):1251–1260. 118

Kern, R., van Hateren, J. H., Michaelis, C., Lindemann, J. P., and Egelhaaf, M. (2005). Function of a fly motion-sensitive neuron matches eye movements during free flight. *Plos Biol.*, 3(6):1130–1138. 7

Kimmerle, B., Eickermann, J., and Egelhaaf, M. (2000). Object fixation by the blowfly during tethered flight in a simulated three-dimensional environment. *J. Exp. Biol.*, 203(11):1723–1732. 82

Kimmerle, B., Warzecha, A. K., and Egelhaaf, M. (1997). Object detection in the fly during simulated translatory flight. *J. Comp. Physiol. A*, 181(3):247–255. 82

Krapp, H. G. and Hengstenberg, R. (1996). Estimation of self-motion by optic flow processing in single visual interneurons. *Nature*, 384:463–466. 7

Krapp, H. G. and Hengstenberg, R. (1997). A fast stimulus procedure to determine local receptive field properties of motion-sensitive visual interneurons. *Vision Res.*, 37(2):225–234. 7, 9

Land, M. and Fernald, R. (1992). The evolution of eyes. *Annu. Rev. Neurosci.*, 15(1):1–29. 5

Land, M. F. (1997). Visual acuity in insects. *Annu. Rev. Entomol.*, 42:147–177. 5

Land, M. F. and Collett, T. S. (1974). Chasing behavior of houseflies (*Fannia-Canicularis*)—description and analysis. *J. Comp. Physiol. A*, 89(4):331–357. 8, 109

Laughlin, S. B. (1994). Matching coding, circuits, cells, and molecules to signals: General principles of retinal design in the fly's eye. *Prog. Retin. Res.*, 13(1):165–195. 5, 78

Lehmann, F. O. and Dickinson, M. H. (1997). The changes in power requirements and muscle efficiency during elevated force production in the fruit fly *Drosophila melanogaster*. *J. Exp. Biol.*, 200(7):1133–1143. 9, 35, 95

Lindemann, J. P., Kern, R., Michaelis, C., Meyer, P., van Hateren, J. H., and Egelhaaf, M. (2003). Flimax, a novel stimulus device for panoramic and highspeed presentation of behaviourally generated optic flow. *Vision Res.*, 43(7):779–791. 9

Lindemann, J. P., Kern, R., van Hateren, J. H., Ritter, H., and Egelhaaf, M. (2005). On the computations analyzing natural optic flow: quantitative model analysis of the blowfly motion vision pathway. *J. Neurosci.*, 25(27):6435–48. 6, 113

Liu, G., Seiler, H., Wen, A., Zars, T., Ito, K., Wolf, R., Heisenberg, M., and Liu, L. (2006). Distinct memory traces for two visual features in the *Drosophila* brain. *Nature*, 439(7076):551–556. 81

Maddess, T. and Laughlin, S. B. (1985). Adaptation of the motion-sensitive neuron H1 is generated locally and governed by contrast frequency. *Proc. R. Soc. Lond. B*, 225(1239):251–275. 115

Marr, D. (1982). *Vision: A Computational Investigation into the Human Representation and Processing of Visual Information*. W. H. Freeman, San Francisco. 139, 140

Marsh, D., Kennedy, J. S., and Ludlow, A. R. (1978). Analysis of anemotactic zigzagging flight in male moths stimulated by pheromone. *Physiol. Entomol.*, 3(3):221–240. 12

Mayer, M., Vogtmann, K., Bausenwein, B., Wolf, R., and Heisenberg, M. (1988). Flight control during free yaw turns in *Drosophila melanogaster*. *J. Comp. Physiol. A*, 163(3):389–399. 10

Miall, R. C. (1978). Flicker fusion frequencies of 6 laboratory insects, and response of compound eye to mains fluorescent ripple. *Physiol. Entomol.*, 3(2):99–106. 19, 33

Nalbach, G. (1993). The halteres of the blowfly *Calliphora*. I. Kinematics and dynamics. *J. Comp. Physiol. A*, 173:293–300. 1

Neumann, T. R. and Bülthoff, H. H. (2002). Behavior-oriented vision for biomimetic flight control. In *Proceedings of the EPSRC/BBSRC International Workshop Biologically-Inspired Robotics: The Legacy of W. Grey Walter*. 8

O'Carroll, D. C. (2001). Motion adaptation and evidence for parallel processing in the lobula plate of the bee-fly *Bombylius major*. In Zanker, J. and Zeil, J., editors, *Motion vision: Computational, neural and ecological constraints*, pages 381–394. Springer Verlag, Berlin. 115

Olberg, R. M. (1981). Parallel encoding of direction of wind, head, abdomen, and visual-pattern movement by single interneurons in the dragonfly. *J. Comp. Physiol. A*, 142(1):27–41. 3

Parsons, M. M., Krapp, H. G., and Laughlin, S. B. (2006). A motion-sensitive neurone responds to signals from the two visual systems of the blowfly, the compound eyes and ocelli. *J. Exp. Biol.*, 209(22):4464–4474. 3

Rajashekhar, K. P. and Shamprasad, V. R. (2004). Golgi analysis of tangential neurons in the lobula plate of *Drosophila melanogaster*. *J. Biosci.*, 29(1):93–104. 7

Reichardt, W. (1961). Autocorrelation, a principle for the evaluation of sensory information by the central nervous system. In Rosenblith, W., editor, *Sensory Communication*, pages 303–317. MIT Press, New York. 8, 113

Reichardt, W. and Poggio, T. (1976). Visual control of orientation behavior in fly. 1. Quantitative analysis. *Q. Rev. Biophys.*, 9(3):311–375. 67, 80, 109, 168

Reichardt, W. and Wenking, H. (1969). Optical detection and fixation of objects by fixed flying flies. *Naturwissenschaften*, 56(8):424–425. 8, 53

Reiser, M. B. and Dickinson, M. H. (2003). A test bed for insect-inspired robotic control. *Philos. T. Roy. Soc. A*, 361(1811):2267–2285. 8, 144

Reiser, M. B., Humbert, J. S., Dunlop, M. J., Del Vecchio, D., Murray, R. M., and Dickinson, M. H. (2004). Vision as a compensatory mechanism for disturbance rejection in upwind flight. In *Proc. of the 2004 American Control Conference*, volume 1, pages 311–316. 155

Sane, S. P. and Dickinson, M. H. (2002). The aerodynamic effects of wing rotation and a revised quasi-steady model of flapping flight. *J. Exp. Biol.*, 205(8):1087–1096. 161

Sayeed, O. and Benzer, S. (1996). Behavioral genetics of thermosensation and hygrosensation in *Drosophila*. *Proc. Natl Acad. Sci.*, 93(12):6079–6084. 3

Schilstra, C. and Van Hateren, J. H. (1999). Blowfly flight and optic flow. I. Thorax kinematics and flight dynamics. *J. Exp. Biol.*, 202(11):1481–1490. 8, 10

Schuppe, H. and Hengstenberg, R. (1993). Optical properties of the ocelli of *Calliphora erythrocephala* and their role in the dorsal light response. *J. Comp. Physiol. A*, 173(2):143–149. 3

Sherman, A. and Dickinson, M. H. (2003). A comparison of visual and haltere-mediated equilibrium reflexes in the fruit fly *Drosophila melanogaster*. *J. Exp. Biol.*, 206(2):295–302. 2

Snyder, A. W. (1979). Physics of vision in compound eyes. In Autrum, H., editor, *Handbook of Sensory Physiology*, pages 225–313. Springer, Berlin. 5, 142

Srinivasan, M. V., Lehrer, M., Kirchner, W. H., and Zhang, S. W. (1991). Range perception through apparent image speed in freely flying honeybees. *Visual Neurosci.*, 6(5):519–535. 8, 12, 88, 105, 119

Srinivasan, M. V., Poteser, M., and Kral, K. (1999). Motion detection in insect orientation and navigation. *Vis. Res.*, 39(16):2749–2766. 5, 6, 11, 115

Srinivasan, M. V., Zhang, S. W., and Chandrashekara, K. (1993). Evidence for 2 distinct movement-detecting mechanisms in insect vision. *Naturwissenschaften*, 80(1):38–41. 14

Srinivasan, M. V., Zhang, S. W., Lehrer, M., and Collett, T. S. (1996). Honeybee navigation en route to the goal: Visual flight control and odometry. *J. Exp. Biol.*, 199(1):237–244. 12, 14, 152

Stange, G. (1981). The ocellar component of flight equilibrium control in dragonflies. *J. Comp. Physiol.*, 141(3):335–347. 3

Stark, W. S., Ivanyshyn, A. M., and Greenberg, R. M. (1977). Sensitivity and photopigments of r1-6, a 2-peaked photoreceptor, in *Drosophila*, *Calliphora* and *Musca*. *J. Comp. Physiol. A*, 121(3):289–305. 34

Strausfeld, N. J. (1989). Beneath the compound eye: Neuroanatomical analysis and physiological correlates in the study of insect vision. In *Facets of Vision*, pages 317–359. Springer, Berlin. 5

Strauss, R., Schuster, S., and Götz, K. G. (1997). Processing of artificial visual feedback in the walking fruit fly *Drosophila melanogaster*. *J. Exp. Biol.*, 200(9):1281–1296. 9

Straw, A. D., Warrant, E. J., and O'Carroll, D. C. (2006). A 'bright zone' in male hoverfly (*Eristalis tenax*) eyes and associated faster motion detection and increased contrast sensitivity. *J. Exp. Biol.*, 209(21):4339–4354. 7, 136

Sugiura, H. and Dickinson, M. H. (in prep.). Direct force measurement of *Drosophila* in flight. 137

Tammero, L. F. and Dickinson, M. H. (2002a). Collision-avoidance and landing responses are mediated by separate pathways in the fruit fly, *Drosophila melanogaster*. *J. Exp. Biol.*, 205(18):2785–2798. 10, 16, 87, 99, 166

Tammero, L. F. and Dickinson, M. H. (2002b). The influence of visual landscape on the free flight behavior of the fruit fly *Drosophila melanogaster*. *J. Exp. Biol.*, 205(3):327–343. 8, 10, 14, 16, 87, 119, 143, 152, 155, 167, 174, 175

Tammero, L. F., Frye, M. A., and Dickinson, M. H. (2004). Spatial organization of visuomotor reflexes in *Drosophila*. *J. Exp. Biol.*, 207(1):113–122. 10, 11, 15, 16, 17, 18, 35, 36, 37, 46, 53, 54, 86, 87, 91, 94, 108, 112, 116, 119, 123, 124, 134, 155, 158, 161, 176

Taylor, G. K. (2001). Mechanics and aerodynamics of insect flight control. *Biol. Rev.*, 76(4):449–471. 1

Van Hateren, J. H. and Schilstra, C. (1999). Blowfly flight and optic flow II. Head movements during flight. *J. Exp. Biol.*, 202(11):1491–1500. 117, 118

Von Holst, E. and Mittlestaedt, H. (1950). Das Reafferenzprinzip. *Naturwissenschaften*, 37(20):464–476. 8, 11

Vosshall, L. (2000). Olfaction in *Drosophila*. *Curr. Opin. Neurobiol.*, 10(4):498–503. 3

Wagner, H. (1986). Flight performance and visual control of flight of the free-flying housefly (*Musca Domestica L.*) I. Organization of the flight motor. *Philos. T. Roy. Soc. B*, 312(1158):527–551. 10

Warzecha, A. K. and Egelhaaf, M. (1996). Intrinsic properties of biological motion detectors prevent the optomotor control system from getting unstable. *Philos. T. Roy. Soc. B*, 351(1347):1579–1591. 148, 166

Webb, B. (1999). A framework for models of biological behaviour. *Int. J. Neural Syst.*, 9(5):375–81. 139

Webb, B. (2006). Validating biorobotic models. *J. Neural Eng.*, 3(3):R25–R35. 140

Wehrhahn, C. (1984). Ocellar vision and orientation in flies. *Proc. R. Soc. Lond. B*, 222(1228):409–411. 3

Wilson, M. (1978). Functional organization of locust ocelli. *J. Comp. Physiol.*, 124(4):297–316. 3

Wu, C. F. and Pak, W. L. (1975). Quantal basis of photoreceptor spectral sensitivity of *Drosophila melanogaster*. *J. Gen. Physiol.*, 66(2):149–168. 34

Zanker, J. M., Egelhaaf, M., and Warzecha, A. K. (1991). On the coordination of motor output during visual flight control of flies. *J. Comp. Physiol. A*, 169(2):127–134. 116

Zanker, J. M., Srinivasan, M. V., and Egelhaaf, M. (1999). Speed tuning in elementary motion detectors of the correlation type. *Biol. Cybern.*, 80:109–116. 6, 114